

FIELD INVESTIGATION AND HYDROLOGICAL
MODELLING OF A SUB-ARCTIC WETLAND SYSTEM
BY SLURP AND WATFLOOD

LIANG JING



**Field Investigation and Hydrological Modelling of a
Sub-arctic Wetland System by SLURP and
WATFLOOD**

by

Liang Jing

A thesis submitted to the
School of Graduate Studies
in partial fulfilment of the
requirements for the degree of
Master of Engineering

Faculty of Engineering and Applied Science
Memorial University of Newfoundland

July 2009

St. John's

Newfoundland

Abstract

The wetlands existing as bogs, fens, swamps, marshes and shallow water comprise 14% of Canadian land. Recently, there are growing research interests in the hydrological characteristics of arctic and subarctic wetland systems in the need for more efficiently conserve wetlands and assess climate change related impacts. This research targeted the Deer River watershed near Churchill, Manitoba, which presents a typical subarctic wetland system in the Hudson Bay Lowlands. An extensive field investigation was first conducted from 2006 to 2008 to facilitate in-depth understanding of the wetland hydrology; and two semi-distributed hydrological models, SLURP and WATFLOOD, were employed to simulate the hydrologic cycle in the targeted subarctic wetland.

The 28-year historic data (1978 - 2005) revealed a steady elevation of mean temperature and accumulative precipitation in the summertime (late June – early October). The 3-year field observation (2006-2008) also provided evidence to indicate a warming climate in the watershed. Frost table, soil moisture and streamflow were monitored and analyzed to advance the acknowledgement of the climatic, geographical and hydrological characteristics of the subarctic wetlands. The frost tables at the monitored transects were declining and reciprocal at their distances to the stream channels because of the subsurface flow within organic layer moving towards the stream and accelerating the thaw of frozen soil. Following the major recharge period during the snowmelt, soil moisture contents in the shallow layers of the wetland kept declining over time

throughout the summer. The water discharges were low before September due to low precipitation and strong evapotranspiration as well as expansion of storage capacity of the organic soil layers, and then gradually increased due to the intensive precipitation in the fall. All the monitored streams showed prolonged responses to precipitation due to the combined effects of shallow impermeable frost table, porous soil, and varied soil storage capacity.

Based on the watershed delineation by River Tools and TOPAZ, SLURP and WATFLOOD were applied to further justify the conclusions from field investigation and examine their applicability on subarctic wetlands. The results also revealed the distinguishable hydrological features of sub-arctic wetlands. It was observed that the snowmelt in the spring season produced the highest peak discharges and contributed to the majority of the annual streamflow. Peaks of the simulated spring flows from both models were to some extent lower than the observed ones. This could be attributed to the effects of extensive wetland ponds and shallow permafrost tables which could restrict the infiltration of rainwater and drive the snowmelt to form spring flow peaks. It was also shown that most of the small or moderate rainfall events during the summertime were unable to generate noticeable surface runoff possibly due to canopy interception, depression storage, porous soil layers, descending permafrost table and intensive evapotranspiration. A thorough comparison between SLURP and WATFLOOD was conducted from the aspects of modelling structure, formulation, parameters, and results, which indicated that SLURP presented a slightly better overall performance than WATFLOOD in most of the years at both watershed- and sub-basin level simulation.

Acknowledgements

I would first like to thank my supervisor, Dr. Bing Chen for his guidance and help during this journey. His knowledge and talent in the academic domain have greatly facilitated the development and success of my research. His friendships and concerns have given me a comfortable study environment and made the 2-year study a memorable one. I wish to thank him for his sincere suggestions and recommendations.

Special thanks go to the School of Graduate Studies and the Faculty of Engineering and Applied Science at Memorial University of Newfoundland for providing me research scholarships and teaching assistantships, as well as Manitoba Hydro, ArcticNet, and Churchill Northern Studies Center (CNSC) which offered me additional funds for field work in Churchill, Manitoba. Those unique experiences have absolutely enriched my life and stimulated my interests in the field.

I would also like to thank Dr. Kenneth Snelgrove at Memorial University of Newfoundland, Dr. Tim Papakyriakou at the University of Manitoba, and Dr. Nicholas Kouwen at the University of Waterloo for their kind help and advice. My great appreciation also go to Dr. LeeAnn Fishback, Kyle Swystun, Robert Whitten, Katy Lapenski, Mike Coffey, Bing Han and Xiang Liu for their assistance in the field work.

To my group mates, Jing Ping and Pu Li, thank you for being with me during the last

three years. To all my fellow graduate students, your help and encouragement is always precious gift to me. To all my friends, I have finally come to the end of this journey.

I would like to express my thanks to my parents in three words: I Love You. I don't know how much further I will go in my research, and I don't know how tough it will be when I start my career, but I do know I can conquer every single mountain in my life with your boundless love and encouragement. Thank you for always believing in me. I will not let you down.

Finally, to my girl friend, Jingjing Cai: thank you for being with me through thick and thin, for offering me your suggestions and help, and for taking care of my everyday life. Trust me, this is a great new start rather than the destination: I hope we can both have a good future career and enjoy our time together for the rest of our lives.

Table of Contents

ABSTRACT	II
ACKNOWLEDGEMENTS	IV
TABLE OF CONTENTS	VI
LIST OF FIGURES	IX
LIST OF TABLES	XIII
LIST OF ABBREVIATIONS AND SYMBOLS	XIV
CHAPTER 1 INTRODUCTION	1
1.1 Background	1
1.2 Objectives	4
1.3 Organization	5
CHAPTER 2 LITERATURE REVIEW	6
2.1 Wetland Hydrology	6
2.2 Field Survey	9
2.3 Hydrological Modelling	11
2.4 SLURP and WATFLOOD	19
CHAPTER 3 CHARACTERIZATION OF SUB-ARCTIC WETLAND SYSTEMS – FIELD INVESTIGATION IN THE DEER RIVER WATERSHED	23
3.1 Introduction	23
3.2 The Study Area	24
3.3 Field Investigation	32
<i>3.3.1 Datasets</i>	32
<i>3.3.2 Calculations</i>	33
<i>3.3.3 Field Work Summary</i>	37
3.4 Results and Discussion	43
<i>3.4.1 Variation of Temperature and Precipitation</i>	43
<i>3.4.2 Distribution of Frost Table</i>	50
<i>3.4.3 Profile of Soil Moisture and Temperature</i>	64
<i>3.4.4 Fluctuation of Water Stage and Streamflow</i>	76
3.5 Summary	86
CHAPTER 4 MODELLING OF THE DEER RIVER WATERSHED BY SLURP	89
4.1 SLURP	89
<i>4.1.1 Vertical Water Balance Model</i>	89
<i>4.1.2 Horizontal Water Budget</i>	96
4.2 Watershed Delineation by TOPAZ	99
4.3 Land Cover Classification	102
4.4 Meteorological and Streamflow data	104

4.5 Sensitivity Analysis	105
4.6 Calibration	109
4.7 Verification	125
4.8 Modelling of the Chesnaye Sub-basin	148
4.8.1 <i>Delineation of the Chesnaye Sub-basin</i>	148
4.8.2 <i>Land Cover</i>	148
4.8.3 <i>Meteorological and Streamflow data</i>	149
4.8.4 <i>Modelling Results</i>	149
4.9 Summary	163
CHAPTER 5 MODELLING OF THE DEER RIVER WATERSHED BY WATFLOOD	164
5.1 WATFLOOD	164
5.1.1 <i>Interception</i>	167
5.1.2 <i>Surface Storage</i>	167
5.1.3 <i>Infiltration</i>	167
5.1.4 <i>Initial Soil Moisture</i>	168
5.1.5 <i>Evapotranspiration</i>	168
5.1.5.1 <i>Potential Evapotranspiration</i>	168
5.1.5.2 <i>Actual Evapotranspiration</i>	170
5.1.6 <i>Snowmelt</i>	171
5.1.7 <i>Interflow</i>	171
5.1.8 <i>Groundwater Recharge</i>	172
5.1.9 <i>Overland Flow</i>	172
5.1.10 <i>Base Flow</i>	172
5.1.11 <i>Channel Routing</i>	173
5.1.12 <i>Wetland Routing</i>	173
5.1.13 <i>Lake Routing</i>	174
5.2 Watershed Delineation by TOPAZ and EnsimHydrologic	175
5.3 Land Cover Classification	181
5.4 Meteorological and Streamflow data	181
5.5 Sensitivity Analysis	182
5.6 Calibration	186
5.7 Verification	202
5.8 Modelling of the Chesnaye Sub-basin	224
5.8.1 <i>Delineation of the Chesnaye Sub-basin</i>	224
5.8.2 <i>Land Cover</i>	224
5.8.3 <i>Meteorological and Streamflow data</i>	224
5.8.4 <i>Modelling Results</i>	224
5.9 Summary	235
CHAPTER 6 COMPARISON BETWEEN SLURP AND WATFLOOD	236
6.1 Introduction	236
6.2 Difference in Modelling Structure	237
6.3 Difference in Simulation Methodologies	239

6.3.1 <i>Interception and Surface Storage</i>	239
6.3.2 <i>Snowmelt Process</i>	240
6.3.3 <i>Evapotranspiration</i>	244
6.3.3.1 SLURP	244
6.3.3.2 WATFLOOD	248
6.4 Difference in Modelling Results	255
6.4.1 <i>Spring Snowmelt and Runoff</i>	255
6.4.2 <i>Summer Rainfall Events</i>	257
6.4.3 <i>Fall Rainfall Events</i>	258
6.4.4 <i>Rainfall-Runoff Relationship</i>	258
6.4.5 <i>Uncertainty Analysis</i>	260
6.4.5.1 Resolution of the modelling inputs	260
6.4.5.2 Quality of the modelling inputs	260
6.4.5.3 Calibration of the modelling parameters	261
6.4.5.4 Effects of permafrost table and ponds	262
6.5 Summary	266
CHAPTER 7 CONCLUSIONS AND RECOMMENDATIONS	268
7.1 Summary	268
7.2 Significance of Research	271
7.3 Recommendations for Future Work	272
REFERENCES	274
APPENDIX A	288

List of Figures

Figure 3.1 Contour map of the Deer River Watershed and the Chesnaye Sub-basin from River Tools [®]	26
Figure 3.2 Drainage map of the Deer River Watershed from River Tools [®]	27
Figure 3.3 Delineation of the Deer River Watershed from River Tools [®]	28
Figure 3.4a Locations of the stream gauging stations (5, 6, 7, 10) and automated weather station (Rail Spur) in the Chesnaye Sub-basin	29
Figure 3.4b Locations of gauging and weather stations in the Deer River Watershed (After Google Earth [®])	31
Figure 3.6a Land coverage of downstream regions in the Deer River watershed	40
Figure 3.6b Land coverage of midstream regions in the Deer River watershed	41
Figure 3.6c Land coverage of upstream regions in the Deer River watershed	42
Figure 3.7 (a) Cumulative summertime precipitation P_{cum} and (b) mean summertime air temperature T_{avg} at the Churchill airport (June 20 th – October 3 rd , 1978-2008)	45
Figure 3.8 Variation of daily evapotranspiration and air temperature in (a) 2006, (b) 2007 and (c) 2008 at Rail Spur	48
Figure 3.9 Variation of daily evapotranspiration and precipitation in (a) 2006, (b) 2007 and (c) 2008 at Rail Spur	49
Figure 3.10 Depth of frost table in 2006 summertime at (a) Stations 5, (b) Station 6, and (c) Station	55
7, and (d) Station 10	56
Figure 3.11 Depth of frost table in 2007 summertime at (a) Station 5, (b) Station 6, (c) Station	57
7, and (d) Station 10	58
Figure 3.12 Frost table vs. (a) precipitation and (b) air temperature at Station 5 in 2006 summertime (RB: Right Bank; LB: Left Bank)	59
Figure 3.13 Frost table vs. (a) precipitation and (b) air temperature at Station 6 in 2006 summertime (RB: Right Bank; LB: Left Bank)	60
Figure 3.14 Frost table vs. (a) precipitation and (b) air temperature at Station 7 in 2006 summertime (RB: Right Bank; LB: Left Bank)	61
Figure 3.15 Frost table vs. (a) precipitation and (b) air temperature at Station 5 in 2007 summertime (RB: Right Bank; LB: Left Bank)	62
Figure 3.16 Frost table vs. (a) precipitation and (b) air temperature at Station 6 in 2007 summertime (RB: Right Bank; LB: Left Bank)	63
Figure 3.17 Frost table vs. (a) precipitation and (b) air temperature at Station 7 in 2007 summertime (RB: Right Bank; LB: Left Bank)	64
Figure 3.18 Frost table vs. (a) precipitation and (b) air temperature at Station 10 in 2007 summertime (RB: Right Bank; LB: Left Bank)	65
Figure 3.19 Soil moisture at stream banks of (a) Station 5, (b) Station 6, and (c) Station 7 in the summertime of 2006	66
Figure 3.20 Soil moisture at stream banks of (a) Station 5, (b) Station 6, (c) Station 7 and (d) Station 10	67
Figure 3.21 Variation of daily soil moisture and (a) precipitation and (b) evapotranspiration in the summertime of 2006 at Rail Spur (SM: Soil Moisture)	68
Figure 3.22 Variation of daily soil moisture and (a) precipitation and (b) evapotranspiration in the summertime of 2007 at Rail Spur (SM: Soil Moisture)	69
Figure 3.23 Variation of daily soil moisture and (a) precipitation and (b) evapotranspiration in	70

the summertime of 2008 at Rail Spur (SM: Soil Moisture)	72
Figure 3.24 Multiple soil layers temperature, air temperature and (a) P and (b) ET in the summertime of 2006 at Rail Spur (June 20 th – Oct 3 rd , ST: Soil temperature; <i>P</i> : Precipitation; <i>ET</i> : Evapotranspiration)	73
Figure 3.25 Multiple soil layers temperature, air temperature and (a) P and (b) ET in the summertime of 2007 at Rail Spur (June 20 th – Oct 3 rd , ST: Soil temperature; <i>P</i> : Precipitation; <i>ET</i> : Evapotranspiration)	74
Figure 3.26 Multiple soil layers temperature, air temperature and (a) P and (b) ET in the summertime of 2008 at Rail Spur (June 20 th – Oct 3 rd , ST: Soil temperature; <i>P</i> : Precipitation; <i>ET</i> : Evapotranspiration)	75
Figure 3.27 Discharge – Stage relationships of (a) Station 5, (b) Station 6, (c) Station 7, and (d) Station 10 from 2006 to 2008	78
Figure 3.28 Discharge – Velocity relationships of (a) Station 5, (b) Station 6, (c) Station 7, and (d) Station 10 from 2006 to 2008	79
Figure 3.29 Plot of evapotranspiration, precipitation and water discharge in 2006 at (a) Stations 5 and (b) Station 7	80
Figure 3.30 Plot of evapotranspiration, precipitation and water discharge in 2007 at (a) Stations 5, (b) Station 6, (c) Station 7, and (d) Station 10	82
Figure 3.31 Plot of evapotranspiration, precipitation and water discharge in 2008 at (a) Stations 5, (b) Station 6 and (c) Station 10	83
Figure 3.32 Response of hourly water discharge to precipitation at (a) Station 5 (July 31 st – August 3 rd , 2007) and (b) Station 10 (August 15 th – August 17 th , 2007)	84
Figure 3.33 Plot of evapotranspiration, precipitation and discharge of (a) Stations 5 and (b) Station 7 in 2007	85
Figure 4.1 Schematic of the SLURP vertical water balance model (Kite, 1997)	94
Figure 4.2 Delineation of the Deer River Watershed through TOPAZ	100
Figure 4.3 River network of the Deer River Watershed generated by TOPAZ	101
Figure 4.4 Land Cover Classification of the Deer River Watershed by IDRISI [®]	103
Figure 4.5 Sensitivity analysis of the key parameters of SLURP	108
Figure 4.6 Simulated and observed daily hydrographs for the Deer River Watershed in 1978	112
Figure 4.7 Simulated and observed daily hydrographs for the Deer River Watershed in 1979	113
Figure 4.8 Simulated and observed daily hydrographs for the Deer River Watershed in 1980	114
Figure 4.9 Simulated and observed daily hydrographs for the Deer River Watershed in 1981	115
Figure 4.10 Simulated and observed daily hydrographs for the Deer River Watershed in 1982	116
Figure 4.11 Simulated and observed daily hydrographs for the Deer River Watershed in 1983	117
Figure 4.12 Simulated and observed daily hydrographs for the Deer River Watershed in 1984	118
Figure 4.13 Simulated and observed daily hydrographs for the Deer River Watershed in 1985	119
Figure 4.14 Simulated and observed daily hydrographs for the Deer River Watershed in 1986	120
Figure 4.15 Simulated and observed daily hydrographs for the Deer River Watershed in 1987	121
Figure 4.16 Simulated and observed monthly hydrographs for the Deer River Watershed from 1978 to 1987	122
Figure 4.17 Simulated and observed annual hydrographs for the Deer River Watershed from 1978 to 1987	123
Figure 4.18 Simulated and observed daily hydrographs for the Deer River Watershed in 1988	128
Figure 4.19 Simulated and observed daily hydrographs for the Deer River Watershed in 1989	129
Figure 4.20 Simulated and observed daily hydrographs for the Deer River Watershed in 1990	130
Figure 4.21 Simulated and observed daily hydrographs for the Deer River Watershed in 1991	131
Figure 4.22 Simulated and observed daily hydrographs for the Deer River Watershed in 1992	132
Figure 4.23 Simulated and observed daily hydrographs for the Deer River Watershed in 1993	133

Figure 4.24 Simulated and observed daily hydrographs for the Deer River Watershed in 1994	134
Figure 4.25 Simulated and observed daily hydrographs for the Deer River Watershed in 1995	135
Figure 4.26 Simulated and observed daily hydrographs for the Deer River Watershed in 1996	136
Figure 4.27 Simulated and observed daily hydrographs for the Deer River Watershed in 1997	137
Figure 4.28 Simulated and observed daily hydrographs for the Deer River Watershed in 1998	138
Figure 4.29 Simulated and observed daily hydrographs for the Deer River Watershed in 1999	139
Figure 4.30 Simulated and observed daily hydrographs for the Deer River Watershed in 2000	140
Figure 4.31 Simulated and observed daily hydrographs for the Deer River Watershed in 2001	141
Figure 4.32 Simulated and observed daily hydrographs for the Deer River Watershed in 2002	142
Figure 4.33 Simulated and observed daily hydrographs for the Deer River Watershed in 2003	143
Figure 4.34 Simulated and observed daily hydrographs for the Deer River Watershed in 2004	144
Figure 4.35 Simulated and observed monthly hydrographs for the Deer River Watershed from 1988 to 2004	145
Figure 4.36 Simulated and observed annual hydrographs for the Deer River Watershed from 1988 to 2004	146
Figure 4.37 Delineation of the Chesnaye Sub-basin by TOPAZ	151
Figure 4.38 River network of the Chesnaye Sub-basin by TOPAZ	152
Figure 4.39 Land cover classification of the Chesnaye Sub-basin by IDRISI®	153
Figure 4.40 Simulated and observed daily hydrographs by SLURP for Station 5 in 2006	154
Figure 4.41 Simulated and observed daily hydrographs by SLURP for Station 7 in 2006	155
Figure 4.42 Simulated and observed daily hydrographs by SLURP for Station 5 in 2007	156
Figure 4.43 Simulated and observed daily hydrographs by SLURP for Station 6 in 2007	157
Figure 4.44 Simulated and observed daily hydrographs by SLURP for Station 7 in 2007	158
Figure 4.45 Simulated and observed daily hydrographs by SLURP for Station 10 in 2007	159
Figure 4.46 Simulated and observed daily hydrographs by SLURP for Station 5 in 2008	160
Figure 4.47 Simulated and observed daily hydrographs by SLURP for Station 6 in 2008	161
Figure 4.48 Simulated and observed daily hydrographs by SLURP for Station 10 in 2008	162
Figure 5.1 Group Response Unit and runoff routing concept (Donald, 1992)	165
Figure 5.2 Schematic of the runoff generation algorithm in WATFLOOD	166
Figure 5.3 Boundary of the Deer River Watershed in EnsimHydrologic®	176
Figure 5.4 DEM of the Deer River Watershed in EnsimHydrologic®	177
Figure 5.5 Channel network of the Deer River Watershed in EnsimHydrologic®	178
Figure 5.6 Gridded cells of the Deer River Watershed in EnsimHydrologic®	179
Figure 5.7 Gridded cells, boundary, elevation and channel network of the Deer River Watershed in EnsimHydrologic®	180
Figure 5.8 Sensitivity analysis of the key parameters of WATFLOOD	184
Figure 5.9 Simulated and observed daily hydrographs for the Deer River Watershed in 1978	189
Figure 5.10 Simulated and observed daily hydrographs for the Deer River Watershed in 1979	190
Figure 5.11 Simulated and observed daily hydrographs for the Deer River Watershed in 1980	191
Figure 5.12 Simulated and observed daily hydrographs for the Deer River Watershed in 1981	192
Figure 5.13 Simulated and observed daily hydrographs for the Deer River Watershed in 1982	193
Figure 5.14 Simulated and observed daily hydrographs for the Deer River Watershed in 1983	194
Figure 5.15 Simulated and observed daily hydrographs for the Deer River Watershed in 1984	195
Figure 5.16 Simulated and observed daily hydrographs for the Deer River Watershed in 1985	196
Figure 5.17 Simulated and observed daily hydrographs for the Deer River Watershed in 1986	197
Figure 5.18 Simulated and observed daily hydrographs for the Deer River Watershed in 1987	198
Figure 5.19 Simulated and observed monthly hydrographs for the Deer River Watershed from 1978 to 1987	199
Figure 5.20 Simulated and observed annual hydrographs for the Deer River Watershed from	

1978 to 1987	200
Figure 5.21 Simulated and observed daily hydrographs for the Deer River Watershed in 1988	204
Figure 5.22 Simulated and observed daily hydrographs for the Deer River Watershed in 1989	205
Figure 5.23 Simulated and observed daily hydrographs for the Deer River Watershed in 1990	206
Figure 5.24 Simulated and observed daily hydrographs for the Deer River Watershed in 1991	207
Figure 5.25 Simulated and observed daily hydrographs for the Deer River Watershed in 1992	208
Figure 5.26 Simulated and observed daily hydrographs for the Deer River Watershed in 1993	209
Figure 5.27 Simulated and observed daily hydrographs for the Deer River Watershed in 1994	210
Figure 5.28 Simulated and observed daily hydrographs for the Deer River Watershed in 1995	211
Figure 5.29 Simulated and observed daily hydrographs for the Deer River Watershed in 1996	212
Figure 5.30 Simulated and observed daily hydrographs for the Deer River Watershed in 1997	213
Figure 5.31 Simulated and observed daily hydrographs for the Deer River Watershed in 1998	214
Figure 5.32 Simulated and observed daily hydrographs for the Deer River Watershed in 1999	215
Figure 5.33 Simulated and observed daily hydrographs for the Deer River Watershed in 2000	216
Figure 5.34 Simulated and observed daily hydrographs for the Deer River Watershed in 2001	217
Figure 5.35 Simulated and observed daily hydrographs for the Deer River Watershed in 2002	218
Figure 5.36 Simulated and observed daily hydrographs for the Deer River Watershed in 2003	219
Figure 5.37 Simulated and observed daily hydrographs for the Deer River Watershed in 2004	220
Figure 5.38 Simulated and observed monthly hydrographs for the Deer River Watershed from 1988 to 2004	221
Figure 5.39 Simulated and observed annual hydrographs for the Deer River Watershed from 1988 to 2004	222
Figure 5.40 Gridded cells, boundary, elevation and channel network of the Chesnaye Sub-basin in EnsimHydrologic®	226
Figure 5.41 Simulated and observed daily hydrographs by WATFLOOD for Station 5 in 2006	227
Figure 5.42 Simulated and observed daily hydrographs by WATFLOOD for Station 7 in 2006	228
Figure 5.43 Simulated and observed daily hydrographs by WATFLOOD for Station 5 in 2007	229
Figure 5.44 Simulated and observed daily hydrographs by WATFLOOD for Station 6 in 2007	230
Figure 5.45 Simulated and observed daily hydrographs by WATFLOOD for Station 7 in 2007	231
Figure 5.46 Simulated and observed daily hydrographs by WATFLOOD for Station 10 in 2007	232
Figure 5.47 Simulated and observed daily hydrographs by WATFLOOD for Station 5 in 2008	233
Figure 5.48 Simulated and observed daily hydrographs by WATFLOOD for Station 10 in 2008	234
Figure 6.1 Simulated and observed daily hydrographs for the Deer River Watershed in 1979	242
Figure 6.2 Simulated and observed daily hydrographs for the Deer River Watershed in 1992	243
Figure 6.3 Monthly evapotranspiration at D. River N. Belcher from 1978 to 1987	251
Figure 6.4 Monthly evapotranspiration at D. River N. Belcher from 1988 to 2004	252
Figure 6.5 (a) Simulated and observed daily hydrographs (b) daily evapotranspiration for Station 5 in 2006	253
Figure 6.6 (a) Simulated and observed daily hydrographs (b) daily evapotranspiration for Station 7 in 2007	254
Figure 6.7 Variation of Modelling efficiencies for SLURP and WATFLOOD in the Deer River Watershed from 1978 to 2004	263
Figure 6.8 Response of daily discharge to the precipitation by SLURP in 1997	264
Figure 6.9 Response of daily discharge to the precipitation by WATFLOOD in 1983	265

List of Tables

Table 2.1 List of some hydrological models and descriptions	16
Table 3.1 Coordinates of the gauging and weather stations and concerned ponds	30
Table 3.2 Summary of the monitoring years	37
Table 3.3 Summary of the field trips	38
Table 3.4 Standard deviation, mean and CV of P_{cum} and T_{avg} over a 31-year summertime period at the Churchill airport (June 20 th – October 3 rd , 1978-2008, Environment Canada)	46
Table 3.5 Variance of daily temperature, precipitation and evapotranspiration during the summertime at Rail Spur (June 20 th – October 3 rd , 2006 - 2008)	46
Table 3.6 Average summertime frost table at Stations 5, 6, 7 in 2006 (June 20 th –October 3 rd)	53
Table 3.7 Average frost table at Stations 5, 6, 7 and 10 in 2007 (June 20 th – October 3 rd)	54
Table 3.8 F-test of soil moisture contents at Stations 5, 6, 7 in 2006	67
Table 3.9 F-test of soil moisture contents at Stations 5, 6, 7 and 10 in 2007	67
Table 3.10 Statistical analysis between soil temperature and air temperature ($\alpha = 0.05$)	67
Table 4.1 Manning's roughness coefficient for different land covers (Parmley, 2000)	98
Table 4.2 Optimized criteria for the land cover classification	103
Table 4.3 Sensitivity analysis of SLURP parameters	107
Table 4.4 Final Values of the parameters for each land cover use for modelling the Deer River Watershed	111
Table 4.5 Modelling efficiencies during SLURP daily calibration in the Deer River Watershed	124
Table 4.6 Modelling efficiencies during SLURP calibration in the Deer River Watershed	124
Table 4.7 Modelling efficiencies during SLURP daily verification in the Deer River Watershed	147
Table 4.8 Modelling efficiencies during SLURP verification in the Deer River Watershed	147
Table 5.1 Sensitivity analysis of WATFLOOD parameters	185
Table 5.2 Final Values of the parameters for each land cover used for modelling the Deer River Watershed	188
Table 5.3 Modelling efficiencies during WATFLOOD daily calibration in the Deer River Watershed	201
Table 5.4 Modelling efficiencies during WATFLOOD calibration in the Deer River Watershed	201
Table 5.5 Modelling efficiencies during WATFLOOD daily verification in the Deer River Watershed	223
Table 5.6 Modelling efficiencies during WATFLOOD verification in the Deer River Watershed	223
Table A.1 Coordinate margins of each sub-basin of the Deer River Watershed	288
Table B.1 Modelling outputs from SLURP and WATFLOOD from 1978 to 2004	291

List of Abbreviations and Symbols

$[\delta T_p]$	Correction to T_p' in iteration process (dimensionless)
a	Surface albedo (dimensionless)
A'	Coefficient in SLURP interception calculation (dimensionless)
A_b	Area of the basin element (m^2)
A_{cs}	Main channel cross section area (m^2)
AET	Actual evapotranspiration rate (mm/h)
$AK2$	Intermediate zone resistance parameter (dimensionless)
alb	All-wave albedo for each land class (dimensionless)
$albe$	All-wave albedo in which the measurement is made (dimensionless)
a_o	Clear-sky albedo (dimensionless)
API	Antecedent Precipitation Index (dimensionless)
ASA	Aggregate Simulation Area
a_z	Regular zenith values of clear-sky albedo (dimensionless)
a_{zd}	Zenith value of dry-season snow-free clear-sky albedo (dimensionless)
a_{zz}	snow-free zenith values of clear-sky albedo (dimensionless)
B	Net long-wave radiation loss for soil-plant surfaces (mm eq./d)
B'	Coefficient in SLURP interception calculation (dimensionless)
b_0	Constant in Morton CRAE model (dimensionless)
b_1	Coefficient in WATFLOOD lake routing (dimensionless)
b_2	Coefficient in WATFLOOD lake routing (dimensionless)
b_3	Coefficient in WATFLOOD lake routing (dimensionless)
b_4	Coefficient in WATFLOOD lake routing (dimensionless)
b_5	Coefficient in WATFLOOD lake routing (dimensionless)
c_0	Constrained variable (dimensionless)
C_1	Constant in SLURP flow routing (dimensionless)
C_2	Constant in SLURP flow routing (dimensionless)
C_3	Constant in SLURP flow routing (dimensionless)
C_4	Constant in SLURP flow routing (dimensionless)
c_s	Kinetic wave speed (m/s)
C_t	Temperature reduction coefficient (dimensionless)
CV	Coefficients of variation (dimensionless)
D	Relative drying power (dimensionless)
$D1$	Depth of water on the soil surface (mm)
d_1	Constant in Morton CRAE model (W/m^2)

d_2	Constant in Morton CRAE model (dimensionless)
<i>Day_no</i>	Julian day of each year (dimensionless)
DEM	Digital Elevation Model
<i>digit</i>	Value from the satellite dataset (dimensionless)
d_{mj}	Distance from the location of station j to the point of m (km)
d_r	Inverse relative earth-sun distance (dimensionless)
d_r	Relative distance between the sun and the earth (dimensionless)
DRNG	Groundwater recharge (mm)
D_s	Depression storage (m^3)
DT	Switch of the daylight saving (dimensionless)
DUZ	Depth of upper zone storage released as interflow (mm)
DV	Deviation of runoff volume (dimensionless)
e^0	Mean saturated vapor pressure at mean daily air temperature (kPa)
e_a	Mean ambient vapor pressure (kPa)
E_A	Actual evapotranspiration (mm/day)
E_a	Drying power (mm eq./d)
e_a^*	Saturated vapour pressure at the air temperature (kPa)
e_a^0	saturated vapor pressure corresponding to air temperature (kPa)
E_{max}	Energy limited transpiration rate (mm)
E_p	Potential evapotranspiration (mm/day)
E_s	Soil limited transpiration rate (mm)
e_s^0	Saturated vapor pressure corresponding to soil surface temperature (kPa)
ET	Evapotranspiration
E_t	Actual transpiration rate (mm)
ET_0	Evapotranspiration (mm/day)
E_w	Wet-environment evaporation (mm/day)
F	Total depth of infiltrated water (mm)
FFCAP	Constant representing the field capacity (dimensionless)
<i>field</i>	Filed capacity as fraction (dimensionless)
FPET	Coefficient of IET (dimensionless)
FPET2	Second reduction coefficient (dimensionless)
FT	Frost table depth
f_T	Vapour coefficient ($W/mbar/m^2$)
FTALL	Forest vegetation coefficient (dimensionless)
f_u	Wind speed function
FULL	Theoretical depth soil pores are full of water (mm)

f_z	Constant in Morton CRAE model (W/mbar/m ²)
G	Incident global radiation (mm eq./d)
G_e	Relative evaporation (dimensionless)
G_E	Extra-atmospheric global radiation (mm eq./d)
GIS	Geological Information System
G_o	Clear-sky global radiation (mm eq./d)
GRU	Group Response Unit
G_s	Soil heat flux (mm eq./d)
G_{sc}	Solar constant (1,367 W/m ²)
H	Altitude (m)
H_a	Absolute pressure (psi)
h_{cha}	Height of water in channel (m)
H_s	Pressure at the water surface (psi)
h_u	Unit pressure change corresponding to unit depth (psi/m)
H_v	Average change in elevation over distance (m)
h_{wet}	Height of water in wetland (m)
I	Intercepted precipitation (mm)
I_1	Inflows at time 1 (m ³ /s)
I_2	Inflows at time 2 (m ³ /s)
IET	Interception evapotranspiration (mm/h)
Inf	Current infiltration rate (mm/day)
Inf_{max}	maximum infiltration rate (mm/day)
IZS	Intermediate zone storage (mm)
J	Julian day of the year (dimensionless)
j	Turbidity coefficient (dimensionless)
Jan_value	Snowmelt rate of each land cover on January 1 st (mm/day/°C)
$July_value$	Snowmelt rate of each land cover on July 1 st (mm/day/°C)
k	Coefficient of surface storage (dimensionless)
K	Hydraulic conductivity (mm/h)
k_1	Retention constant for fast store (day)
K_1	Storage constant (dimensionless)
k_2	Retention constant for slow store (day)
k_{cond}	Hydraulic conductivity (m/s)
K_n	Short wave radiation (MJ/m ² /h)
K_r	Recession constant (dimensionless)
k_v	Friction distance (dimensionless)

<i>L</i>	Distance to the stream (m)
<i>LAI</i>	Leaf Area Index
<i>LB</i>	Left Bank
<i>L_{loc}</i>	Local longitude west of Greenwich (degree)
<i>L_n</i>	Long-wave radiation (MJ/m ² /h)
<i>LST</i>	Local solar time (h)
<i>L_{std}</i>	Longitude of the standard meridian in the local time zone (degree)
<i>L_v</i>	Distance to the nearest channel (m)
<i>LZF</i>	Lower zone function constant (dimensionless)
<i>LZS</i>	Lower zone storage (mm)
<i>m</i>	Average moisture content (dimensionless)
<i>M</i>	Hourly snowmelt depth (mm/h)
<i>m₀</i>	Initial soil moisture content (dimensionless)
<i>max</i>	Maximum possible soil water contents (mm)
<i>MF</i>	Melting factor (mm/°C/h)
<i>n</i>	Manning's roughness coefficient (dimensionless)
<i>NDVI</i>	Normalized Difference Vegetation Index (dimensionless)
<i>NIR</i>	Near infrared pixel intensity (band 2) (dimensionless)
<i>n_s</i>	Number of stations (dimensionless)
<i>NSE</i>	Nash and Sutcliffe efficiency (dimensionless)
<i>O₁</i>	Outflow at time 1 (m ³ /s)
<i>O₂</i>	Outflow at time 2 (m ³ /s)
<i>Outflow</i>	Flow moving out of the lake (m ³ /s)
<i>P</i>	Total precipitation (mm)
<i>p</i>	Atmospheric temperature (°C)
<i>P_A</i>	Long-term average precipitation (mm)
<i>P_{cum}</i>	Cumulative summertime precipitation (mm)
<i>P_e</i>	Accumulated rainfall excess (mm)
<i>PET</i>	Potential evapotranspiration rate (mm/h)
<i>P_i</i>	Amount of precipitation in hour <i>i</i> (mm)
<i>Pot</i>	Capillary potential at the wetting front (mm)
<i>p_s</i>	Atmospheric pressure at sea level (kPa)
<i>PWP</i>	Permanent wilting point (mm)
<i>PWR</i>	Coefficient in the lower zone function (dimensionless)
<i>Q</i>	Entering discharge from upstream boundary (m ³ /s)
<i>q₀</i>	Unit-width reference discharge (m ³ /s)

Q_0	Daily observed flow (m^3/s)
$Q_{l,out}$	Outflow from rapid storage (m^3/s)
$Q_{average}$	Mean observed flow (m^3/s)
$q_{channel}$	Net income flows of the channel (m^3/s)
Q_{in}	Inflow (m^3/s)
q_{in}	Lateral flow (m^3/s)
q_{in}	Lateral flow contributing to the channel inflow (m^3/s)
q_{int}	Interflow (m^3/s)
q_l	Overland flow (m^3/s)
q_{loss}	Less evaporation (m^3/s)
q_{loss}	Evaporation loss (m^3/s)
q_{lz}	Base flow (m^3/s)
Q_m	Daily modeled flow (m^3/s)
Q_N	Net radiation (mm eq./d)
Q_n	Net radiation ($\text{MJ}/\text{m}^2/\text{day}$)
Q_{out}	Outflow (m^3/s)
$q_{O_{wet}}$	Lateral wetland outflow (m^3/s)
Q_r	Channel inflow (m^3/s)
q_{stream}	Precipitation falling on the stream (m^3/s)
q_{stream}	Sum of streamflow (m^3/s)
q_{swevp}	Evaporation loss off the wetland surface (m^3/s)
q_{swrain}	Flow contribution from the precipitation (m^3/s)
q_{wet}	Net income flows of the wetland (m^3/s)
R	Pixel intensity in the red visible range (band 1) (dimensionless)
R_1	Melt rate of SLURP ($\text{mm}/\text{day}/^\circ\text{C}$)
R_2	Restricted degree-day snowmelt rate ($\text{mm}/\text{day}/^\circ\text{C}$)
R_3	Combined channel roughness and length parameter (dimensionless)
R_a	Total incoming extraterrestrial solar radiation (mm)
RB	Right Bank
REC	Coefficient in WATFLOOD interflow calculation (dimensionless)
RETN	Retention constant (mm)
RG	Groundwater flow (mm/day)
RH	Relative humidity (dimensionless)
RI	Interflow (mm/day)
$RL\uparrow$	incident outgoing long wave radiation (W/m^2)
$RL\downarrow$	incident incoming long wave radiation (W/m^2)

R_n	Daily net radiation flux (MJ/m ² /day)
R_n	Net radiation (mm eq./d)
R_{ni}	Incident net radiation (W/m ²)
RP	Percolation (mm/day)
R_{si}	Incident incoming short wave radiation (W/m ²)
R_T	Net radiation for soil-plant surface at air temperature (mm eq./d)
R_v	Hydraulic radius (m)
s	Slope of the vapour pressure curve (kPa/°C)
S	Ratio of observed to maximum sunshine duration (dimensionless)
$s(T_d)$	Slope of the saturation-vapour pressure temperature curve (kPa/°C)
S_0	Channel bottom slope (dimensionless)
S_1	Current contents of the fast storage (mm)
$S_{1,max}$	Maximum capacity of the fast storage (mm)
S_2	Current contents of the slow storage (mm)
$S_{2,max}$	Maximum capacity of the slow storage (mm)
SAT	Soil saturation level (mm)
S_c	Correction factor for perturbation in earth's rotation rate (h)
S_d	Maximum value of depression storage (m ³)
S_i	Internal slope (dimensionless)
SM	Soil Moisture
S_m	Daily snowmelt rate (mm/day)
$SPORE$	Constant representing the saturation point (dimensionless)
S_s	Storage (m ³)
ST	Soil temperature
$Storage$	Storage of the lake (m ³ /s)
$store$	Current soil water contents (mm)
S_{water}	Water stage (m)
SWE	Snow Water Equivalent
T	Air temperature (°C)
t	Total infiltration time (hour)
T_a	Air temperature (°C)
T_{avg}	Mean summertime air temperature (°C)
$T_{avg,d}$	Mean temperature (°F)
T_{base}	Temperature at which snow starts to melt (°C)
$T_{critical}$	Melting temperature(°C)
T_D	Dew-point temperature (°C)

T_i	Incident near surface air temperature (K)
t_{loc}	Local civil time (0-24)
TOPAZ	TOpographic PArameteriZation
T_p	Potential evapotranspiration equilibrium temperature ($^{\circ}\text{C}$)
T_p'	Initial values for T_p ($^{\circ}\text{C}$)
T_s	Soil surface temperature ($^{\circ}\text{C}$)
U	Wind speed at 2 m above ground (m/s)
U_2	Wind speed at 2 m above ground (m/s)
USGS	U.S. Geological Survey
UZS	Upper zone storage (mm)
UZSI	Upper zone storage indicator (dimensionless)
V	Average velocity of the flow from land cover to the channel (m/s)
v	Saturation vapour pressures (kPa)
v_D	Saturation vapour pressures at T_D (kPa)
v_p	Saturation vapour pressure at T_p (kPa)
v_p'	Initial values for v_p (kPa)
w	Main channel width (m)
W	Precipitable water vapour (kPa)
$wilt$	Wilting point as fraction (dimensionless)
w_s	Sunset hour angle (radian)
X	Weighting constant (dimensionless)
Z	Noon regular zenith distance of sun (dimensionless)
z	Average angular zenith distance of sun (dimensionless)
Z_0	Aerodynamic roughness length for each land cover (dimensionless)
α	Priestley-Taylor coefficient (dimensionless)
α'	Constant in Morton CRAE model ($^{\circ}\text{C}$)
α_c	Conversion factor ($\text{mm}/\text{W}/\text{m}^2/\text{day}$)
α_l	Degrees of lag (degree)
β	Downward slope (dimensionless)
β'	Constant in Morton CRAE model ($^{\circ}\text{C}$)
β_a	Degrees of attenuation (degree)
β_s	Empirical coefficient (dimensionless)
β_s	Shape constant (dimensionless)
γ	Psychometric constant ($0.066 \text{ kPa}/^{\circ}\text{C}$)
γ	Deviation of the normal to the surface (dimensionless)
γp_s	Constant in Morton CRAE model ($\text{mbar}/^{\circ}\text{C}$)

Δ	Slope of saturated vapor pressure curve (kPa/°C)
δ	Solar declination (rad)
Δ_p	Slope of saturation vapour pressure curve at T_p (kPa/°C)
Δ_p'	Initial values for Δ_p (kPa/°C)
δ_t	Difference between the mean monthly max and min temperature (°F)
Δt	Time step (s)
Δx	Channel length (m)
ε_0	Surface emissivity (dimensionless)
ε_a	Atmospheric emissivity (dimensionless)
ζ	Stability factor (dimensionless)
η	Radius vector of sun (dimensionless)
θ	Solar incidence angle (rad)
θ_j	Observation at station j
θ_m	Objective unknown value at location m
λ	heat transfer coefficient (mbar/°C)
λ_v	Latent heat of vaporization (MJ/m ² /h)
ρ	Increase in atmospheric radiation due to clouds (dimensionless)
ρ_w	Mass density of water (kg/m ³)
σ	Stefan-Boltzman constant (5.67×10^{-8} W/m ² /K ⁴)
τ	Transmittance of clear sky to direct beam solar radiation (dimensionless)
τ_a	Part of τ that is the result of absorption (dimensionless)
τ_{sw}	Atmospheric transmissivity from elevation (dimensionless)
φ	Latitude (degree)
ω	Solar time angle (rad)

Chapter 1 Introduction

1.1 Background

Wetlands comprise 14% of the Canadian land and exist as bogs, fens, swamps, marshes and shallow water (Price and Waddington, 2000). Their considerable impact on water storage and distribution, water quality, carbon and nitrogen cycle, climate change and ecosystems has been noticed (Price *et al.*, 2005). To understand and clarify the hydrological characteristics of wetland systems is inevitable and crucial for the purposes of modeling the water cycle and predicting how the water cycle may vary in the next century. Recently, public recognition of their environmental significance has highlighted the need for in-depth understanding of hydrological processes in order to more efficiently conserve wetlands and assess climate related impacts especially in the northern regions (Rouse *et al.*, 1997; Woo and Young, 2003; Woo and Young, 2006; Ström and Christensen, 2007). Arctic and subarctic regions are sensitive to climatic conditions and occupying a crucial position of maintaining the integration of the global environment as well as the arctic communities. A recent report of the Arctic Climate Impact Assessment demonstrated that the temperature of arctic areas had been increasing sharply at twice of the average rate of other regions in the world; moreover, the precipitation had been increasing as well at a rate of 8% (Arctic Council and the International Arctic Science Committee, 2004).

Many previous studies targeting the subarctic wetlands/watersheds have been conducted

based on field investigations providing valuable data sources (Bello and Smith, 1990; Quinton and Roulet, 1998; Woo and Young, 2003). These investigations mainly aimed at the aspects of geological features, meteorological conditions, soil and vegetation, streamflow, etc. It was concluded that the sufficient water supplement, which comprises of snowmelt water, precipitation, local groundwater flow, streamflow and inundation from lakes, was the determinant factor of the existence of the wetlands (Winter and Woo, 1990; Woo and Young, 2006). Two distinguished flow mechanisms that occur in hummocky terrain and organic/mineral two layers system were reported (Woo and Marsh, 2005). Channel runoff from snowmelt and precipitation is primarily delayed by lakes in the vicinity and the particular permafrost (Quinton and Roulet, 1998; Leenders and Woo, 2002; Hayashi *et al.*, 2007). Soil features of the subarctic wetlands also influence the hydrologic processes because the porosity and hydraulic conductivity dramatically decline with depth (Quinton and Marsh, 1998; Carey and Woo, 1998; Carey and Woo, 1999; Woo and Marsh, 2005; Carey *et al.*, 2007). Recently, precipitation and temperature increase have attracted much attention which couples with change in magnitude of water supply, permafrost degradation, even complete drying (Waddington *et al.*, 1998; Payette *et al.*, 2001; Woo and Young, 2006). Temperature of the subarctic region, especially the Hudson Bay Lowlands was observed as steady increasing in the past several decades (Rouse *et al.*, 1997; Rouse, 1998; Eaton and Rouse, 2001).

Hydrological modelling plays important role along with field investigation in discovering the attributes of the subarctic wetlands. Traditionally, a large number of hydrological models have been developed and applied to simulate the watershed and/or wetland

systems (Quick and Pipes, 1977; Beven *et al.*, 1984; Abbott *et al.*, 1986; Bergström, 1992; Shah *et al.*, 1996a & 1996b; Bicknell *et al.*, 1997; Richard and Gratton, 2001; Cheng *et al.*, 2002; Moreda *et al.*, 2006; Xu *et al.*, 2006). Canadian researchers have made significant contributions to the field, especially through the development and application of the two semi-distributed hydrological models, SLURP and WATFLOOD. SLURP (Kite, 1975) was developed for the simulation of macro-scale basins and is famed for its unique concept of dividing the whole catchment into multiple aggregate simulation areas (ASA) to allow the prediction at both the outlet and interior points with distributed parameters (Haberlandt and Kite, 1998; Su *et al.*, 2000; Shin and Kim, 2007; St Laurent and Valeo, 2007; Armstrong and Martz, 2008; Brown *et al.*, 2008). WATFLOOD was developed at the University of Waterloo (Tao and Kouwen, 1989) under the concept of evenly dividing the watershed into group response units (GRU) and widely used for simulating watershed hydrology within Canada and beyond (Fassnacht *et al.*, 1999; Shaw *et al.*, 2005; Pirroniro *et al.*, 2006; Dibike and Coulibaly, 2007). However, there are only a few attempts to use these models to study subarctic wetlands (Mancell *et al.*, 2000; Zhang *et al.*, 2000; Linden and Woo, 2003; Boswell and Olyphant, 2007). There is still a gap between the acknowledged attributes and the actual hydrological characteristics of the subarctic wetlands, especially the water balance and how it interacts with climatic conditions, vegetation cover and permafrost zones. It has been suggested that one of the best ways of studying subarctic wetlands could be the integration of field investigation and hydrological modelling, which would require knowledge of the water cycle process both qualitatively and quantitatively. Such integrated studies are highly desired, especially in the need for more efficient wetland conservation and assessment of climate change

related impacts in the Canadian northern regions.

1.2 Objectives

This research attempts to help fill the existing knowledge gaps of the subarctic wetland hydrology, especially water flow and how it interacted with frost table and precipitation, as well as quantification of these hydrology parameters, by conducting an integrated study based on field investigation and model simulation in a typical wetland system in the Hudson Bay Lowlands, the Deer River watershed near Churchill, Manitoba. This objective entails the following major research tasks:

- 1) To conduct field surveys and collect meteorological and hydrological data in order to extract basic wetland characteristics in the Deer River watershed;
- 2) To apply two semi-distributed hydrological models, SLURP and WATFLOOD to the targeted wetland system to facilitate in-depth understanding of the wetland hydrology and justify the conclusions from the field investigation; and
- 3) To compare the two models from the aspects of modelling structure, formulation, parameters, and results based on the field observations and historic data for examining their capacity and feasibility in modeling subarctic wetlands.

Results from both field and modelling work will be advantageous in contributions from acknowledging the hydrological characteristics of subarctic wetlands. This research will represent a promising effort of characterizing and modelling the wetland hydrology which would benefit wetland conservation and climate change assessment and adaptation in the northern regions.

1.3 Organization

Chapter 2 reviews literatures regarding subarctic wetland hydrology from both field investigation and numerical modelling perspectives. Particularly, the previous studies by SLURP and WATFLOOD have been discussed in details to elicit the aim of this research. Chapter 3 presents a field survey in a subarctic wetland system in the Deer River watershed, Manitoba and discusses the hydrological characteristics including the variations of frost tables, soil moisture contents and streamflows, as well as the climatic and geographical conditions during the monitored seasons. Chapters 4 and 5 present the simulation mechanism of SLURP and WATFLOOD, respectively, along with simulation results at both the watershed and sub-basin scales. Discussions on modeling calibration, validation, and sensitivity analysis are also included. Chapter 6 compares SLURP and WATFLOOD from perspectives of modelling structure, formulations, parameters, and outputs and explores their capability and efficiency in modeling subarctic wetlands. The last chapter summarizes the major research findings and contributions, and also provides recommendations for the future work.

Chapter 2 Literature Review

2.1 Wetland Hydrology

Previous studies focusing on the northern regions have provided evidence in recognizing the hydrological process and the reflection of climate variation in subarctic wetlands. For example, Winter and Woo (1990) stated that adequate water source was the primary factor of the existence of subarctic wetlands. Quinton and Roulet (1998) demonstrated the relationship between flux and water storage of a subarctic wetland, and conceptualized the discharge response delay to precipitation which is attributed to large storage capacity of pools. Woo and Young (2006) also noted that reliable water supply which comprises of snowmelt water, localized ground water discharge, streamflow, and inundation by lakes and sea during the thawed season played a determinant role in wetland sustainability. Besides these, water flow within northern wetlands is highly sensitive to precipitation because of particular porous soil characteristic and shallow impermeable frost table. Leenders and Woo (2002) examined runoff from the subalpine willow-shrub zone, and conducted modelling to elicit that the ice content which impedes percolation had more notable effect on water flow rather than SWE (Snow Water Equivalent) or temperature. Woo and Marsh (2005) reviewed the frozen soil and permafrost hydrology in Canada from 1999 to 2002, showing two distinctive flow mechanisms of subarctic wetlands related to permafrost and frost table fluctuation. One is normal in hummocky terrain with inter-hummocky surface flow and subsurface lateral flow. The other commonly happens in the two-layer (organic and mineral) system where water could flow in particular pipes.

Hayashi *et al.* (2007) reported that subsurface flow was strongly dependent on frost table based on simulations of cycles in wetland systems.

Soil features of subarctic wetlands have been previously investigated by many studies and preliminary results indicate that organic soil, which comprises acrotelm and catotelm layers, is underlain by mineral soil which has negligible capability of water infiltration (Carey and Woo, 1999; Woo and Marsh, 2005). Quinton and Marsh (1998) stated that hydraulic conductivity declines with depth due to increasing humidification of peat and moreover, Carey and Woo (1998) found that discontinuity between organic and mineral layers led to the explicit vertically hydraulic reduction. Carey and Woo (2000) studied on subarctic slopes and concluded that pipeflow is ephemeral when water table is close to the surface and diminishes during summertime when water table is drawn downward. Carey *et al.* (2007) estimated hydraulic and pore characteristics of organic soil in the Wolf Creek Basin, Yukon, deduced that hydraulic conductivity and active layer porosity both decline with depth.

Climatic conditions have been addressed in much recent subarctic wetland research. Of significance is that temperature rise is coupled with precipitation increase (Waddington *et al.*, 1998; Payette *et al.*, 2001; Woo and Young, 2006). Basically, temperature rise is coupled with expected consequences which can be summarized as change in the magnitude of water supply and loss, permafrost degradation, and enhanced melt extent. Winter (2000) classified wetlands into mountainous, plateau and high plains, broad basin of interior drainage, riverine, flat coastal as well as hummocky glacial and dune landscapes

and reported that wetlands which depended on precipitation as water source were the most vulnerable to climate change. Rouse *et al.* (1997) examined historical records and reported a temperature increase of more than 1 °C in parts of the arctic and subarctic regions in North America during the last century. These regions are vulnerable to climate warming because it would probably lead to the completely drying of deltas and lakes. More interestingly, climate warming would alter the fundamental characteristics of permafrost and peatlands which might bring impacts on local ecosystems and water cycles. Another consequence is that the warmer and drier climate condition can convert the wetlands from a carbon sink to a source which will aggravate the global warming. Woo and Young (2006) emphasized that a continued warming trend would result in the elimination of lingering snowbanks and meltwater-fed wetlands in the high arctic region. Some numerical modelling studies also demonstrated the variation of subarctic climate. Rouse (1998) developed a water balance model and implemented it for northern Hudson Bay Lowlands to illustrate that annual precipitation would increase with temperature rise because of longer evaporation periods, excluding dry years with less precipitation and greater water deficit. Eaton and Rouse (2001) observed a similar tendency by analyzing recent 30 years meteorological data of northern Hudson Bay Lowlands and that the increase of precipitation is not as notable as temperature. Corell (2006) stated that arctic temperature had been increasing at approximately twice the rate of the rest of the world.

Although previous research has contributed much to the understanding of hydrological behaviour of subarctic wetlands, the relationship between hydrological functions and wetland's physical properties, such as soil properties, vegetation variation and the

characteristics of permafrost, is still lack of attention. One of the best ways of acquiring this information is the combination of field survey and hydrological modelling, which enables acknowledging the water cycle process both qualitatively and quantitatively.

2.2 Field Survey

Field survey is the most reliable information and data source of studying the subarctic wetland. Many studies targeting the subarctic and arctic regions were based on field investigation and have produced valuable data sources. Generally, the hydrological parameters which could be obtained through field surveys include: geological information (land use, elevation, slope, etc), meteorological data (temperature, precipitation, wind, radiation, etc), soil properties (temperature, moisture, porosity, ground heat flux, hydraulic conductivity, infiltration rate, etc), vegetation conditions (species, leaf area index, etc), streamflow (discharge, velocity, depth, etc) and others (frost table, water table, etc). If the study areas are inaccessible because of the harsh geological or weather conditions, recent geological information system (GIS) and information acquiring technologies, such as remote sensing and aerial photograph, could be used to gain necessary data.

Bello and Smith (1990) monitored the hourly summertime evaporation from a small tundra lake in the Hudson Bay Lowlands which filled the gap of field data regarding summer evaporation. Lakes in the northern regions, such as the Hudson Bay Lowlands, are very special because of their shallowness and likelihood of being ephemeral which

promotes thorough mixing and a uniform temperature distribution. In this research, field work started from a geological survey and concentrated on the terrain features of a selected lake. Depths of soil layers, permafrost table, net radiation, air temperature were measured. Local land cover conditions and statistical climate records of Churchill were obtained. Data analysis drew the conclusion that local advection is the major factor of the large fluxes of latent heat which exceeds the available radiant energy over the summer.

Quinton and Roulet (1998) examined the relationship between water discharge and storage within a typical subarctic patterned wetland in Quebec, Canada. Basic topographical conditions and vegetation species were measured or investigated. A 5-m meteorological tower was set in the study area and air temperature, relative humidity, net radiation as well as wind speed were measured. Rainfall volume, ground heat flux, hydraulic conductivity, snow water equivalent, daily snowmelt and water levels were monitored, respectively. Total basin discharge was measured and computed at the basin outlet through the flume and continuous stage readings. Based on the field survey data analysis, it was concluded that the discharge response of pattern wetlands is distinctive because the large storage capacity of the wetland pools intensively affects the runoff contributions. Woo and Young (2003) studied the hydrological features of patchy wetlands in high arctic regions to help fill the gap of related knowledge on polar desert environment. The study area was chosen at Resolute in Nunavut because it has an accessible high arctic environment. Geological information was obtained from literatures and field survey that the whole area was covered by weathered rocks and underlain by limestone. Water table was maintained relative high and measured by ten transects each

with perforated and screened pipes which extended to the outside region of the area. Frost table was measured twice weekly by pounding a steel bar into the ground until it reached the frozen layer. Outflow was monitored by placing a flume at each outlet with a water-level recorder which converted the stage data to discharge data. Field investigation supported the conclusion that saturated soil conditions together with insulating properties of the organic layer creates shallow frost table and relatively high water table in the summertime.

These studies supply some ideas about how to measure hydrological parameters in the sub-arctic region, including permafrost table, net radiation, air temperature, etc. GIS technology should be applied as an excellent reinforcement to the conventional measuring methods. In this thesis, field work was conducted during the summertime with an automated weather station deployed and frost table, soil moisture, soil temperature as well as streamflow monitored. Satellite images were also used to generate the river networks and land coverage of the study basin.

2.3 Hydrological Modelling

Hydrological modelling also plays a significant role in acknowledging the features of the subarctic wetlands. Numerous models have been developed to simulate watershed hydrology in general, such as HEC-1, PRMS (Precipitation-Runoff Modelling System), SSARR (Streamflow Synthesis and Reservoir Regulation), SRM (Snowmelt Runoff Model), UBC, and TOPMODEL (Table 2-1). Most of the models listed in Table 2-1 are

semi-distributed models which are based on the emergence of high spatial resolution data, the development of GIS technologies and the increasing functions of computers. They are defined as semi-distributed because some of the input parameters are not fully distributed and have to be simplified as lumped for each land cover type due to the accessibilities of data resource. On the other hand, lumped models have also been historically used under the concept that all of the parameters are spatially averaged together to create uniformity. Shah *et al.* (1996a & 1996b) applied both Système Hydrologique Européen (SHE) and a stochastic rainfall field model to the Upper Wye Catchment, Wales, UK. It was reported that there is interaction between antecedent conditions and spatial rainfall averaging which limited the performance of the lumped model. Xu *et al.* (2006) tested a monthly conceptual lumped water balance model, NOPEX-6, in the Mälaren basin Sweden for the purpose of clarifying the effects of precipitation data error on the model's performance. The results showed that the model was mainly influenced by the systematic error rather than the random error. Moreda *et al.* (2006) calibrated parameters for Continuous Antecedent Precipitation Index (CONT-API) model with the Nash-Sutcliffe Efficiency ranging from 69% to 78% in the Susquehanna River Basin. The primary advantage of the semi-distributed models is that they account for the spatial variability of the watershed with all the variables being represented and calibrated. They can provide greater amounts of spatially distributed information rather than simplified and lumped average values that never occur in the reality. Moreover, spatial resolution of the simulation and conceptualization of physical processes can be greatly improved and useful in the semi-distributed models when the model is coupled to other distributed models such as pollutant transport model. Nonetheless, new challenges still exist for semi-distributed

models, such as how to determine an appropriate resolution for both data availability and model performance, and how to estimate insufficient data.

Although many hydrological models have been developed and used, only a few models specifically target subarctic wetlands. In recent decades, interest in modelling subarctic wetland hydrology has been spurred by many research and management requirements. Weick and Rouse (1991a) reported the effects of advection which was from a cold polar sea to a warmer terrestrial land, on the energy balance of the Hudson Bay Lowlands. Field work was conducted in the summer of 1987 and was followed by a boxing model (Weick and Rouse, 1991b) which documented the divergence and convergence of the energy balance in a boundary layer. The results indicated that the Bowen ratio, under any wind direction, decreases away from the coast and the horizontal convergence and divergence are more obvious near the coast. Zhang *et al.* (2000) developed a process based, spatially distributed hydrological model ARHYTHM (ARctic HYdrological and THERmal Model) and applied it to Imnavait watershed in northern Alaska. This model is capable of determining the flow directions in each sub-catchment and the entire drainage network, as well as simulating various basic physical processes, including snow ablation, subsurface flow, overland flow and channel flow routing, soil thawing and evapotranspiration. Simulated results showed reasonable agreement with field measurement and satellite imagery except for the spring runoff which could be explained by not considering the effect of snow damming. It was also reported that spatially distributed modelling had promising applicability in the high latitude regions.

Based on a series of assumptions regarding net groundwater flow and radial symmetry, Mancell *et al.* (2000) applied WETLANDS, a multidimensional water flow model that dynamically links pond water, ground water and saturated soil layers, to simulate pond water and groundwater table in a cypress-pine flatwood forest (CPFF) wetland of the Santa Fe River in Florida. Comparison of observed and simulated results suggested that the hydrology of the CPFF wetland was dominated by the seasonal cumulative net water input (NMI). Elevations of both pond water and groundwater showed similar trends as the variation of NWI. Van der Linden and Woo (2003) attempted to seek a suitable level of hydrological models by using SLURP and LIARDFLOW model to simulate the runoff of the Liard River basin which is a representative subarctic region. It was reported that it is not always necessary to choose a complex model rather than a simple one because the runoff generation process may be sensitive to some processes. This conclusion was also supported by Michaud and Sorooshian (1994), and Refsgaard and Knudsen (1996). Boswell and Olyphant (2007) analyzed the hydrological characteristics of the Lake Station Wetland Restoration Site (LSWRS) within the extensive Great Marsh of Indiana by using a three dimensional, transient and variably-saturated groundwater model. Numerical simulations identified more rarely saturated zones which required hydrological remediation from regular ones. The results also revealed that topography, rainfall history and antecedent conditions played significant roles in the hydrology of restoration wetlands.

Although previous studies, limited modelling efforts focused on the typical sub-arctic wetlands in Canada, especially the Hudson Bay Lowlands in northern Manitoba, which is

the second largest wetland in Canada. To better preserve the wetland habitats and serve the local communities, there is still a gap between the acknowledged attributes and the actual hydrological characteristics of the subarctic wetlands, especially water flow and how it interacts with frost table and precipitation, as well as quantification of these hydrology parameters. For example, permafrost table is one of the most significant attributes of the subarctic wetlands because of its unique capability of inhibiting the water percolation and related consequences from its fluctuation. However, it has only been concerned in some of the studies and its spatial distribution in the spring peak and summertime is not well studied. In this thesis, to fill this gap, an extensive field investigation focusing on the hydrological features of the Deer River watershed near Churchill, Manitoba has been conducted from 2006 to 2007. Some important hydrological parameters which are not commonly studied in previous studies, such as frost table, soil moisture and temperature, were monitored through the 3-year summers. To quantitatively assess these features from the past three decades, two semi-distributed hydrological models, SLURP and WATFLOOD are used to simulate the water cycle of this typical subarctic wetland. These are two popular hydrological models that have been developed and widely used in Canada, even other places in the world because their structures allow the simulation to be conducted at the outlet and interior points of a basin. However, both of them have been rarely applied to Canadian subarctic wetlands, especially in Hudson Bay Lowlands in previous research. This thesis will help to fill the knowledge gap of how typical hydrological models would fit the situation in the sub-arctic wetlands and advance the development of specialized models for the those areas.

Table 2.1 List of some hydrological models and descriptions

Name	Description
AGNPS (Cho <i>et al.</i> , 2008)	AGNPS (AGricultural Non-Point Source) is a physically-based, distributed model which has been developed by the USDA (United States Department of Agriculture). It can simulate the runoff and soil erosion with curve number (CN) and Universal Soil Loss Equation (USLE).
ARNO (Todini, 1996)	ARNO was named by its first application to the Arno River. It is a semi-distributed conceptual model and in widespread use for both flood forecasting and atmosphere processes. The most important advantage of ARNO model appears at the spatial probability distribution of soil moisture capacity and varying contributing areas.
EPIC (Williams <i>et al.</i> , 1989)	ERIC (Erosion-Productivity Impact Calculator), as a comprehensive model which comprises of hydrological processes, weather prediction, nutrient flows, etc, can simulate the daily soil erosion status over hundreds of years and even interpret functional changes of the ecosystems.
HBV (Bergström, 1992)	HBV (Hydrologiska Byråns Vattenbalansmodell) is a widely used hydrological transport model which was initially developed in Scandinavia. It includes conceptual numerical computations or descriptions of meteorological interpolations, snow accumulation and melt, evapotranspiration, soil moisture, runoff generation and routing.
HEC-1 (Duru and Hjelmfelt, 1994)	HEC-1 model is originally from US Army Corp of Engineers. It can predict and control the runoff generation through surface roughness coefficient, initial moisture loss and constant rate of infiltration. Moreover, it contains a kinematic wave approach which could affect the model outputs.
HSPF (Bicknell <i>et al.</i> , 1997)	HSPF (Hydrological Simulation Program – Fortran) was completed by the USGS and U.S. EPA as a successor of the SWM (Stanford Watershed Model). This model is designed to assess and predict the land use scenario, reservoir operations, and even pollutants transportation because it has embedded water quality modules besides general hydrological processes. Multiple unit areas can be modelled for flexible time step between 1 minute and 1 day.
MODHYDROLOG (Chiew and McMahon, 1994)	MODHYDROLOG is a physically-based model that has been extensively applied in Australia for the purposes of simulating the runoff generation as well as evapotranspiration. This model could be repeatedly applied independently for multiple subareas within one catchment under spatially varied parameters.

MOHID Land (Galvão <i>et al.</i> , 2005)	MOHID Land was developed by the Technical University of Lisbon and integrated into the WMS (Water Modeling System)-MOHID. MOHID Land is capable of simulating water and sediment transport as well as water quality with a dynamic time stepping. Evapotranspiration is treated as a dynamic boundary condition.
PRMS (Cary, 1984)	PRMS (Precipitation-Runoff Modelling System) is another deterministic distributed model developed by the USGS. It can divide the watershed into homogeneous response units (HRU) or interconnected channel segments. Parameter optimization and sensitivity analysis ensures the model to compute the discharge from normal or extreme rainfall events based on daily time step.
SHE (Abbott <i>et al.</i> , 1986)	SHE (Système Hydrologique Européen, all called MIKE SHE) is a physically-based and spatially distributed hydrological model which has been widely used in Europe. Besides the basic function of simulating the water cycle from rainfall to channel discharge, adaptive modular enables SHE to handle solute transport, particle tracking as well as geochemical reactions.
SRM (Richard and Gratton, 2001)	SRM (Snowmelt Runoff Model) is a typical semi-distributed model and more applicable for high mountain regions. Runoff control parameters include runoff coefficients, which are functional at determining the water loss (e.g. evapotranspiration, infiltration), and recession coefficient which accounts for the immediate surface runoff.
SSARR (U.S. Army Corps of Engineers, 1987)	SSARR (Streamflow Synthesis and Reservoir Regulation) was developed and distributed by the North Pacific Division, U.S. Army Corps of Engineers. It is a deterministic conceptual model which contains a watershed model and a streamflow and reservoir regulation model. The watershed model comprises of two sub-models to synthesize the heatwater from rainfall and snowmelt. The routing method is "cascade of reservoirs" technique which concerns the lag and attenuation of flood wave.
SWM (Crawford and Linsley, 1966)	SWM (Stanford Watershed Model) was the first physically-based model that integrated all the concepts for basin chemistry hydrology on hourly time step. Unique and advanced features of this model could be summarized as the use of nominal soil moisture storage and its continuous varied water source, and cumulative frequency distributions for infiltration. SWMM and HSPF are all its successful successors.
SWMM (Park <i>et al.</i> , 2008)	SWMM (Storm Water Management Model), as a comprehensive mathematical model, was designed for modelling the quantity and quality of urban water cycle. The watershed is delineated into subcatchments based on the variety of hydrological attributes. Flow routing is computed by a combination of the continuity equation and Manning's equation.

<p>TOPMODEL (Beven <i>et al.</i>, 1984)</p>	<p>TOPMODEL is a physically-based, distributed watershed model which simulating the water cycle by predicting the movement of the water table. This model has been widely and extensively used because its code is available and it requires less parameter than regular models. A watershed could be divided into grids or sub-watersheds and the surface is defined as surface zone, saturated zone and root zone. However, this model is more accurate to moderate topography and grid size should be less than 50 m.</p>
<p>UBC (Quick and Pipes, 1977)</p>	<p>UBC model was initially developed for the prediction of Fraser River in British Columbia in Canada. Computation is based on sub-areas and initial outputs of each sub-area are used as inputs for the subsequent network flow model to generate the water budget of the whole basin. Elevation is an important parameter and related with temperature, precipitation, and channel flow characteristics.</p>
<p>XINANJIANG (Cheng <i>et al.</i>, 2002)</p>	<p>XINANJIANG rainfall-runoff model was developed in the 1970s in China and used as a soil moisture accounting model. Water budget and channel routing are two independent components during simulating and optimization. Calculations are based on delineated sub-areas and runoff is transformed into discharge by a linear system. This model has been widely used across China from humid areas to semi-humid areas.</p>

2.4 SLURP and WATFLOOD

SLURP (Kite, 1975) was developed for simulating and predicting hydrological features in macroscale basins. It has a concept of dividing the whole catchment into multiple aggregate simulation areas (ASA) and using a number of distributed parameters and data. To solve the problem of insufficient precipitation data in modelling macroscale basins, Haberlandt and Kite (1998) performed hydrological simulation using SLURP in the Mackenzie River Basin in the north-western Canada and discovered that better interpolation techniques and the use of combined precipitation data could improve the model results. Su *et al.* (2000) used SLURP to simulate hydrologic processes, especially water level variations over a 28-year period from 1969 in two different scale watersheds in Saskatchewan. It was illustrated that SLURP was able to predict water level variation accurately and was sensitive to the scale effect which is related to snow redistribution. St Laurent and Valeo (2007) improved the SLURP by adding a new subroutine of snowmelt and the results showed the additions in simulating the physical snowmelt when the air temperature exceeded 0 °C. Shin and Kim (2007) applied SLURP to assess snowmelt processes in the mountainous watersheds of South Korea under changing climatic conditions by using CCCma and CGCM2 models with SRES A2 and B2 scenarios. Validation results showed that the time of peak snowmelt runoff was advanced about one month in that mountainous region. Armstrong and Martz (2008) employed SLURP to study the impact of “generalizing” land cover conditions on the hydrological response at Wolf Creek and suggested that reducing the resolution of land cover generally has limited influence on the runoff simulation. Unlike traditional hydrological models which are

calibrated and validated at the basin outlet, Brown *et al.* (2008) analyzed MODIS imagery and compared SLURP outputs in terms of performance regarding the ability to simulate the snow cover change.

SLURP was chosen among other models because it divides watershed into sub-watersheds and has been widely used for macroscale areas. The sub-watershed concept allows runoff concentration to be calculated for each element maximally based on the topographical conditions. Each land cover within each sub-watershed has its own concentration time based on its mean distance to the channel, which precisely represents the natural process. Evapotranspiration can be computed from three options for various scenarios. The built-in calibration function allows most of the important parameters to be optimized automatically within predefined ranges. However, some hydrologic equations are simplified in SLURP as compared with WATFLOOD, such as infiltration and subsurface flow. Furthermore, it requires either datasets of net radiation, sunshine hours or global radiation to compute evapotranspiration, which may not be available and have to be estimated under some circumstances. These advantages and disadvantages could be justified in the modelling work of this thesis.

WATFLOOD was developed at the University of Waterloo (Tao and Kouwen, 1989) and has been updated continuously. It is a semi-distributed hydrological model which adopts the concept of dividing the watershed into segments and cells. Fassnacht *et al.* (1999) used WATFLOOD along with CLASS land surface scheme for simulation of the Grand River in Ontario, Canada. The results showed that the adjusted radar images produced

15% inaccuracy while corrected gauged precipitation yield 35% deviation from observed flow. This demonstrated that radar data are more applicable to the winter simulation than the corrected gauge data. Shaw *et al.* (2005) developed an expert system - WATPAZ which was an ArcInfo macro language interface between TOPAZ and WATFLOOD, and capable of extracting physiographic data from a Digital Elevation Model (DEM) to supply WATFLOOD. Its grouped response units allow a large drainage basin to be subdivided without compromising either computational efficiency or hydrological variability. Pirroniro *et al.* (2006) coupled a hydrodynamic model, ONE-D with WATFLOOD to evaluate how the climatic conditions would affect the flow regimes of three large lakes in Alberta, Canada. It was reported that the water level fluctuations were found to be more variable during the simulation. Moreover, spring snowmelt runoff was estimated to be earlier and reduced considerably. Dibike and Coulibaly (2007) applied two types of hydrological models, physically based distributed WATFLOOD and the lumped model HBV-96 to simulate the flow regimes of the Saguenay River in Quebec, Canada. It was summarized that both of the two models had limited efficiencies and different responses with downscaled temperature and precipitation data, whereas they performed well with historical data.

WATFLOOD was also selected because it is a typical semi-distributed model which subdivides the watershed into segments and adds a wetland routine and reservoir chain. The segments contain geological information and interface with modern radar meteorological data. Land cover information is also embedded into each unit and WATFLOOD has a distinguished wetland subroutine which is able to route and

re-distribute runoff within wetlands. Snow sublimation is also considered in the model to compensate the snowmelt. The model is used under DOS environment to speed up repetitive calculations. All of the inputs and outputs could be viewed and edited from Ensim Hydrological (Canadian Hydraulics Centre and Water Survey Canada, 2007), which is a hydrological software developed by Canadian Hydraulics Center. Nonetheless, some limitations include: the segment concept could mislead the flow direction at large scale; snowmelt process is a function of temperature and its rate is defined as a constant; the wetland subroutine requires many parameters of the wetland; the default time step is hourly which requires hourly input data and could introduce error when only daily data is available, etc. Results from the modeling work will advance the understanding of subarctic wetland hydrology, substantiate the application scope of both models, and also reveal the more appropriate scheme for modelling the subarctic wetlands that can support and benefit future model modification work.

Chapter 3 Characterization of Sub-arctic Wetland Systems – Field Investigation in the Deer River Watershed

3.1 Introduction

To fill the gap of understanding of subarctic hydrology associated with climatic conditions, especially water flow and how it interacts with frost table and precipitation, an extensive field investigation focusing on the hydrological features of the Deer River Watershed near Churchill, Manitoba was conducted during the summertime from 2006 to 2008. Data analysis indicates that the summertime air temperature and precipitation has been rising in the past decades. Frost table at stream banks have a reverse proportional relationship to their distances to the streams, and air temperature appears as the dominant factor influencing the fluctuation of the frost table in the summertime. Surface soil moisture becomes more saturated closer to the stream whereas soil moisture at deep layers are significantly influenced by evapotranspiration and dramatically fluctuate throughout the summer. The monitoring streams show a delayed response to precipitation due to the combined effects from the shallow impermeable frost table, porous soil characteristics, and varied storage capacity of organic layers. Such findings presented by this research will be helpful for understanding the water cycle in subarctic wetlands, advancing the understanding of subarctic wetland hydrology, and benefit the hydrology modelling work of the Deer River Watershed.

3.2 The Study Area

The Deer River Watershed is located in the northern part of the Hudson Bay Lowlands (Figure 3.1). Specifically, as shown in Figure 3.2, it lies in between latitudes 57°25'N to 58°25'N and longitudes 94°3'W to 95°16'W. The watershed occupies approximately 5,000 km² and mainly consists of tundra and boreal coniferous forest. The elevation gradually descends from 232 m in southwest to 16 m in northeast. The watershed features the typical subarctic hummock surface and permafrost table.

The Deer River Watershed is a broad polygonized peat plateau which consists of high and low centered polygons (Dredge and Nixon, 1979). The vegetation is predominantly lichen-heath, in which lichen occupies between 67 to 83% of the whole plain (Bello and Smith, 1990). Specifically, Eaton and Rouse (2001) described the other vascular species which can be found in sedge fen near Churchill, including water sedge, northern bog sedge, mud sedge, scrub birch, trailing willow, deer grass, and purple saxifrage. It was also noted that a thin layer of moss presents in almost 15% of the total area. Soil characteristics of the Deer River Watershed has also been studied and addressed by previous research. For example, Reeve *et al.* (2000) collected data from Hudson Bay Lowlands and showed hydraulic conductivity drops from 4.2×10^{-6} m/s at a depth of 1 m to 1.5×10^{-6} m/s at a depth of 2 m. Wessel and Rouse (1994) stated that volumetric water content of peat soil and hummock is capable of reaching at 80 to 90% and 50 to 60%, respectively. To further understand and characterize the meteorological conditions and hydrological features of the Deer River Watershed, a monitoring network composed of 10

gauging stations and 2 automated weather stations was established with the support from Manitoba Hydro, ArcticNet, University of Manitoba and Churchill Northern Studies Center (Figure 3.4b). Their coordinates are listed in Table 3.1.

In order to well understand the wetland hydrology and the interactions between climate and water cycle, the Deer River Watershed was delineated from a 3 arc second DEM, which was obtained from the National Map Seamless Server of the U.S. Geological Survey (USGS, 2007), by River Tools[®]. A small representative sub-basin, the Chesnaye Sub-basin, in the downstream of the Deer River was selected as the study area to conduct a demonstration field investigation for intensive monitoring work. Figure 3.3 shows the delineated sub-basins and the Chesnaye Sub-basin. All the coordinates of the sub-basins are listed in Appendix A.

The Chesnaye Sub-basin contains 4 stream gauging stations and 1 automated weather station as shown in Figure 3.4a. As part of downstream region of the Deer River Watershed, it is located approximately 70 km south of Churchill, Manitoba, Canada. The Chesnaye Sub-basin is extremely flat with elevations varying slightly around 52 m. It has the typical hummocky terrain with two main streams flow into the Deer River. The vegetation cover is mainly tundra and shrub with little coniferous forest along the streams. Many disconnected lakes and ponds stretch over the basin. A Canada VIA railway goes through the basin from north to south which enables the field investigation run smoothly.

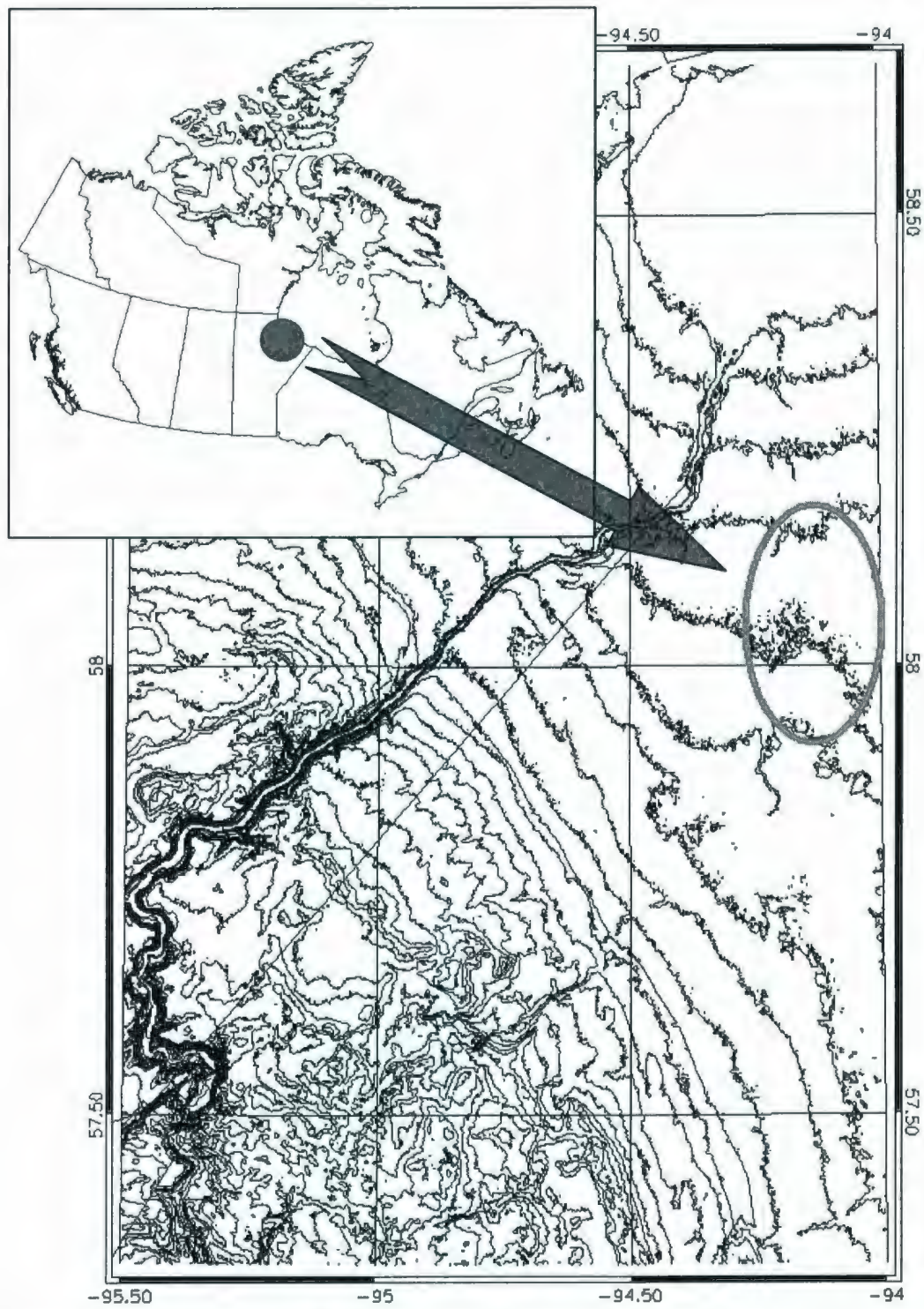


Figure 3.1 Contour map of the Deer River Watershed and the Chesnaye Sub-basin from

River Tools®

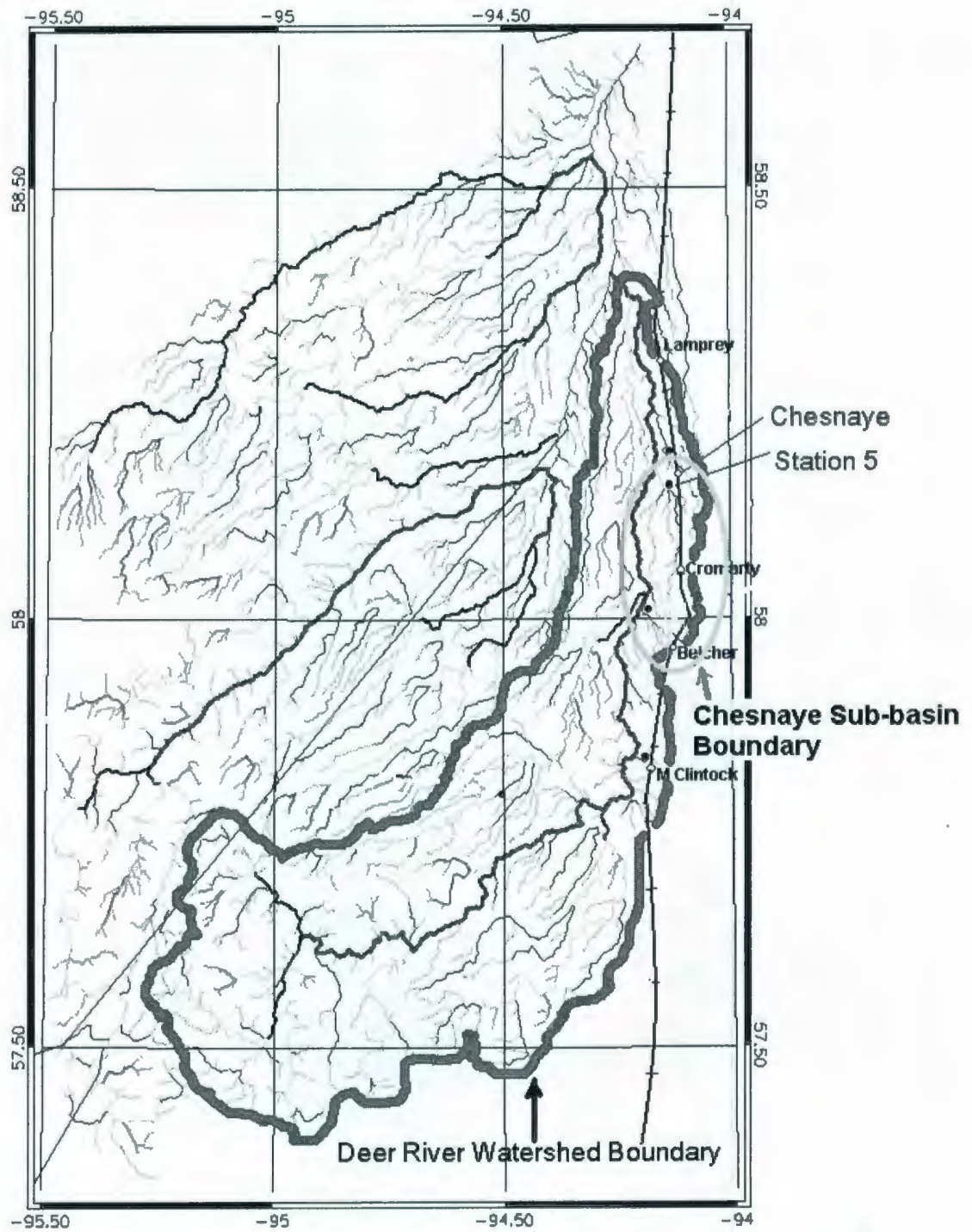


Figure 3.2 Drainage map of the Deer River Watershed from River Tools®

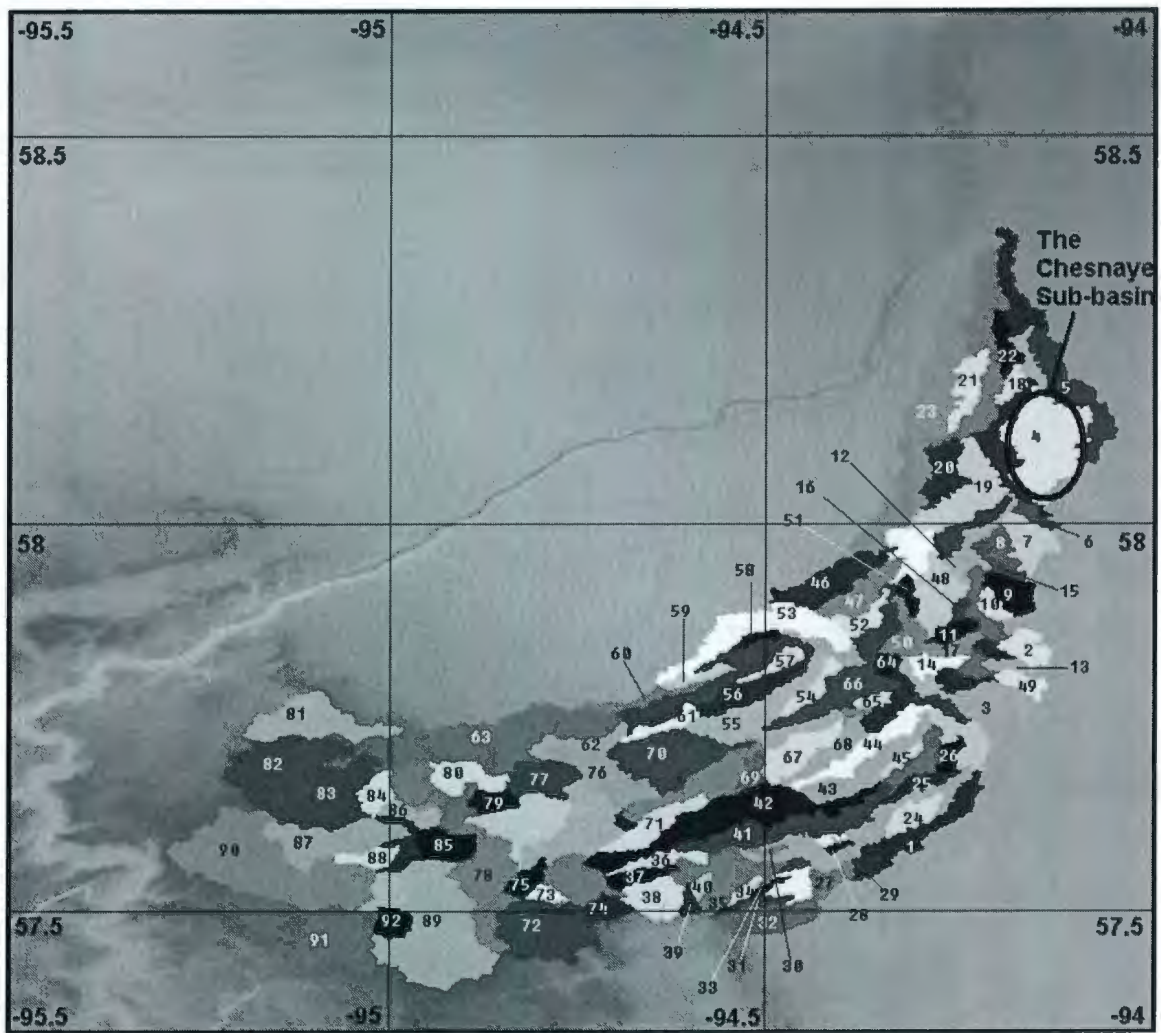


Figure 3.3 Delineation of the Deer River Watershed from River Tools[®]

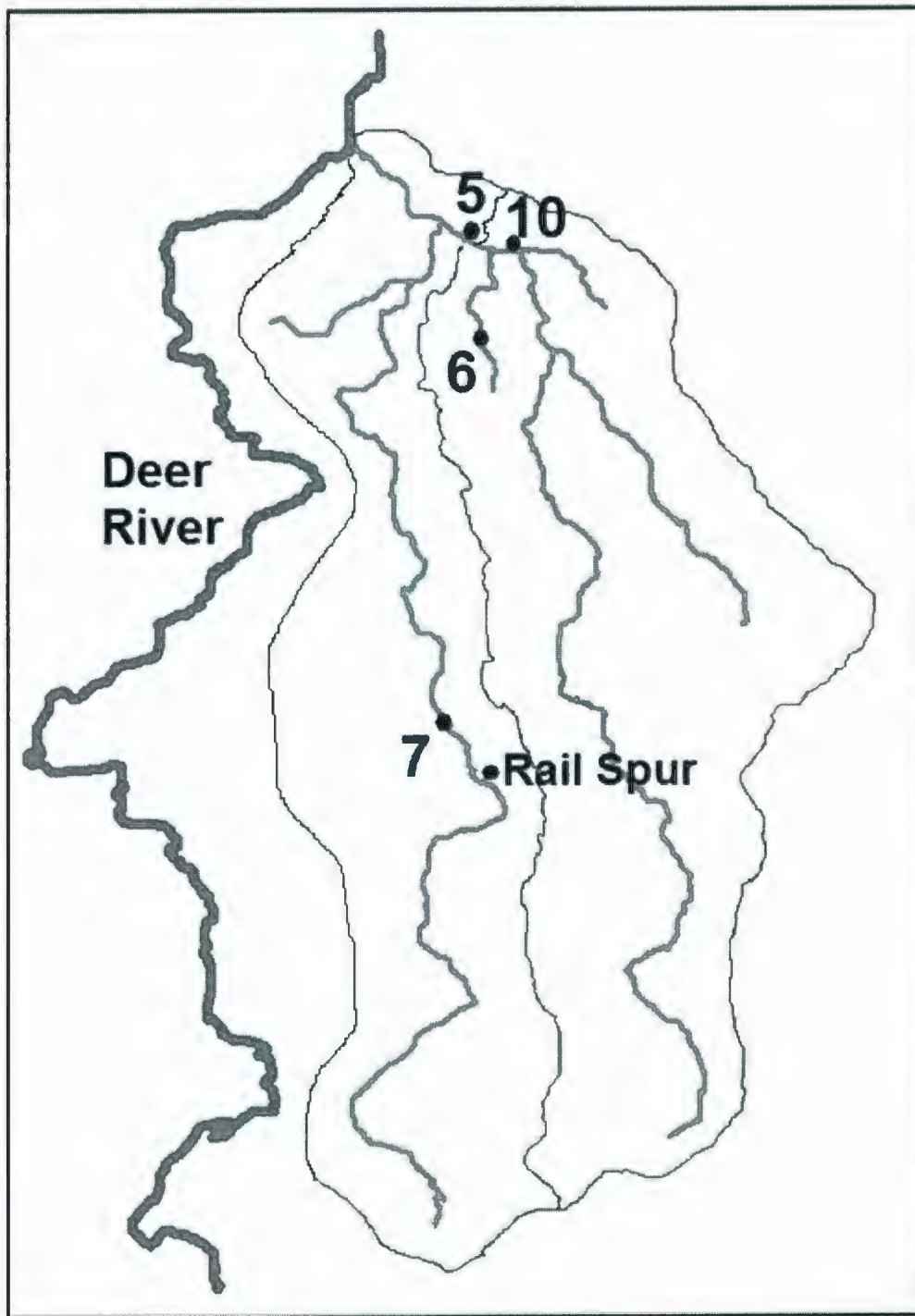


Figure 3.4a Locations of the stream gauging stations (5, 6, 7, 10) and automated weather station (Rail Spur) in the Chesnaye Sub-basin

Table 3.1 Coordinates of the gauging and weather stations and concerned ponds

Station name	Coordinates	
Station 1 (Hydro)	58°00'54.00"N	94°11'44.00"W
Station 2 (M.Clintock, Hydro)	57°47'51.35"N	94°12'53.59"W
Station 3 (Goose Creek)	58°34'02.00"N	93°59'55.00"W
Station 4 (Goose Creek)	58°33'02.00"N	94° 5'16.00"W
Station 5 (Chesnaye)	58°12'42.48"N	94° 8'56.33"W
Station 6 (Chesnaye)	58°11'46.91"N	94° 8'28.12"W
Station 7 (Rail Spur)	58°08'53.21"N	94° 8'34.84"W
Station 8	58°15'30.83"N	94° 9'59.76"W
Station 9 (Hydro)	57°47'54.00"N	94°30'7.00"W
Station 10 (Chesnaye)	58°12'19.56"N	94° 8'35.46"W
Pond 1	58°11'03.83"N	94° 8'46.44"W
Pond 2	58°10'52.05"N	94° 8'23.49"W
Weather Station 1	57°50'21.00"N	94°12'20.00"W
Weather Station 2 (Rail Spur)	58°09'38.00"N	94° 8'35.00"W



Figure 3.4b Locations of gauging and weather stations in the Deer River Watershed (After Google Earth®)

3.3 Field Investigation

Hydrological parameters were obtained at four stations (Stations 5, 6, 7 and 10) during the summertime from 2006 to 2008 within the Chesnaye Sub-basin as shown in Figure 3.4a. The detailed field investigation methods are provided by Jing and Chen (2007). In this research, the following datasets have been acquired through the fieldwork and from other related sources:

3.3.1 Datasets

A. Hourly meteorological data which includes air temperature, dew temperature, cumulative precipitation, incident short wave radiation, relative humidity, wind speed and direction, soil temperature and soil moisture was obtained from the local automated weather station at Rail Spur. Evapotranspiration was computed by Penman-Monteith Equation. Historical meteorological data (June 20th – October 3rd, 1978-2008) was obtained from Environment Canada at the Churchill airport.

B. Stream gauging data from those 4 stations, which includes water level (HOBO[®] pressure transducer, 2-4 minutes interval), flow velocity and discharge (Sontek[®] ADV Flowtracker, 2 weeks interval) and water sampling (2 weeks interval).

C. Frost table depth and surface soil moisture at multiple transects (2m, 4m, 6m and 8m) of both banks of each station (2 weeks interval); Estimation of vegetation coverage.

D. Besides regular field investigation of the Chesnaye Sub-basin, helicopter recon was conducted on June 20th, 2007. From the observation in flight and sampling work at upstream locations, significantly different vegetation coverage, topographic and hydrological conditions were identified. For example, the forest occupies approximately 70% of the land area and the remaining is mainly covered by shrubs at upstream of the basin. As a comparison, at Station 5, the land coverage of forest, shrubs and tundra are around 10%, 20% and 70%, respectively. Figure 3.5 shows the helicopter recon route and Figures 3.6a, 3.6b and 3.6c display the downstream, midstream and upstream land coverage.

3.3.2 Calculations

Water stage was automatically recorded by HOBO[®] pressure transducers installed at the stream bottom of each station. Based on pre-calibration, absolute pressure values stored in the transducer could be converted to relative pressure from the water surface to the bottom. Absolute water depth could be calculated by:

$$S_{water} = \frac{H_a - H_s}{h_u} \quad (3-1)$$

where S_{water} is the water stage (m); H_a is the absolute pressure (psi); H_s is the pressure at the water surface (psi); and h_u stands for the unit pressure change corresponding to unit depth (psi/m). Flow velocity was measured by SonTek[®] ADV Flow Tracker at multiple points for each station and discharge could be automatically calculated. Then the relationship between stage and discharge can be regressed from the days when discharge

was measured, in order to estimate continuous real-time discharge in the whole summer.

Frost table was monitored by pounding steel bar which has a maximum detection of 1.5 m. Soil moisture was measured by using detection probe at 5 cm depth and vegetation cover was observed and estimated.

Meteorological parameters were derived from automated weather station (AWS) located at Mile Marker 467, Rail Spur (58° 09' 38"N, 94° 08' 35.4"W). Basic surface meteorology (air temperature and pressure, precipitation, relative humidity and wind speed), incident incoming short wave radiation, soil temperature (at 0, 5, 10, 25, 50, and 75cm depth) and soil moisture (at 5 and 25 cm depth) were hourly sampled and recorded on Campbell Scientific CR-1000 data logger. Daily evapotranspiration was determined using FAO-56 Penman-Monteith Equation. This method is appropriate for a well watered grass crop and is not recommended for quantitative analysis (Allen *et al.*, 1998):

$$ET_0 = \frac{0.408\Delta(R_n - G_s) + \gamma \frac{900}{T + 273} U_2 (e^0 - e_a)}{\Delta + \gamma(1 + 0.34U_2)} \quad (3-2)$$

where ET_0 is evapotranspiration (mm/day); R_n is daily net radiation flux (MJ/m²/day); G_s is sensible heat flux into soil (MJ/m²/day); γ is psychometric constant (0.066 kPa/°C); T is air temperature (°C); U_2 is wind speed at 2 m above ground (m/s); e^0 is mean saturated vapor pressure at mean daily air temperature (kPa); e_a is mean ambient vapor pressure (kPa); and Δ stands for the slope of saturated vapor pressure curve (kPa/°C).

$$e_a = e^0 \times RH \quad (3-3)$$

where RH is the relative humidity

$$\Delta = \frac{e_s^0 - e_a^0}{T_s - T_a} \quad (3-4)$$

where e_s^0 and e_a^0 stand for saturated vapor pressure (kPa) corresponding to soil surface temperature T_s (derived from Rail Spur Station) and air temperature T_a ($^{\circ}\text{C}$), respectively; and R_n could be obtained by converting the incident net radiation as shown in the following equation:

$$R_n = \left(\frac{\sum_{i=1}^{24} R_{ni}}{24} \times 3600 \times 24 \right) / 10^6 \quad (3-5)$$

where R_{ni} is the incident net radiation (W/m^2); R_{si} is the incident incoming short wave radiation (W/m^2) and derived from the automated weather station at Rail Spur. R_{si} can also be computed as (Bastiaanssen, 1995; Samani *et al.*, 2007):

$$R_{ni} = (1-a)R_{si} + RL \downarrow - RL \uparrow - (1-\varepsilon_0)RL \downarrow \quad (3-6)$$

where a is the surface albedo (dimensionless); $RL \downarrow$ and $RL \uparrow$ are the incident incoming and outgoing long wave radiation (W/m^2); and ε_0 stands for the surface emissivity (dimensionless). The following equation should be used if instant short-wave radiation is not available:

$$R_{si} = G_{sc} \cos \theta d_r \tau_{sw} \quad (3-7)$$

where G_{sc} represents the solar constant ($1,367 \text{ W}/\text{m}^2$); d_r is the inverse relative earth-sun distance (Allen *et al.*, 1998), calculated as:

$$d_r = 1 + 0.033 \cos\left(\frac{2\pi}{365} J\right) \quad (3-8)$$

where J is the Julian day of the year. τ_{sw} is the atmospheric transmissivity from elevation

(Z) (Allen *et al.*, 1998) and computed by:

$$\tau_{sw} = 0.75 + 2 \times 10^{-5} (Z) \quad (3-9)$$

θ is the solar incidence angle (rad) which can be expressed as:

$$\begin{aligned} \cos(\theta) = & \sin(\delta) \sin(\phi) \cos(\beta) - \sin(\delta) \cos(\phi) \sin(\beta) \cos(\gamma) \\ & + \cos(\delta) \cos(\phi) \cos(\beta) \cos(\omega) \\ & + \cos(\delta) \sin(\phi) \sin(\beta) \cos(\gamma) \cos(\omega) \\ & + \cos(\delta) \sin(\beta) \sin(\gamma) \sin(\omega) \end{aligned} \quad (3-10)$$

where δ is the solar declination (rad) and calculated from (Allen *et al.*, 1998):

$$\delta = 0.409 \sin\left(\frac{2\pi}{365} J - 1.39\right) \quad (3-11)$$

ϕ stands for the latitude and defined as 58.2° in this research; β is the downward slope and marked as 0.002 for the study area; γ is the deviation of the normal to the surface from the local meridian and given 0.605 for the study area; and ω is the solar time angle (rad) which could be calculated from the following equations:

$$\omega = \frac{\pi}{12} (LST - 12) \quad (3-12)$$

$$LST = t_{loc} + 0.06667(L_{std} - L_{loc}) + S_c - DT \quad (3-13)$$

$$S_c = 0.1645 \sin(2b) - 0.1255 \cos(b) - 0.025 \sin(b) \quad (3-14)$$

$$b = \frac{2\pi(J - 81)}{364} \quad (3-15)$$

where LST is the local solar time (h); t_{loc} is the local civil time (0-24); L_{std} and L_{loc} are the longitude of the standard meridian in the local time zone and the local longitude west of Greenwich (degree), respectively; L_{std} and L_{loc} are defined as 90° and 94° based on the geological location of the Hudson Bay; DT is the switch of the daylight saving and

chosen as 0; and S_c is the correction factor for perturbation in earth's rotation rate (h). $RL\downarrow$ and $RL\uparrow$ are calculated from the following equations:

$$RL\downarrow = \varepsilon_a \sigma T_i^4 \quad (3-16)$$

$$\varepsilon_a = 0.85(-\ln\tau_{sw})^{0.09} \quad (3-17)$$

$$RL\uparrow = \varepsilon_0 \sigma T_s^4 \quad (3-18)$$

$$\begin{aligned} \varepsilon_0 &= 0.95 + 0.01 \times LAI & LAI < 3 \\ \varepsilon_0 &= 0.98 & LAI \geq 3 \end{aligned} \quad (3-19)$$

where ε_a stands for atmospheric emissivity; σ is the Stefan-Boltzman constant (5.67×10^{-8} W/m²/K⁴); T_i and T_s are the incident near surface air temperature and surface temperature (K), respectively; ε_0 stands for the surface emissivity which is assumed as 0.96 for the whole study area (dimensionless); and LAI is the Leaf Area Index (dimensionless).

3.3.3 Field Work Summary

Field work in the summertime of 2006 was conducted by Dr. Kathy Young and her research team from York University. Our research team from Memorial University worked collaboratively with University of Manitoba, York University and the Churchill Northern Studies Center to accomplish the field work in the summer of 2007 and 2008. Detailed study years and trips information are listed in Tables 3.2 and 3.3, respectively.

Table 3.2 Summary of the monitoring years

Year	Meteorological data	Frost table	Soil moisture	Stream discharge
2006	√	√	√	√
2007	√	√	√	√
2008	√	-	√	√

Table 3.3 Summary of the field trips

Trip #.	Time	Visiting Stations	Team member
1	06/20/2006	Stations 5, 6	Dr. Kathy Young, Peter Graham, Hossein Zahedi
2	06/25/2006	Stations 5, 6, 7	Dr. Kathy Young, Peter Graham, Hossein Zahedi
3	06/28/2006	Stations 5, 6	Dr. Kathy Young, Peter Graham, Hossein Zahedi
4	07/01/2006	Stations 5, 6	Dr. Kathy Young, Peter Graham, Hossein Zahedi
5	07/10/2006	Stations 5, 6, 7	Dr. Kathy Young, Peter Graham, Hossein Zahedi
6	07/16/2006	Stations 5, 6, 7	Dr. Kathy Young, Peter Graham, Hossein Zahedi
7	07/24/2006	Stations 5, 6, 7	Dr. Kathy Young, Peter Graham, Hossein Zahedi
8	08/21/2006	Stations 5, 6, 7	Dr. Kathy Young, Peter Graham, Hossein Zahedi
9	06/20/2007	Stations 5 and 10	Dr. Bing Chen, Liang Jing, Robert Whitten
10	06/29/2007	Stations 5, 6 and 10	Liang Jing, Robert Whitten, Katie LapenSkie
11	07/11/2007	Stations 5, 6 and 10	Robert Whitten, Mike Coffey, Katie Lapenskie
12	07/27/2007	Station 7	Robert Whitten, Mike Coffey, Katie Lapenskie
13	08/08/2007	Stations 5, 6 and 10	Robert Whitten, Mike Coffey, Katie Lapenskie
14	08/17/2007	Station 7	Robert Whitten, Mike Coffey, Katie Lapenskie
15	08/22/2007	Stations 5, 6 and 10	Robert Whitten, Mike Coffey, Katie Lapenskie
16	08/29/2007	Stations 5 and 7	Dr. Ken Snelgrove, Mike Coffey, Sandy Liu
17	09/26/2007	Stations 5, 6 and 7	Liang Jing, Robert Whitten, Bing Han
18	10/03/2007	Stations 5, 6 and 10	Liang Jing, Robert Whitten, Phil Greenwood
19	07/13/2008	Stations 5, 6 and 10	Liang Jing, Kyle Swystun
20	10/16/2008	Stations 5, 6 and 10	LeeAnn Fishback, Carley Basler, Jackie Dunn, Adam Brisson



Figure 3.5 Route of the helicopter recon (photo by Liang Jing)

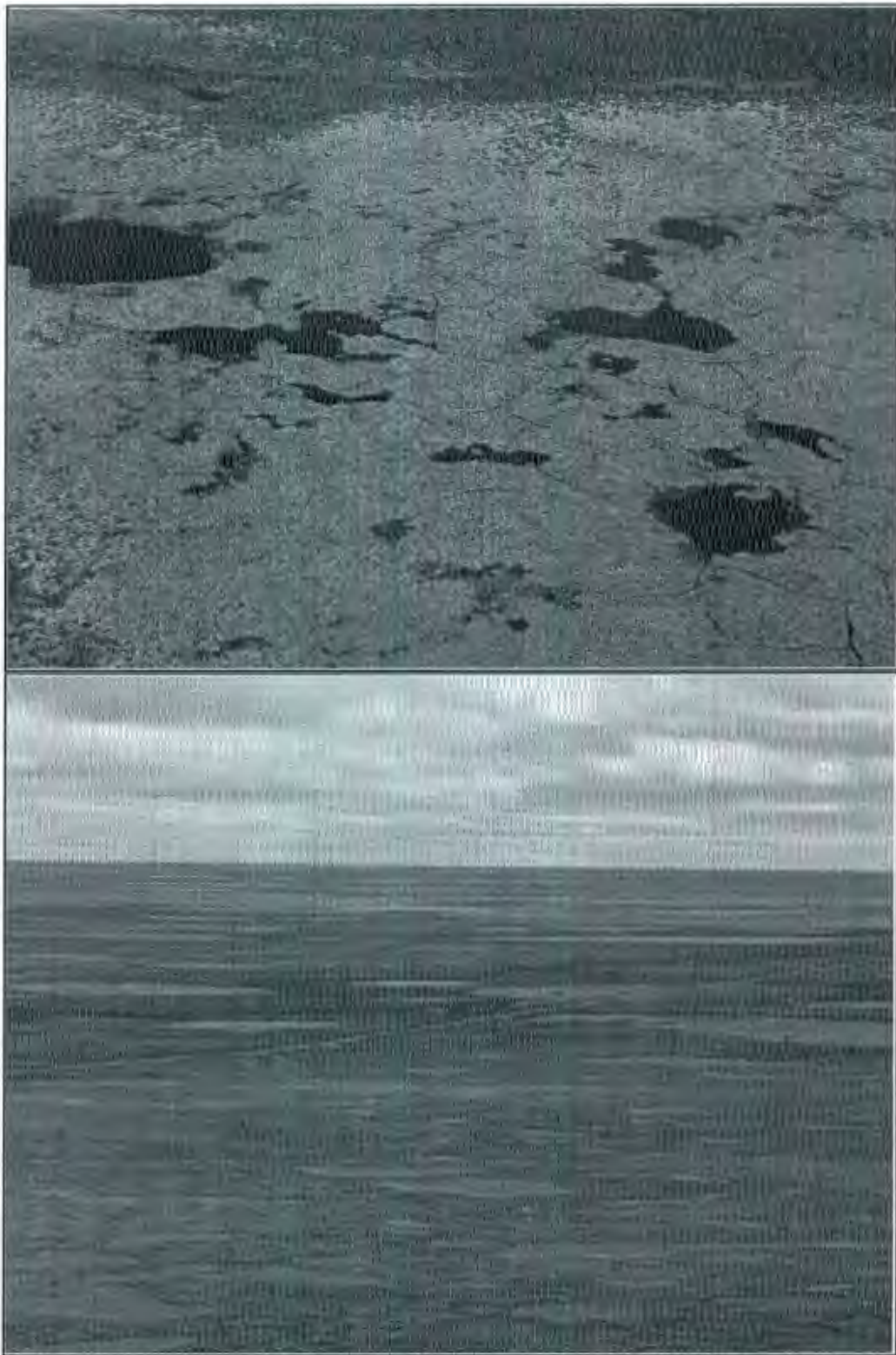


Figure 3.6a Land coverage of downstream regions in the Deer River watershed (photo by Liang Jing)



Figure 3.6b Land coverage of midstream regions in the Deer River watershed (photo by Liang Jing)



Figure 3.6c Land coverage of upstream regions in the Deer River watershed (photo by Liang Jing)

3.4 Results and Discussion

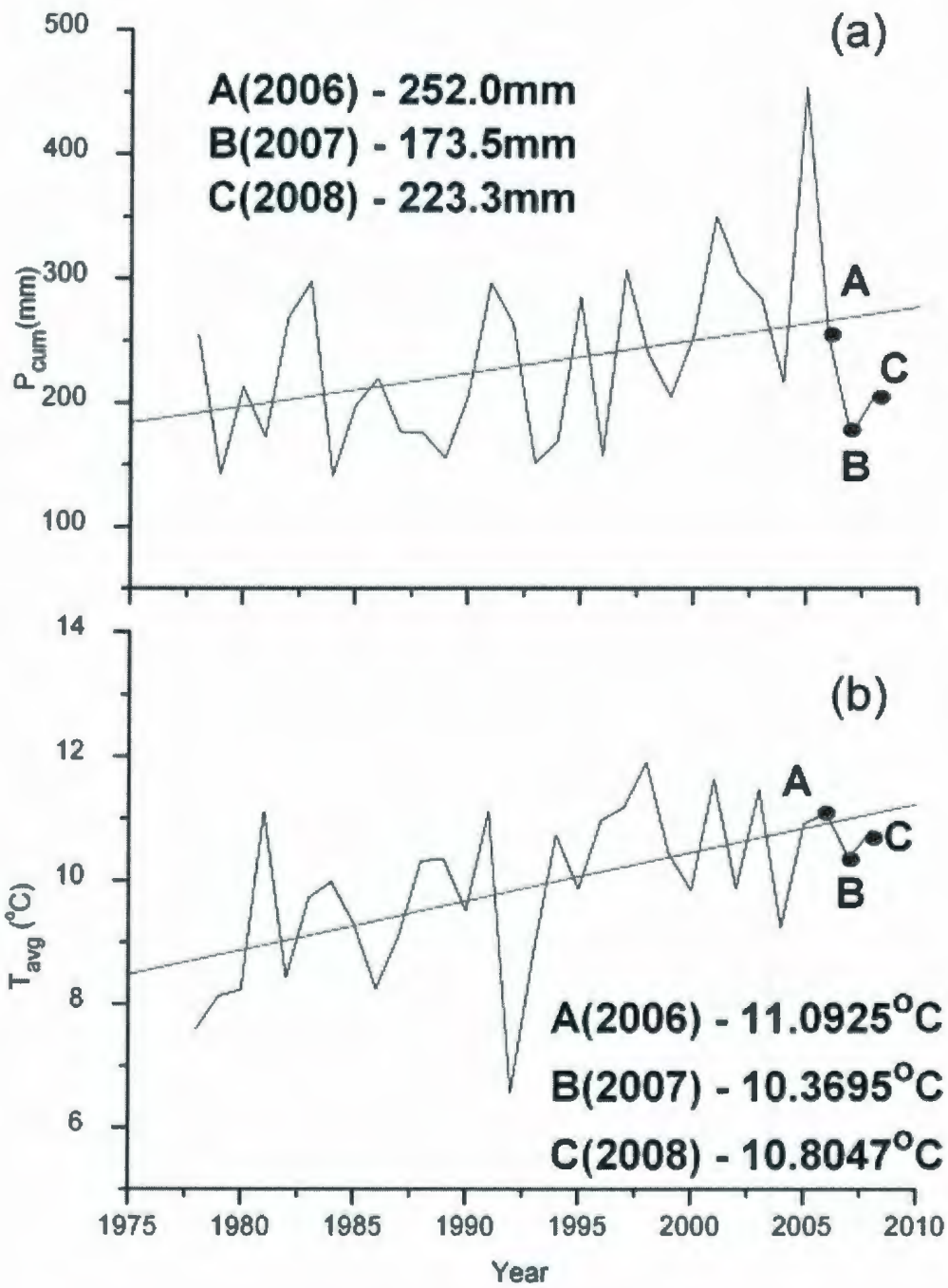
Data analysis has been conducted and the results indicate that summertime air temperature and precipitation has been rising in the past decades, leading to the inference that frost table has been descending. Soil moisture contents in the shallow layers of the wetland kept declining over time throughout the summer. The water discharges were low before September due to low precipitation and strong evapotranspiration as well as expansion of storage capacity of the organic soil layers, and then gradually increased due to the intensive precipitation in the fall.

3.4.1 Variation of Temperature and Precipitation

Climatic condition changes have been disclosed through the analysis of the 31-year historical data obtained at the Churchill airport (Environment Canada) and the 3-year monitoring data collected from the automated weather station in the Chesnaye Sub-basin. Figure 3.7 shows the variation of the cumulative summertime precipitation (P_{cum}) and mean summertime air temperature (T_{avg}) during the past 31 years, with P_{cum} ranging from 141 (1984) to 454 mm (2005) and T_{avg} ranging from 6.6 (1992) to 11.9 °C (1998). The linear trendlines indicate slight and steady elevations of summertime temperature and precipitation. To further quantify the variations, the coefficients of variation ($CV = \text{standard deviation}/\text{mean}$) are calculated for each 5-year period in the past 31 years (Table 3.4). As a comparison with those in the 1990s, T_{avg} has been continually rising by 1 °C every decade and P_{cum} has kept increasing particularly with a jump of around 20% in the 2000s. These results show warmer and wetter summers in recent years in the subarctic

regions near Churchill. In addition, it is notable that the fluctuations of P_{cum} , of which CV values range from 0.21 to 0.39, behave more dramatically over time than that of T_{avg} in the past 31 years.

Table 3.5 shows the variance of air temperature, evapotranspiration and precipitation in the summertime (June 20th – October 3rd) from 2006 to 2008 at Rail Spur. Of significance is the remarkable fluctuation of the summertime air temperature in both 2007 and 2008, which has higher maximum and lower minimum values as well as decrease in average as compared with those of 2006. Despite the notable mean temperature decrease, the warm climate is becoming severe and the elevating fluctuation reflects the unsteady status of the global climate. P_{cum} of 2007 is almost identical with that of 2006 regardless of different distributions. Most of the rainfall events in the summertime of 2007 are moderate (e.g., daily maximum value decreases by 43% from 2006's level) and occurs in the September (Figure 3.9b). By contrast, precipitation is distributed in several rainfall events with greater amount during July and August in 2006 (Figure 3.9a). On the other hand, P_{cum} of 2008 has the same temporal distribution as that of 2006 with smaller amount (Figure 3.9c). These two observations of temperature and precipitation are also confirmed as shown in Figure 3.7 that T_{avg} and P_{cum} decreases in 2007 at the Churchill airport. The cumulative summertime evapotranspiration (Equation 3-2) of 2007 is the minimum within the 3-year observance which could be explained by the lowest mean daily air temperature.



Note: Historical data is obtained from Environment Canada

Figure 3.7 (a) Cumulative summertime precipitation P_{cum} and (b) mean summertime air temperature T_{avg} at the Churchill airport (June 20th – October 3rd, 1978-2008)

Table 3.4 Standard deviation, mean and CV of P_{cum} and T_{avg} over a 31-year summertime period at the Churchill airport (June 20th – October 3rd, 1978-2008, Environment Canada)

	Standard deviation		Mean		CV = σ/μ	
	P_{cum} (mm)	T_{avg} (°C)	P_{cum} (mm)	T_{avg} (°C)	P_{cum} (mm)	T_{avg} (°C)
1978-1982	53.6	1.4	210.2	8.7	0.26	0.16
1983-1987	58.4	0.7	206.3	9.3	0.28	0.07
1988-1992	59.4	1.8	219.0	9.6	0.27	0.19
1993-1997	75.5	1.0	213.7	10.3	0.35	0.10
1998-2002	57.0	1.0	270.1	10.7	0.21	0.09
2003-2008*	107.7	0.9	275.9	10.6	0.39	0.08

*This period has 6 years.

Table 3.5 Variance of daily temperature, precipitation and evapotranspiration during the summertime at Rail Spur (June 20th – October 3rd, 2006 - 2008)

	Maximum			Minimum			Average			Sum		
	2006	2007	2008	2006	2007	2008	2006	2007	2008	2006	2007	2008
T (°C)	20.2	23.8	24.0	0.8	-1.2	0.5	11.4208	10.4577	11.3666	-	-	-
P (mm/day)	31.7	18.1	20.7	0	0	0	-	-	-	185.8	195.9	135.1
ET (mm/day)	4.5	4.9	5.9	0.1	0.1	0.1	-	-	-	174.0	153.9	167.0

Note: T is the daily air temperature; P is the precipitation; and ET is the evapotranspiration.

The 3-year observation at Rail Spur also shows a significantly proportional relationship between air temperature and evapotranspiration in the summertime. Evapotranspiration has the similar fluctuation as air temperature as explicitly shown in Figure 3.8. In Figure 3.8a, evapotranspiration is observed at its local minimum level on July 2nd and August 1st, 2006 (0.2 and 0.2 mm/day) when air temperature correspondingly drops down to its local lowest levels (9.3 °C and 7.7 °C). Viewed from Figure 3.8b, for instance, both maximum and minimum values of evapotranspiration coincide with the ones of air temperature on July 11th and July 22nd, 2007. Similar relationship can be found in Figure 3.8c where evapotranspiration and air temperature are both at the maximum levels on July 22nd, 2008. This evidence emphasizes that air temperature is one of the dominant factors of summertime evapotranspiration in the subarctic wetlands. On the other hand, precipitation also influences evapotranspiration process because it determines water availability and air humidity. Meanwhile, it plays an important role in raising the evapotranspiration with an average lag time of 1 day because it brings sufficient water into the wetland system. For example, daily evapotranspiration reaches its local bottom (0.2 mm/day) on July 11th, 2007, along with the local minimum daily temperature (6.5 °C). With the gradually increasing temperature, heavy rainfalls occurs on July 10th and 11th, 2007 (6.1 and 3.8 mm/day, respectively); consequently, the daily evapotranspiration rises up to 2.8 mm on July 12th, 2007 (Figure 3.9b). The similar phenomena could be observed on August 2nd, 2007, as well as July 2nd, July 14th, August 1st, 2006 (Figure 3.9a) and August 21st, 2008 (Figure 3.9c).

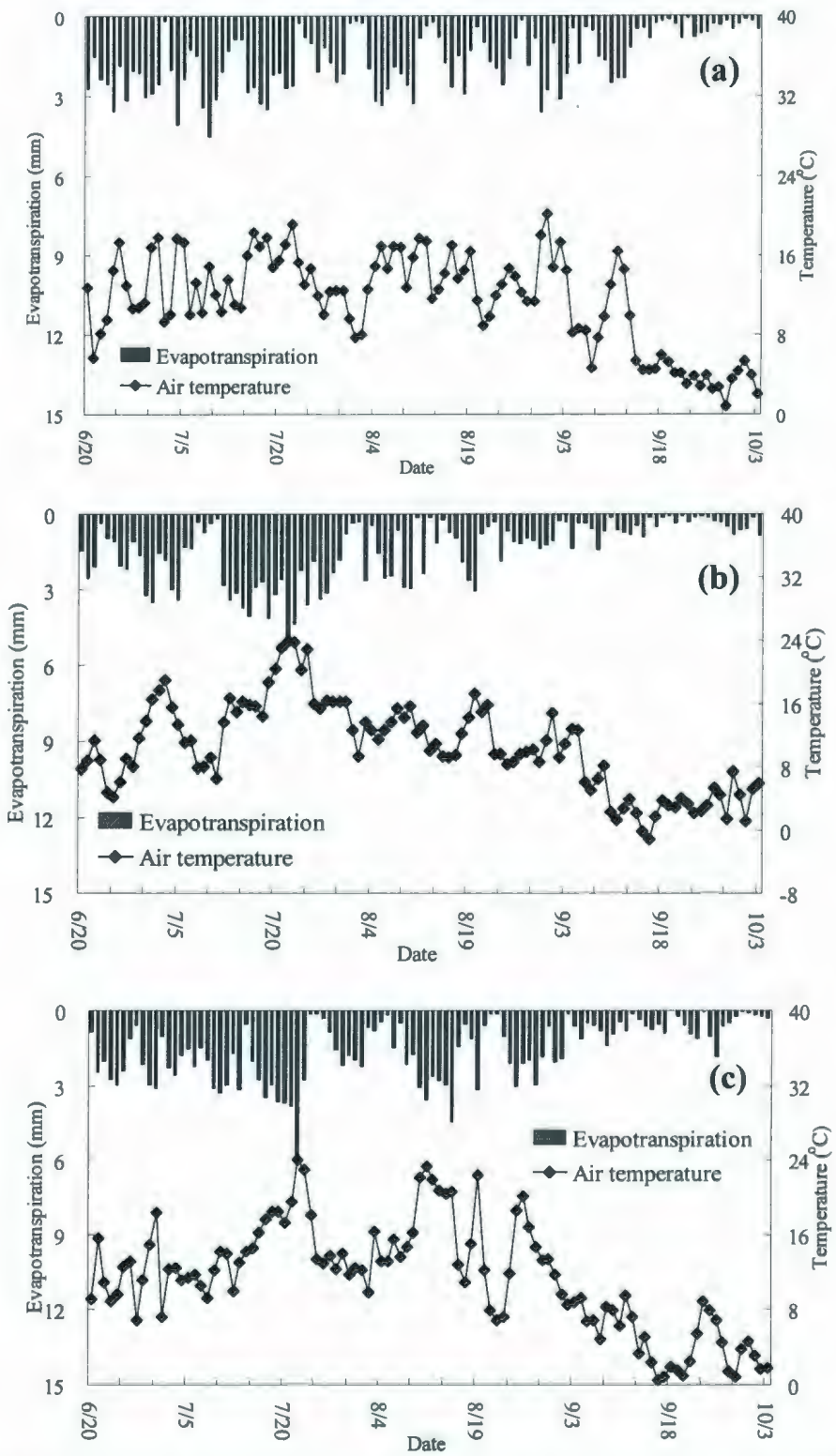


Figure 3.8 Variation of daily evapotranspiration and air temperature in (a) 2006, (b) 2007 and (c) 2008 at Rail Spur

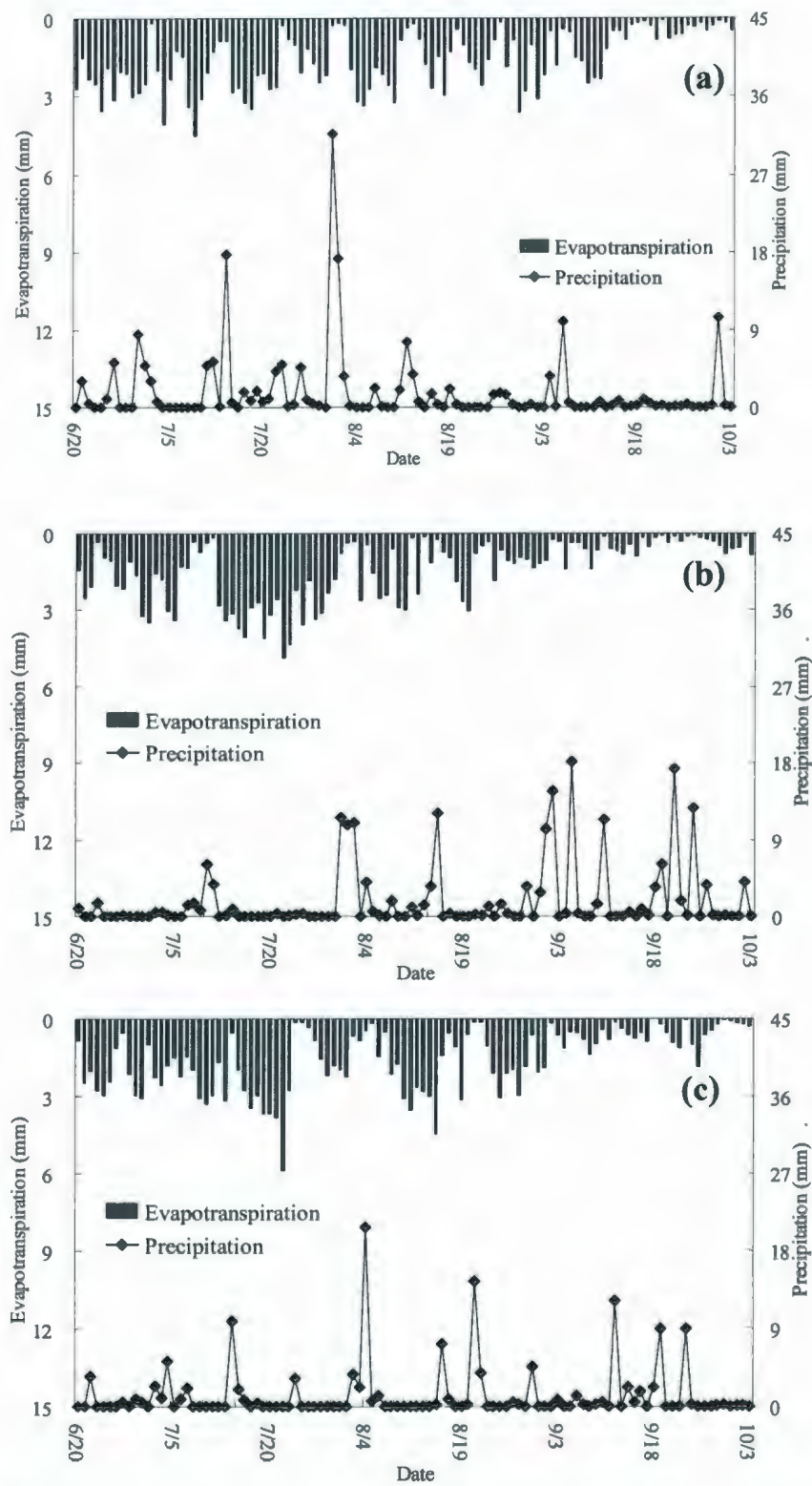


Figure 3.9 Variation of daily evapotranspiration and precipitation in (a) 2006, (b) 2007 and (c) 2008 at Rail Spur

3.4.2 Distribution of Frost Table

Figures 3.10 and 3.11 show the spatial and temporal distribution of the frost table at the monitoring stations during the summertime of 2006 and 2007. It indicates a reverse proportional relationship between frost table depth and its distance to the stream. There are a number of possible factors which may contribute to this phenomenon, such as influence of water contents from stream flow and subsurface flow, low albedo vegetations and insulation effect from deep snow cover may play important roles in the process. Soil moisture tends to be higher as one gets closer to the stream because of the percolation from the stream flow. Moreover, subsurface flow penetrating the organic layer is towards the stream which may accelerate the thaw of frozen soil. Dark forests near the streams have much lower albedo than the lichens and moss covered hollows which are far away from the streams. This difference of albedo may cause the near stream frost table to be lower than the distant locations because of the acceleration of the ice thaw. Moreover, greater insulation that can intensify the permafrost melt should be considered at near stream locations where the snow cover is deeper. The similar evidences have also been reported by the previous studies (Woo and Marsh, 2005; Woo and Young, 2006). The average summertime frost table at each station in 2006 and 2007 also supports this deduction. For example, frost table at 6 m away from the stream is much shallower than the locations at 2 and 4 m (Table 3.6, Station 5; Table 3.7, Stations 5 and 7). Spatial distribution of the frost table at each station is further demonstrated by the results from F-test. Greater F values stand for significant spatial variance of the depth of frost table, following by the less possibility of Prob. > F. For example, both banks of Station 5 have values of Prob. > F less than 0.05 (Table 3.6), indicating the differences among frost

tables at near stream and distant locations are significant. This difference could still be observed even the value of Prob. > F is more than 0.05. However, most of the results in 2007 (Table 3.7) do not apparently show that spatial distribution. This may be due to the errors from field measurements.

Another interesting finding is that, the average summertime frost table in 2007 is much deeper in most stations (Tables 3.6 and 3.7), indicating a trend of warmer summer. A good example could be seen from the right bank at Station 5. The records for 2, 4 and 6 m are 1030, 987 and 588 mm in 2006 and 1265, 1253 and 1112 mm in 2007, showing remarkable increase at 23%, 27% and 99%, respectively. Records from Stations 6 and 7 also agree with this increasing observation. One probable reason for this is on account of the higher temperature during July and August in which most of the sampling work was conducted in 2007 (Figure 3.9b). Although the mean summertime (June 20th – October 3rd) air temperature of 2007 is 1 °C lower than that of 2006, the average value during July and August of 2007 (13.4766 °C) is higher than that of 2006 (13.4729 °C) with more intensive fluctuation. Moreover, larger amount of precipitation and less evapotranspiration in the summertime of 2007 results in plentiful subsurface flow which maybe another important cause of deeper frost table.

Figures 3.12 to 3.18 demonstrate the relationships among frost table, air temperature and precipitation at the monitoring stations during the summertime of 2006 and 2007. Generally, air temperature appears as the dominant factor leading the fluctuation of frost table during the two monitoring seasons. For example, viewed from Figure 3.15b, the

frost tables at each transect continuously keeps descending throughout the summer of 2007 when air temperature remains between 11 – 23 °C. This fact, along with the relatively high thermal capacity of soil stabilizes the temperature field of the stream banks and makes the frost table descend due to sufficient ground heat flux. The same phenomenon could be observed in most figures regarding temperature and frost table. On the other hand, the influence of precipitation on frost table is not as significant as that of air temperature, which is illustrated in Figure 3.15a that the frost table keeps descending regardless rainfall events. This is due to insufficient precipitation, relatively high air temperature and excessive evapotranspiration which jointly diminishes the subsurface flow within the organic layer and barely affects the frost table.

Table 3.6 Average summertime frost table at Stations 5, 6, 7 in 2006 (June 20th –October 3rd)

	Station 5			Station 6			Station 7		
	L(m)*	FT(mm)**	Prob. > F***	L	FT	Prob. > F	L	FT	Prob. > F
	2	1030		2	417		2	523	
Right	4	987	0.013	4	325	0.119	4	-	0.066
Bank	6	588		6	338		6	-	
	8	364		8	358		8	301	
	2	1349		2	358		2	347	
Left	4	1171	0.003	4	333	0.783	4	431	0.232
Bank	6	576		6	349		6	-	
	8	647		8	321		8	241	

*L is distance to the stream

**FT is frost table depth

***Prob. > F means the probability of having equal frost tables (Prob. > F is less than 0.05 if the differences are significant).

Table 3.7 Average frost table at Stations 5, 6, 7 and 10 in 2007 (June 20th – October 3rd)

	Station 5			Station 6			Station 7			Station 10		
	L* (m)	FT**(mm)	Prob. > F****	L	FT	Prob. > F	L	FT	Prob. > F	L	FT	Prob. > F
Right Bank	2	1265		2	1098		2	558		2	1078	
	4	1253	0.814	4	914	0.681	4	204	0.495	4	1022	0.693
	6	1112		6	1117		6	269		6	1294	
Left Bank	2	983		2	1134		2	433		2	1258	
	4	748	0.606	4	939	0.831	4	490	0.913	4	876	0.424
	6	762		6	1080		6	488		6	989	

*L is distance to the stream

**FT is frost table depth

***Prob. > F means the probability of having equal frost tables (Prob. > F is less than 0.05 if the differences are significant)

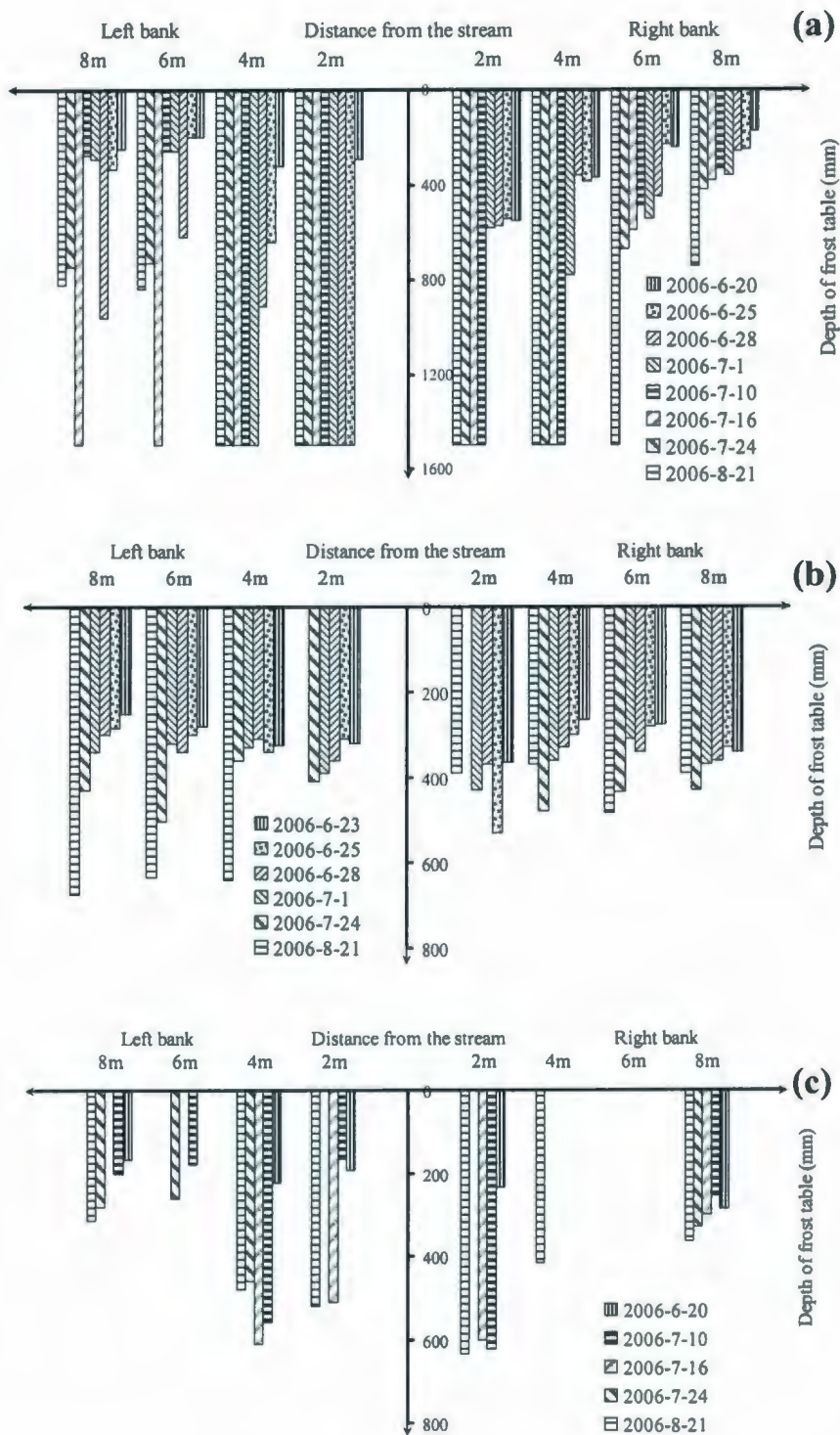


Figure 3.10 Depth of frost table in 2006 summertime at (a) Stations 5, (b) Station 6, and (c) Station 7

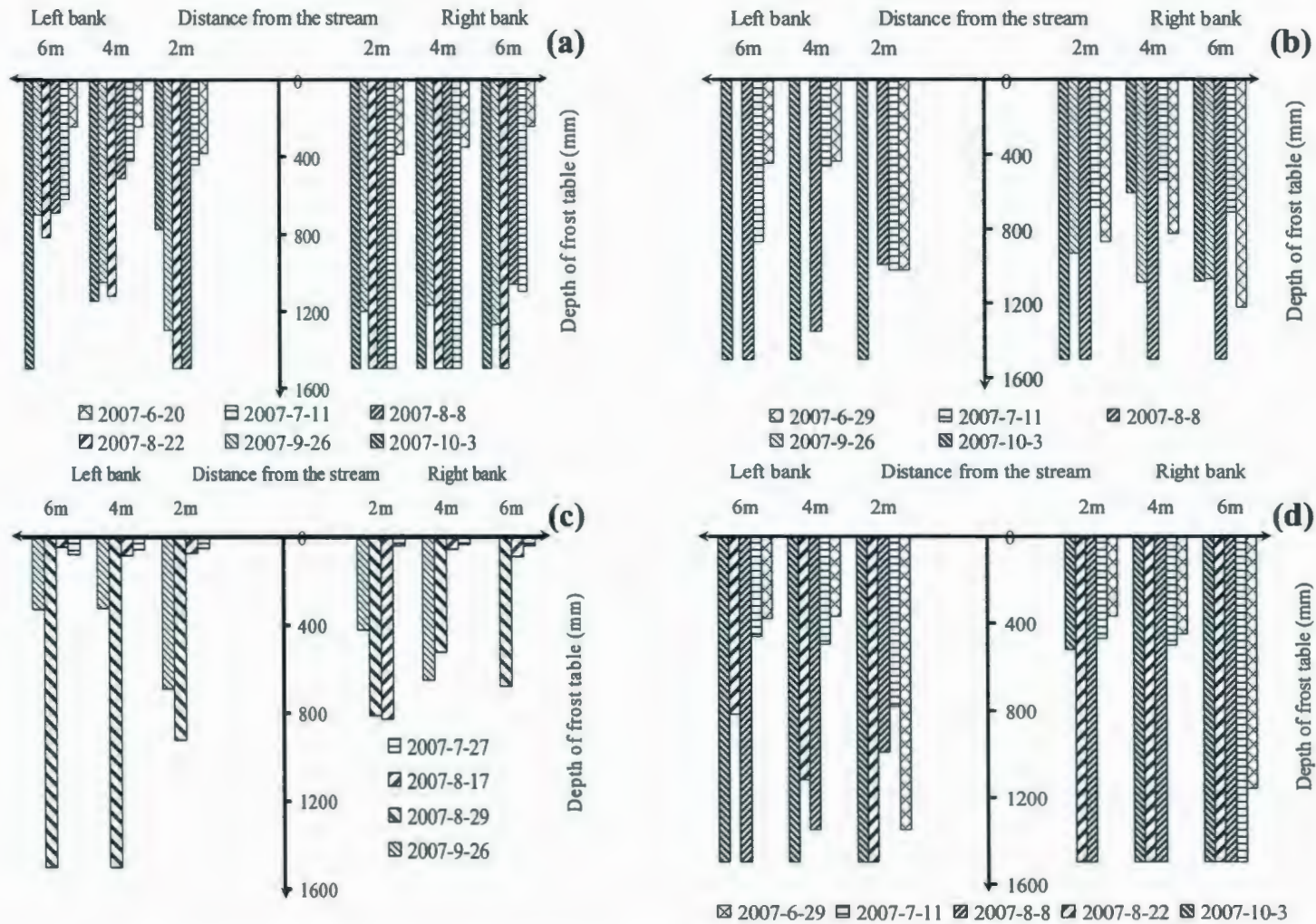


Figure 3.11 Depth of frost table in 2007 summertime at (a) Station 5, (b) Station 6, (c) Station 7, and (d) Station 10

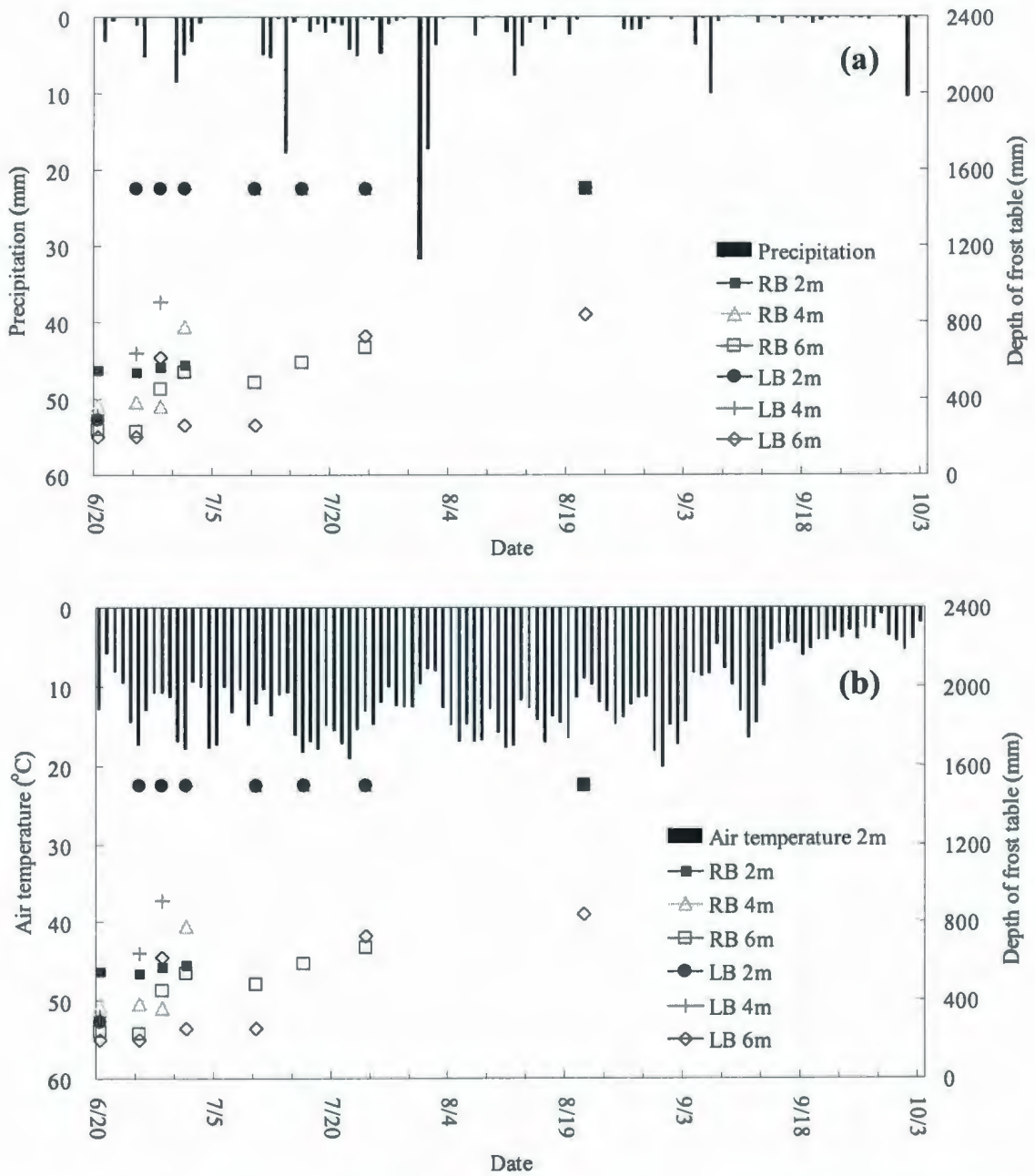


Figure 3.12 Frost table vs. (a) precipitation and (b) air temperature at Station 5 in 2006 summertime (RB: Right Bank; LB: Left Bank)

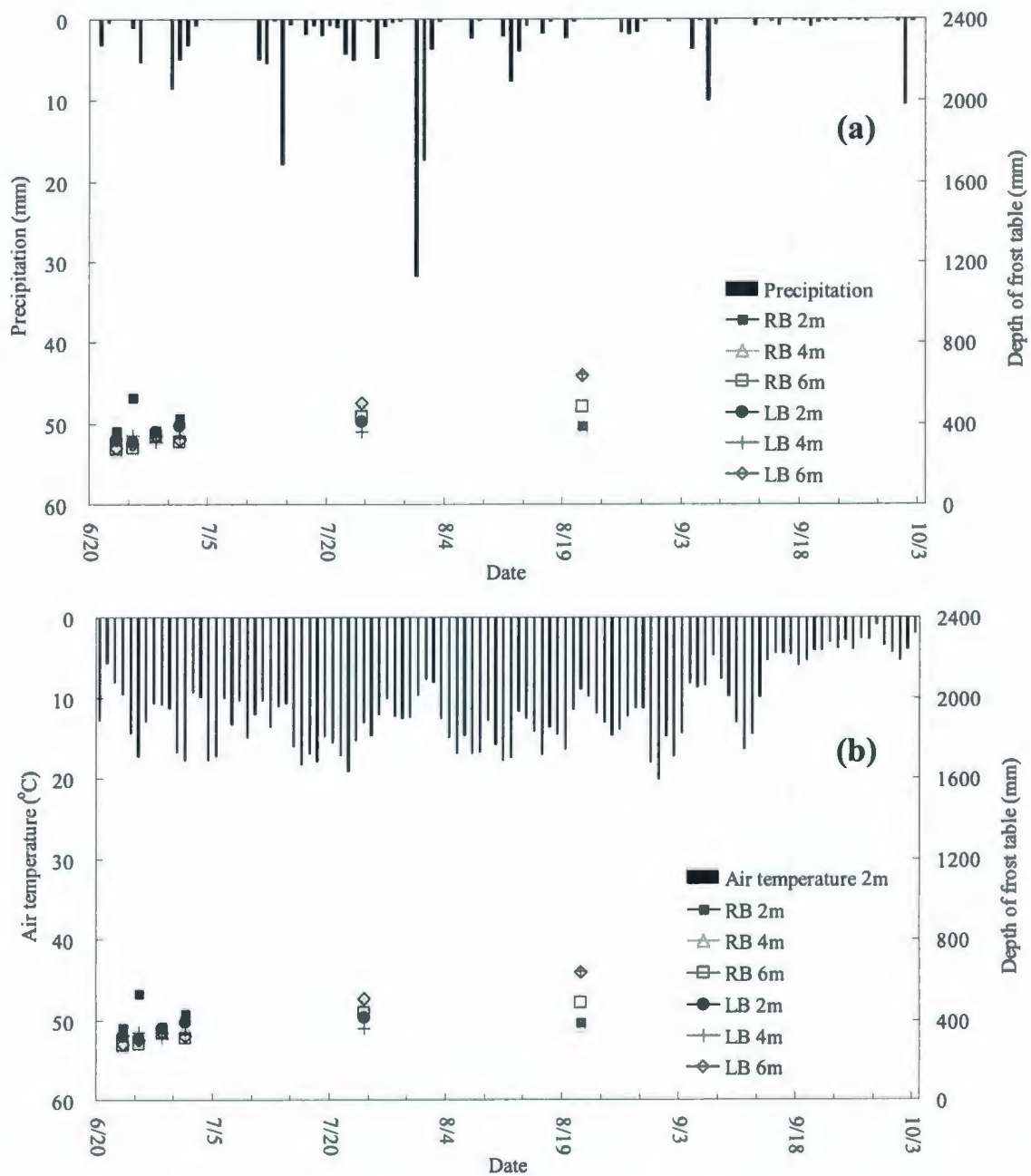


Figure 3.13 Frost table vs. (a) precipitation and (b) air temperature at Station 6 in 2006 summertime (RB: Right Bank; LB: Left Bank)

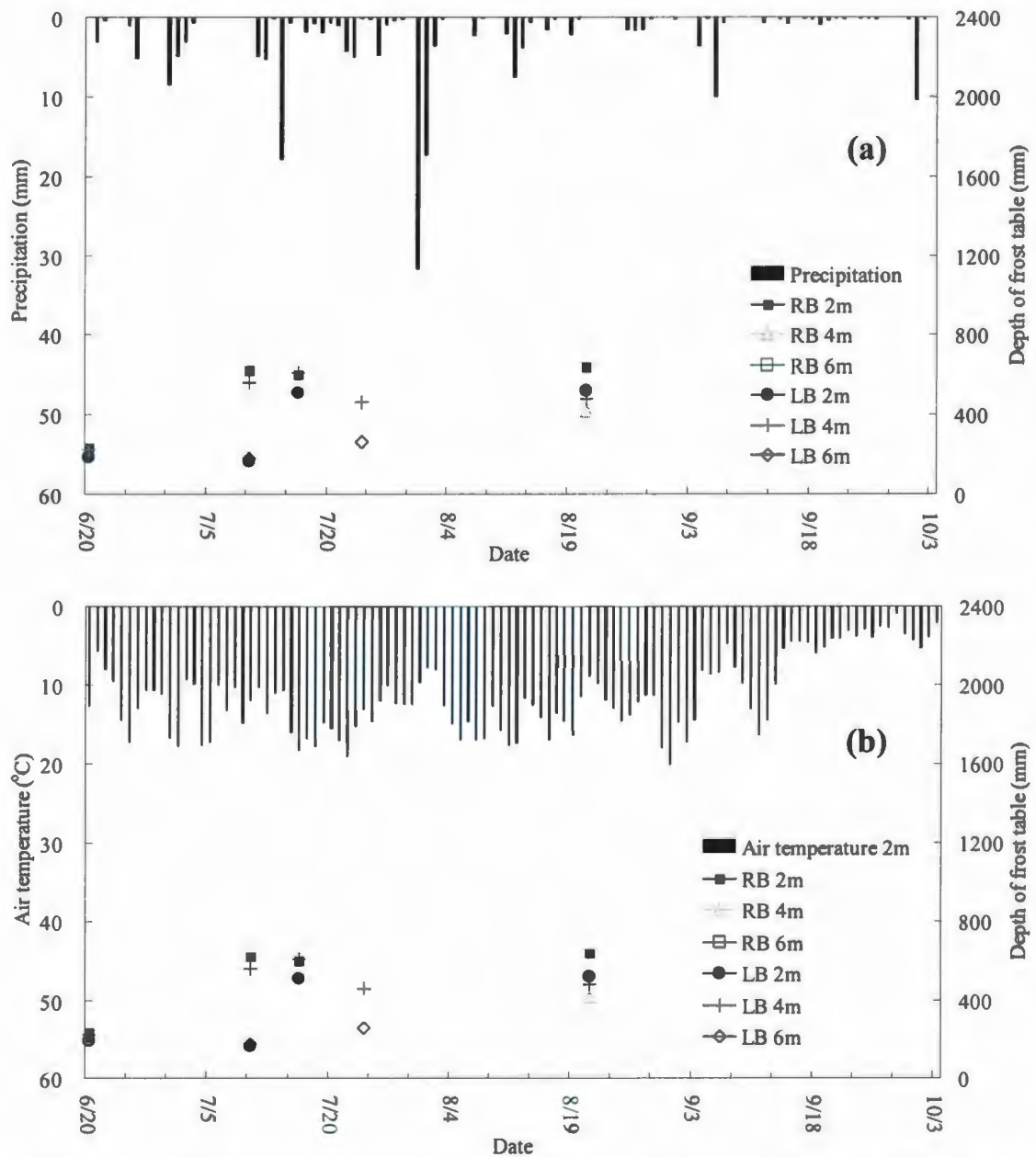


Figure 3.14 Frost table vs. (a) precipitation and (b) air temperature at Station 7 in 2006 summertime (RB: Right Bank; LB: Left Bank)

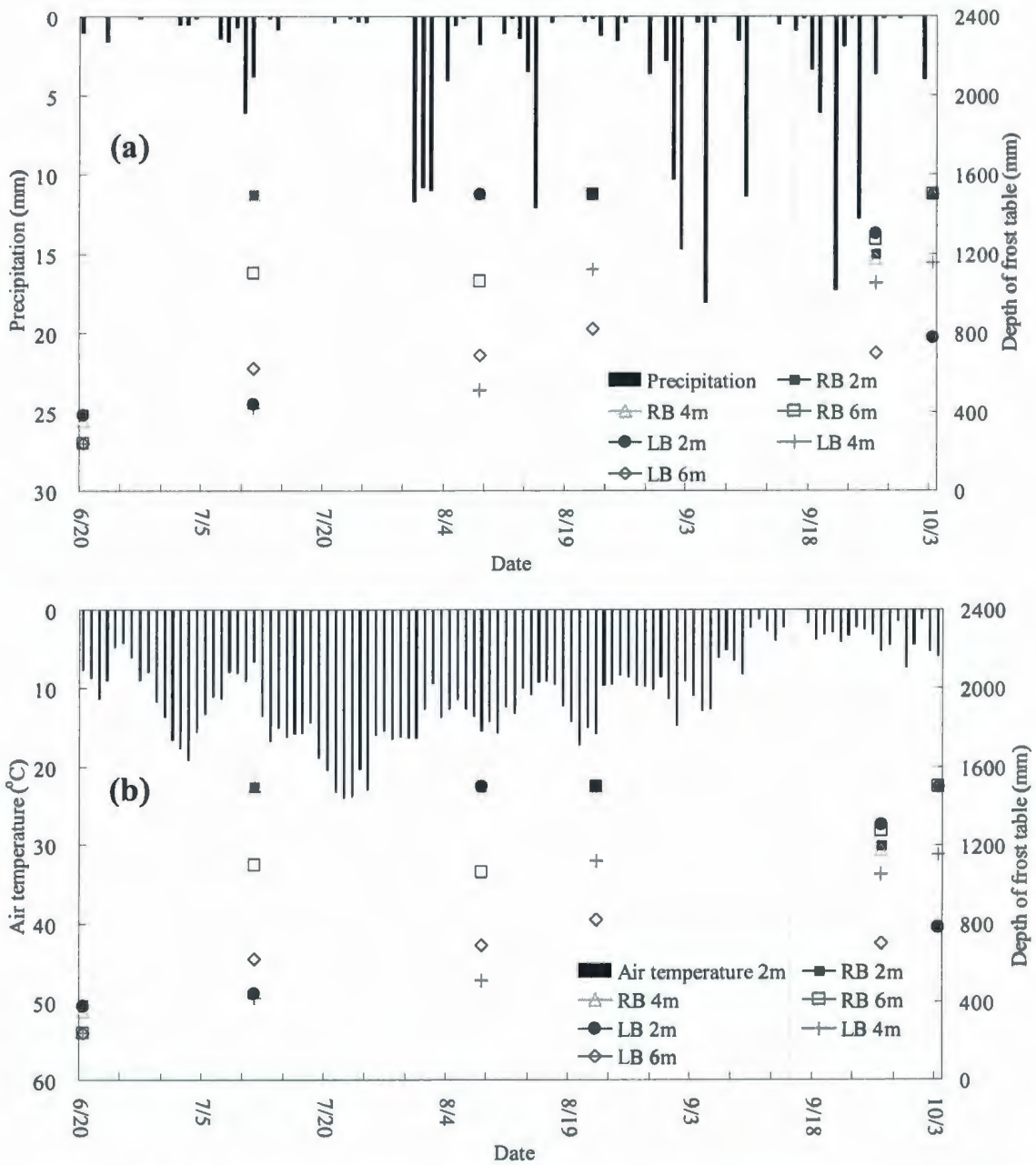


Figure 3.15 Frost table vs. (a) precipitation and (b) air temperature at Station 5 in 2007 summertime (RB: Right Bank; LB: Left Bank)

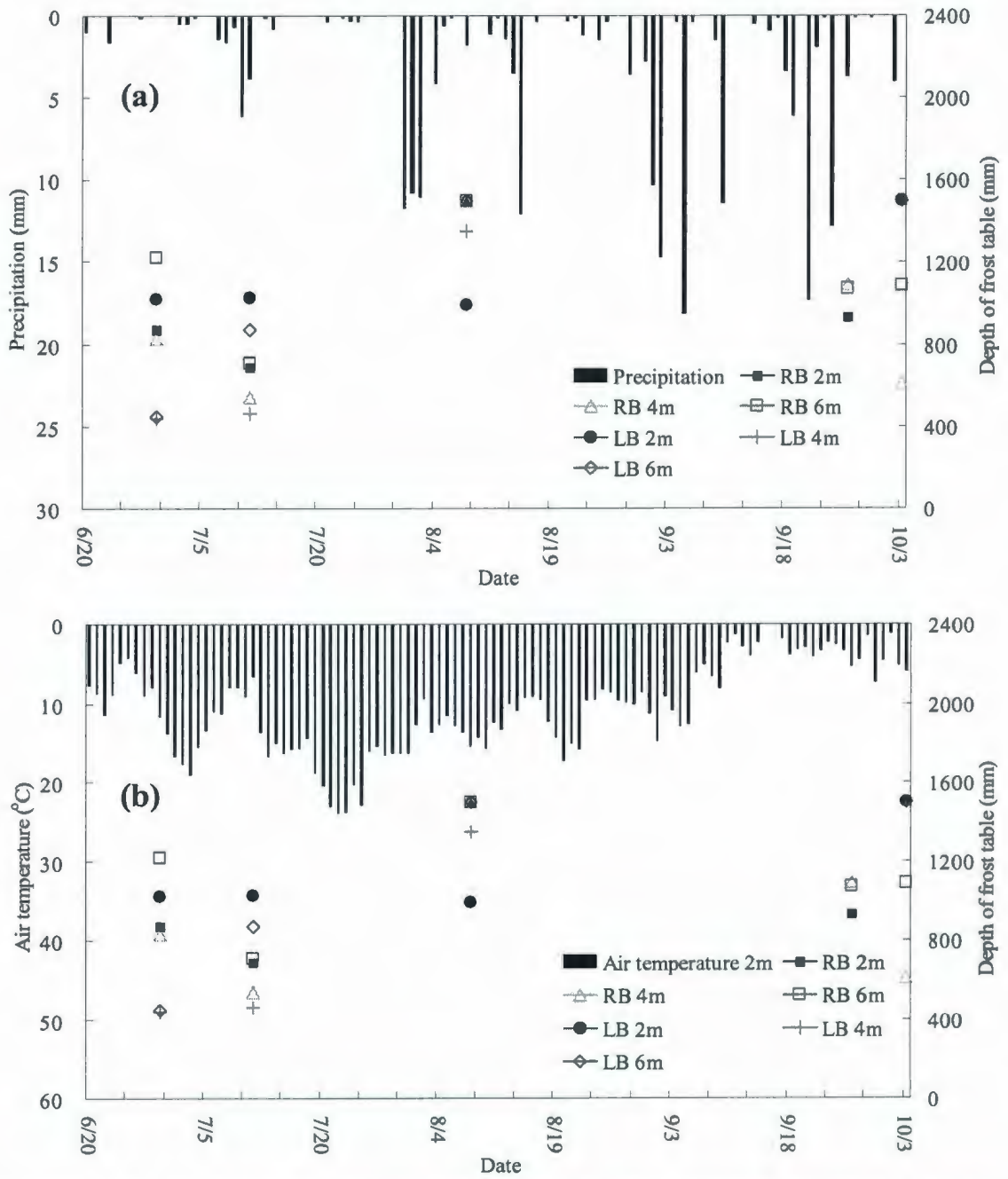


Figure 3.16 Frost table vs. (a) precipitation and (b) air temperature at Station 6 in 2007 summertime (RB: Right Bank; LB: Left Bank)

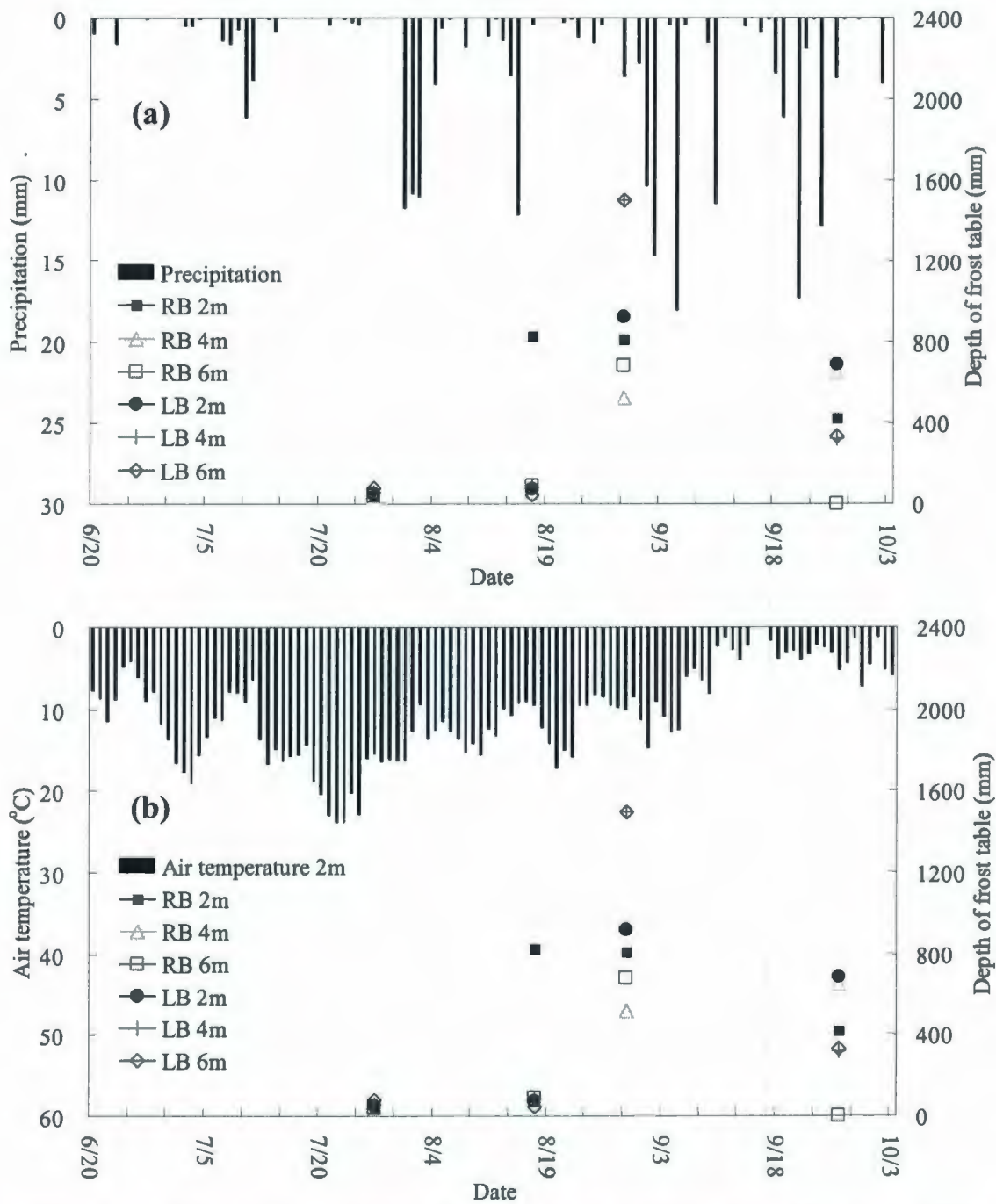


Figure 3.17 Frost table vs. (a) precipitation and (b) air temperature at Station 7 in 2007 summertime (RB: Right Bank; LB: Left Bank)

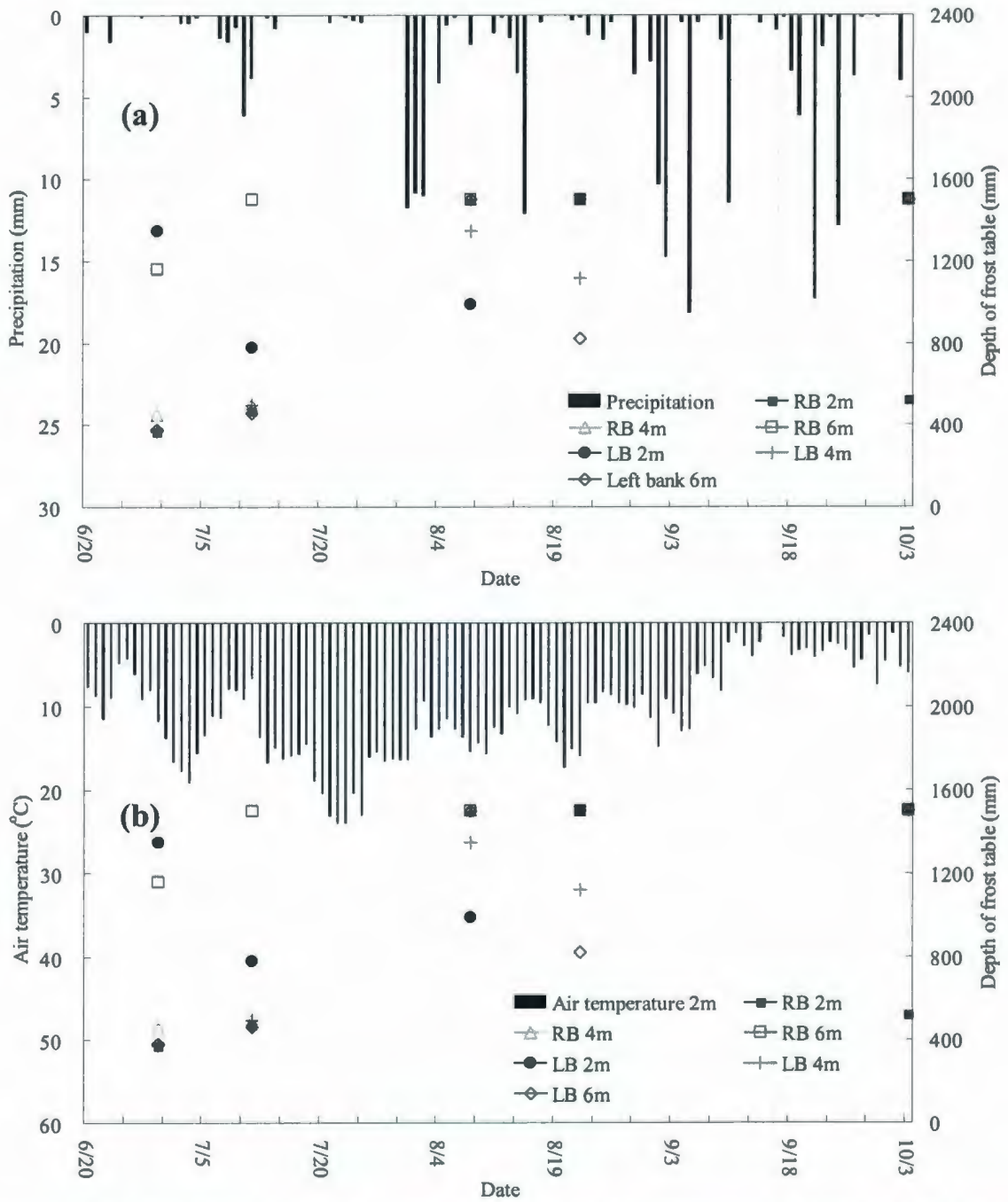


Figure 3.18 Frost table vs. (a) precipitation and (b) air temperature at Station 10 in 2007 summertime (RB: Right Bank; LB: Left Bank)

3.4.3 Profile of Soil Moisture and Temperature

Surface soil moisture (5 cm depth) was monitored at multiple transects of each station in the summertime of 2006 and 2007. Figures 3.19 and 3.20 demonstrate a spatial trend that the soil layers become more saturated as one gets closer to the stream, which could be clearly viewed from the observations at the left banks of Stations 5 and 7 in both monitoring seasons. In 2006, for instance, the average surface soil moisture contents at the left bank of Station 5 are 38.2%, 24.5%, 21.8% and 17.9%, respectively, with the locations ranging from 2, 4, 6 and 8 m away from the stream. On account of the presence of extraordinarily high hydraulic conductivity of the organic soil texture (Reeve *et al.*, 2000) and steep slope, near stream locations gain more water from the stream and the vicinity because the intensity of this infiltration process is inversely proportional to the distance from the stream. Despite most data following this descending trend, surface soil moisture contents at some transects show a reverse trend, for example, the transects in the right banks of Stations 5, 7 and 10 in 2007. This finding could be attributed to the presence of frost table, soil texture and land slope. Frost table descends as approaching to the stream, which represents that active organic layer become deeper and infiltration occurs more easily with less resistance because the storage capacity increases. Therefore, some distant transects, if frost table is shallow enough, are possibly to be saturated near the ground surface, leading to higher soil moisture contents than those close to the stream.

Another interesting observation is that the temporal differences of surface soil moisture in both seasons are not as significant as spatial differences during the summertime as shown in Tables 3.8 and 3.9. F value is defined by model mean square, which represents the

temporal effects, over error mean square which accounts for the spatial effects, comparing the weighting of time and location to the fluctuation of soil moisture. Hence, in terms of this, greater F values stand for significant temporal effect to the variance of surface soil moisture at each transect, following by the less possibility of Prob. > F. The results indicate that transects at Stations 5 and 7 have stable temporal distributions of surface soil moisture contents which can be supported by their relatively low F values, high Prob. > F values as well as Figures 3.19 and 3.20. This phenomenon can be mainly explained by the fact that the soil moisture tests were conducted at the surface layer where water content is replenished by precipitation, evaporation as well as the ponds in vicinity. Nonetheless, surface soil moisture contents at some locations such as Stations 6 and 10 behave discretely over time which is due to the flooding events in September when inundation submerges low-lying banks.

These findings show the distinguished soil features of the subarctic wetland systems, which are also supported by the observations obtained from the automated weather station at Rail Spur. Automated weather station at Rail Spur also provides solid evidence of temporally stable soil moisture as well as soil temperature features in the summertime from 2006 to 2008. The primary finding is that following the major recharge period during the snowmelt, soil moisture contents at deep layers are more saturated and stable (Figures 3.21-3.23) which could be explained by the water table lying above. Meanwhile, soil moisture of shallow soil layers (e.g., at 5 cm depth) has strong relationship with evapotranspiration and dramatically fluctuate throughout the summer in each year because of the water loss from intensive evapotranspiration and the lack of precipitation.

For instance, soil moisture at 5 cm depth decreases sharply on July 15th, July 31st 2006 and July 11th, August 2nd 2007 (Figure 3.21a and 3.22a) when precipitation occurs whereas soil moisture at 25 cm depth is relatively stable. Another possible explanation for this phenomenon can be related to the descending frost table which elongates the active organic layer and drives the water table downwards, reducing the water supplement (Carey and Woo, 1999; Carey and Woo, 2001). Soil temperature at the shallow layers (e.g., 0, 5 and 10 cm depth) varies continually and more or less accords with the air temperature in the summertime as shown in Figures 3.24 to 3.26. In comparison, soil temperature at the deep layers (e.g., 50 and 75 cm depth) remains stable (around 0 °C) during the summers, which could be attributed to the fact that permafrost table lying below. The most exceptional zone is the mid soil layer temperature (at depth of 25 cm) which lies between 0.23 and 5.86 °C throughout the whole summer in 2006. This may be due to the shallow water table that submerges this particular soil layer and the relatively high water contents that enables ground heat flux being attenuated to stabilize the temperature. To quantify the differences between the air temperatures the soil temperatures at multiple layers, t-tests have been conducted with the aim of examining whether the mean values of soil temperatures and air temperatures are equal or distinct. The greater the t value, the more distinct difference exists between the soil temperature and the air temperature. The results (Table 3-10) indicate that the soil temperatures at ground surface (0 cm) in each summer are almost the same as air temperature and this similarity diminishes as the soil layer becomes deeper.

Table 3.8 F-test of soil moisture contents at Stations 5, 6, 7 in 2006
(June 20th – October 3rd)

	Station 5		Station 6		Station 7	
	F*	Prob. > F**	F	Prob. > F	F	Prob. > F
Right	17.71	<0.0001	6.64	0.0002	0.95	0.463
Left	1.31	0.286	9.27	<0.0001	0.32	0.863

*F is determined by model mean square over error mean square

**Prob. > F means the probability of having equal soil moisture (Prob. > F is greater than 0.1 if the temporal differences are not significant)

Table 3.9 F-test of soil moisture contents at Stations 5, 6, 7 and 10 in 2007
(June 20th – October 3rd)

	Station 5		Station 6		Station 7		Station 10	
	F	Prob. > F	F	Prob. > F	F	Prob. > F	F	Prob. > F
Right	1.45	0.276	8.2	0.008	1.85	0.216	4.06	0.033
Left	0.92	0.498	178.87	<0.0001	1.69	0.245	2.89	0.079

Table 3.10 Statistical analysis between soil temperature and air temperature ($\alpha = 0.05$)

		Depth (cm)	0	5	10	25	50	75
2006	Mean difference*		0.31	1.30	3.71	8.23	11.52	11.96
	t for H ₀		1.08	4.51	12.52	27.73	36.54	37.58
	Prob> t **		0.2810	4×10 ⁻⁶	10 ⁻²³	5×10 ⁻⁵⁵	3×10 ⁻⁶⁸	10 ⁻⁶⁹
2007	Mean difference		-0.33	0.08	2.29	7.69	10.65	11.09
	t for H ₀		-0.77	0.23	5.58	18.25	23.47	24.20
	Prob> t		0.4404	0.8182	10 ⁻⁷	8×10 ⁻³⁷	6×10 ⁻⁴⁷	10 ⁻⁴⁸
2008	Mean difference		-0.64	-0.45	1.84	8.03	11.52	12.11
	t for H ₀		-0.78	-0.56	2.54	13.40	20.40	21.45
	Prob> t		0.4339	0.5750	10 ⁻²	5×10 ⁻³⁰	10 ⁻⁵¹	10 ⁻⁵⁴

* Mean difference between the soil temperature and the air temperature in the summertime (Air temperature - Soil temperature)

** Prob>|t| stands for the probability of having equal means of the soil temperature with the air temperature

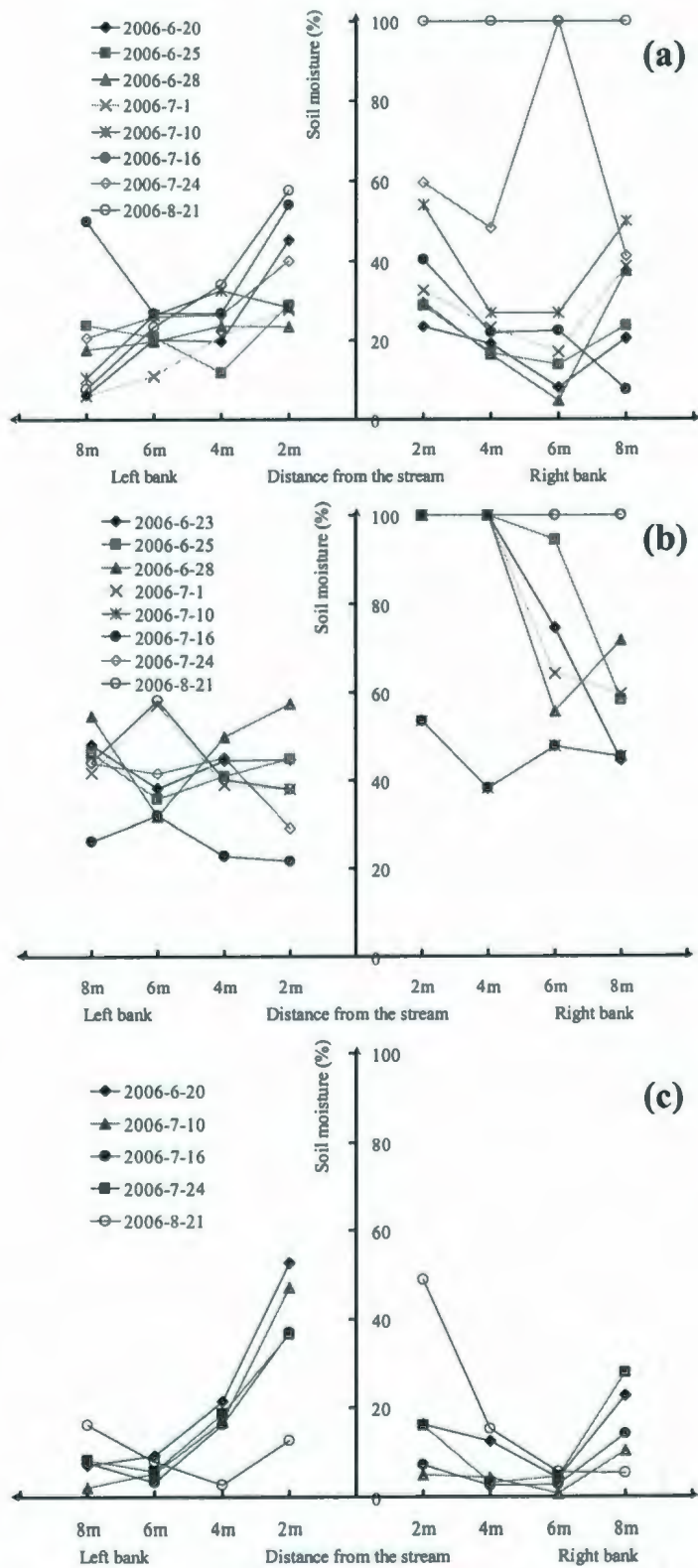


Figure 3.19 Soil moisture at stream banks of (a) Station 5, (b) Station 6, and (c) Station 7 in the summertime of 2006

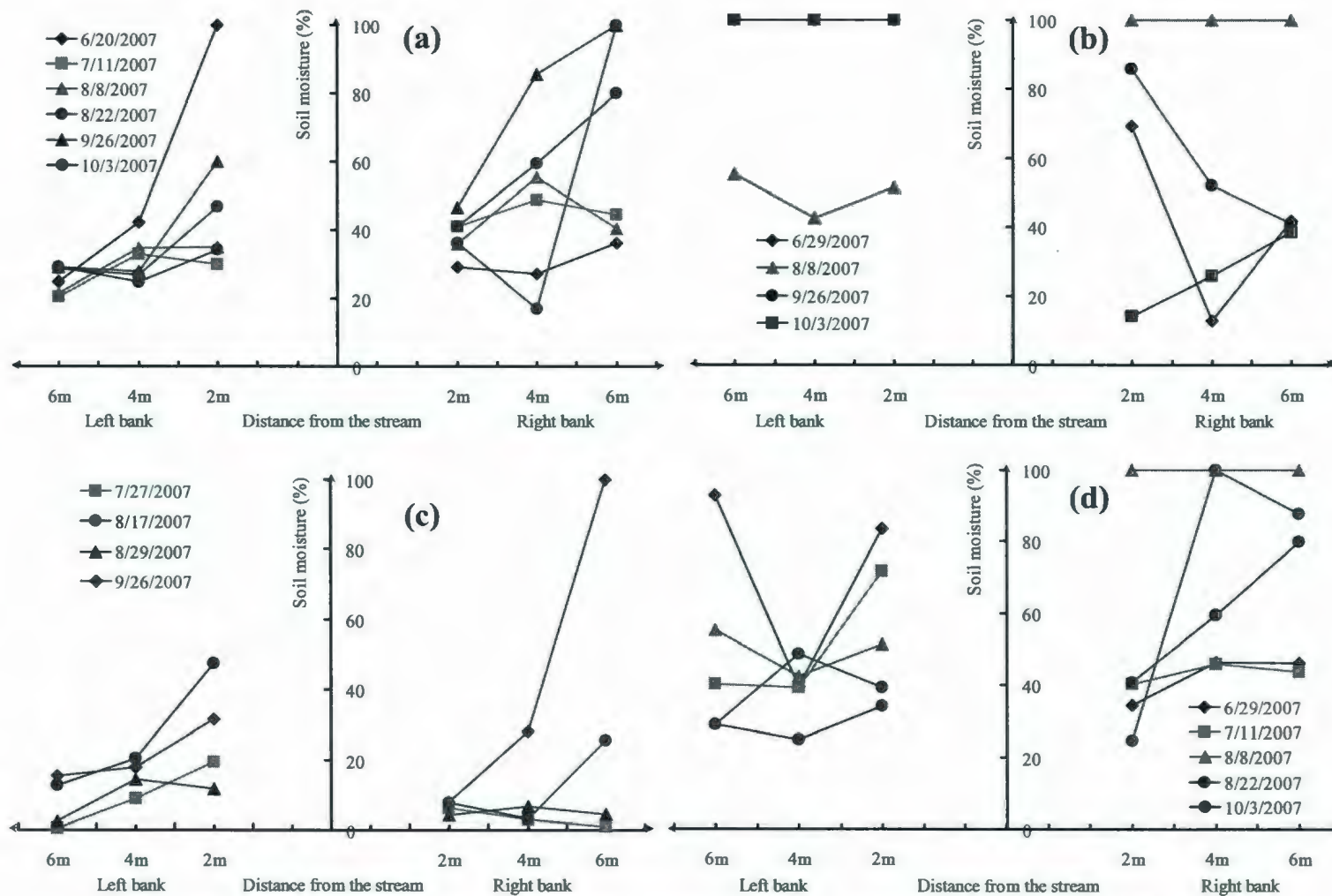


Figure 3.20 Soil moisture at stream banks of (a) Station 5, (b) Station 6, (c) Station 7 and (d) Station 10 in the summertime of 2007

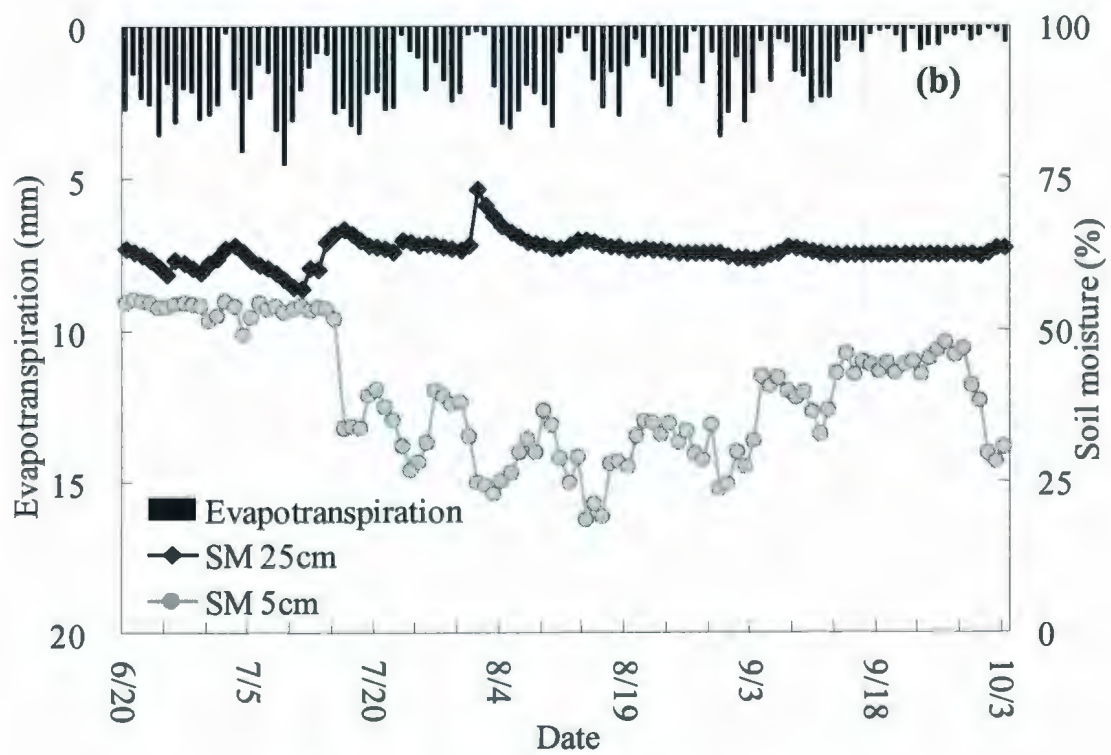
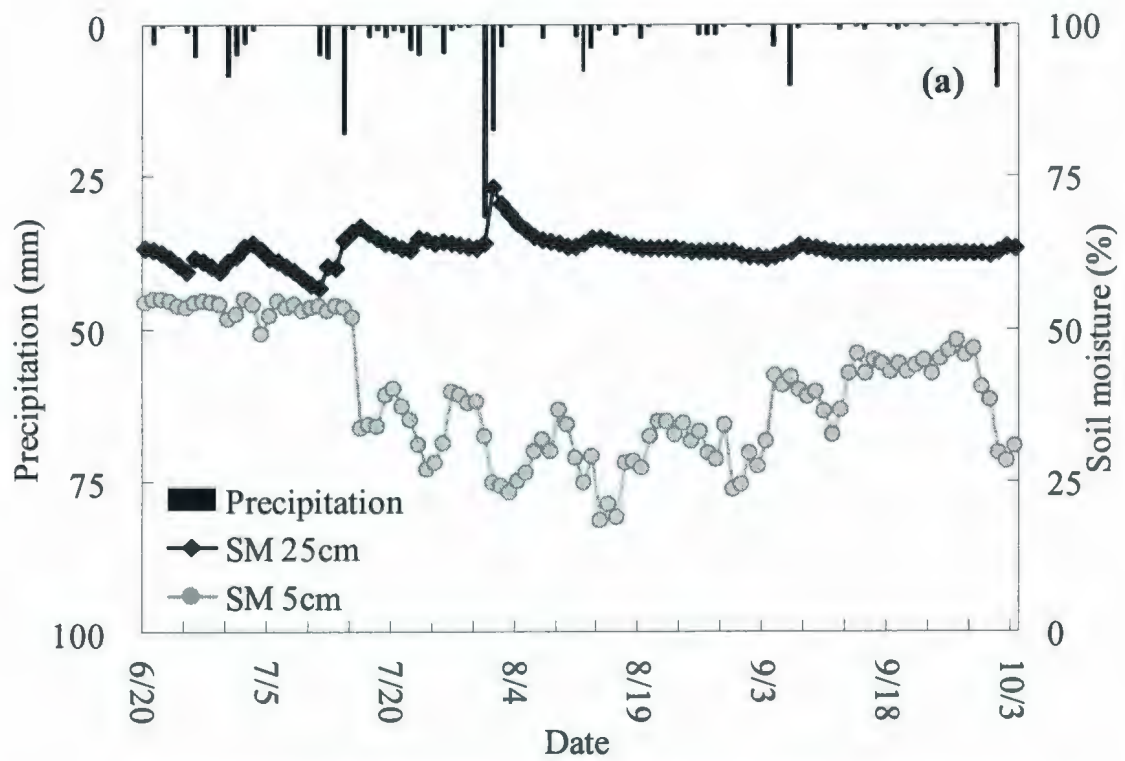


Figure 3.21 Variation of daily soil moisture and (a) precipitation and (b) evapotranspiration in the summertime of 2006 at Rail Spur (SM: Soil Moisture)

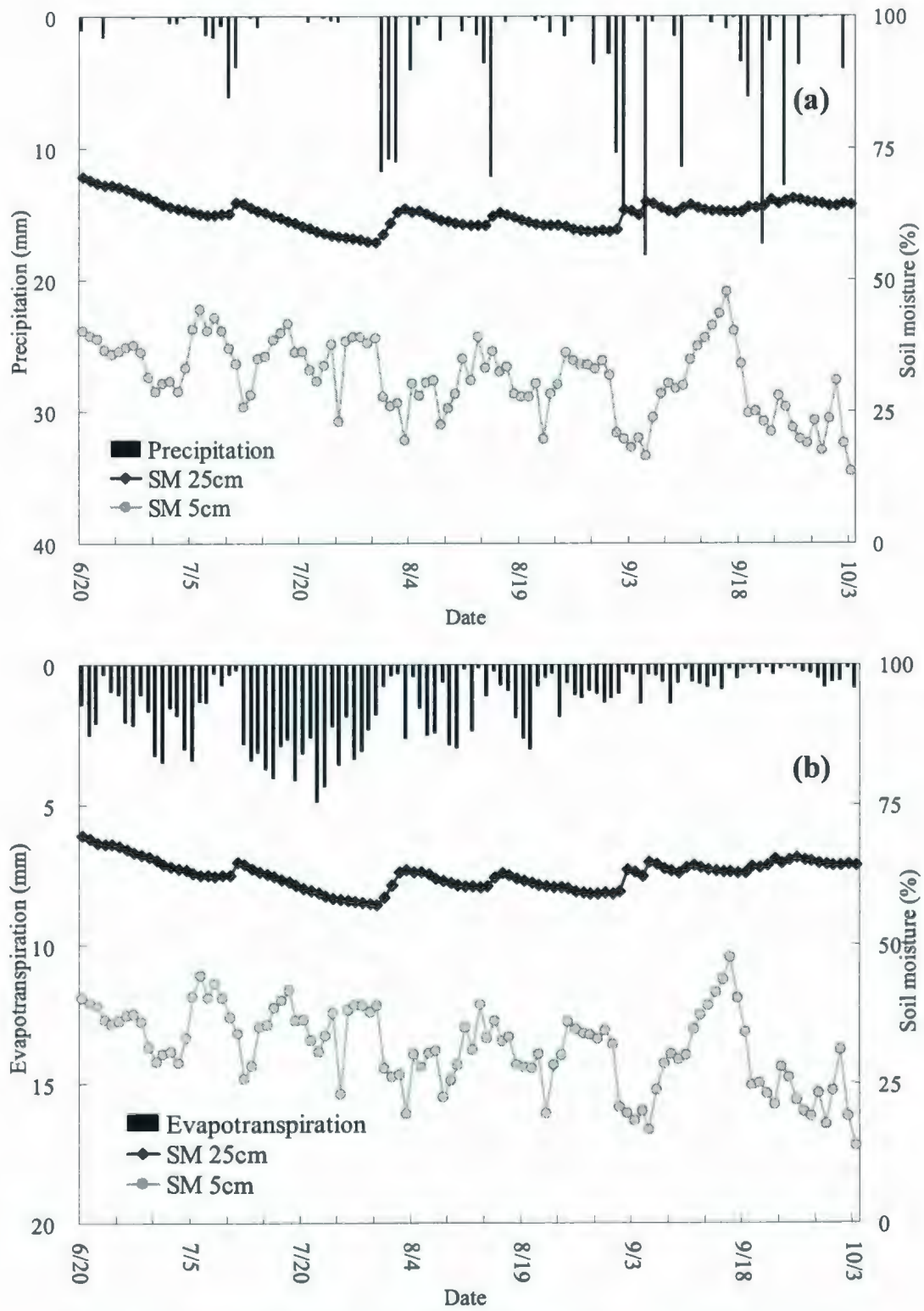


Figure 3.22 Variation of daily soil moisture and (a) precipitation and (b) evapotranspiration in the summertime of 2007 at Rail Spur (SM: Soil Moisture)

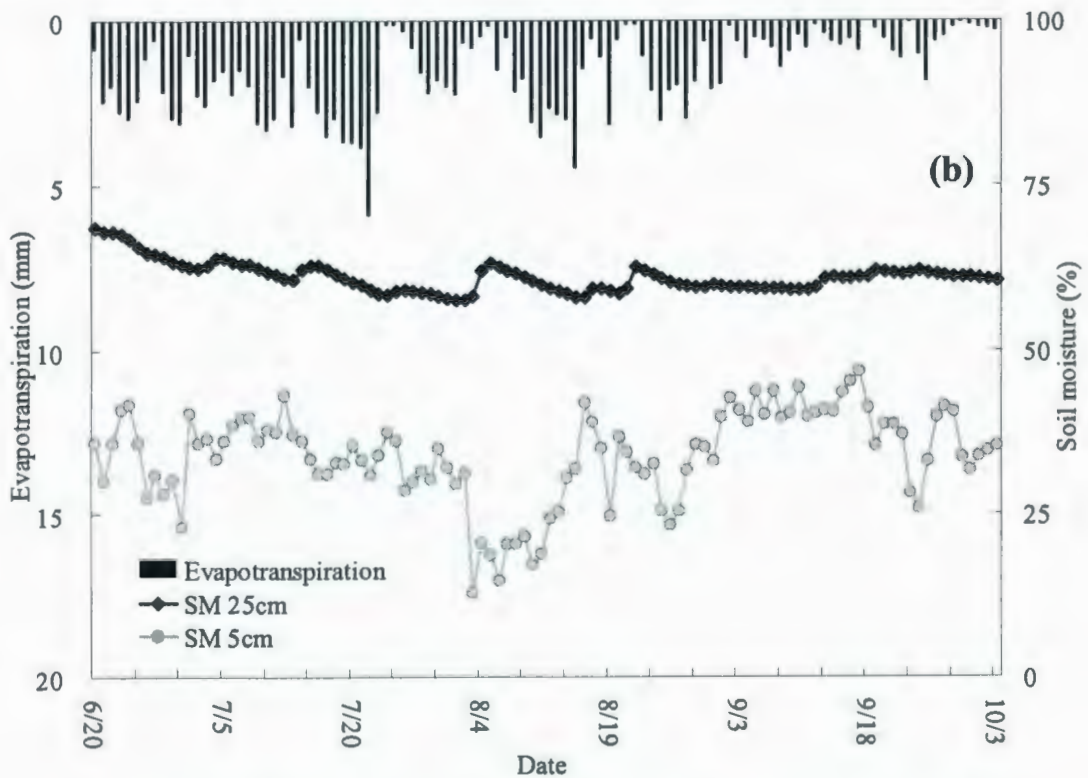
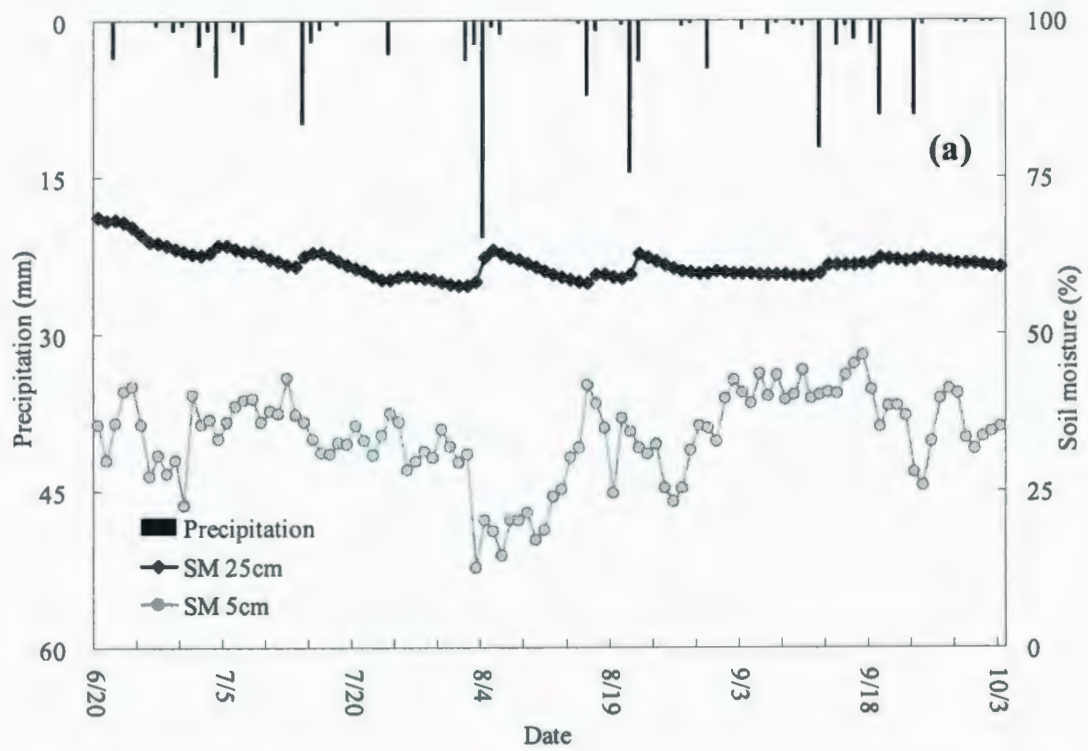


Figure 3.23 Variation of daily soil moisture and (a) precipitation and (b) evapotranspiration in the summertime of 2008 at Rail Spur (SM: Soil Moisture)

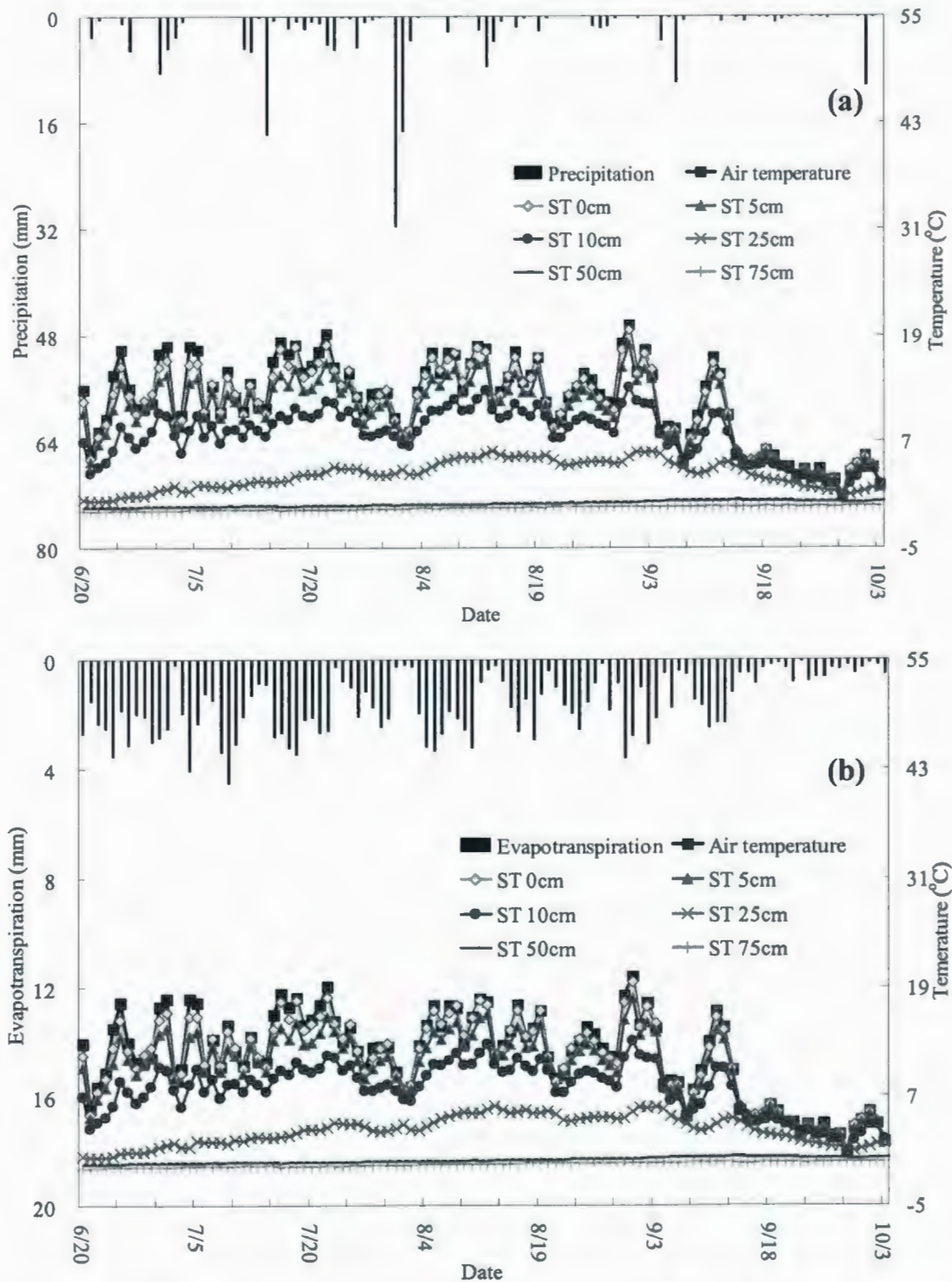


Figure 3.24 Multiple soil layers temperature, air temperature and (a) P and (b) ET in the summertime of 2006 at Rail Spur (June 20th – Oct 3rd, ST: Soil temperature; P: Precipitation; ET: Evapotranspiration)

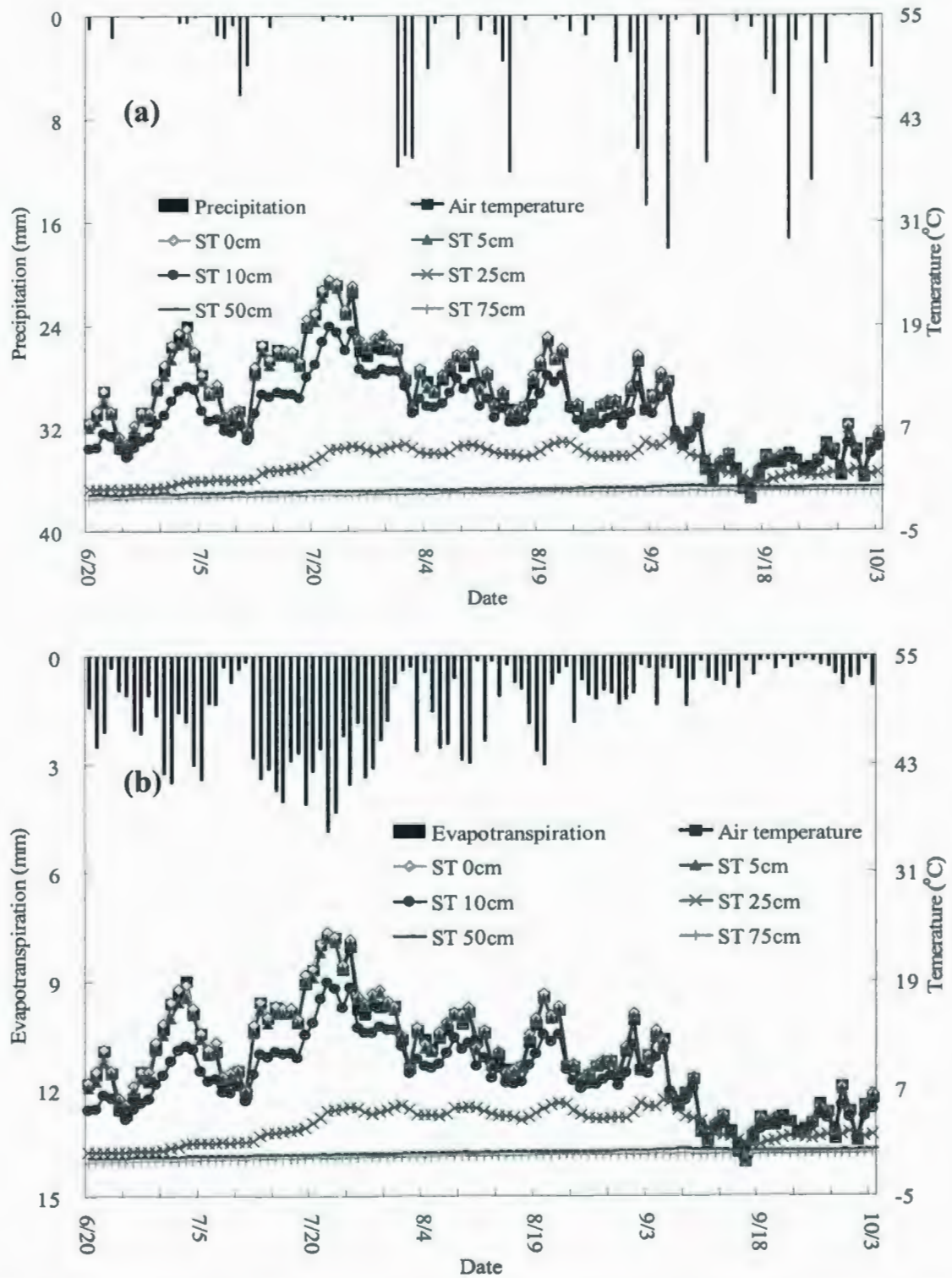


Figure 3.25 Multiple soil layers temperature, air temperature and (a) P and (b) ET in the summertime of 2007 at Rail Spur (June 20th – Oct 3rd, ST: Soil temperature; P: Precipitation; ET: Evapotranspiration)

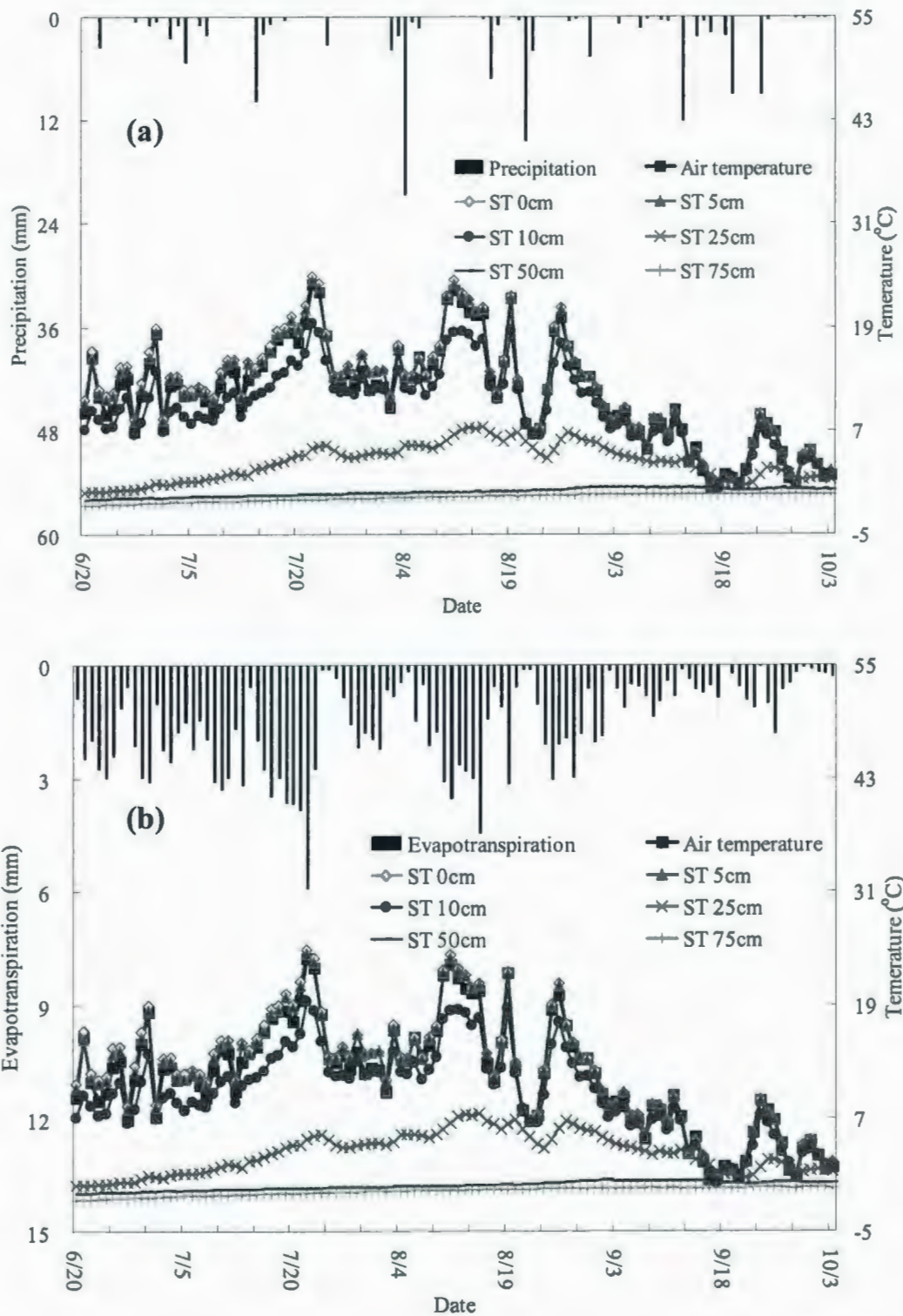


Figure 3.26 Multiple soil layers temperature, air temperature and (a) P and (b) ET in the summertime of 2008 at Rail Spur (June 20th – Oct 3rd, ST: Soil temperature; P: Precipitation; ET: Evapotranspiration)

3.4.4 Fluctuation of Water Stage and Streamflow

Based on the collected data (water stage and flow velocity) from the gauging stations between 2006 and 2008, discharge-stage and discharge-velocity relationships have been generated as illustrated in Figures 3.27 and 3.28. Generally, the discharge is exponentially proportional to the variation of flow velocity and water stage. Based on the formulated regression equations, real-time discharge can be calculated which is critical and helpful for supporting the modeling efforts in this research (Chapter 6).

Viewed from Figures 3.29 to 3.31, the water discharges at the four stations are close to zero before September and then gradually increases due to the high precipitation and lower amounts evapotranspiration. From June to August, air temperature continuously raises up, which causes frost table subsidence and active organic layer expansion. Consequently, the enlarged water storage capacity of soil layers can hold more water from both infiltration of rainfall and increase evapotranspiration opportunity time. On the other hand, precipitation is relative low before the beginning of the wet season in September. Furthermore, evapotranspiration is the most intensive within a year which accelerates the water loss to the atmosphere and reduces the surface runoff. Therefore, most of the small or moderate rainfall events do not generate obvious runoff and the streamflow remains low during the period between June and August. Similar phenomenon has also been observed and reported in a few other subarctic watersheds in Canada (Quinton and Roulet, 1998; Eaton and Rouse, 2001). After heavy rainfall start in September, along with decreased temperature and weakened evapotranspiration, this descending streamflow trend is dramatically changed and a significant increase of water discharge can be

observed. The data collected from Stations 5 and 7 in 2007 remarkably presents such a trend (Figures 3.30a and 3.30c).

When compared to precipitation, a lag time of 1-2 days between peaks of water discharge and rainfall events is observed at most of these headwater stations due to time of runoff concentration impacts. This is virtually significant after September because the raining season has much more water input. For example, when zooming into the plot of hourly precipitation and water discharge (Figure 3.32), the increase of water discharges at Stations 5 and 10 starts 1-1.5 days after the rainfall events occur on July 31st and August 15th, 2007. This delay could be attributed to the considerable water storage capacity of the organic soil layers, distances travelled in soil and channels as well as the slope.

Figure 3.33 shows the variation of water discharges of Stations 5 and 7, and Stations 6 and 10 in 2007, respectively. It is illustrated by Figure 3.4a that Stations 5 and 7 are located in the same drainage catchment which results in a similar discharge fluctuation trend (Figure 3.33a), although discharge of Station 5 behaves less sensitive to the precipitation as a stream junction. Stations 6 and 10 also have an identical discharge trend due to their close locations and affiliation to the same concentration basin (Figure 3.33b).

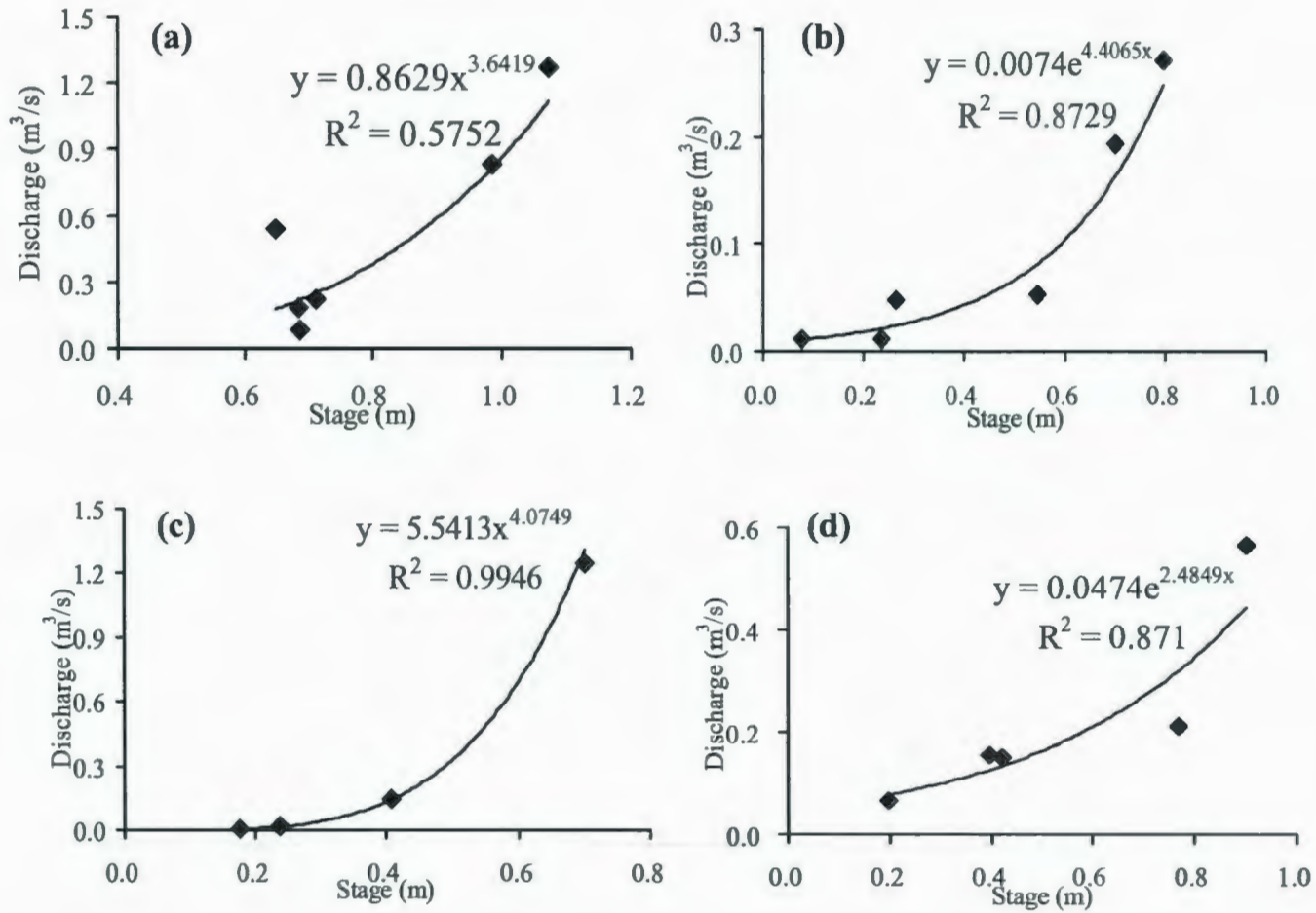


Figure 3.27 Discharge – Stage relationships of (a) Station 5, (b) Station 6, (c) Station 7, and (d) Station 10 from 2006 to 2008

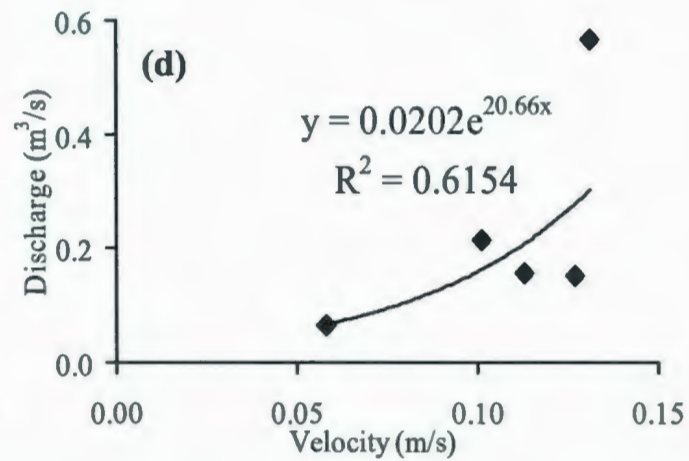
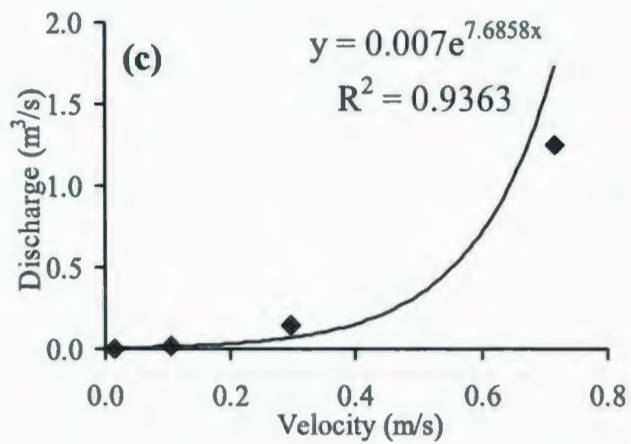
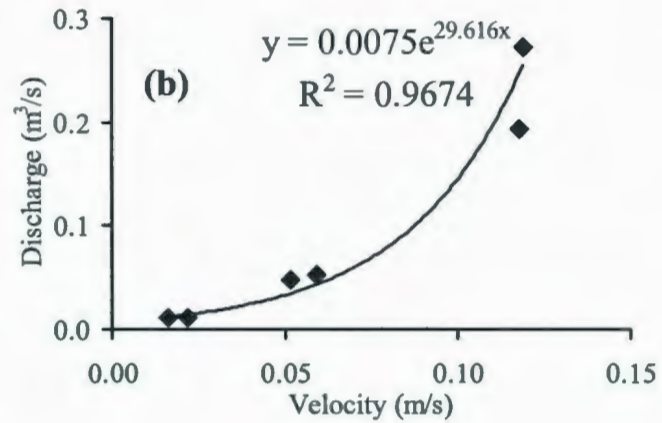
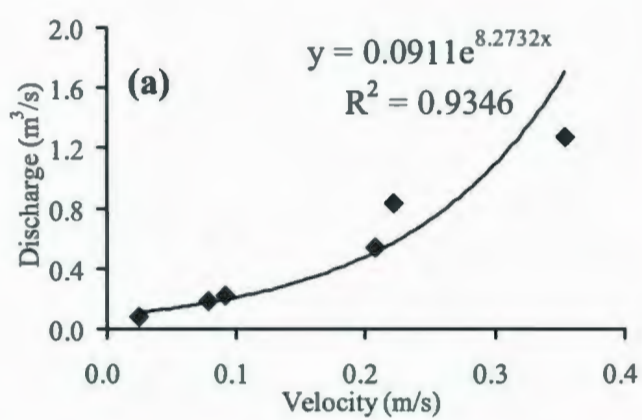


Figure 3.28 Discharge – Velocity relationships of (a) Station 5, (b) Station 6, (c) Station 7, and (d) Station 10 from 2006 to 2008

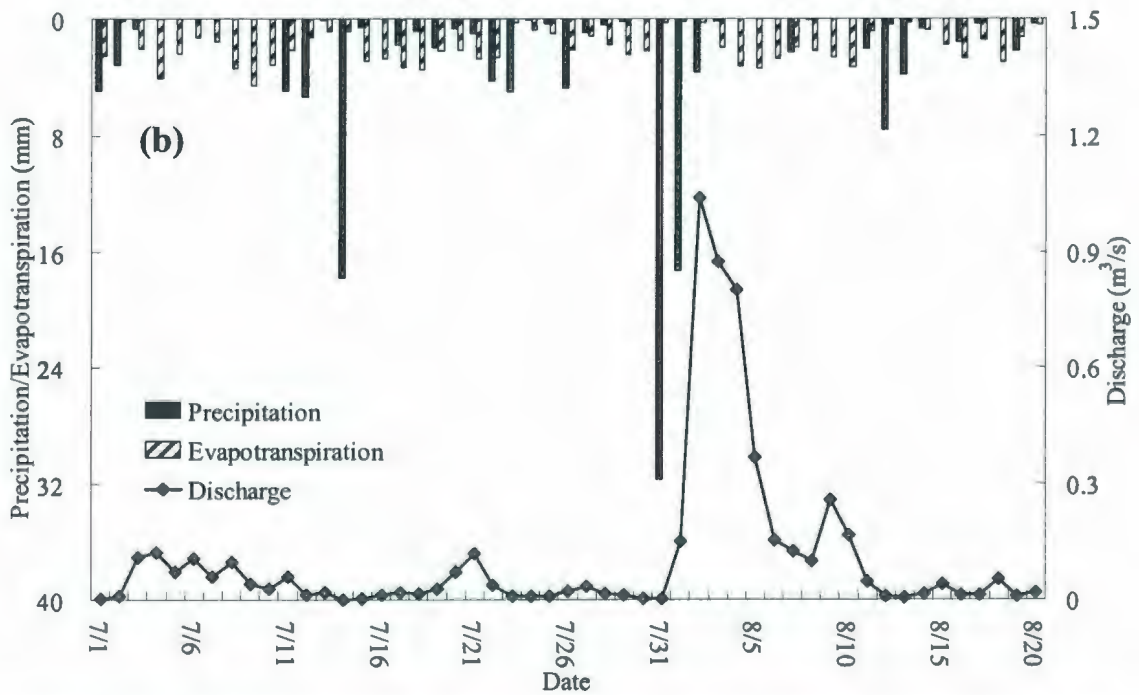
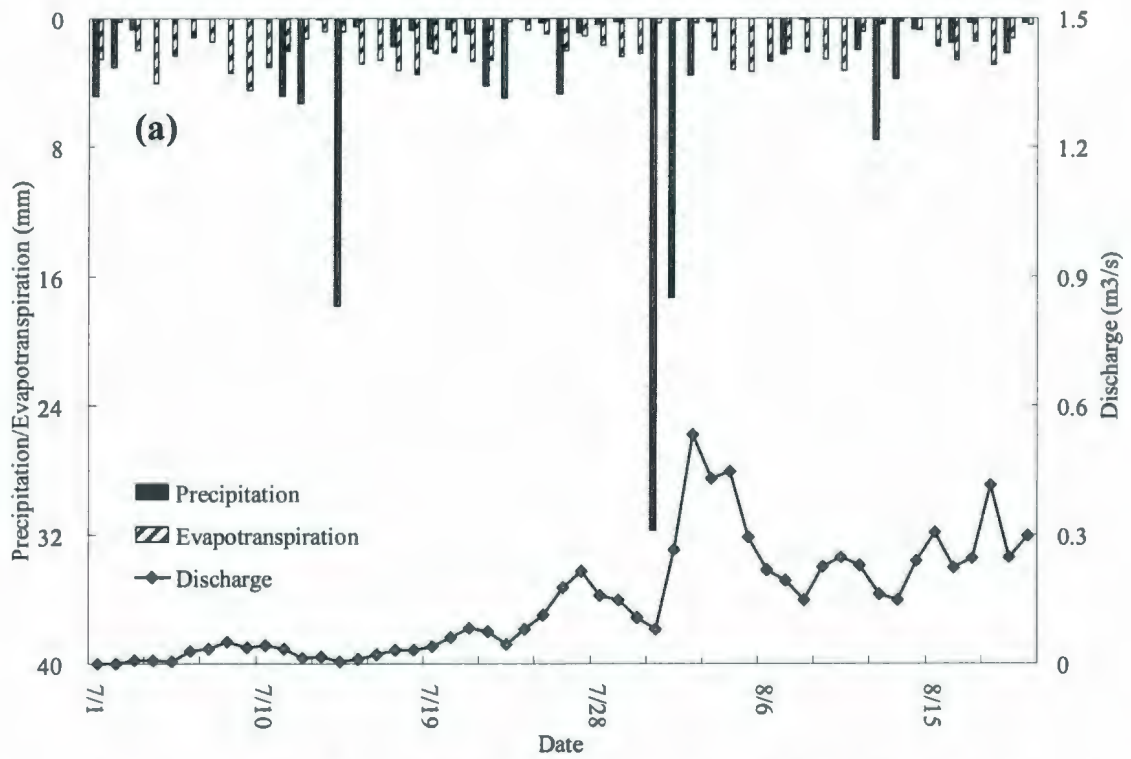
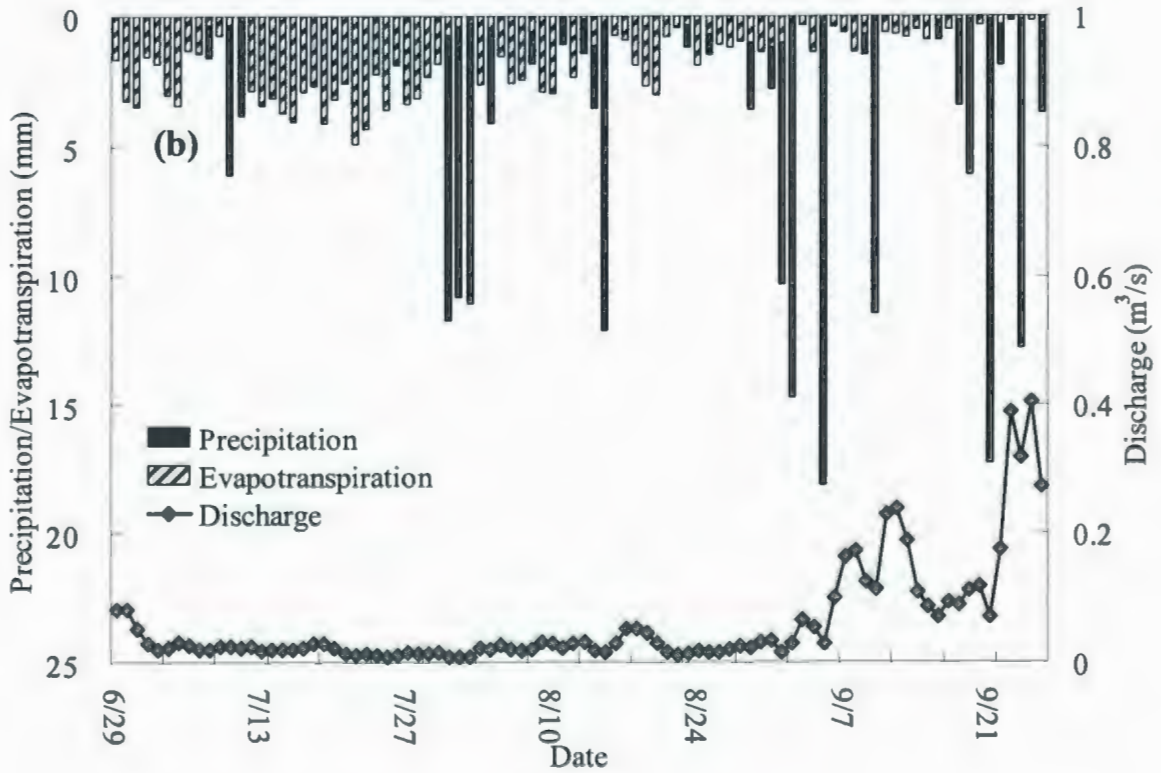
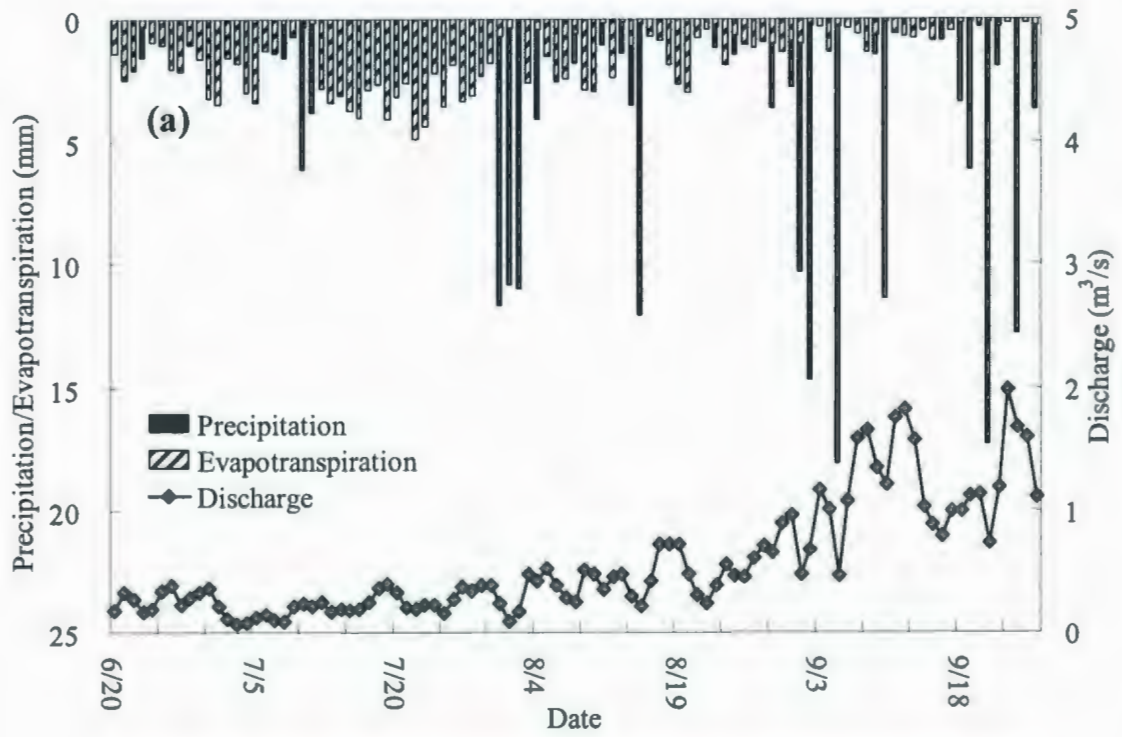


Figure 3.29 Plot of evapotranspiration, precipitation and water discharge in 2006 at (a) Stations 5 and (b) Station 7



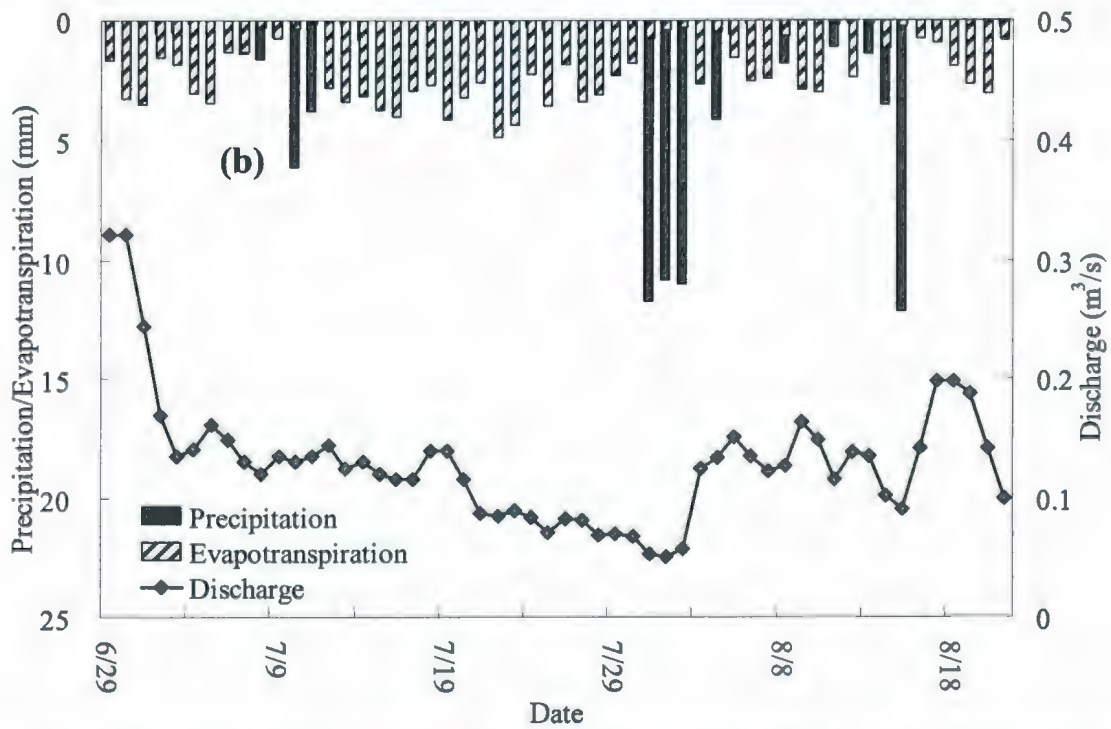
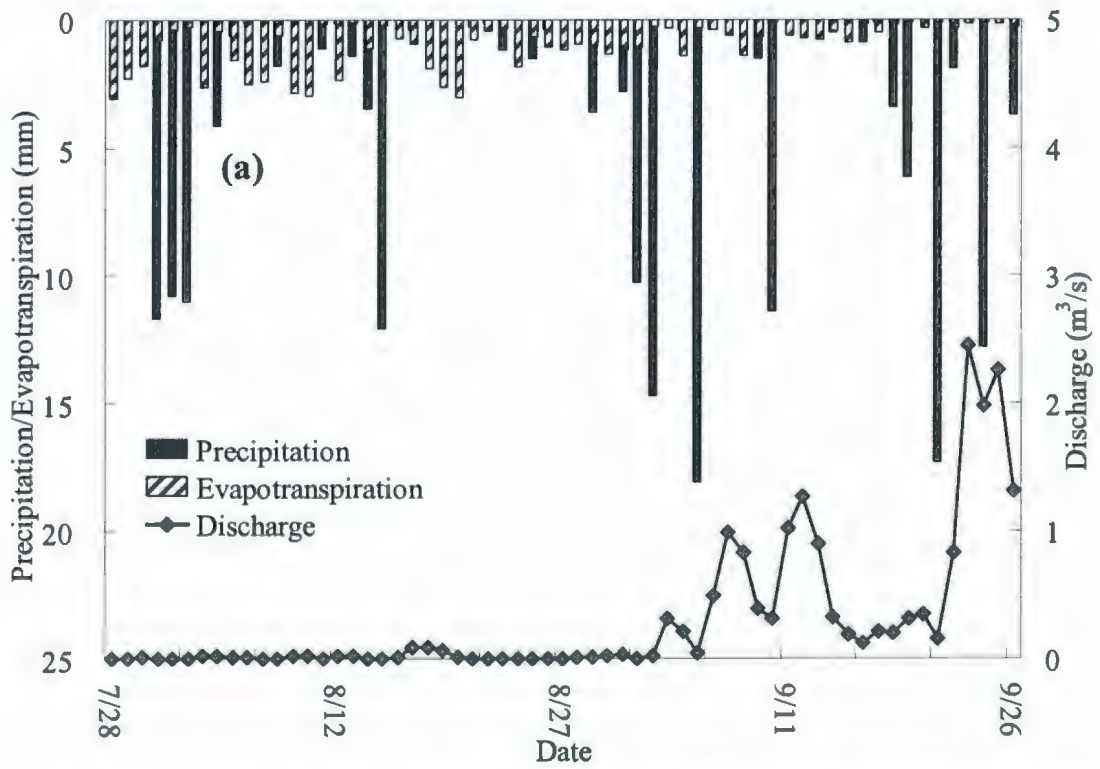


Figure 3.30 Plot of evapotranspiration, precipitation and water discharge in 2007 at (a) Stations 5, (b) Station 6, (c) Station 7, and (d) Station 10

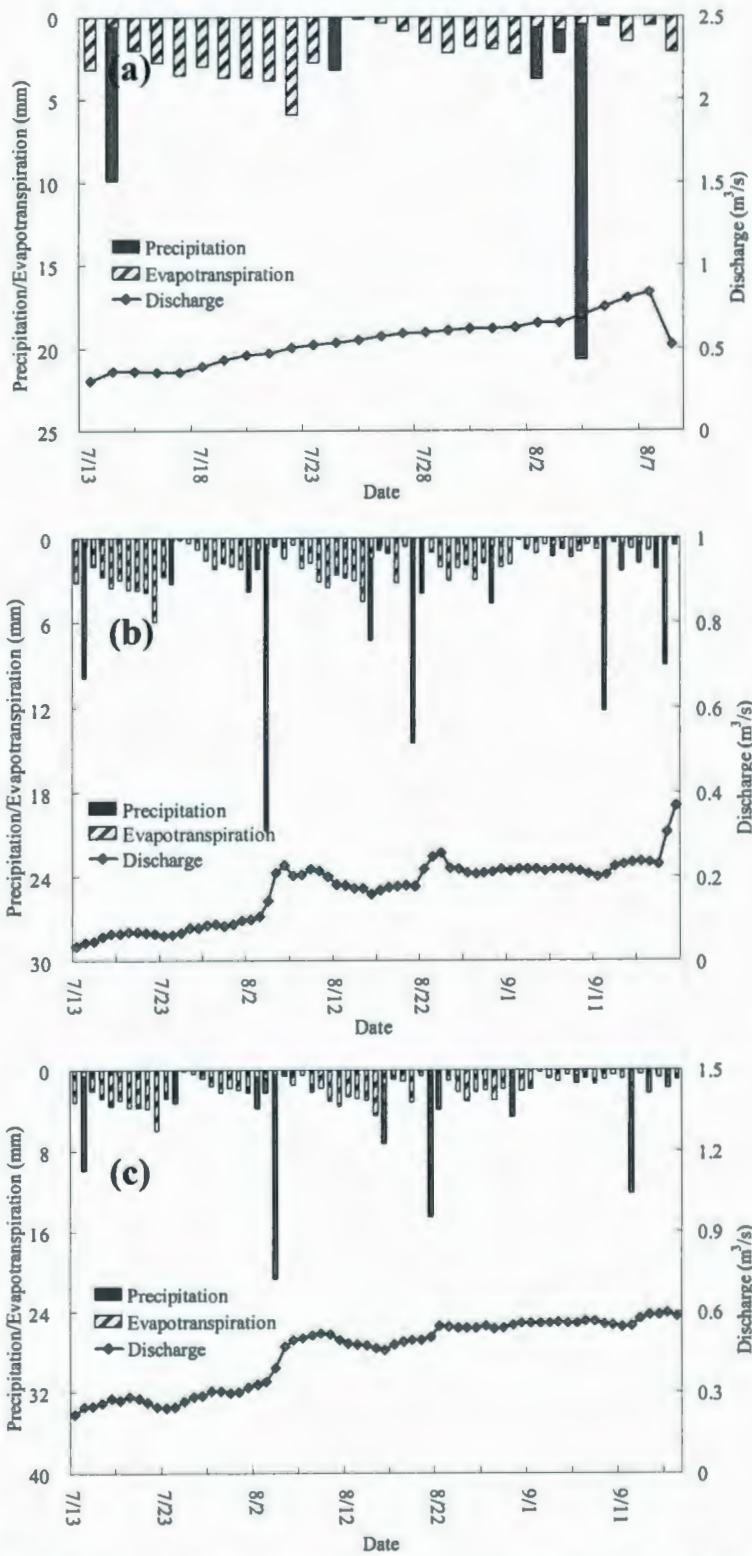


Figure 3.31 Plot of evapotranspiration, precipitation and water discharge in 2008 at (a) Stations 5, (b) Station 6 and (c) Station 10

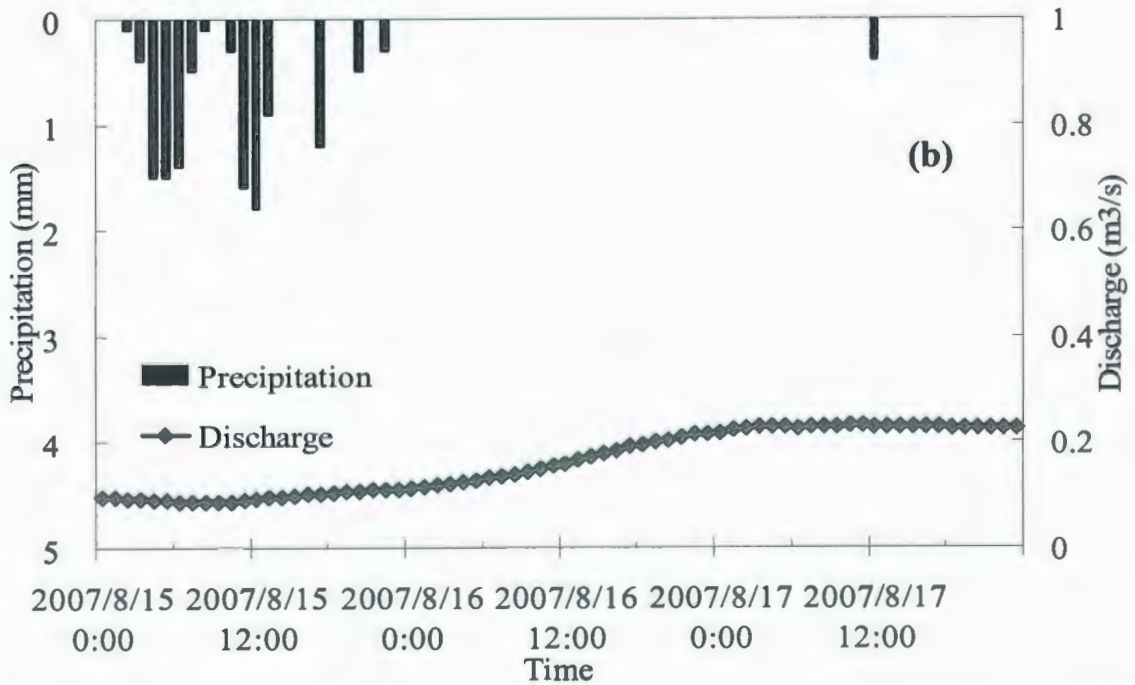
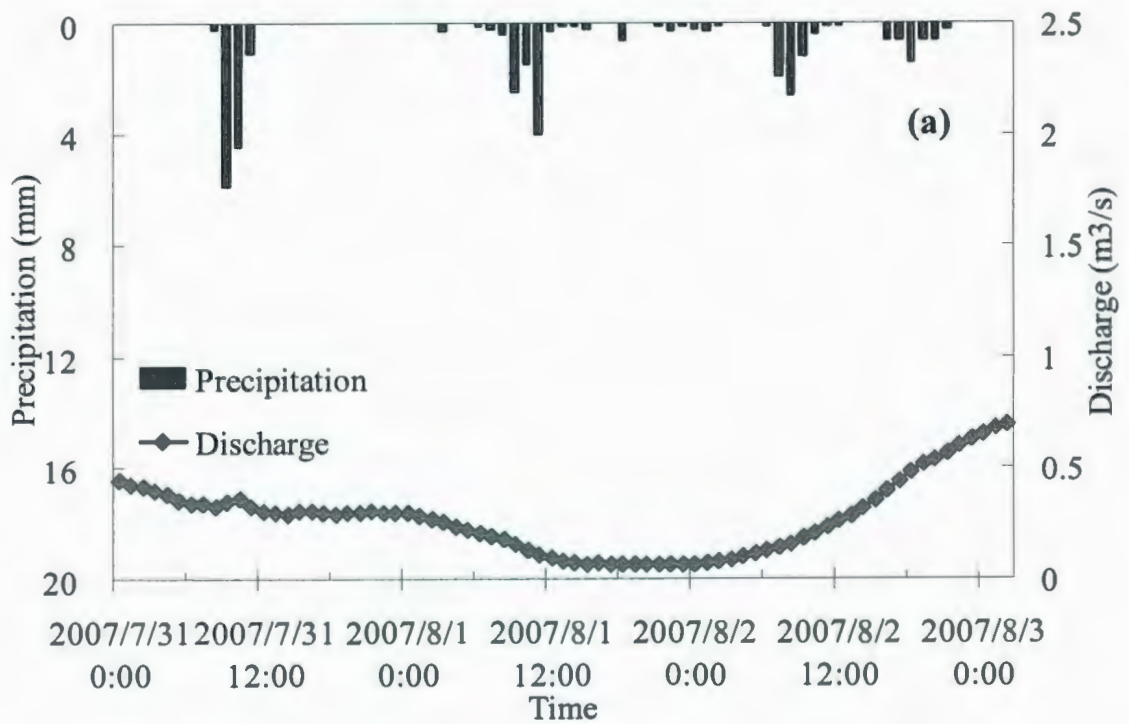


Figure 3.32 Response of hourly water discharge to precipitation at (a) Station 5 (July 31st – August 3rd, 2007) and (b) Station 10 (August 15th – August 17th, 2007)

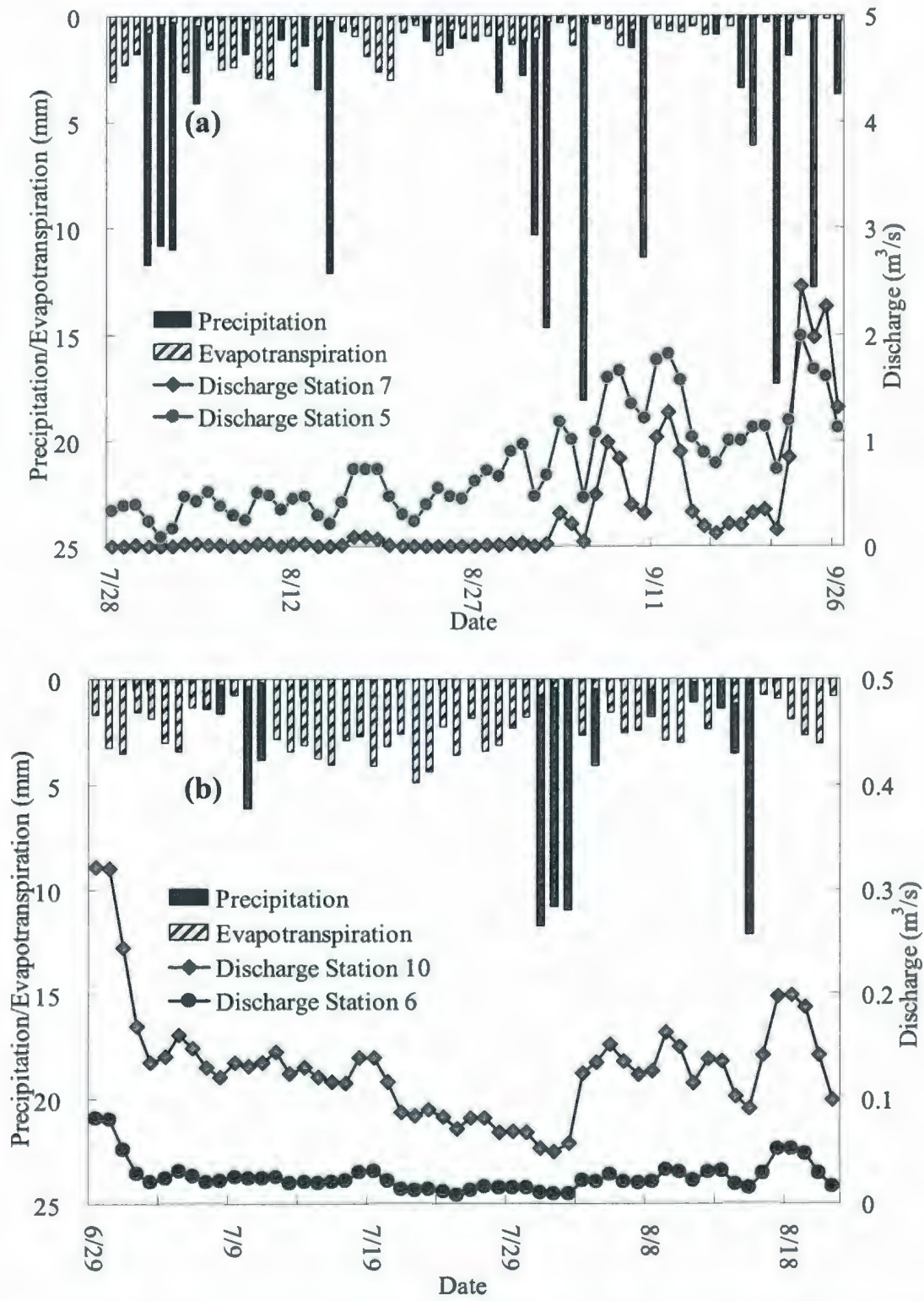


Figure 3.33 Plot of evapotranspiration, precipitation and discharge of (a) Stations 5 and (b) Station 7 in 2007

3.5 Summary

An extensive field investigation focusing on the hydrological features of the Deer River watershed near Churchill, Manitoba was conducted during the summertime from 2006 to 2008. The watershed was first delineated into sub-basins based on its distributed hydrological features and then a monitoring network was established to collect hydrological and meteorological data for an in-depth understanding of the subarctic wetland attributes and the construction of wetland hydrological models. The field activities mainly include: site investigation and background information collection; installation and maintenance of mobile weather stations and flow gauges along the streams; meteorological and hydrological measurement and data collection from the stations on a regular basis; vegetation and land cover information collection through on-site observation; and helicopter recons. Data analysis has been conducted leading to the following major conclusions:

(1) The 31-year data (1978 to 2008) at the Churchill airport presents steady increase of both mean summertime temperature and accumulative summertime precipitation, indicating a change in climatic conditions. Data from the automated weather station at Rail Spur also demonstrates this increase of air temperature and precipitation. Moreover, the 3-year observation at Rail Spur shows the same fluctuation trend between air temperature and evapotranspiration in the summertime. Precipitation also plays an important role because it determines the water availability for evapotranspiration.

(2) Summertime frost tables at stream banks show a reverse proportional relationship to their distances to the streams, indicating strong influences from the stream and subsurface flows. Besides the water percolation from the stream flow, subsurface flow penetrating the organic layer is towards the stream which may accelerate the thaw of frozen soil. Meanwhile, lower albedo vegetations and greater insulation under deeper snow cover at near stream locations may also contribute to this observance. Another interesting finding is that, the average summertime frost table in 2007 is much deeper in most stations, indicating a change of climatic conditions. It can be explained by the fact that air temperature appears as the dominant factor leading the fluctuation of frost table during the two monitoring seasons.

(3) Surface soil moisture becomes more saturated as one gets closer to the stream. This could be attributed to the extraordinarily high hydraulic conductivity and intensive water infiltration. The descending frost table explains some exceptional observance that several remote transects from the streams have higher soil moisture contents. Furthermore, the temporal differences of surface soil moisture are not as significant as spatial differences during the summertime. The automated weather station at Rail Spur also provides solid evidence of temporally stable soil moisture as well as soil temperature features in the summertime from 2006 to 2008. The primary finding is that following the major recharge period during the snowmelt, soil moisture contents at surface layers are significantly influenced by evapotranspiration and dramatically fluctuate throughout the summer. Soil temperature at the shallow layers varies continually and more or less accords with the air temperature in the summertime, whereas soil temperature at the deep layers keeps stable

(around 0 °C) which can be attributed to the fact that permafrost table lying below.

(4) The discharge-stage and discharge-velocity curves were generated based on the collected data from the gauging stations between 2006 and 2008. Throughout the monitoring season, the water discharge generally shows a descending trend before September due to low precipitation and high evapotranspiration as well as expansion of organic soil layers, and then an ascending one through to fall due to large amount of precipitation and decreasing temperature. A concentration time of 1-2 days between peaks of water discharge and rainfall events is also observed which may be attributed to the effect of enlarged water capacity of the organic layer, distances travelled in soil and channels and the slope

Two semi-distributed hydrological models, SLURP and WATFLOOD, will be applied to simulate the hydrological processes of the sub-arctic wetlands in the subsequent chapters. Chapter 4 will focus on modelling the Deer River Watershed and the Chesnaye Sub-basin by SLURP, evaluating the model's performance. Chapter 5 will apply the WATFLOOD to the Deer River Watershed and the Chesnaye Sub-basin. Modelling results will be discussed and effects from both the internal model structures and external hydrological features will be analyzed.

Chapter 4 Modelling of the Deer River Watershed by SLURP

4.1 SLURP

The Semi-distributed Land Use-based Runoff Processes (SLURP) model (Kite, 1997) is a semi-distributed, conceptual continuous hydrological model which fits between the traditional lumped models and fully-distributed models. This daily time-step model was originally developed for meso- and macroscale basins with intermediate complexity, which incorporates necessary physical processes without compromising the simplicity of calculation. SLURP can simulate the hydrological behaviour of a selected watershed, without high demands in data and computational requirements as do fully-distributed models. Basically, the simulation is based on a vertical water balance, and horizontal runoff generation within each simulation unit.

4.1.1 Vertical Water Balance Model

SLURP divides the whole watershed into multiple aggregated simulation areas (ASAs) by Topographic Parameterization (TOPAZ). The D8 flow algorithm (O'Callaghan and Mark, 1984) used in TOPAZ determines flow direction of each DEM grid to its steepest descent neighbour grids and combines related grids to form an ASA. Each ASA is subsequently divided into areas with different types of land cover based on vegetation and soil characteristics and physiographical conditions. A vertical water balance model is sequentially applied to each land cover type within each ASA which contains any number of land covers. The vertical water balance component consists of precipitation, canopy

interception, snowmelt, infiltration, surface runoff, and groundwater outflow (Figure 4.1). The first step within the vertical water balance model is to evaluate and calculate the actual evapotranspiration by either one of the following methods.

1) Complementary Relationship Areal Evapotranspiration (CRAE) model (Morton, 1983). It requires data of hours of bright sunshine and net all-wave radiation to compute the actual evapotranspiration as follows:

$$E_A = 2E_w - E_p \quad (4-1)$$

where E_A is the actual evapotranspiration (mm/day); E_w is the wet-environment evaporation (mm/day) and computed from an empirical equation using the slope of the saturation vapour pressure/temperature curve and net radiation; and E_p is potential evapotranspiration (mm/day) and calculated by solving the energy balance and aerodynamic equations at equilibrium using a modified Penman equation.

2) Granger (1995) method. It uses remotely-sensed surface temperature in a particular feedback relationship with vapour deficit. Hours of bright sunshine and global radiation data is required. Actual evapotranspiration is derived as the following equation:

$$E = \frac{\Delta G_e Q_N + \gamma G_e E_a}{\Delta G_e + \gamma} \quad (4-2)$$

where E is the actual evapotranspiration (mm/day); Δ is the slope of the vapour pressure curve (kPa/°C); G_e is the dimensionless relative evaporation; Q_N is the net radiation (mm eq./d); γ is the psychrometric constant (0.066 kPa/°C); E_a is the drying power (mm eq./d); and G is calculated from the relative drying power as the following equation:

$$G_e = \frac{1}{0.905 + 0.905^{(6.2D)}} + 0.2(1 - D) \quad (4-3)$$

where D is the relative dimensionless drying power and computed from:

$$D = \frac{E_a}{E_a + Q_N} \quad (4-4)$$

where E_a is the drying power and derived from:

$$E_a = f_u(e_a^* - e_a) \quad (4-5)$$

where e_a and e_a^* are the vapour pressure and the saturated vapour pressure at the air temperature (kPa), respectively; and f_u is a wind speed function as shown in the following equations:

$$\begin{aligned} f_u &= a_G + b_G U \\ a_G &= 8.19 + 0.22Z_a \\ b_G &= 1.16 + 0.08Z_a \end{aligned} \quad (4-6)$$

where U is the wind speed at 2 m above ground (m/s); and Z_0 is an aerodynamic roughness length for each land cover.

3) Spittlehouse (1989) method. It calculates the available energy by Priestly and Taylor (1972) approach. Available soil moisture is computed from the field capacity and root zone depth. Hours of bright sunshine and global radiation data is required. This method defines the actual evapotranspiration as a function of plant transpiration:

$$\begin{aligned} E_{\max} &= \alpha \left(\frac{s}{s + \gamma} \right) (R_n - G_s) \\ E_s &= \beta_s \left[\frac{\text{store} - \text{max} \cdot \text{wilt}}{\text{max}(\text{field} - \text{wilt})} \right] \end{aligned} \quad (4-7)$$

where α is the Priestley-Taylor coefficient; s is the slope of the vapour pressure curve (kPa/°C); γ is the psychrometric constant (0.066 kPa/°C); R_n is the net radiation (mm eq./d); G_s is the soil heat flux (mm eq./d); E_{max} is the energy limited transpiration rate (mm); β_s is an empirical coefficient; *store* and *max* are the current and maximum possible soil water contents (mm); *field* and *wilt* are the field capacity and wilting point as fractions; E_s is the soil limited transpiration rate (mm); and E_t is the actual transpiration rate (mm) and defined as the lesser of E_{max} and E_s . Total evapotranspiration is the sum of E_t and E :

$$E = gL \quad (4-8)$$

$$E_{total} = E + E_t \quad (4-9)$$

Where E is the actual evaporation (mm); and L is the depth of water in the canopy (mm).

Precipitation is intercepted by the canopy. The following equation illustrates how much water can pass through the vegetation (Spittlehouse, 1989):

$$I = A' \times LAI \times P^{B'} \quad (4-10)$$

where P is the total precipitation (mm); I is the intercepted precipitation (mm); A' and B' are coefficients; and LAI is the leaf area index of the canopy. Yin and Williams (1997) suggested that LAI can be calculated from $NDVI$ (Normalized Difference Vegetation Index):

$$LAI_i = LAI_{max} \times \frac{(NDVI_i - NDVI_{min})}{(NDVI_{max} - NDVI_{min})} \quad (4-11)$$

where i is the current value and *max* and *min* indicate the maximum and minimum values of $NDVI$, respectively. $NDVI$ is calculated from below:

$$NDVI = \frac{NIR - R}{NIR + R} \quad (4-12)$$

where *NIR* is the near infrared pixel intensity (band 2) and *R* is the pixel intensity in the red visible range (band 1).

Any precipitation will be in the form of snowfall if the daily mean temperature is below or equal to the critical temperature, which is the equilibrium point between water phase and snow phase. When the daily mean temperature exceeds the critical temperature, the snowpack will start to be depleted by the following degree-day snowmelt equation which has been chosen in this study (Anderson, 1973):

$$S_m = R_1 (T - T_{critical}) \quad (4-13)$$

where *T* and *T_{critical}* are the air temperature and melting temperature(°C); *S_m* is the daily snowmelt rate (mm/day); and *R₁*, the melt rate (mm/day/°C) on any day, is calculated from a parabolic interpolation from values for each land cover on January 1st and July 1st as:

$$\begin{aligned} R_1 = & \frac{1}{33306} \times (Jan_value - July_value) \times (Day_no)^2 \\ & + \frac{367}{33306} \times (July_value - Jan_value) \times Day_no \\ & + \frac{1}{91} (92 \times Jan_value - July_value) \end{aligned} \quad (4-14)$$

where *Jan_value* and *July_value* are the snowmelt rate of each land cover on January 1st and July 1st, respectively; *Day_no* is the Julian day of each year. A simplified energy budget method may also be used as the following equation states (Kustas *et al.*, 1994):

$$S_m = R_2 (T - T_{critical}) + \alpha_c Q_n \quad (4-15)$$

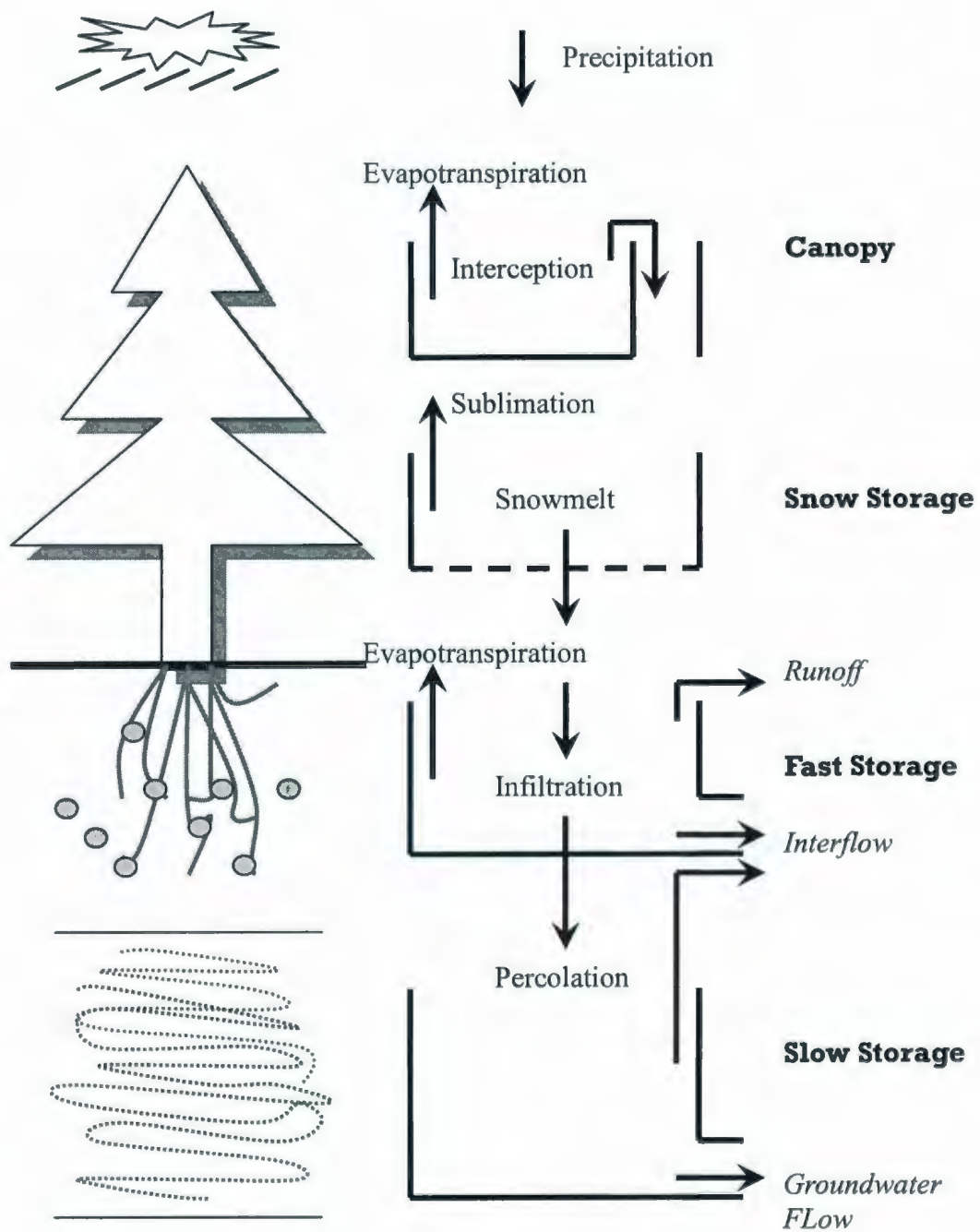


Figure 4.1 Schematic of the SLURP vertical water balance model (Kite, 1997)

where R_2 is the restricted degree-day snowmelt rate and recommended as 2.0 mm/day/°C by Brubaker *et al.*, (1996); Q_n is the net radiation (MJ/m²/day); and α_c is the conversion factor and used as 0.26 mm/W/m²/day by Brubaker *et al.*, (1996).

The subsurface flow processes are simulated between the fast storage and the slow storage which account for the aerated soil layer and groundwater layer, respectively. Rainfall or snowmelt water penetrating from ground surface to the fast storage obeys:

$$Inf = \left(1 - \frac{S_1}{S_{1,max}}\right) \times Inf_{max} \quad (4-16)$$

where S_1 and $S_{1,max}$ are the current contents and maximum capacity of the fast storage (mm), respectively; Inf and Inf_{max} are the current and maximum infiltration rates (mm/day), respectively. The outflow from rapid storage $Q_{1,out}$ can be calculated by:

$$Q_{1,out} = \frac{1}{k_1} \times S_1 \quad (4-17)$$

where k_1 is the retention constant for fast store (day). As Figure 4.1 shows, the outflow from fast storage is separated to percolation and interflow with a ratio as follows:

$$\frac{RP}{RI} = \frac{S_1 / S_{1,max}}{S_2 / S_{2,max}} \quad (4-18)$$

where S_2 and $S_{2,max}$ are the current contents and maximum capacity of the slow storage (mm), respectively; RP and RI stands for percolation and interflow (mm/day), respectively. Groundwater flow is also generated from water percolation by:

$$RG = \frac{1}{k_2} \times S_2 \quad (4-19)$$

where RG is the groundwater flow (mm/day); and k_2 is the retention constant for slow

store (day).

4.1.2 Horizontal Water Budget

After the simulation of vertical water balance, the horizontal water budget can be calculated. Surface runoff, interflow and groundwater flow are first accumulated from each land cover type within each ASA. The combined outflow is converted and accumulated to stream flow and eventually routed to the outlet of the watershed. Runoff from each land cover type within an ASA is routed to the nearest channel and finally to the outlet of the ASA. Manning's equation (Kite, 1997) is used to calculate the average flow velocity over land cover type which can be used to determine the time required to reach the channel:

$$V = (1.49/n)R_v^{2/3}(H_v/L_v)^{1/2} \quad (4-20)$$

where V is the average velocity of the flow from each land cover type to the channel (m/s); n is the Manning's roughness coefficient for each land cover (Table 4.1); R_v is the hydraulic radius (m); H_v and L_v account for the average change in elevation over distance and the distance to the nearest channel (m), respectively. On the other hand, travel time along the channel to the final outlet is computed based on the average distance to the outlet, the slope and the flow velocity over each land cover.

The accumulated flow from the outlet of an ASA has to be routed to the outlet of the downstream ASA based on the flow direction. Two approaches are provided in SLURP to generate the flow direction and network: hydrological storage routing method (Kite,

1997), which has been chosen in this research, and Muskingum-Cunge channel routing method (Cunge, 1967). Storage routing method is simple but sacrifices accuracy, which can be presented as follows:

$$Q_{out} = \alpha_l S_s^{\beta_a} \quad (4-21)$$

$$S_s = (Q_{in} / \alpha_l)^{1/\beta_a} \quad (4-22)$$

where Q_{in} and Q_{out} are inflow and outflow (m^3/s), respectively; S_s is the storage (m^3); and α_l and β_a are the degrees of lag and attenuation required, respectively.

Muskingum-Cunge channel routing method could be selected whenever channel characteristic data including length, slope, average width, depth and roughness are available. It is assumed that depth and discharge have a single-valued relationship and the classic kinetic wave equation is appropriate to be used. The outflow at time 2, O_2 can be calculated from:

$$O_2 = C_1 I_1 + C_2 I_2 + C_3 O_1 + C_4 \quad (4-23)$$

where I_1 and I_2 are inflows at times 1 and 2 (m^3/s), respectively; O_1 is the outflow at time 1 (m^3/s); and C_1 , C_2 , C_3 and C_4 are constants which can be obtained by:

$$\begin{aligned} C_0 &= K_1 - K_1 X + \Delta t / 2 \\ C_1 &= -(K_1 X - \Delta t / 2) / C_0 \\ C_2 &= (K_1 X + \Delta t / 2) / C_0 \\ C_3 &= (K_1 - K_1 X + \Delta t / 2) / C_0 \\ C_4 &= 0.5(q_1 + q_2) \Delta x \Delta t / C_0 \end{aligned} \quad (4-24)$$

where K_1 is the storage constant and calculated by:

$$K_1 = \Delta x / c_s \quad (4-25)$$

where c_s is the kinetic wave speed (m/s) and calculated from

$$c_s = 1.27 \beta_s \frac{S_0^{0.3}}{q_0^{0.4}} n^{0.6} \quad (4-26)$$

where β_s is shape constant and set to 5/3 for rectangular channel; q_0 is a unit-width reference discharge (m^3/s); n is the Manning's roughness coefficient; and Δx is the channel length (m). X is the weighting constant and computed by:

$$X = 0.5 \left[1 - \frac{q_0}{c_s S_0 \Delta x} \right] \quad (4-27)$$

where S_0 is the channel bottom slope (dimensionless).

Table 4.1 Manning's roughness coefficient for different land covers (Parmley, 2000)

Types of land cover	Manning's roughness coefficient (n)
Floodplains – farmland	0.035
Floodplains – light brush	0.050
Floodplains – heavy brush	0.075
Floodplains – trees	0.15
Mountain streams with rocky beds	0.04 - 0.05
Straight, unlined earth canals	0.020
Natural streams – with little vegetation	0.025
Natural streams – clean and straight	0.030
Natural streams – major rivers	0.035
Natural streams – sluggish with deep pools	0.040

4.2 Watershed Delineation by TOPAZ

A 3 arc second (approximately 90 m) resolution DEM for the Deer River Watershed was obtained from the National Map Seamless Server of the USGS (USGS, 2007). There are 1801 columns and 1601 rows in the DEM. The DEM was subsequently processed by TOPAZ which has strong capability of automated digital landscape analysis. There are four subroutines in TOPAZ have been operated to get the delineated sub-watersheds: DEDNM, RASBIN, RASPRO and RASFOR.

Figure 4.2 shows the delineated sub-watersheds of the Deer River Watershed in which No.18 sub-watershed has a national stream gauging station (D. River N. Belcher, ID: 06FD002). The historical records of stream discharge were used for calibration and verification process in the modelling work. Figure 4.3 displays the river network of the Deer River Watershed generated by TOPAZ.

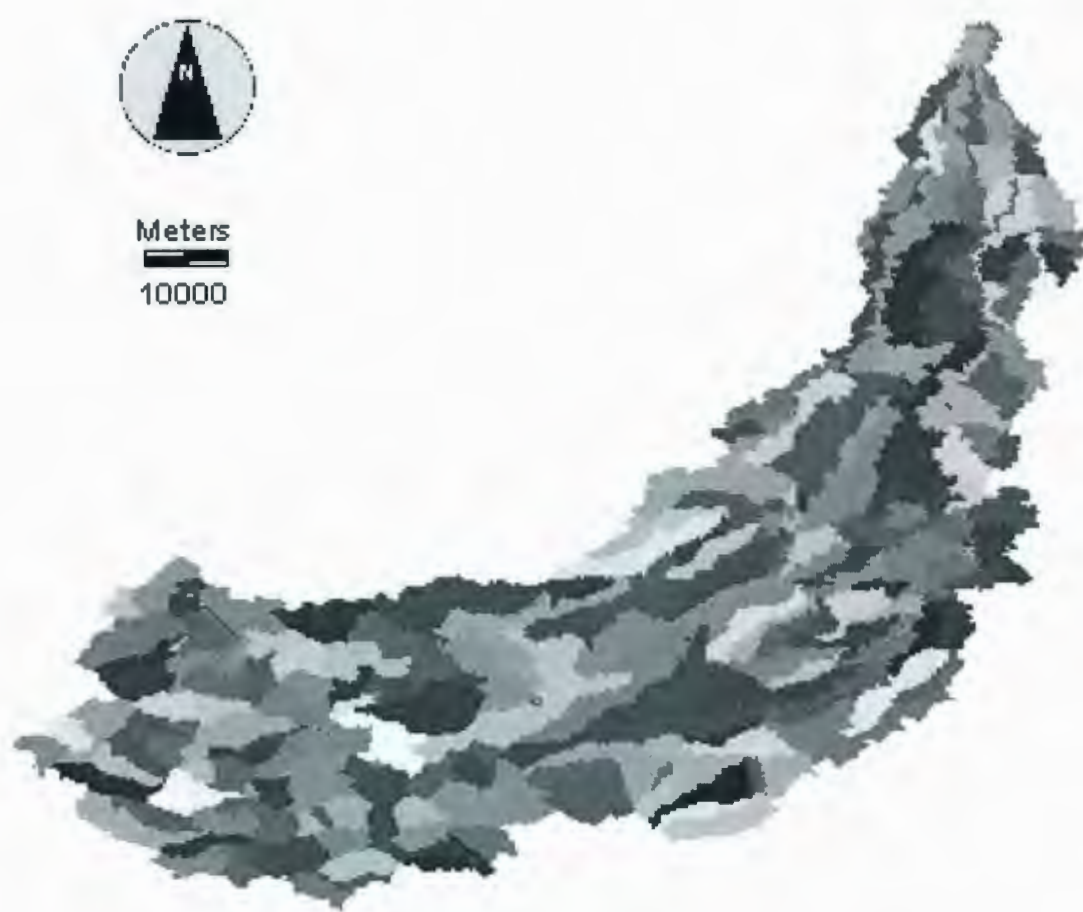


Figure 4.2 Delineation of the Deer River Watershed through TOPAZ

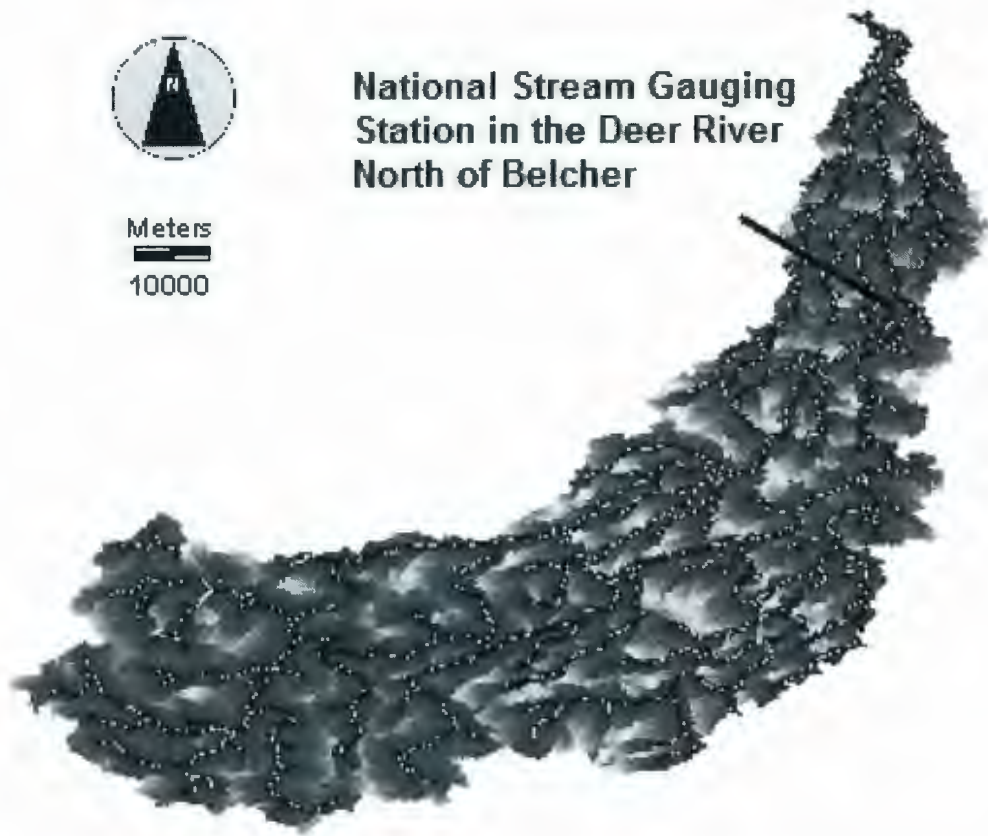


Figure 4.3 River network of the Deer River Watershed generated by TOPAZ

4.3 Land Cover Classification

The land cover dataset (1 km resolution) of the Deer River Watershed was obtained from the SPOT vegetation program (SPOT IMAGE and VITO, 2008). Original NDVI (Normalized Difference Vegetation Index) of July, 2007 was calculated from the dataset by the following equation because there is no snow interference in the summertime:

$$\text{Original_NDVI} = 0.004 \times \text{digit} - 0.1 \quad (4-28)$$

where *digit* is the value from the satellite dataset.

As Figure 4.4 shows, the DEM grids (90 m × 90 m) covering the watershed were assigned with the converted final NDVI values based on the original NDVI values (1 km × 1 km). Each of the original NDVI value was uniformly distributed to 11 × 11 grids. There was 10 m error for distributing each original NDVI to the DEM grids and it was reasonably acceptable. The next step is to classify the NDVI class in order to divide the entire watershed into different types of land cover including water, impervious, marsh, shrub, coniferous and deciduous. Based on the assumption that land cover of the Deer River Watershed has not changed during the past three decades, the converted NDVI values varied from 0.05 to 0.72. Values close to zero represent water and higher value stand for more flourished vegetation. Based on some previous studies (Wang *et al.*, 2003; Guerschman *et al.*, 2003; St Laurent and Valeo, 2007), the classification criteria for the Deer River Watershed were optimized during the model's calibration running and Table 4.2 shows the criteria for the land cover classification.

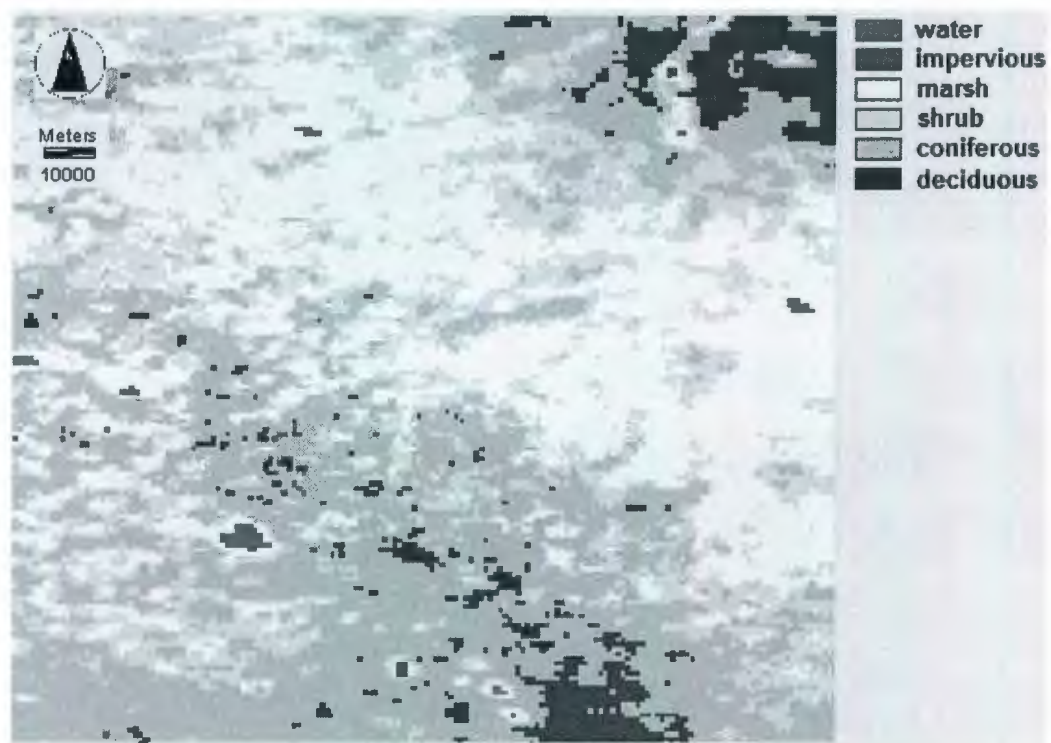


Figure 4.4 Land Cover Classification of the Deer River Watershed by IDRISI®

Table 4.2 Optimized criteria for the land cover classification

Land covers	NDVI* values	
	Lower bound	Upper bound
Water	0.05	0.20
Impervious	0.20	0.30
Marsh	0.30	0.50
Shrub	0.50	0.54
Coniferous	0.54	0.62
Deciduous	0.62	0.72

* Normalized Difference Vegetation Index

4.4 Meteorological and Streamflow data

Meteorological data (1978 – 2004) of Churchill-A Climate Station (ID: 5060600) was purchased from Environment Canada, including daily average temperature, daily accumulated precipitation, daily net radiation, and hourly dew point temperature. Data (1978 – 2004) from the climate station in the town of Churchill (approximately 80 km northwards) was used for modelling work. This station is the only available and nearest station which is a major limitation of this research because it could cause some inaccuracy to the modelling results. All the hourly data was also converted to daily average. Streamflow data (1978 – 2004) was obtained from the gauging station (ID: 06FD002) of Water Survey Canada near Belcher (Figure 4.3, 58°0'54" N 94°11'44" W).

SLURP requires each ASA to be assigned a value from the gauging stations. It weights the contribution from each station by the percentage of grids, which have the closest distance to each station, in the DEM within one ASA. For example, an ASA has 1,000 grids on the DEM. There are three climatic stations (A, B and C) outside or inside this ASA and the distances between each grid and each station are computed. If the results show that 400, 300 and 300 grids are closer to Station A, Station B and Station C, respectively, the final meteorological parameters (e.g. rainfall and temperature) for the whole ASA can be calculated as the sum of 40%*Station-A values, 30%*Station-B values and 30%*Station-C values.

4.5 Sensitivity Analysis

SLURP is a distributed conceptual model which lies between lumped basin models and fully-distributed physically-based models. All the parameters of SLURP have been tested by sensitivity analysis to examine their significance and impacts on modelling results. The parameters were individually adjusted by $\pm 5\%$, $\pm 15\%$ and $\pm 30\%$ and the results were represented by the fluctuation of modelling efficiency. This might not be appropriate because it sacrifices the interrelationship between some parameters. However, due to the time restriction and the complexities of the models, more advanced sensitivity analysis are not able to be conducted. This could be a limitation of this thesis. The Nash and Sutcliffe efficiency (*NSE*) was calculated by the following equation and used as statistical measurement for the goodness of fit of the SLURP:

$$NSE = 1 - \frac{\sum (Q_0 - Q_m)^2}{\sum (Q_0 - Q_{average})^2} \quad (4-29)$$

where Q_0 is the daily observed flow (m^3/s); Q_m is the daily modeled flow (m^3/s); and $Q_{average}$ is the mean observed flow (m^3/s).

Table 4.3 shows the results of sensitivity analysis which indicate that maximum infiltration rate (saturated hydraulic conductivity), retention constant for fast store, maximum capacity for fast store, retention constant for slow store, maximum capacity for slow store, precipitation factor, rain/snow division temperature and snow melt rate in July play significant roles in SLURP. However, precipitation factor is used to compensate the precipitation gauge and since there is no need to calibrate the obtained meteorological

data, it should be set to 1.0 here. Maximum infiltration rate, maximum capacity for slow store and rain/snow division temperature are the three most influential factors (Figure 4.5) among which maximum infiltration rate dominates the infiltration process of SLURP and has the greatest influence (-13.0%) on the modelling efficiency. Snow melt rate in July was manually calibrated and set to 4.0, 3.0 and 2.0 mm/°C/day for water/impervious/marsh, shrub, and coniferous/deciduous areas, respectively (Metcalf and Buttle, 2001).

Hence, the parameters calibrated in the automatic optimization runs of SLURP include (from the most significant to the least significant):

- A. Maximum capacity for slow store
- B. Rain/snow division temperature
- C. Maximum infiltration rate
- D. Retention constant for fast store
- E. Maximum capacity for fast store
- F. Retention constant for slow s

Table 4.3 Sensitivity analysis of SLURP parameters
(The first 10 parameters in bold font can be automatically optimized in the model)

Variation of parameters	↓30%	↓15%	↓5%	↑5%	↑15%	↑30%
Variation of Modelling Efficiencies (%)						
Initial contents of snow store (mm)	+1.5	+0.9	+0.3	-0.3	-1.2	-2.8
Initial contents of slow store (%)	+1.2	+0.7	+0.2	-0.2	-0.7	-1.6
Maximum infiltration rate (mm/day)	-10.4	-3.6	-0.8	+0.5	+1.3	+1.2
Manning's roughness coefficient	0	0	0	0	0	0
Retention constant for fast store (day)	+4.3	+2.3	+0.6	-0.7	-2.5	-4.9
Maximum capacity for fast store (mm)	-4.9	-1.7	-0.4	+0.3	+0.9	+1.4
Retention constant for slow store (day)	-2.0	-0.9	-0.2	+0.2	+0.7	+1.2
Maximum capacity for slow store (mm)	-3.4	-5.0	+0.2	-0.3	-9.8	-13.0
Precipitation factor	-17.1	-7.6	+1.0	-2.2	-20.7	-48.9
Rain/snow division temperature (°C)	-5.0	-6.0	+0.3	-0.3	-8.4	-9.7
Canopy interception A	+2.4	+0.7	+0.2	0	0	0
Canopy interception B	+3.1	+2.1	+0.3	0	0	0
Land cover albedo	0	0	0	0	0	0
LAI in Jan	-0.3	-0.1	-0.1	+0.1	+0.1	+0.3
LAI in Jul	-0.1	-0.1	-0.1	0	0	-0.1
Maximum canopy capacity	-0.2	-0.1	-0.1	+0.1	+0.1	+0.1
Soil heat flux amplitude	0	0	0	0	0	0
Snow melt rate in July (mm/°C/day)	-5.8	-2.7	-0.8	+0.4	+0.5	-1.1
Maximum albedo of snow	0	0	0	0	0	0
Minimum albedo of snow	0	0	0	0	0	0
Temperature lapse rate (°C/100 m)	0	0	0	0	0	0

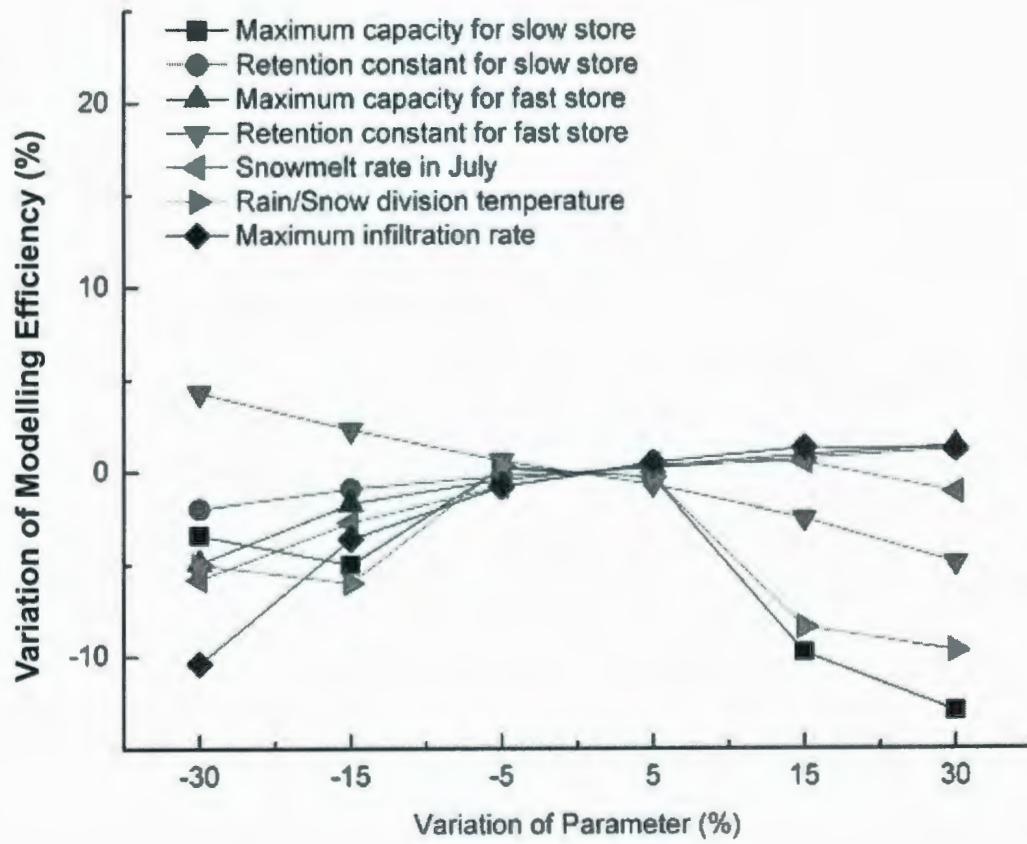


Figure 4.5 Sensitivity analysis of the key parameters of SLURP

4.6 Calibration

Calibration was conducted by using the first 10-year data (1978 – 1987) by both manual adjustments the built-in module of SLURP. All the parameters were calibrated and assigned reasonable values by taking reference from literatures (Su *et al.*, 2000; Metcalfe and Buttle, 2001; Kite, 2002; Thorne, 2004; Woo and Thorne, 2006; St Laurent and Valeo, 2007). After the optimization run, the final values of the parameters are listed in Table 4.4. It should be noted that the initial contents of snow store and slow store were set to close to zero as recommended by Kite, 2002. Figures 4.6 to 4.15 show the daily model outputs during the calibration period (1978 – 1987). Table 4.5 reports the modelling NSE efficiencies and deviation of runoff volume (DV) of all the calibration years. The NSE value lies in between 0 and 1. The closer it is to 1, the better performance the model has. DV represents the difference between standard deviations of both annual simulated and observed runoff, indicating whether the model overestimates or underestimate the runoff.

The model's overall efficiency (52%) is not high and it may be due to the combined effects from not considering the existence of the frost table and ponds, underestimating the water storage capacity of the soil and the errors of the built-in snowmelt routine. However, it performs well in some years. For instance, in 1979, the modelling efficiency reaches 76% with accurate estimation of spring runoff, implying the simulated flow matches well with the observed one (Figure 4.7). The DV values indicate that the annual runoff volumes for most of the calibration years are underestimated for the Deer River (Table 4.5). For example, in 1983, the annual DV is -55.2% which implies that the

fluctuation of the simulated flow is not as intensive as that of the observed flow. This may be explained by the effect of permafrost layer which blocks the percolation of precipitation and snowmelt water and increases the runoff in the watershed during the snowmelt period. On the other hand, not removing enough volume of water from the system through the process of evapotranspiration can also overestimate the runoff during the summer period (Figures 4.10, 4.11 and 4.15). Figures 4.16 and 4.17 show the monthly and annual model outputs during the calibration period (1978 – 1987), respectively. Table 4.6 reports the modelling efficiencies and DV of monthly and annual results. The monthly modelling efficiency (47%) and DV (-39.1%) are slightly lower than the average daily modelling efficiency (52%) and DV (-44.9%) which means monthly modelling results match well with the daily results. It can be concluded that SLURP is not accurate in simulating the snowmelt process and rainfall events in the sub-arctic wetlands because it is not appropriate for the particular region with relatively high water storage capacity and permafrost.

Table 4.4 Final Values of the parameters for each land cover use for modelling the Deer River Watershed

	Water	Impervious	Marsh	Shrub	Coniferous	Deciduous
Initial contents of snow store (mm)	1	1	1	1	1	1
Initial contents of slow store (%)	9.775	8.625	4.238	6.839	5.895	6.205
Maximum infiltration rate (mm/day)	100.9	142.4	106.9	147.7	111.9	105.7
Manning roughness n	0.02	0.08	0.01	0.07	0.02	0.03
Retention constant for fast store (day)	36.97	52.62	5.447	7.480	62.89	40.45
Maximum capacity for fast store (mm)	95.35	133.8	531.2	583.6	373.7	697.0
Retention constant for slow store (day)	130.7	171.0	686.1	745.5	713.0	747.1
Maximum capacity for slow store (mm)	338.7	260.6	361.6	102.9	62.19	63.22
Precipitation factor	1	1	1	1	1	1
Rain/snow division temperature (°C)	-0.03	-0.56	-0.99	-0.93	-0.61	-0.32
Canopy interception A	0	0.5	1	1	1	1
Canopy interception B	1	1	1	1	1	1
Land cover albedo	0	0.15	0.15	0.14	0.13	0.16
LAI in Jan	0	0	2	0.5	5	3
LAI in Jul	0	2	2	4.5	5	10
Maximum canopy capacity	0	2.8	3.8	6.2	5.6	4.3
Soil heat flux amplitude	0.15	0.15	0.15	0.15	0.15	0.15
Snow melt rate in July (mm/°C/day)	4	4	4	3	3	2
Maximum albedo of snow	0.78	0.78	0.78	0.7	0.7	0.7
Minimum albedo of snow	0.37	0.37	0.37	0.37	0.37	0.37
Temperature lapse rate (°C/100 m)	0.75	0.75	0.75	0.75	0.75	0.75

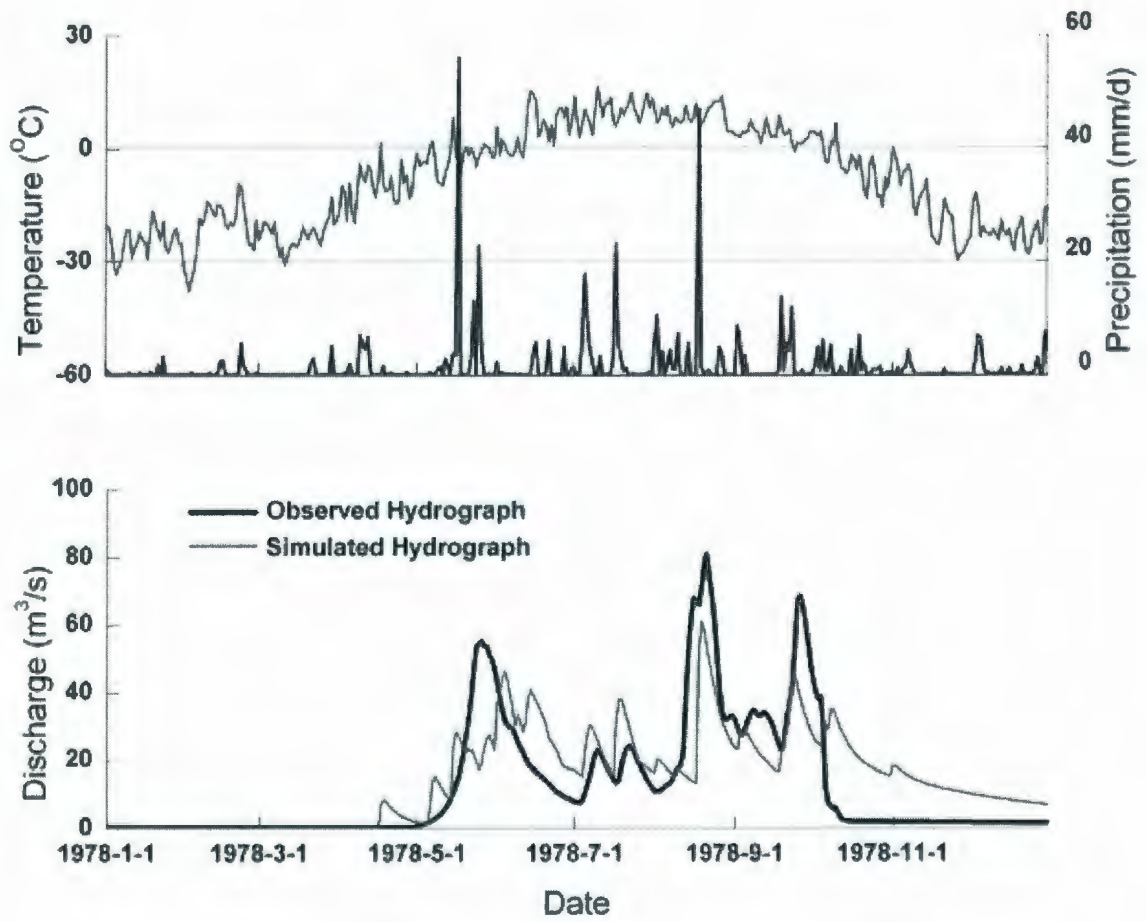


Figure 4.6 Simulated and observed daily hydrographs for the Deer River Watershed in 1978

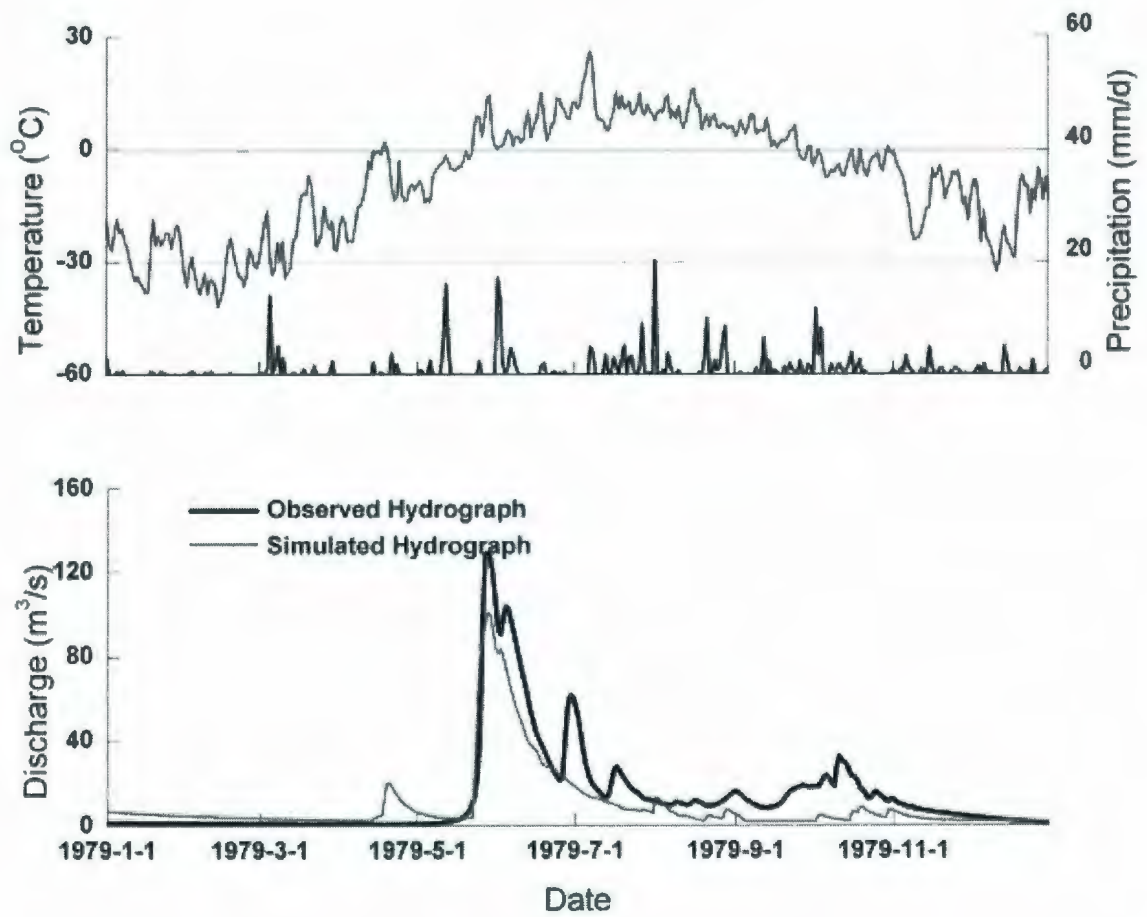


Figure 4.7 Simulated and observed daily hydrographs for the Deer River Watershed in 1979

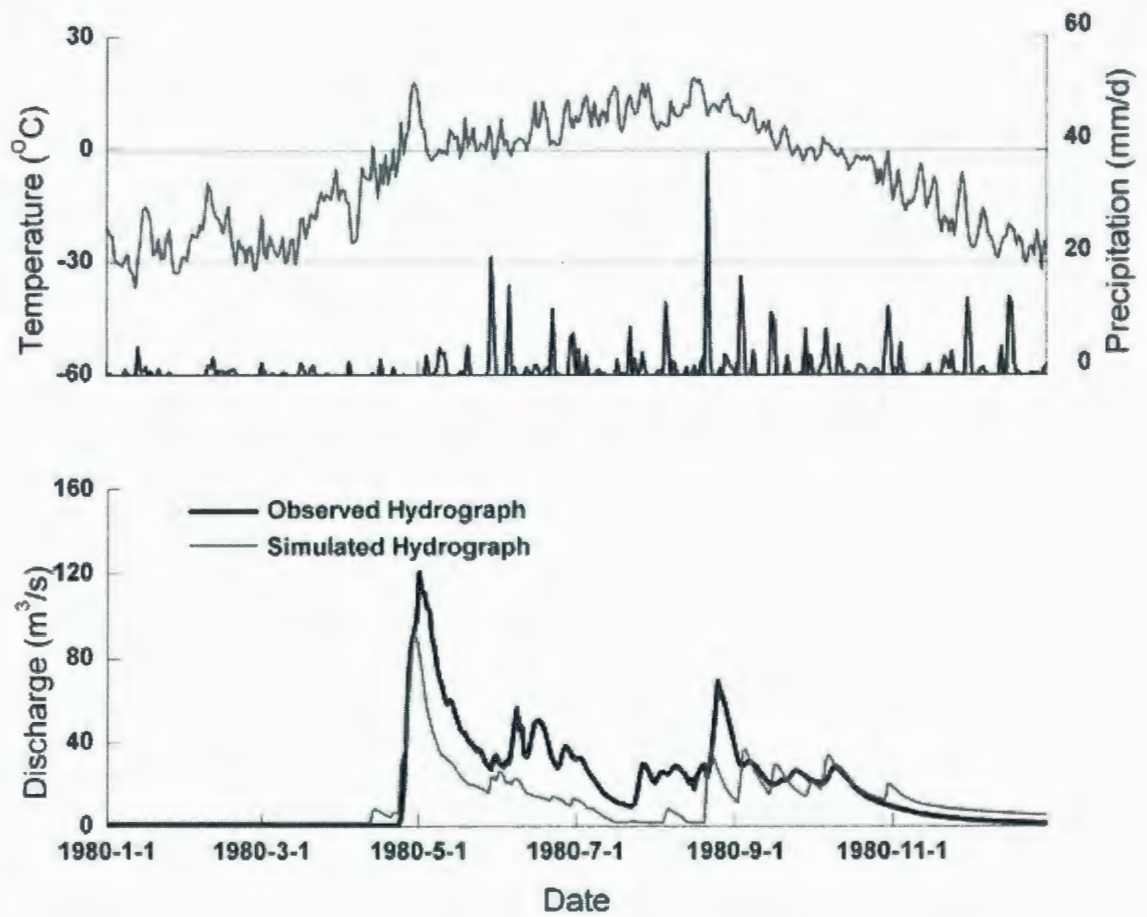


Figure 4.8 Simulated and observed daily hydrographs for the Deer River Watershed in 1980

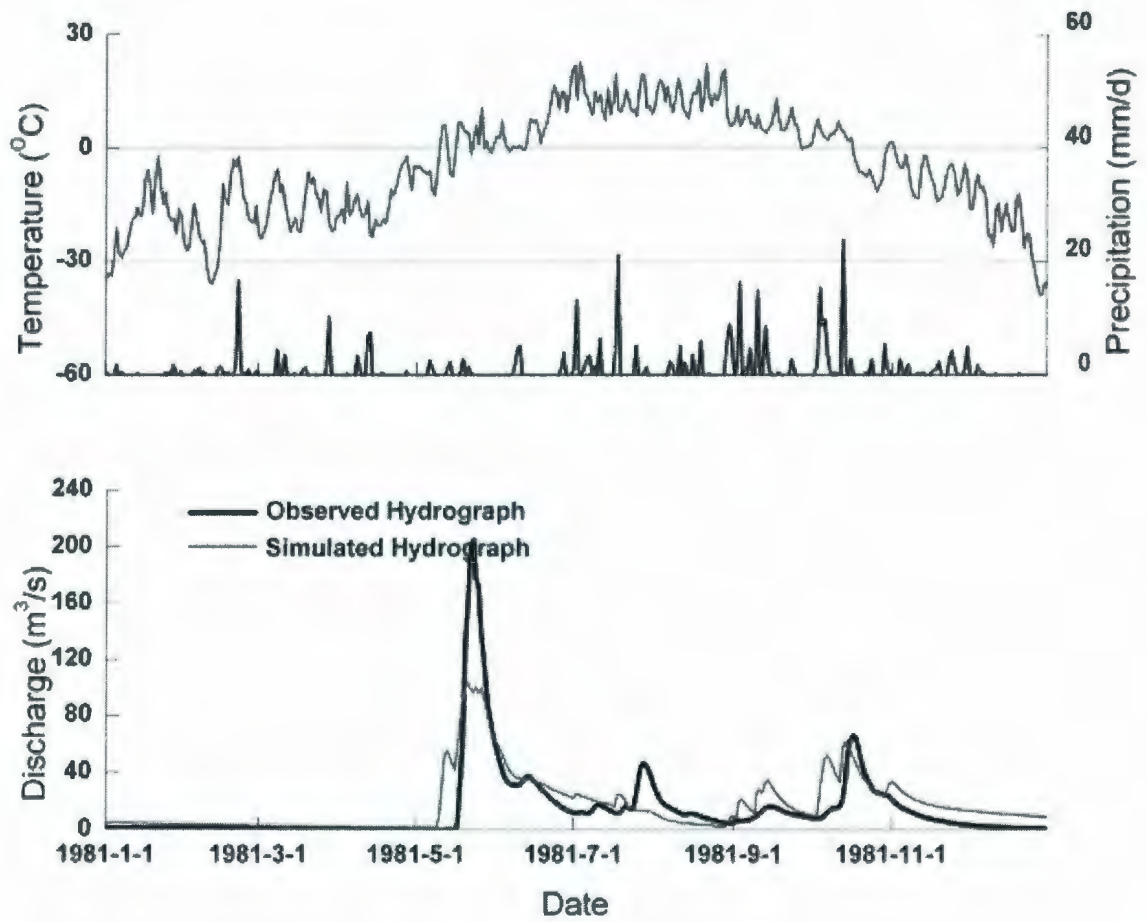


Figure 4.9 Simulated and observed daily hydrographs for the Deer River Watershed in 1981

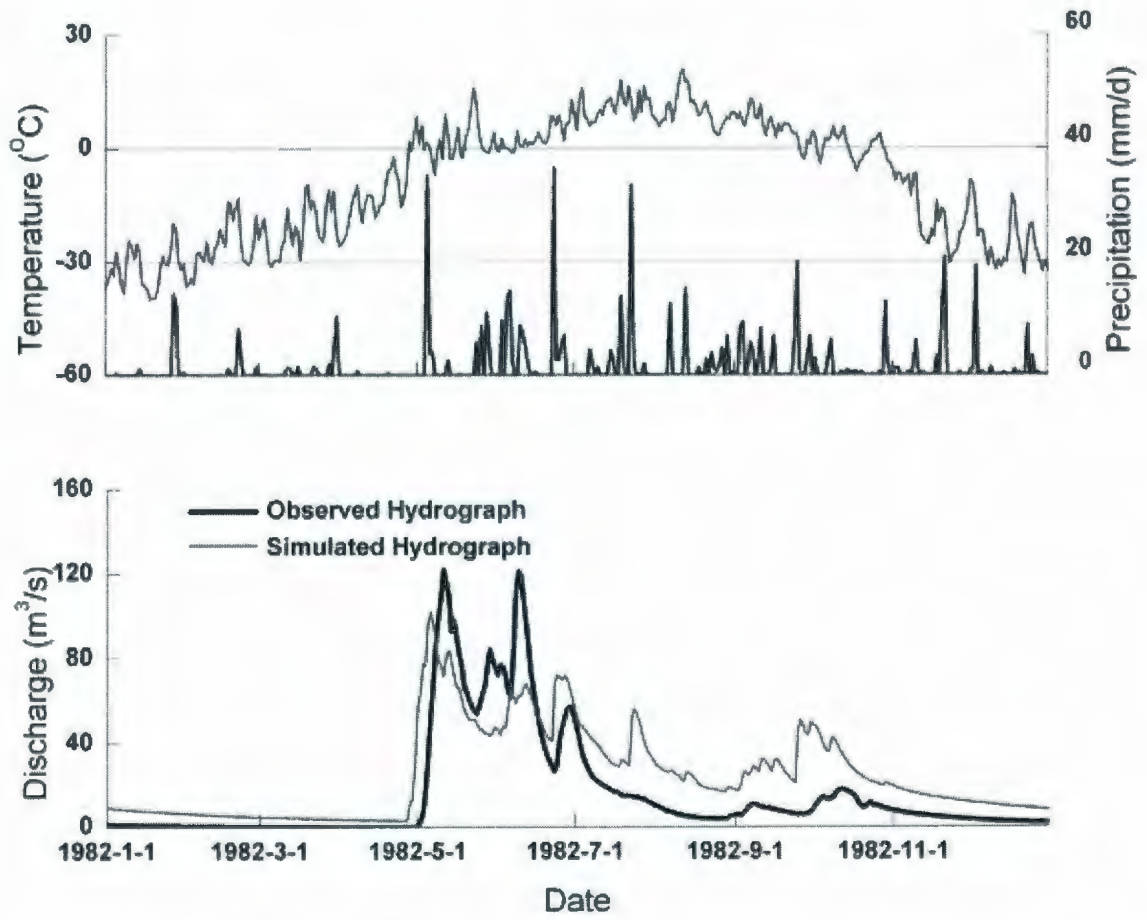


Figure 4.10 Simulated and observed daily hydrographs for the Deer River Watershed in 1982

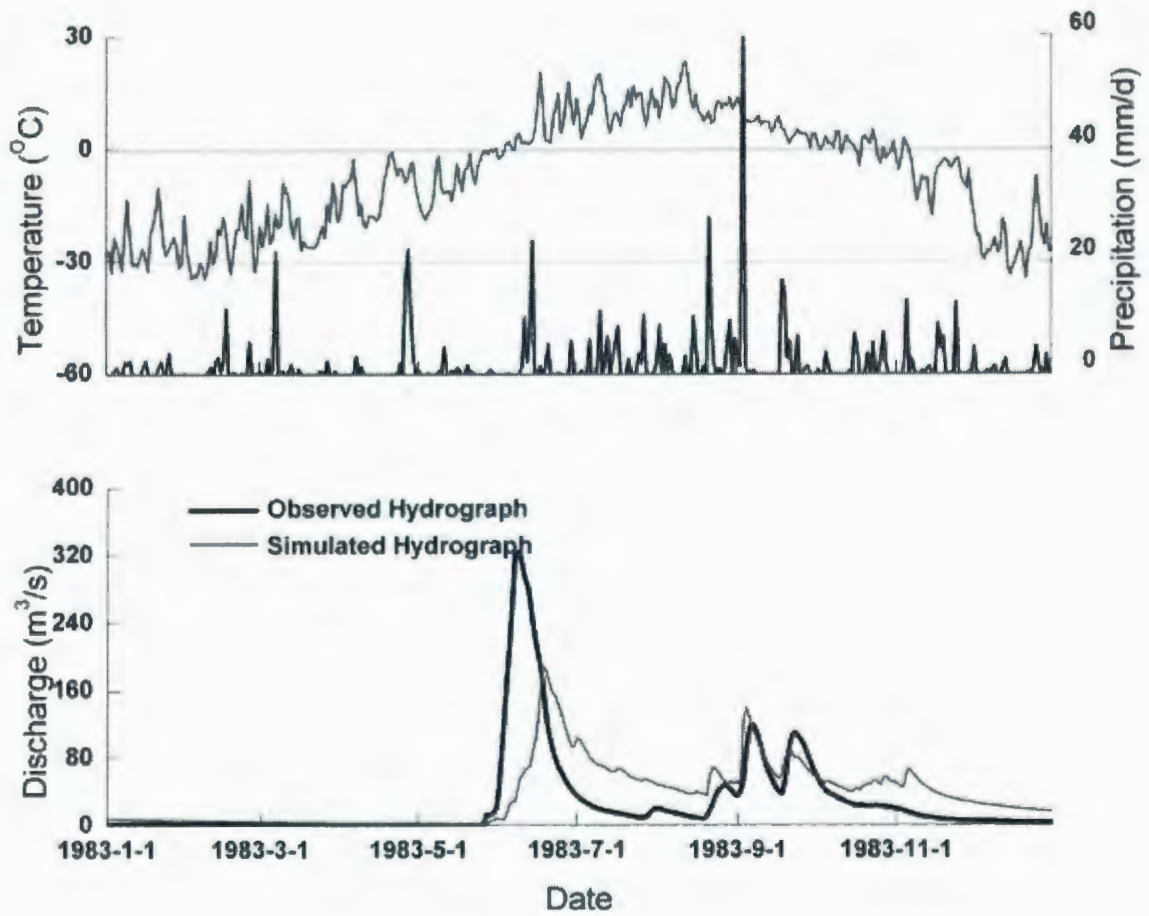


Figure 4.11 Simulated and observed daily hydrographs for the Deer River Watershed in 1983

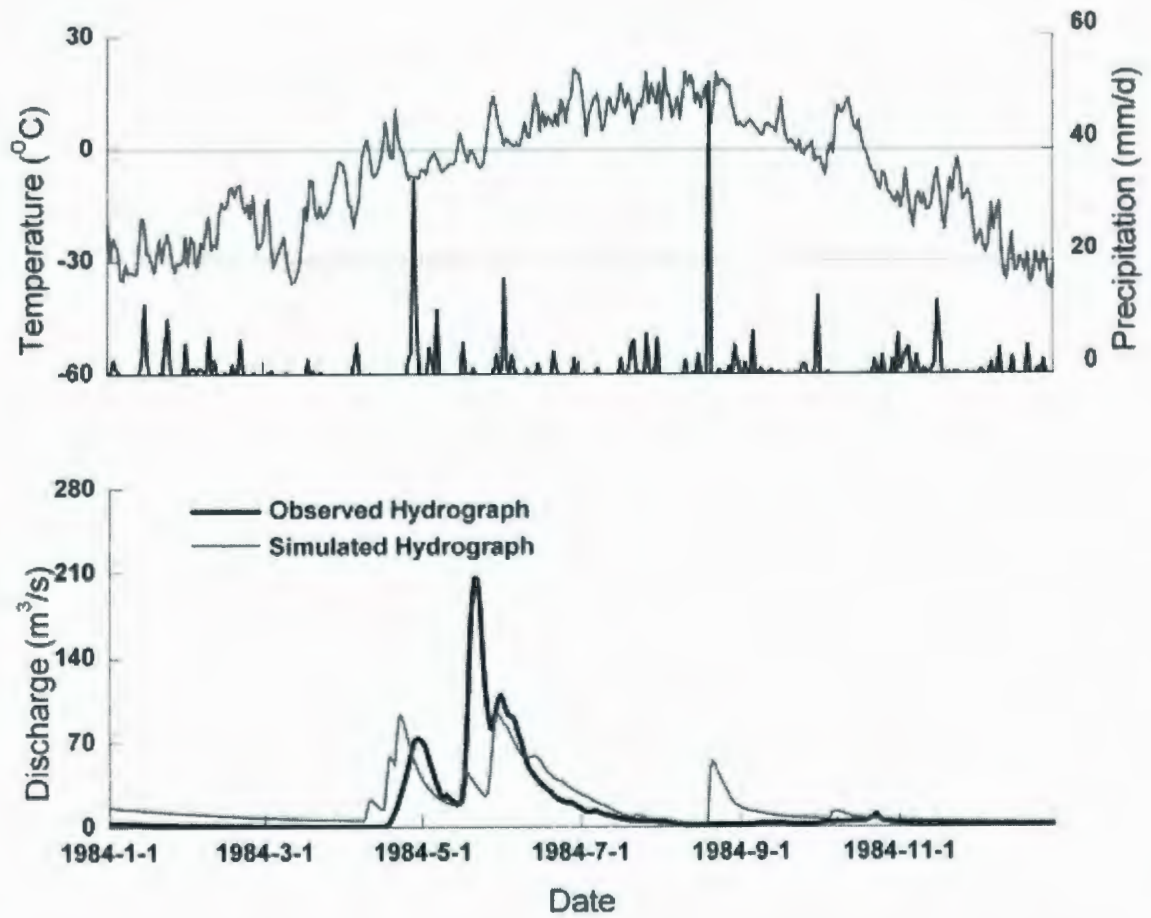


Figure 4.12 Simulated and observed daily hydrographs for the Deer River Watershed in 1984

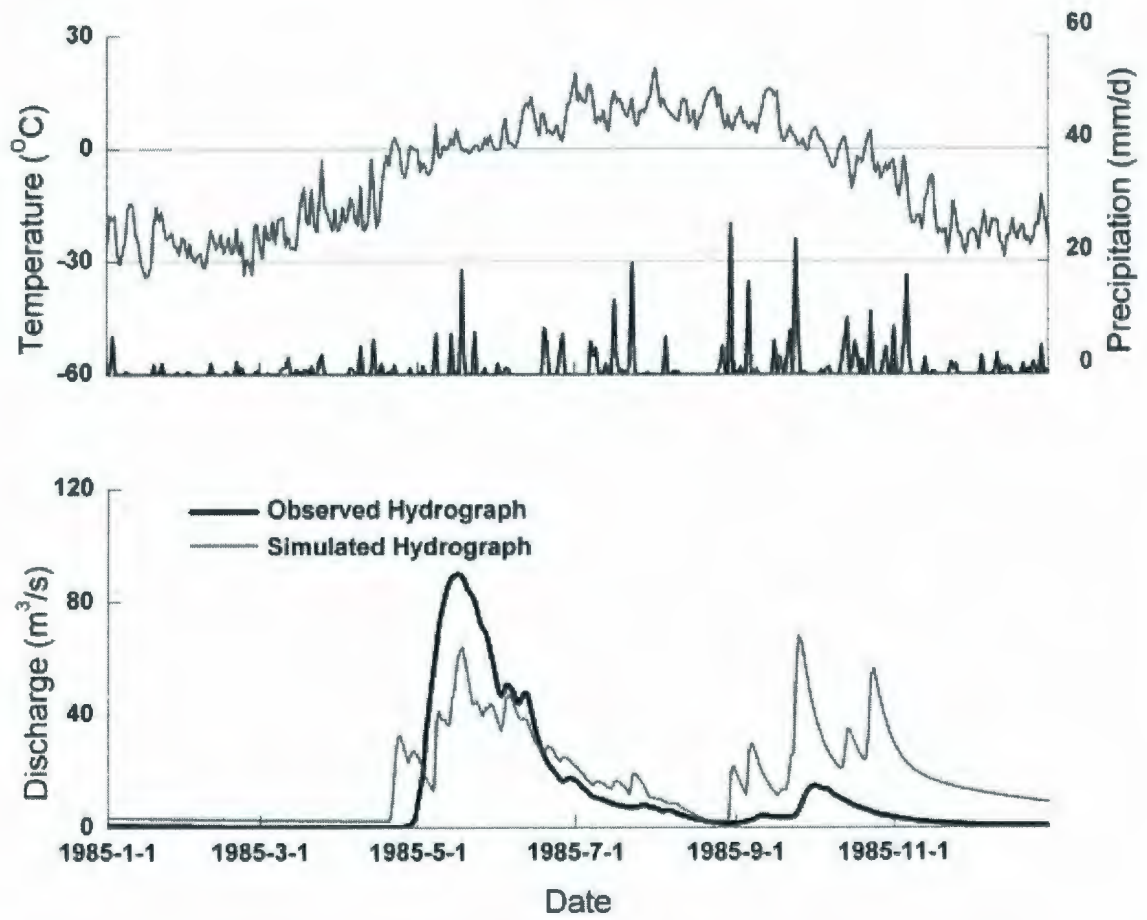


Figure 4.13 Simulated and observed daily hydrographs for the Deer River Watershed in 1985

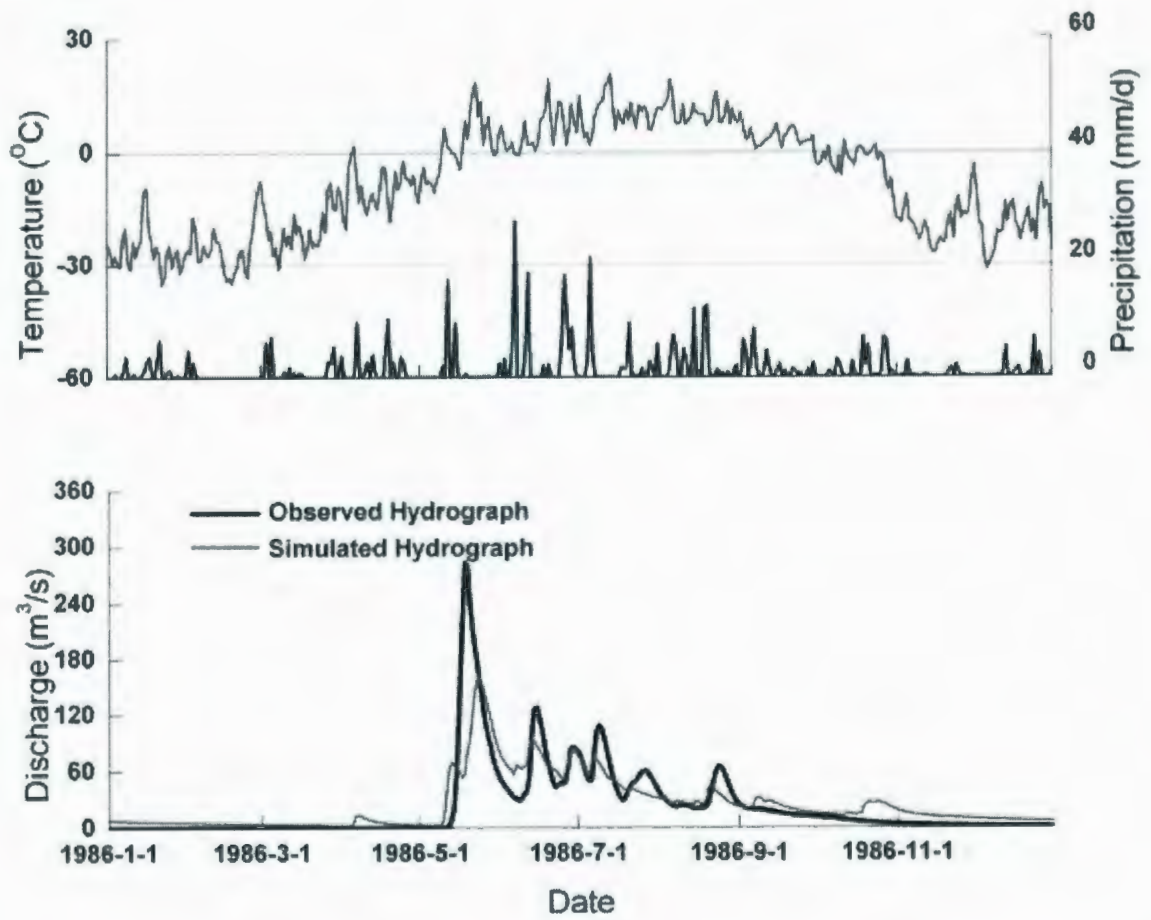


Figure 4.14 Simulated and observed daily hydrographs for the Deer River Watershed in 1986

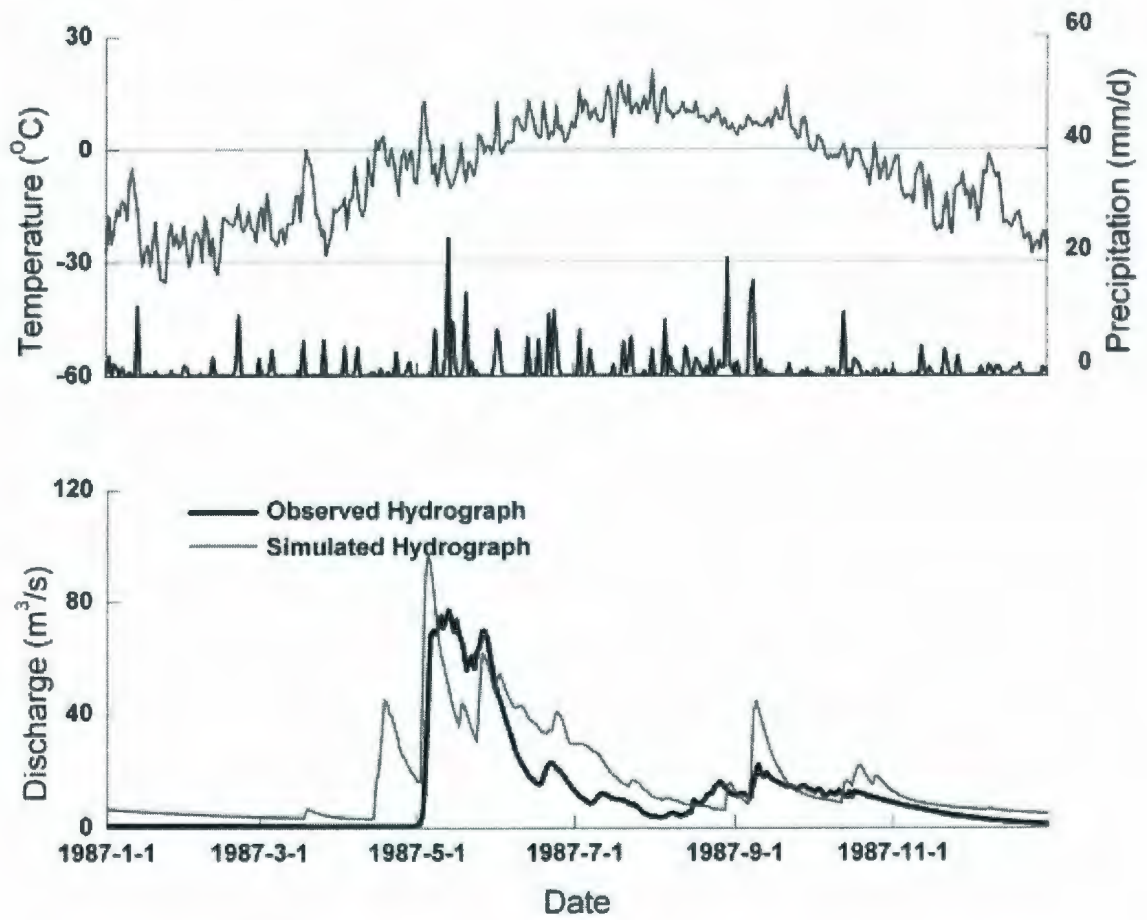


Figure 4.15 Simulated and observed daily hydrographs for the Deer River Watershed in 1987

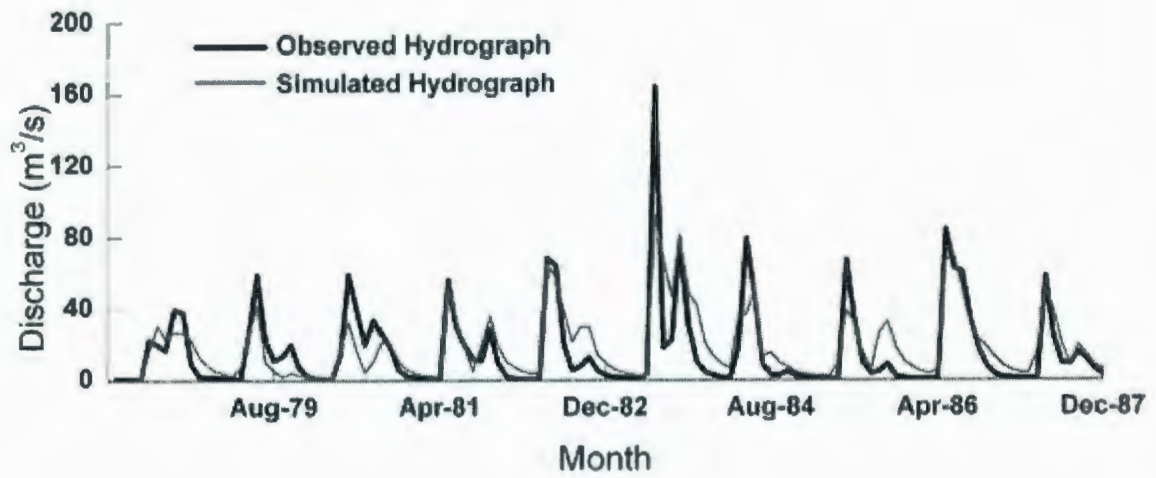


Figure 4.16 Simulated and observed monthly hydrographs for the Deer River Watershed from 1978 to 1987

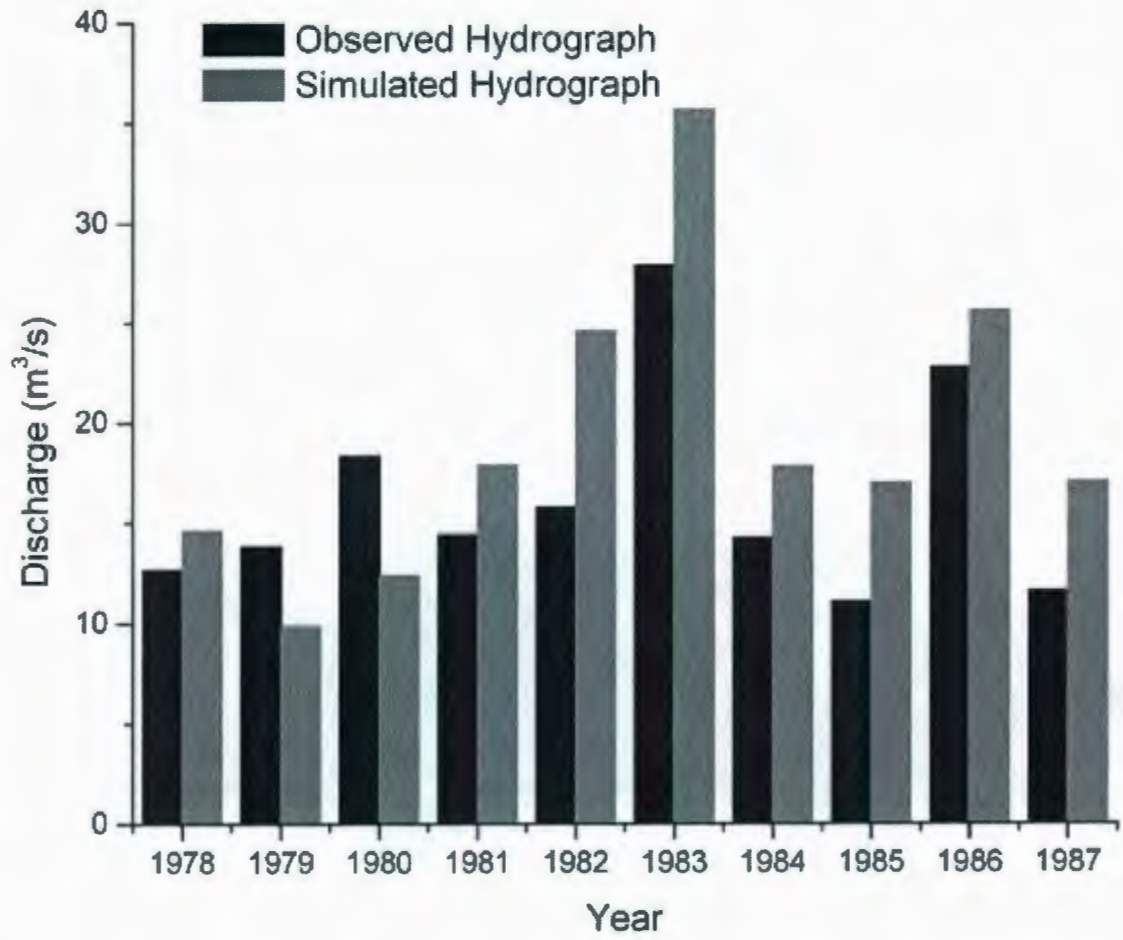


Figure 4.17 Simulated and observed annual hydrographs for the Deer River Watershed from 1978 to 1987

Table 4.5 Modelling efficiencies during SLURP daily calibration in the Deer River Watershed

Year	NSE (%)	DV (%)
1978	54	-46.0
1979	76	-44.1
1980	57	-59.9
1981	66	-45.3
1982	53	-33.9
1983	23	-55.2
1984	40	-60.7
1985	38	-47.2
1986	64	-51.0
1987	48	-5.4
Average.	52	-44.9
Max.	76	-5.4
Min.	23	-60.7

Note: NSE is the Nash and Sutcliffe efficiency; and DV is the deviation of runoff volumes.

Table 4.6 Modelling efficiencies during SLURP calibration in the Deer River

	NSE (%)	DV (%)
Monthly	47	-39.1
Annual	-11	94.3

Note: NSE is the Nash and Sutcliffe efficiency; and DV is the deviation of runoff volumes.

4.7 Verification

Modelling verification was performed for a period of 17 years (1988 – 2004). Figures 4.18 to 4.34 show the modeled and observed daily hydrograph outputs during the verification period. Table 4.7 reports the modelling Nash and Sutcliffe efficiency (NSE) and deviation of runoff volume (DV) of this period.

The NSEs of the verification years are lower than the calibration years with an average at 4%. Nonetheless, the NSEs of the first 10-year period in the verification years (1988 – 1997) are not low, ranging from -27% to 66% with an average at 35%. However, simulation of the last 7 years (1999 – 2004) has negative efficiencies, which might be contributed to a number of possible reasons, including streamflow data measurement, a natural shifting of the channels or the change of meteorological data collection. The observed stream discharge is too small than what it is expected to be. For example, during the summer period (July 20th – October 3rd) of 2001 (Figure 4.31), the precipitation is continuous and 50% more than historical average amount (1978 – 2004). Some extreme heavy rainfall events occur on August 10th and September 21st with total precipitation of 39.5 and 31.5 mm, respectively. However, the streamflow does not actively respond to the rainfall events and keeps stable around 14 m³/s which is much lower than the historical average value of 20 m³/s (1978 – 2004). The same trend can be found in the years of 1998, 2002 and 2003.

Generally, most of the major mismatches between the simulated flow and observed flow

are discovered in the spring snowmelt period and summer/fall raining season. The DVs of the verification years, which range from -81 to 96.3% with an average of -13.6%, support this conclusion (Table 4.7). For example, in the year of 1995, the simulated spring runoff peak is only one third of the observed peak and most of the rainfall events in the summer and fall seasons are underestimated as shown in Figure 4.25. DV of this year is -81% which means that the simulated fluctuation is drastically weaker and the total simulated runoff volume is lower than the observed flow. The simulated runoff in spring which is caused by snowmelt is lower than the observed flow, which may be due to the existence of permafrost table. In SLURP, the degree-day snowmelt algorithm generates snowmelt and puts it into the fast storage tank on any day if air temperature exceeds 0 °C. Because the shallow permafrost table can prevent the water from infiltrating into the fast storage tank, the actual spring runoff will be much higher than the simulated results. Furthermore, this degree-day snowmelt algorithm has a limitation of generating illogical runoff whenever temperature exceeds 0 °C in March or April even it is not possible in the field. Besides the contribution from the permafrost layer, ponds which extensively exist in the Deer River Watershed is another factor which can hold rain water for a period and make the actual observed summer flow less than the simulated flow in some years (e.g. 1992 and 1998). It is implied that modifications to the snowmelt algorithm and adding some routines regarding the frost table as well as the particular soil features may improve the model's performance.

Figures 4.35 and 4.36 show the monthly and annual model outputs during the verification period (1988 – 2004), respectively. Table 4.8 reports the modelling

efficiencies and DV of monthly and annual results. The monthly modelling efficiency (NSE = 21%) and DV (-2.8%) are better than the daily modelling results, indicating some considerable differences between the daily simulated and observed flows are diminished. However, the annual modelling efficiency (NSE = -235%) and DV (97%) imply that the annual simulated runoff volumes are overestimated and much higher than the observed ones. This could be attributed to the suspectable streamflow data during the period of 1998 – 2004.

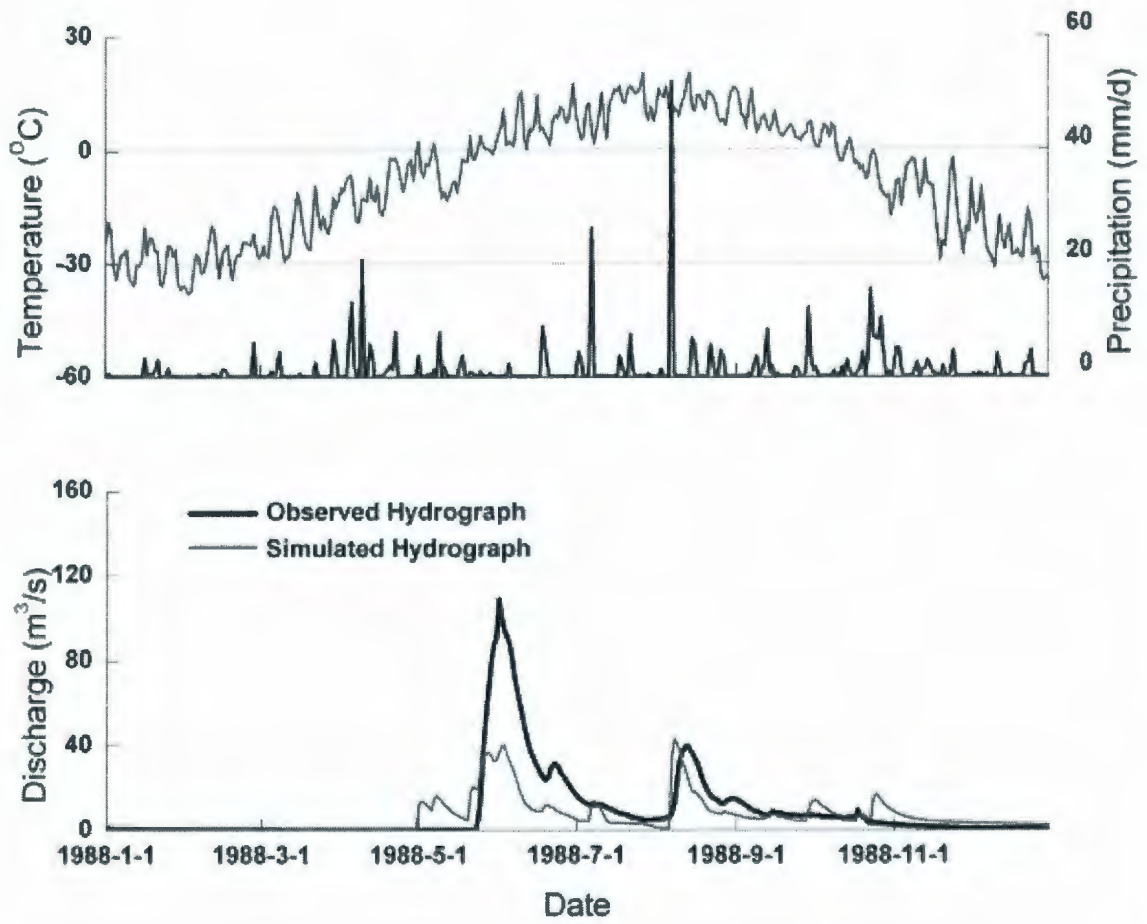


Figure 4.18 Simulated and observed daily hydrographs for the Deer River Watershed in 1988

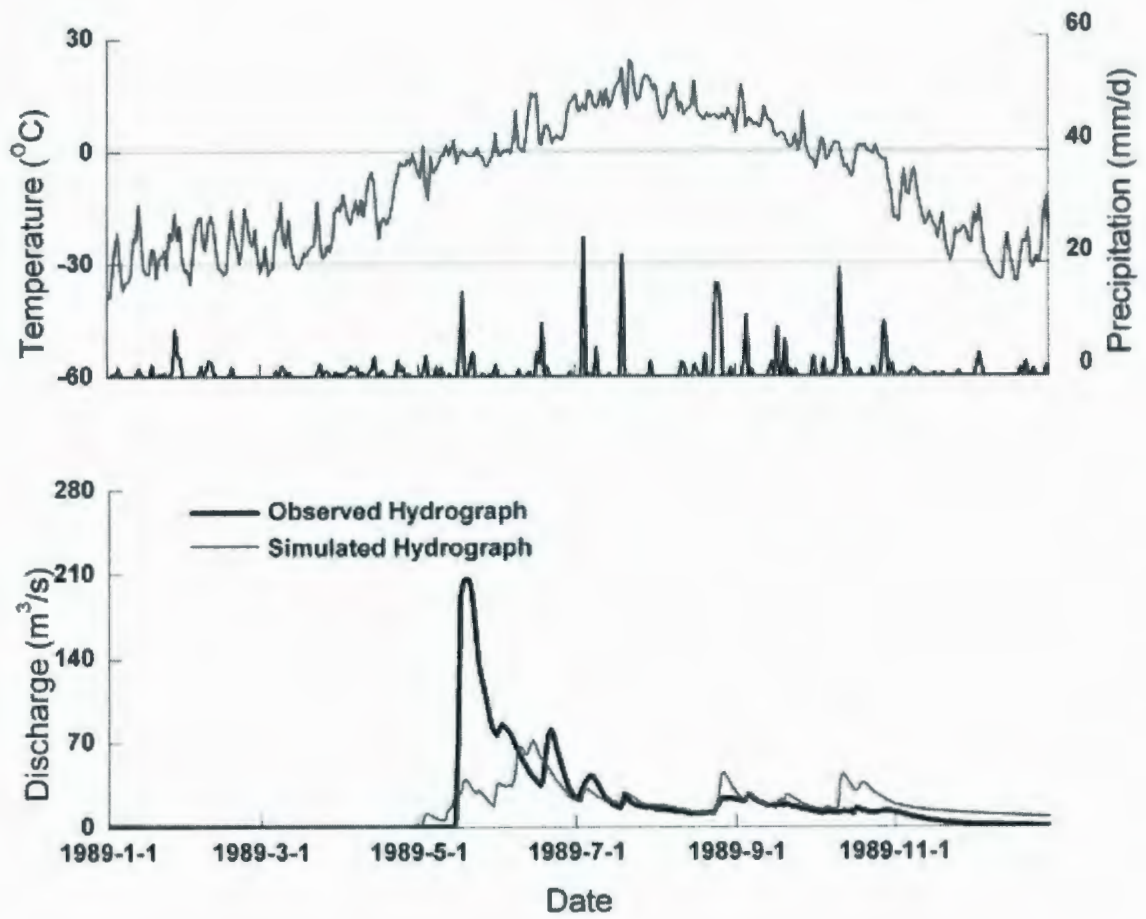


Figure 4.19 Simulated and observed daily hydrographs for the Deer River Watershed in 1989

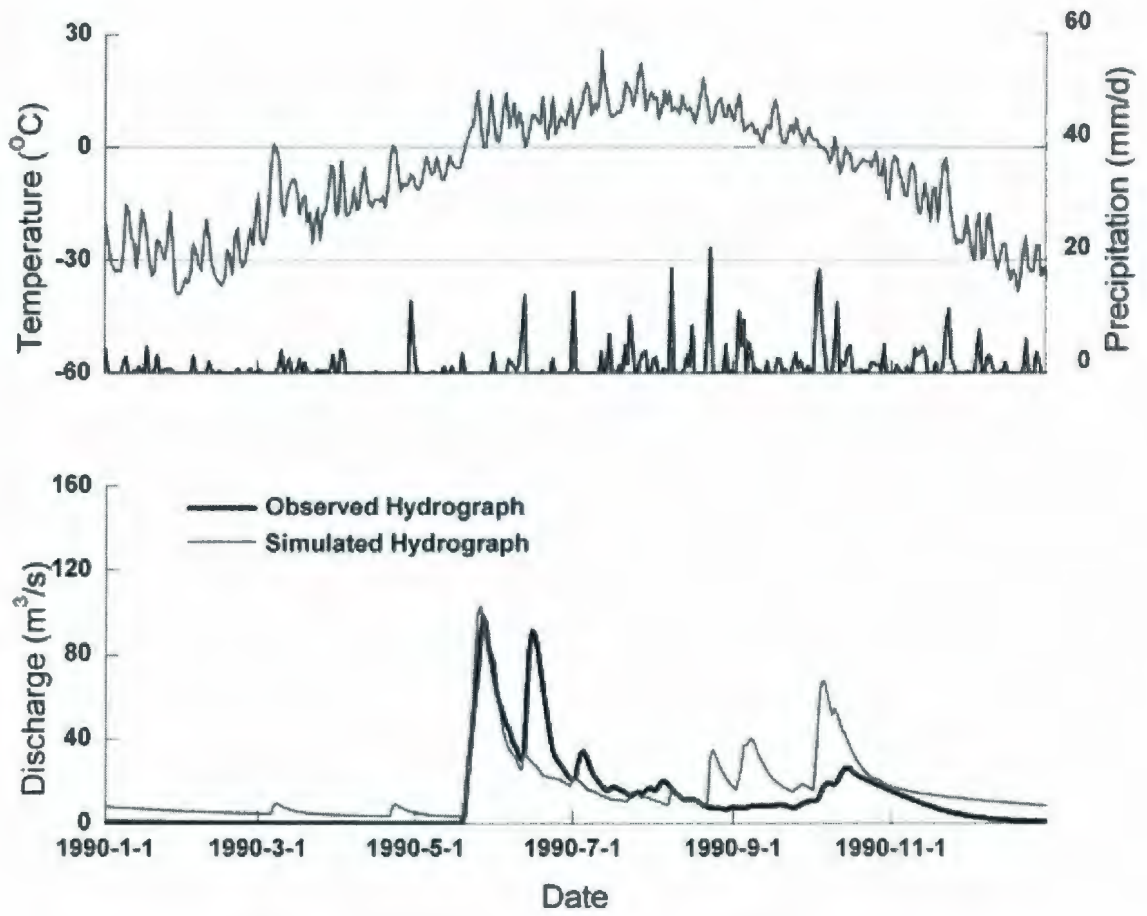


Figure 4.20 Simulated and observed daily hydrographs for the Deer River Watershed in 1990

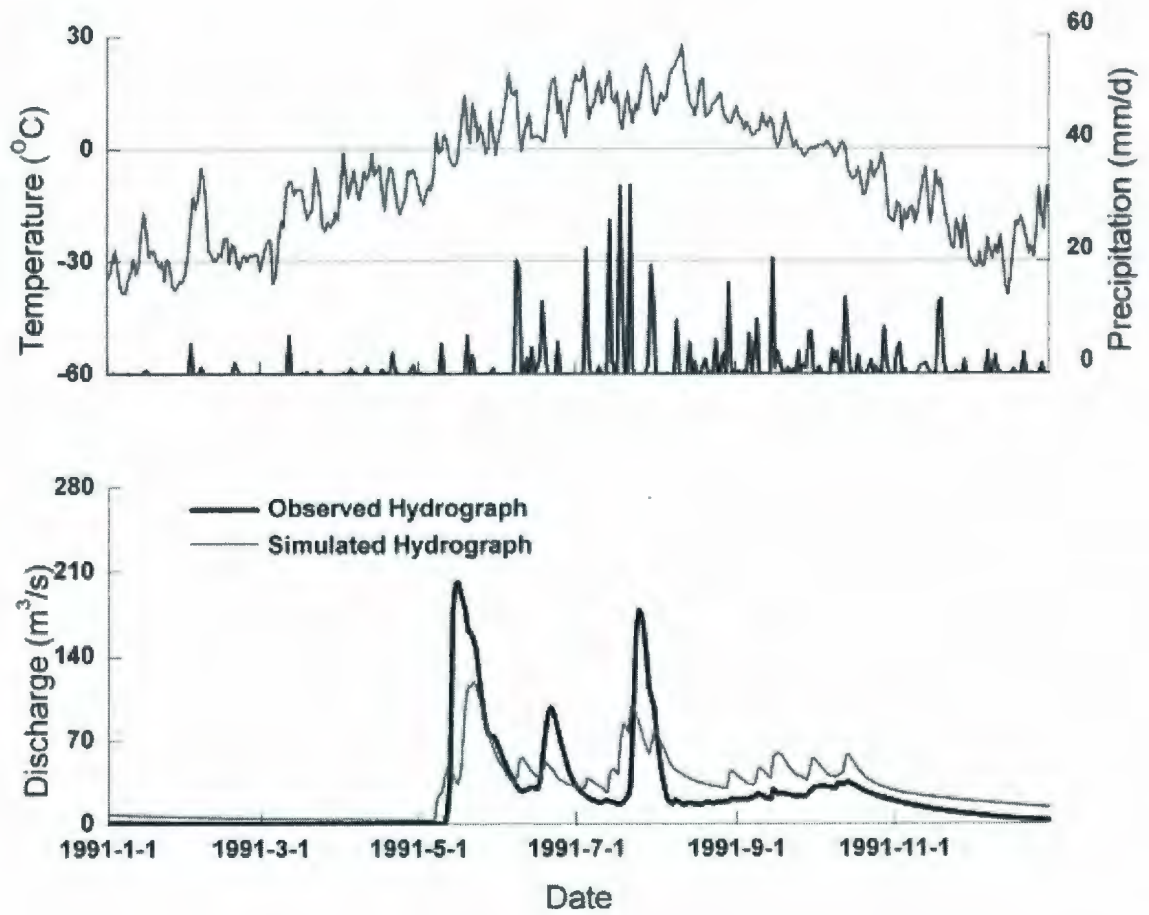


Figure 4.21 Simulated and observed daily hydrographs for the Deer River Watershed in 1991

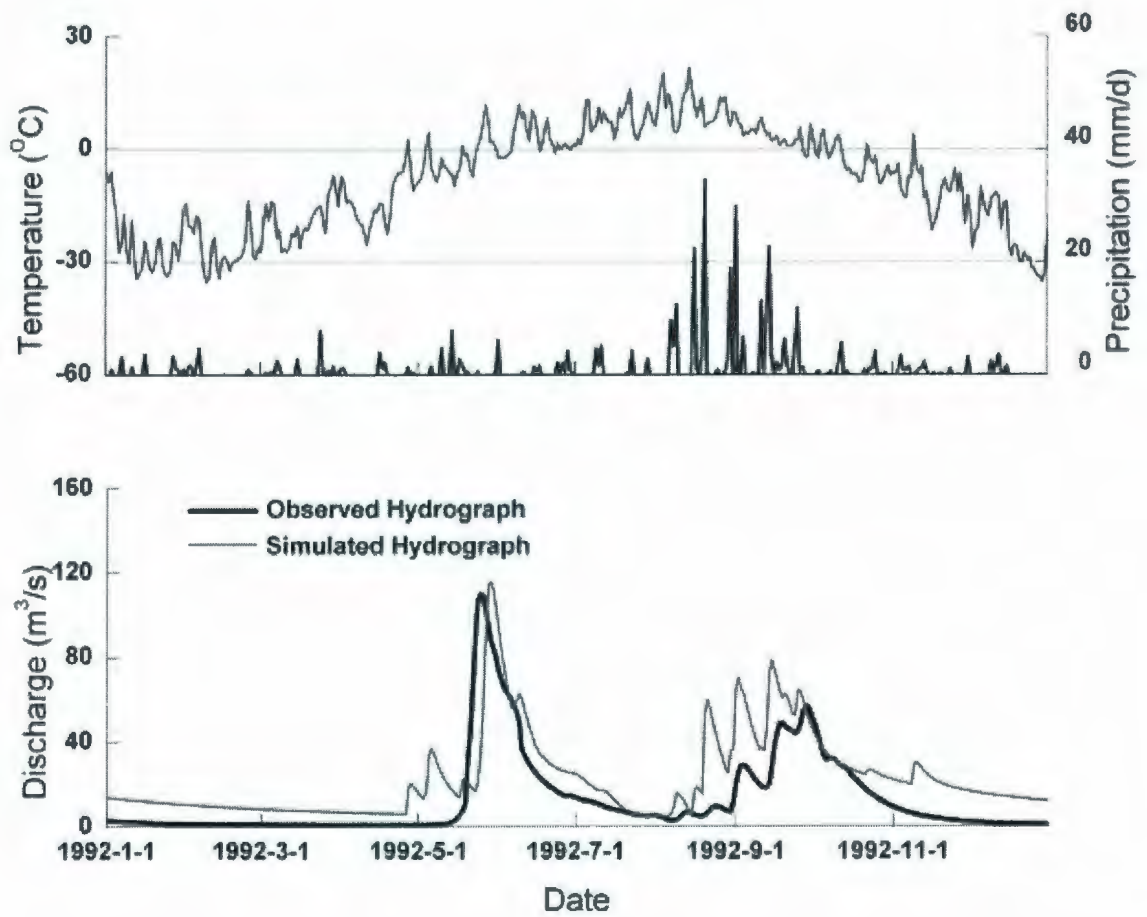


Figure 4.22 Simulated and observed daily hydrographs for the Deer River Watershed in 1992

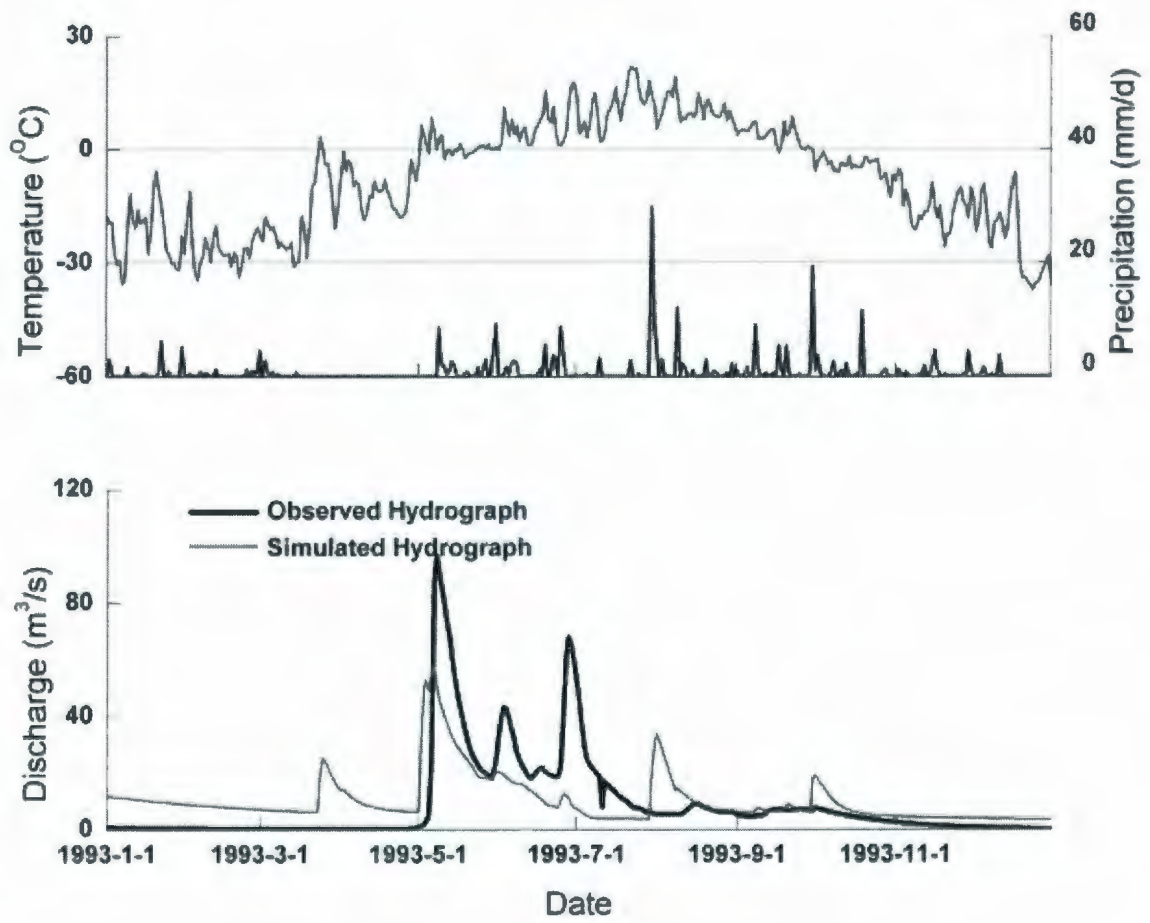


Figure 4.23 Simulated and observed daily hydrographs for the Deer River Watershed in 1993

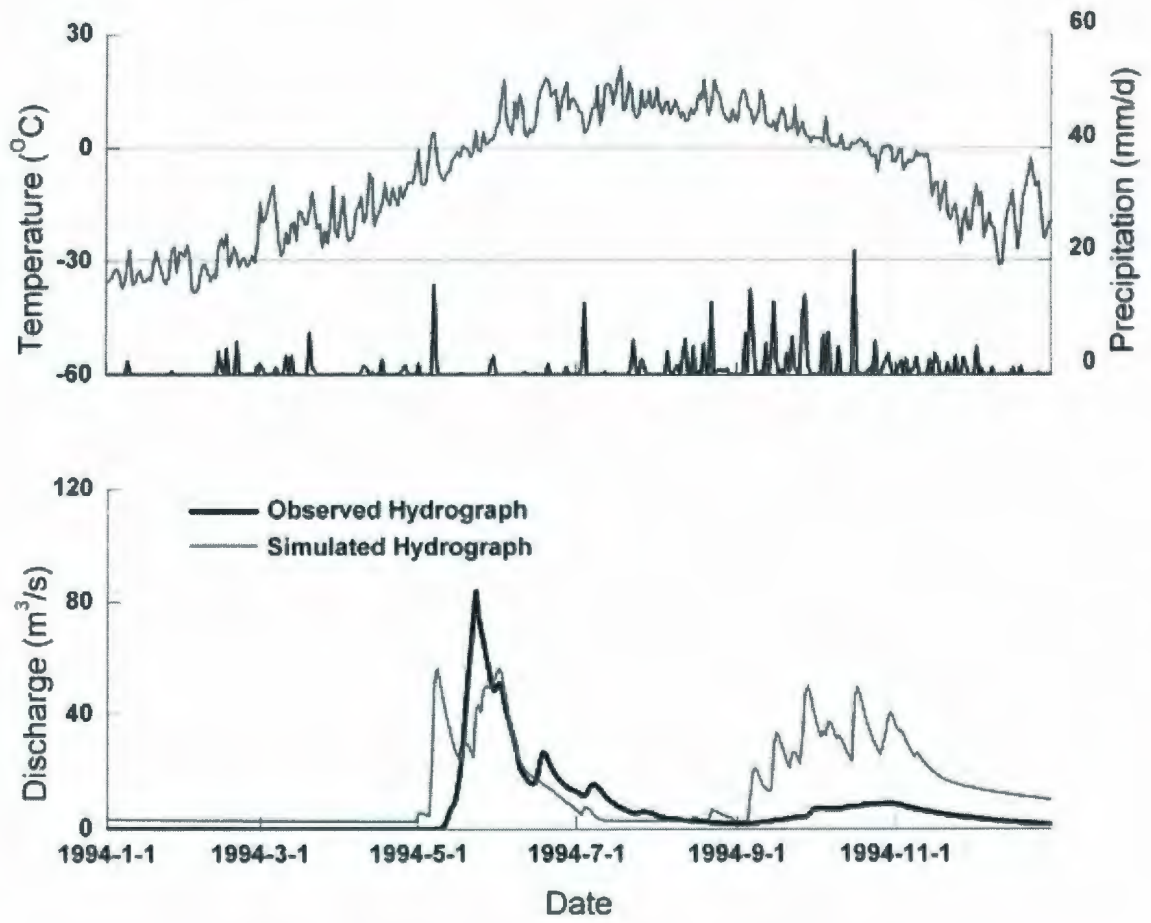


Figure 4.24 Simulated and observed daily hydrographs for the Deer River Watershed in 1994

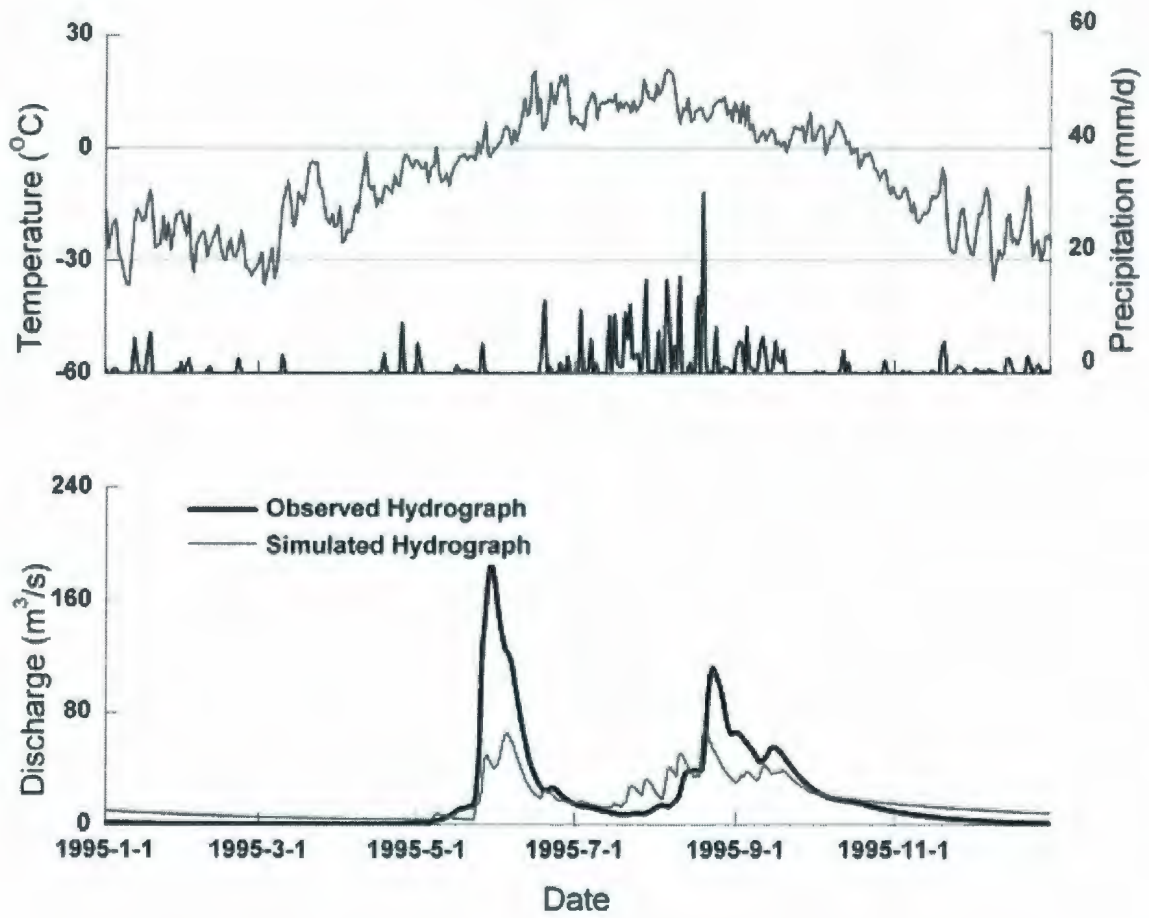


Figure 4.25 Simulated and observed daily hydrographs for the Deer River Watershed in 1995

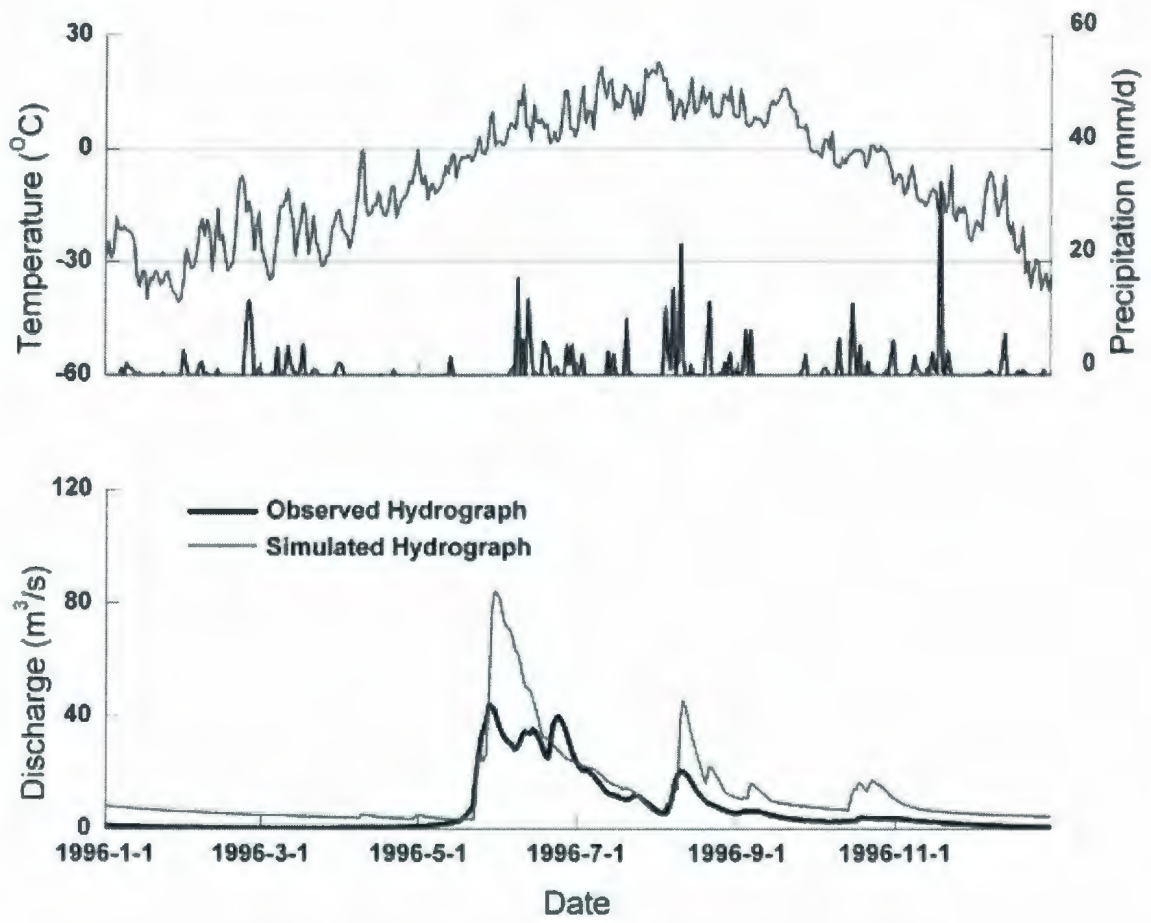


Figure 4.26 Simulated and observed daily hydrographs for the Deer River Watershed in 1996

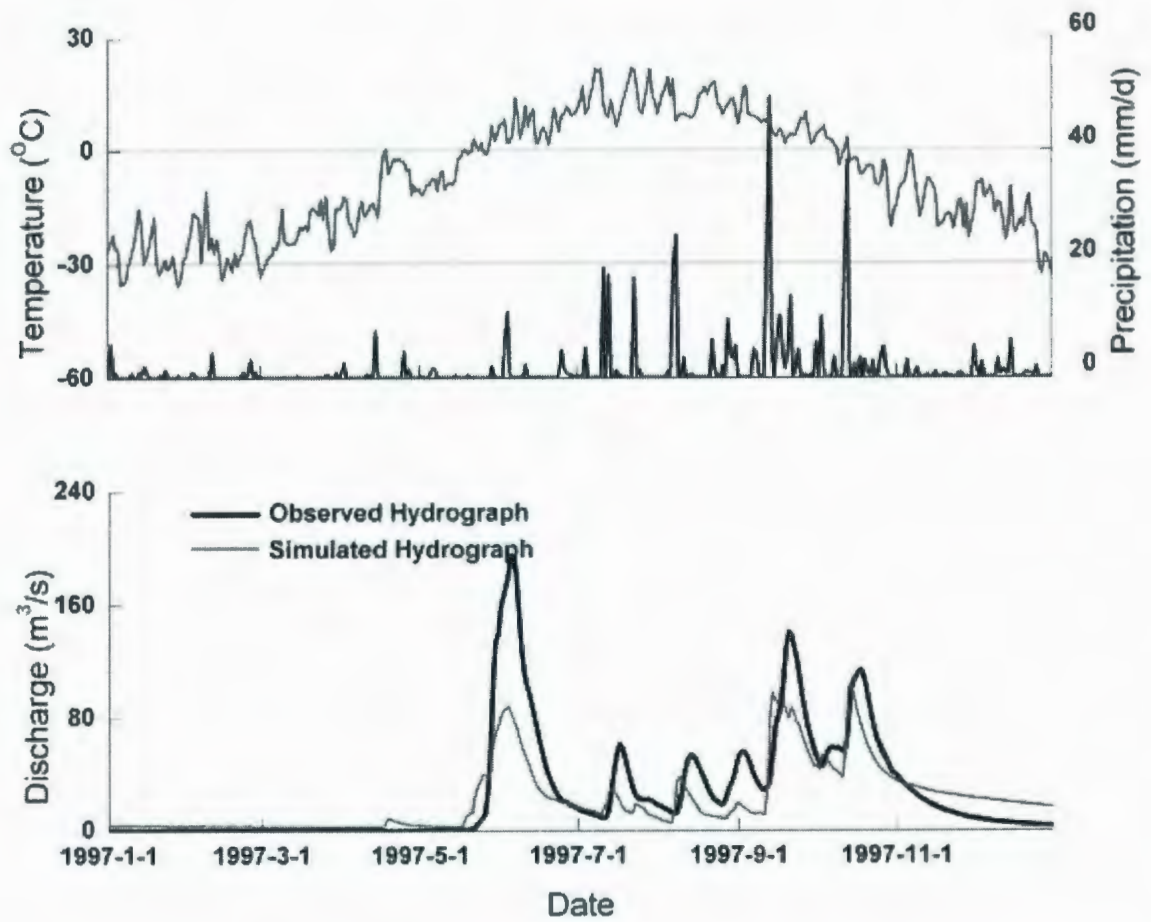


Figure 4.27 Simulated and observed daily hydrographs for the Deer River Watershed in 1997

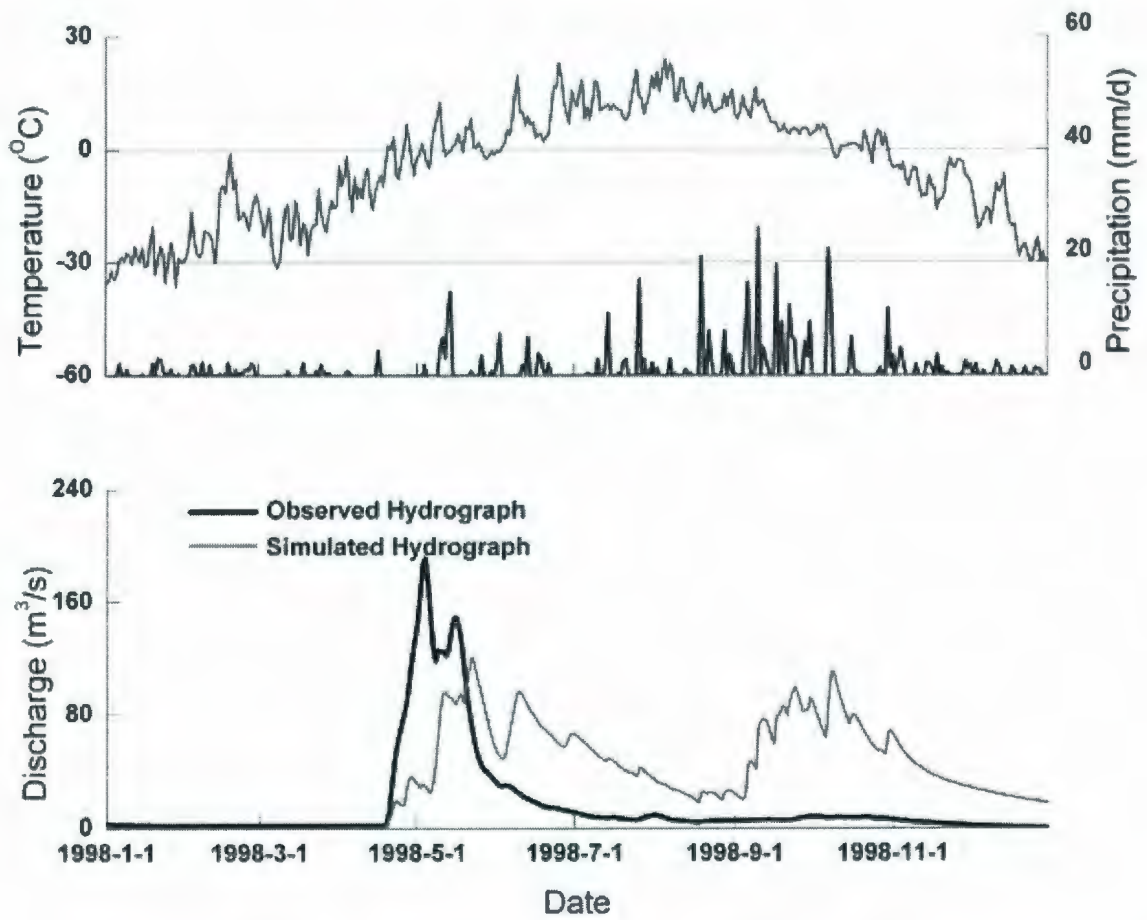


Figure 4.28 Simulated and observed daily hydrographs for the Deer River Watershed in 1998

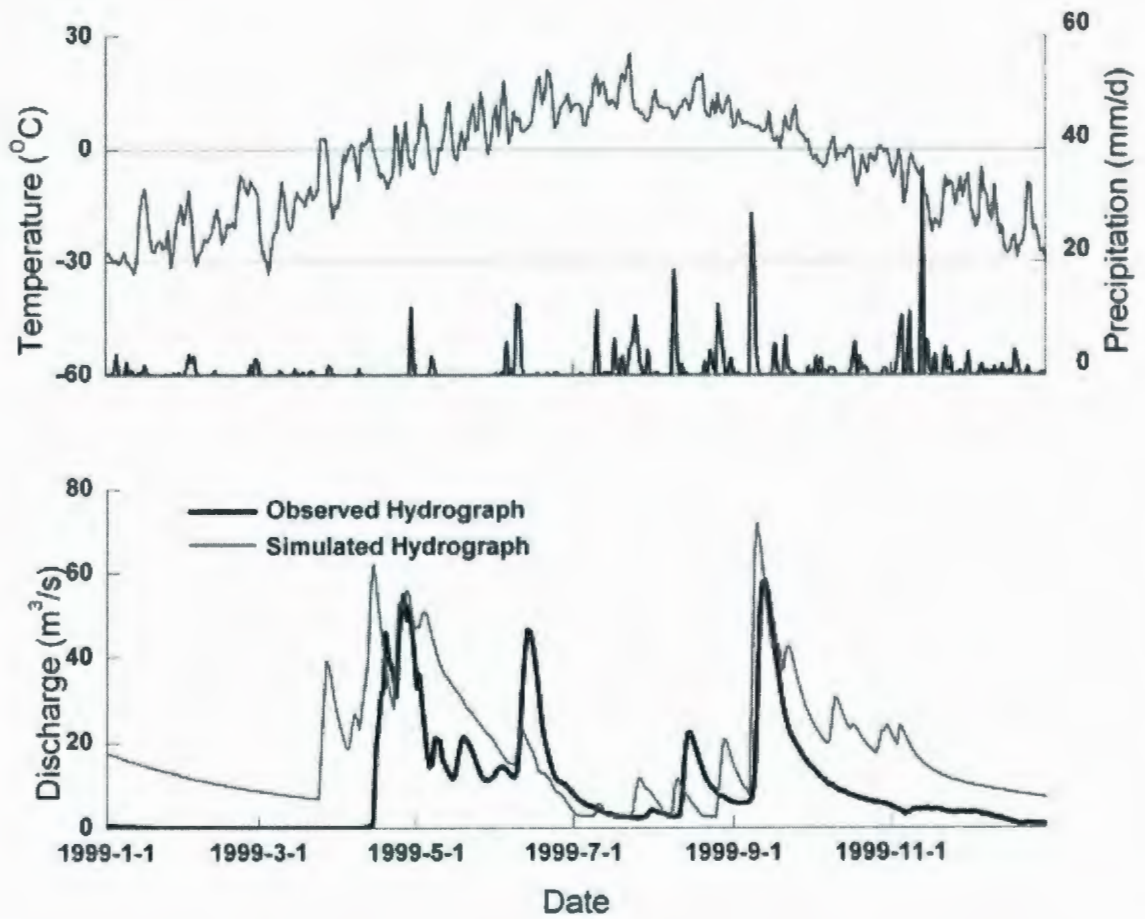


Figure 4.29 Simulated and observed daily hydrographs for the Deer River Watershed in 1999

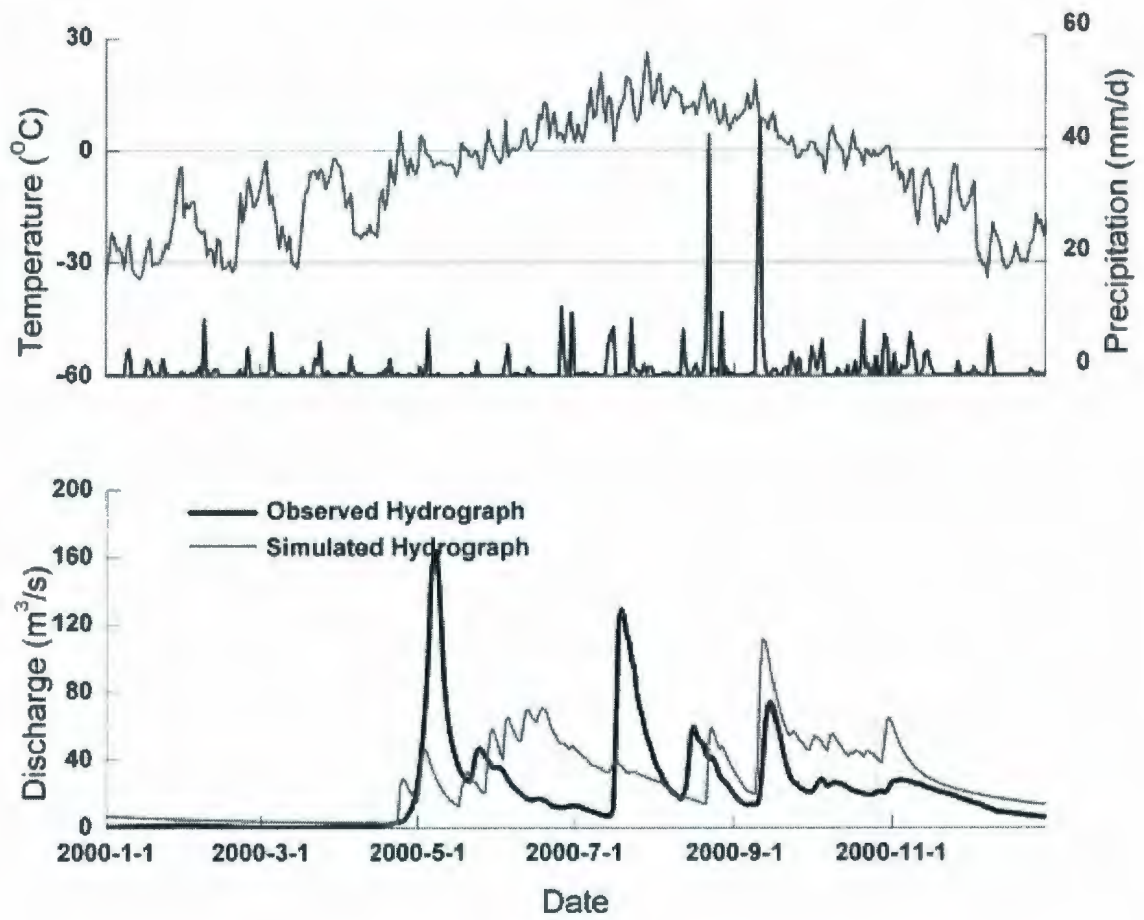


Figure 4.30 Simulated and observed daily hydrographs for the Deer River Watershed in 2000

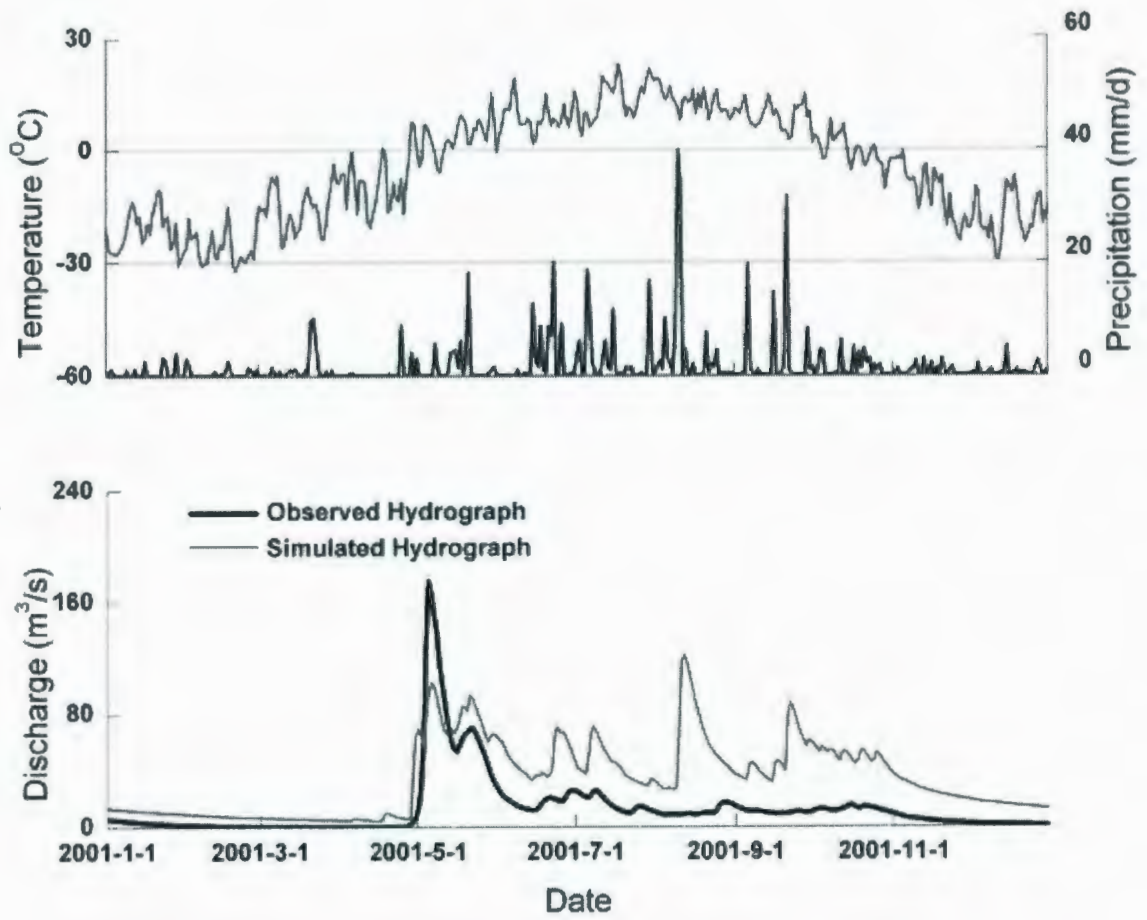


Figure 4.31 Simulated and observed daily hydrographs for the Deer River Watershed in 2001

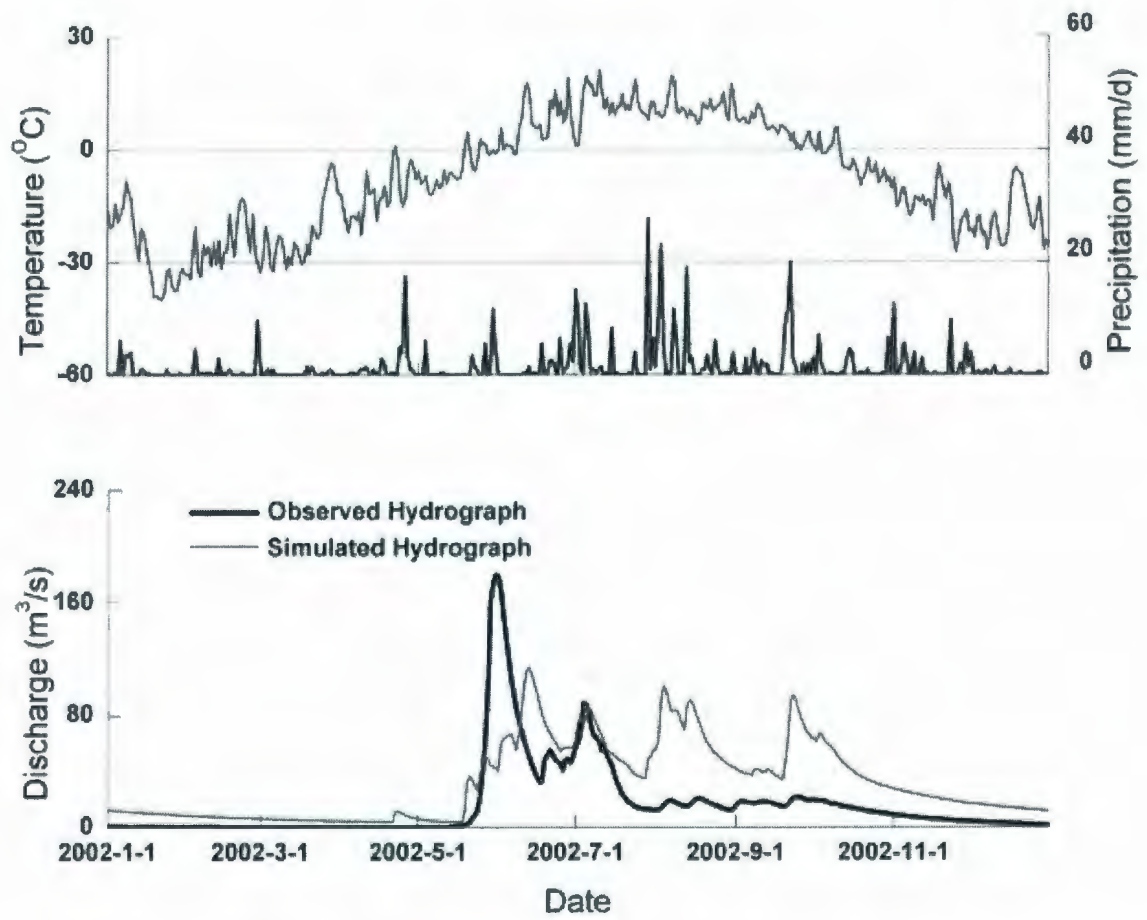


Figure 4.32 Simulated and observed daily hydrographs for the Deer River Watershed in 2002

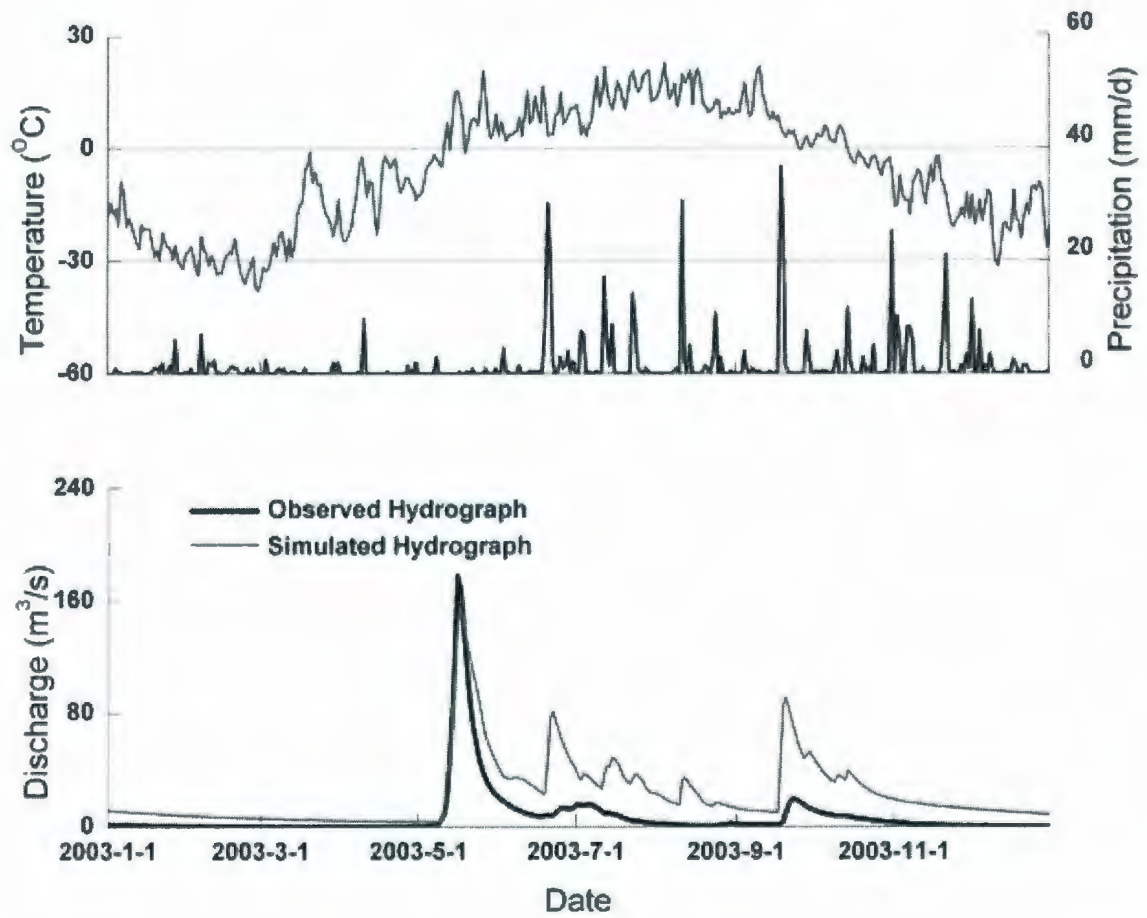


Figure 4.33 Simulated and observed daily hydrographs for the Deer River Watershed in 2003

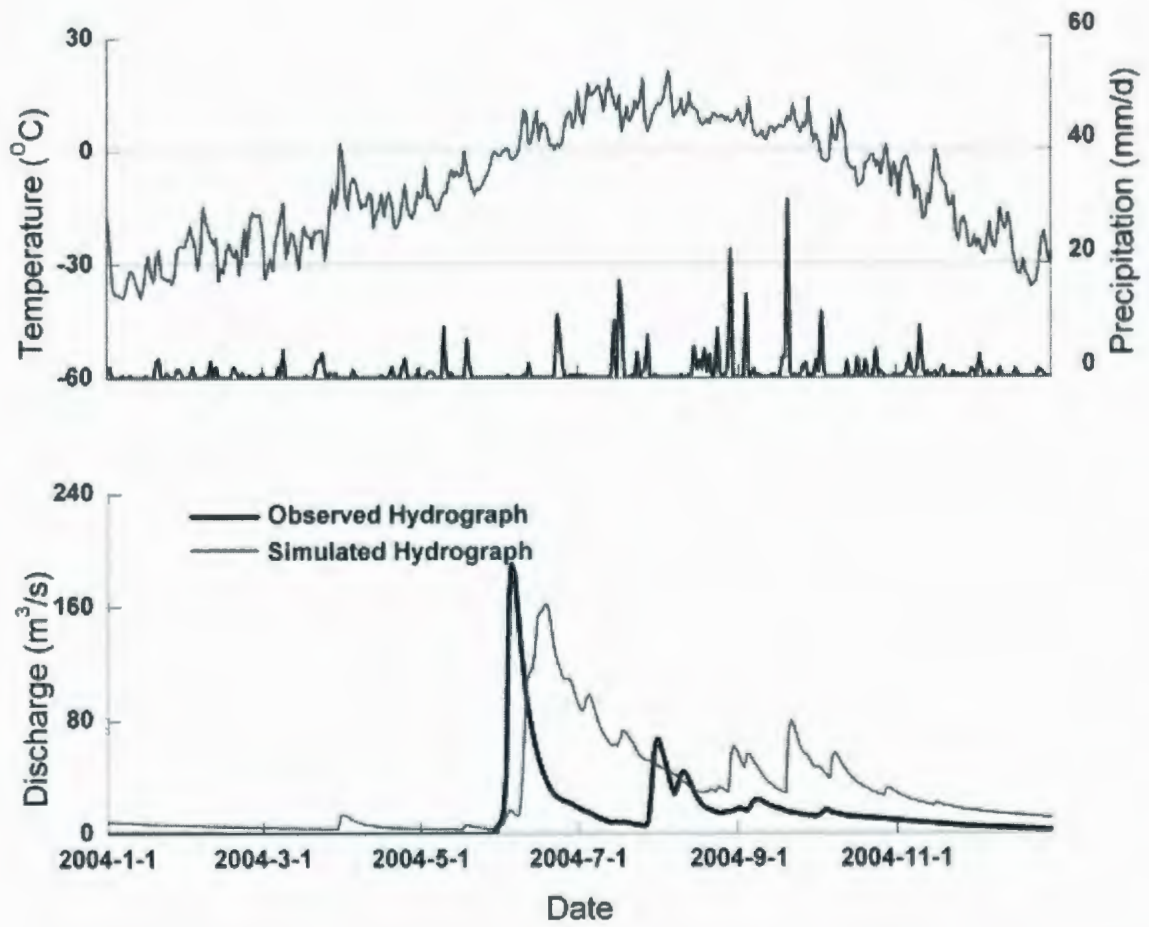


Figure 4.34 Simulated and observed daily hydrographs for the Deer River Watershed in 2004

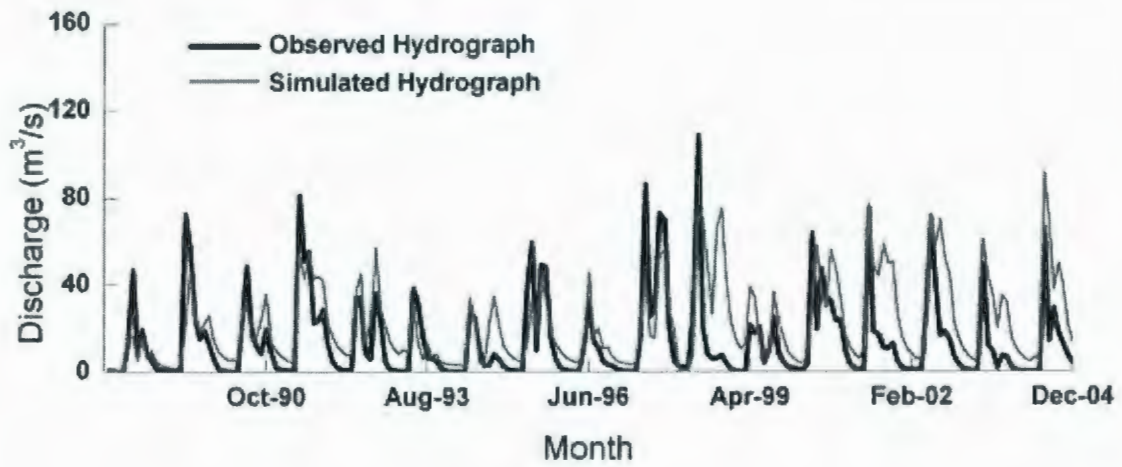


Figure 4.35 Simulated and observed monthly hydrographs for the Deer River Watershed from 1988 to 2004

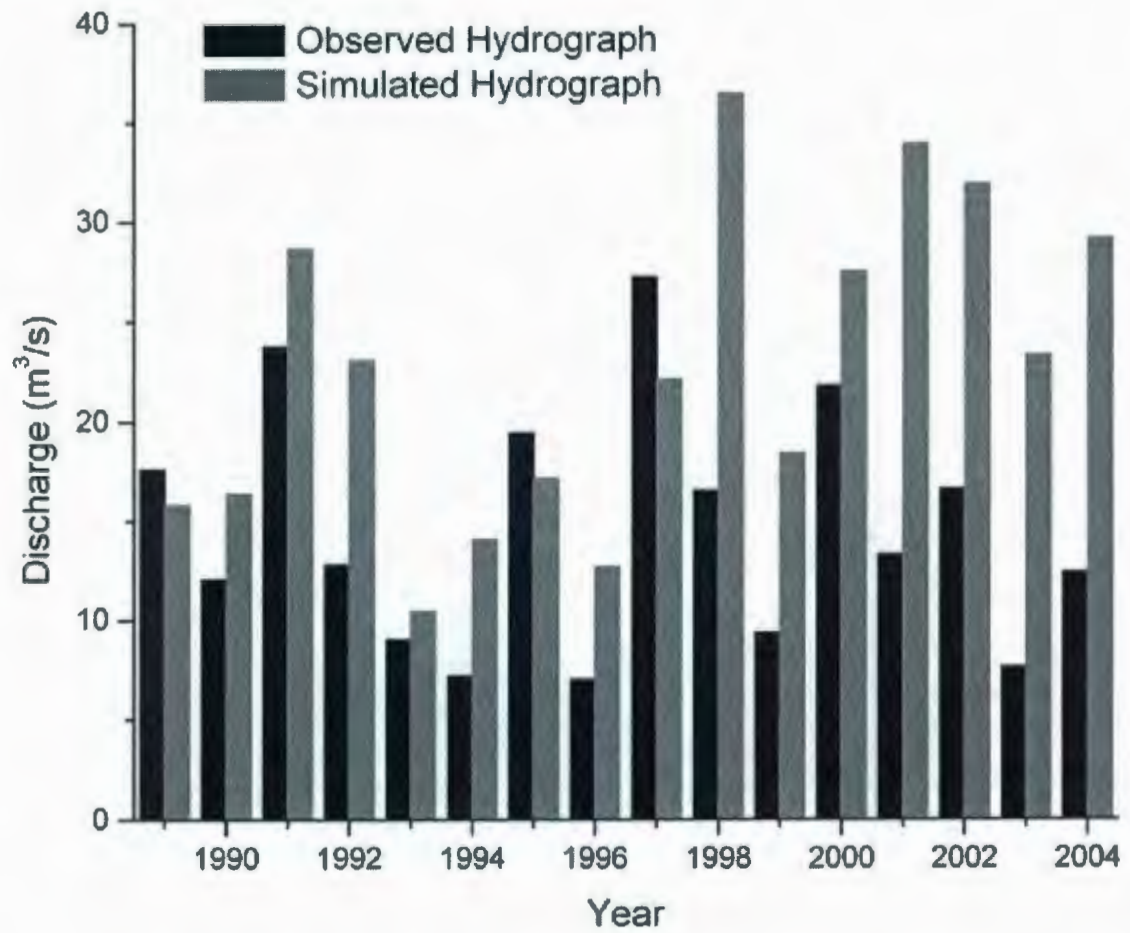


Figure 4.36 Simulated and observed annual hydrographs for the Deer River Watershed from 1988 to 2004

Table 4.7 Modelling efficiencies during SLURP daily verification in the Deer River Watershed

Year	NSE (%)	DV (%)
1988	49	-77.2
1989	32	-80.5
1990	49	-22.6
1991	52	-59.6
1992	31	-1.5
1993	32	-69.0
1994	-27	20.1
1995	52	-81.0
1996	17	96.3
1997	66	-63.8
1998	-61	-11.9
1999	-31	22.8
2000	-3	-34.5
2001	-61	24.6
2002	-10	-10.3
2003	-4	45.2
2004	-121	72.2
Average.	4	-13.6
Max.	66	96.3
Min.	-121	-81.0

Note: NSE is the Nash and Sutcliffe efficiency; and DV is the deviation of runoff volumes.

Table 4.8 Modelling efficiencies during SLURP verification in the Deer River Watershed

	NSE (%)	DV (%)
Monthly	21	-2.8
Annual	-235	97

Note: NSE is the Nash and Sutcliffe efficiency; and DV is the deviation of runoff volumes.

4.8 Modelling of the Chesnaye Sub-basin

To further understand the hydrological features of the subarctic wetland in the summer time at a small scale basin, a typical sub-arctic catchment (the Chesnaye Sub-basin, Figure 3.3) located in the northeast corner of the Deer River Watershed was chosen for detailed field survey and modelling (see Chapter 3). It mainly belongs to the downstream of the river with an average elevation of 52 m. Land cover conditions are limited to tundra, shrub and little coniferous forest. Soil characteristics have been studied and addressed in Section 3.2. An automated weather station was established at Rail Spur since fall 2005. Four stream gauging stations were deployed during each summer and fall from 2006 to 2008 (Figure 3.4a).

4.8.1 Delineation of the Chesnaye Sub-basin

The study area was delineated into 48 sub-catchments by TOPAZ as shown in Figure 4.37. The four stream gauging stations (Stations 5, 6, 7, and 10) are also labelled in the figure. The generated river network is shown in Figure 4.38.

4.8.2 Land Cover

Land cover data (351 columns, 353 rows) of the Chesnaye Sub-basin was extracted from the land classification file (1801 columns, 1601 rows) of the Deer River Watershed. There are five types of land cover in the Chesnaye Sub-basin as shown in Figure 4.39.

4.8.3 Meteorological and Streamflow data

Meteorological data was obtained from the automated weather station at Rail Spur. Streamflow data was obtained from the four gauging stations deployed within the Chesnaye Sub-basin.

4.8.4 Modelling Results

Figures 4.40 to 4.48 show the modelling results from SLURP between 2006 and 2008. It could be observed that most of rainfall events were overestimated during the summertime (July and August). This is usually attributed to the canopy interception, depression storage, soil layer porosity, permafrost table descending and evapotranspiration. Canopy interception is not one of the dominant factors because the vegetation types in the study area are mainly limited to tundra and shrub which have small LAI. Depression storage, which refers to the local small ponds, contributes greatly to receiving and storing the precipitation. Descending frost table reveals more highly porous soil which is capable of taking remarkable amount of precipitation. Evapotranspiration performs as a catalyst of amplifying the soil water storage because of the high temperature and sufficient net radiation. These factors result in the consequence that most of the rainfall water is stored in the local ponds or soil layers, leaving only little water to be discharged in the streams. In the fall (September and October), runoff resulted from rainfall events are estimated closely to the actual observed flow at Stations 6 and 7 (Figures 4.41, 4.43, 4.44 and 4.47). This illustrates that the soil layers are more or less saturated after the summer drainage. Station 5 and Station 10 are underestimated during the whole experiment season (July – September) in 2007 (Figures 4.42 and 4.45). This is concluded as the error due to the

delineation of the watershed which results from the limitation of DEM resolution. The sub-catchment where station 10 is located should be much larger than the one used in the modelling work based on the field investigation and observation by Google Earth®. With the influence of numerous ponds, the simulated flow for Station 10 is lower than the observed record. Due to the fact that Station 5 sums up the water discharge from Stations 6 and 10, its estimation is consequently shorted than observation.

The results support the conclusion from the modelling work of the Deer River Watershed that SLURP overestimates the summer rainfall events because it does not consider the existence of the frost table and ponds. Moreover, reduced runoff may also be explained by the underestimated evapotranspiration from the Morton CRAE model. Nonetheless, it is indicated that SLURP has good modelling performance in small scale (the Chesnaye Sub-basin) as in macro scale (the Deer River Watershed). Future research work regarding the modifications to the modules of snowmelt and runoff concentration will promote the accuracy of SLURP.

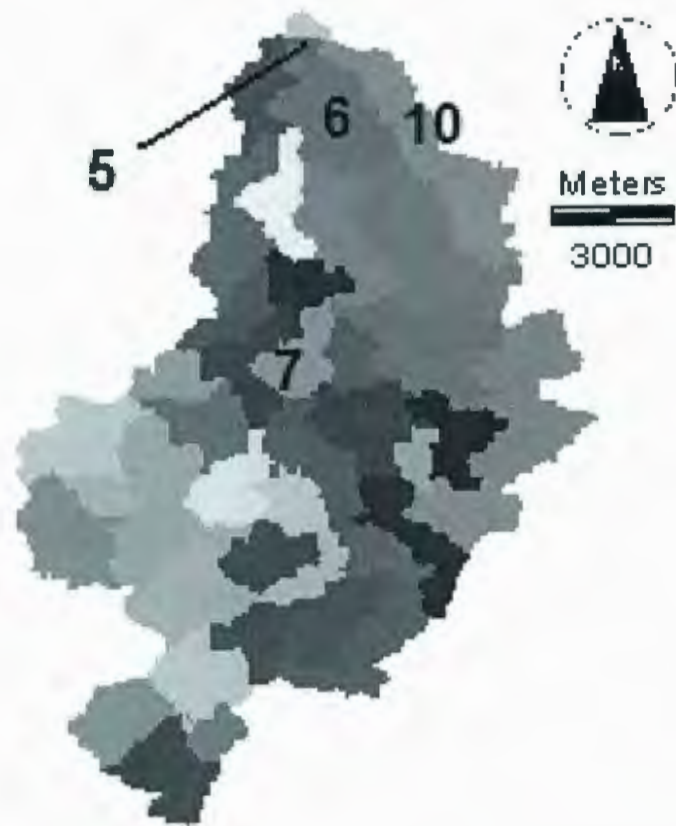


Figure 4.37 Delineation of the Chesnaye Sub-basin by TOPAZ

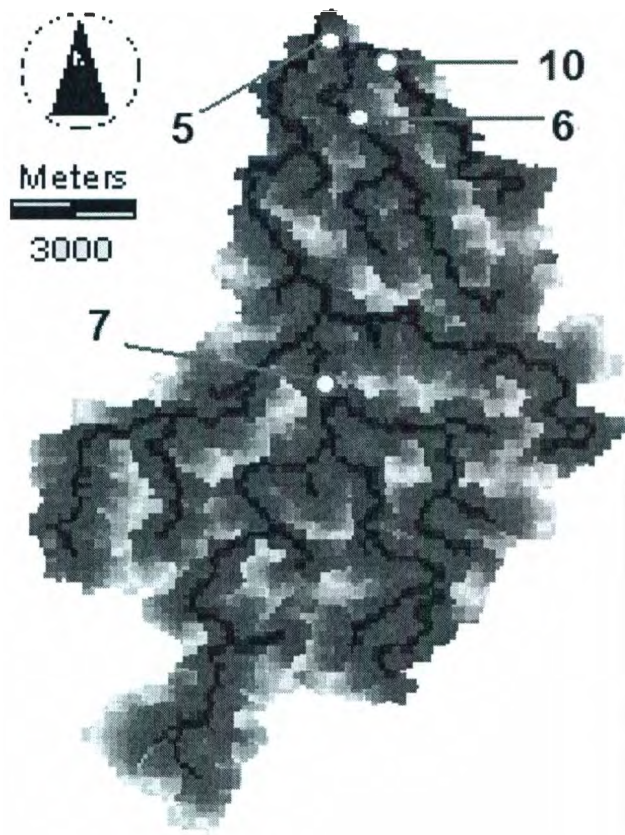


Figure 4.38 River network of the Chesnaye Sub-basin by TOPAZ

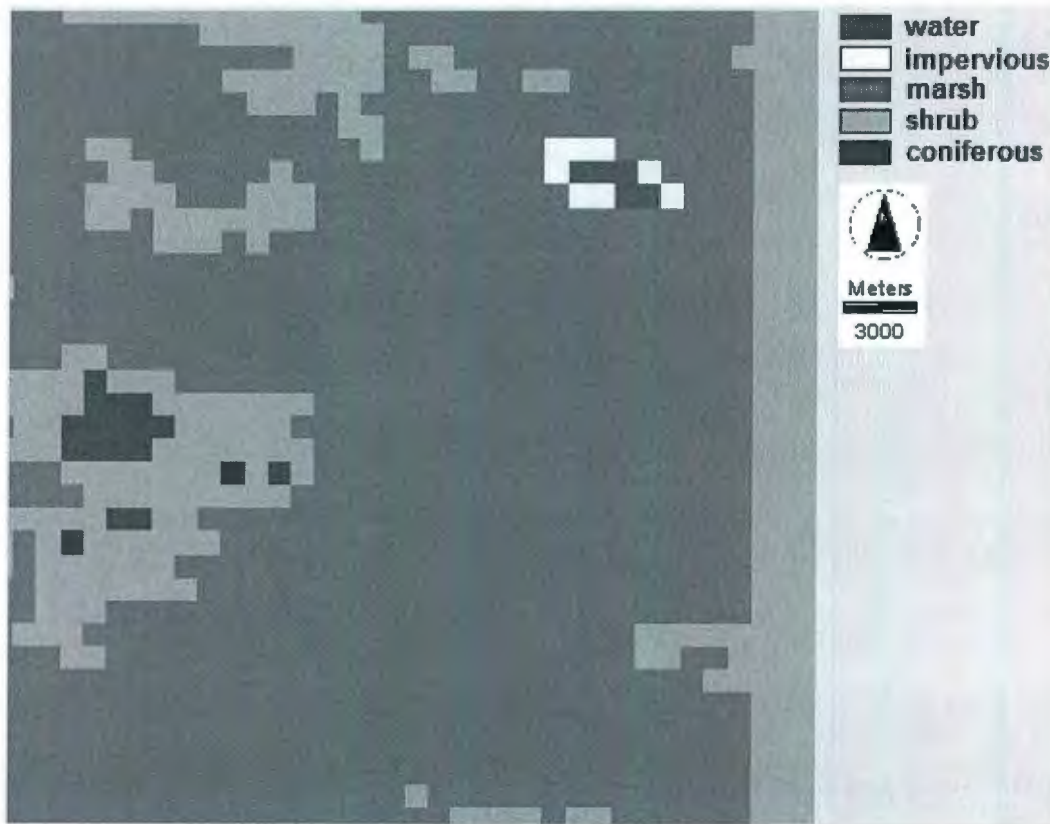


Figure 4.39 Land cover classification of the Chesnaye Sub-basin by IDRISI®

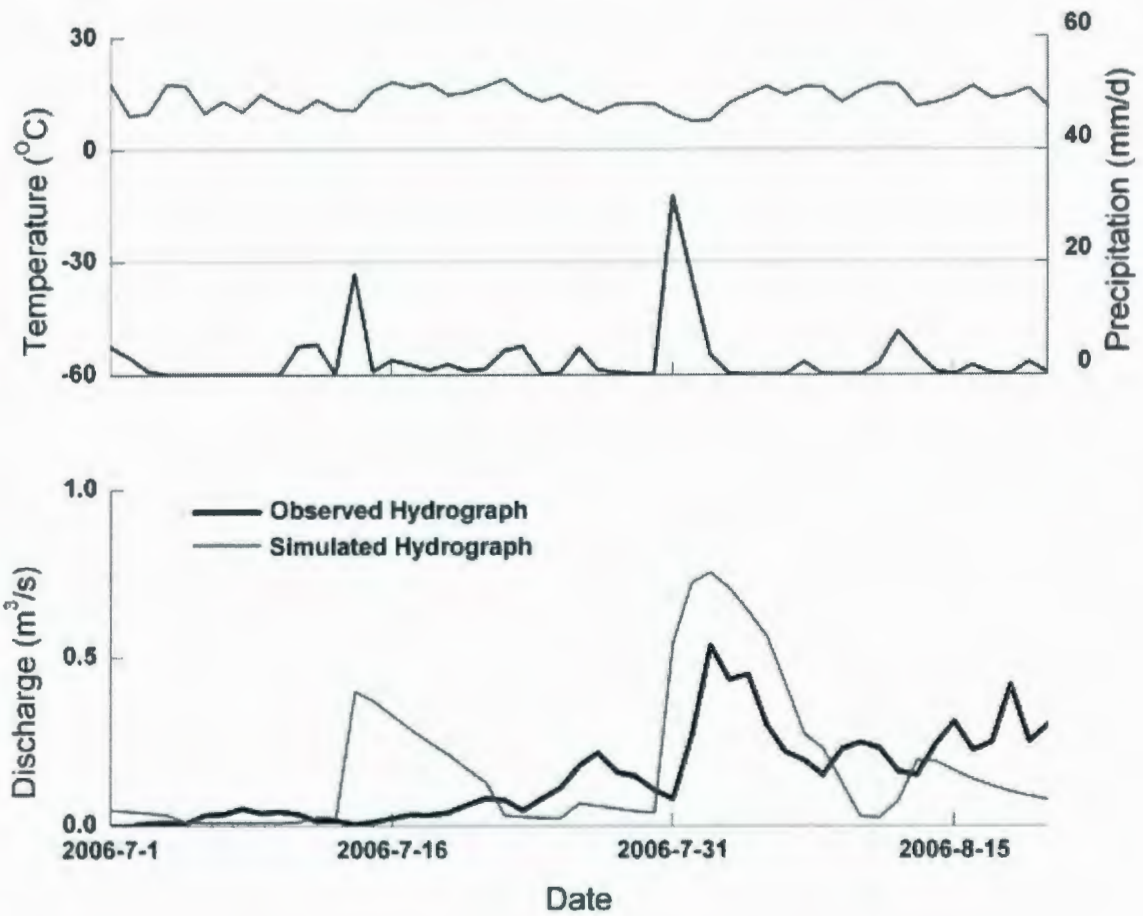


Figure 4.40 Simulated and observed daily hydrographs by SLURP for Station 5 in 2006

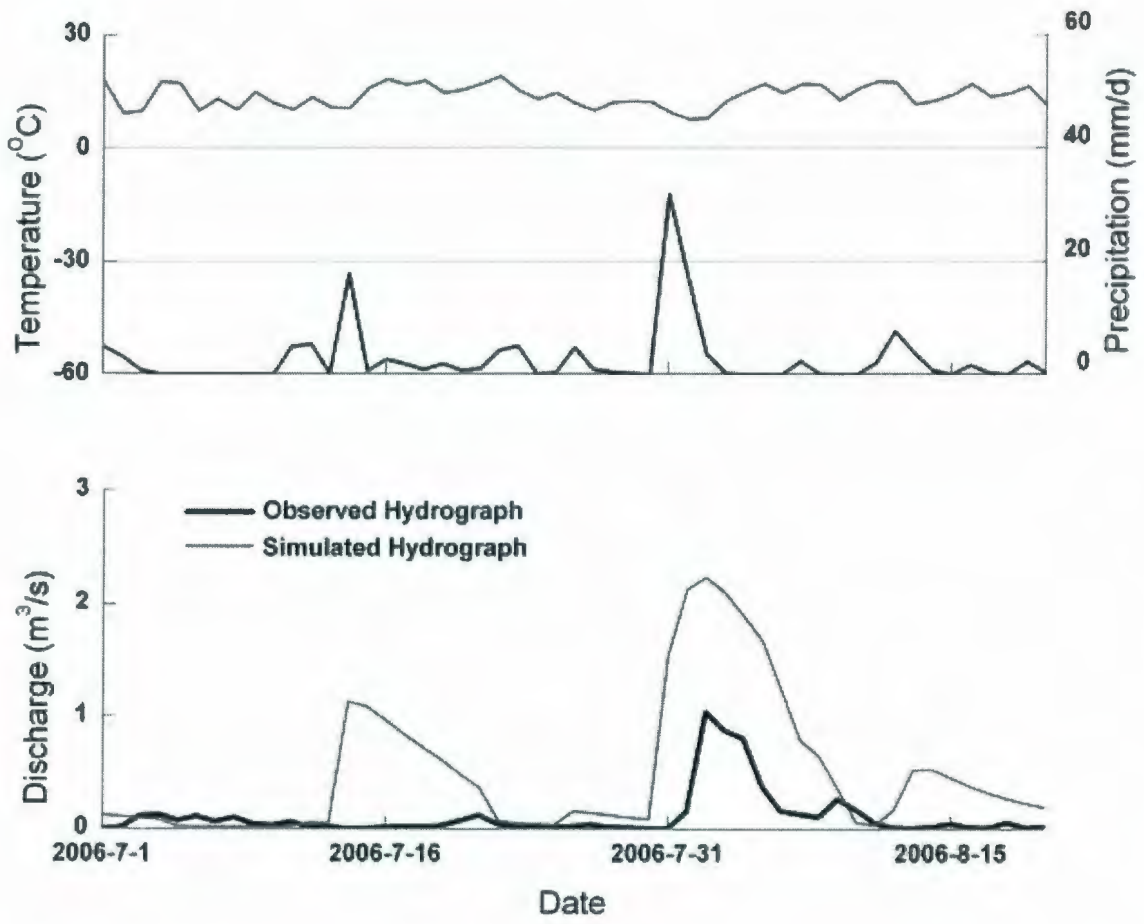


Figure 4.41 Simulated and observed daily hydrographs by SLURP for Station 7 in 2006

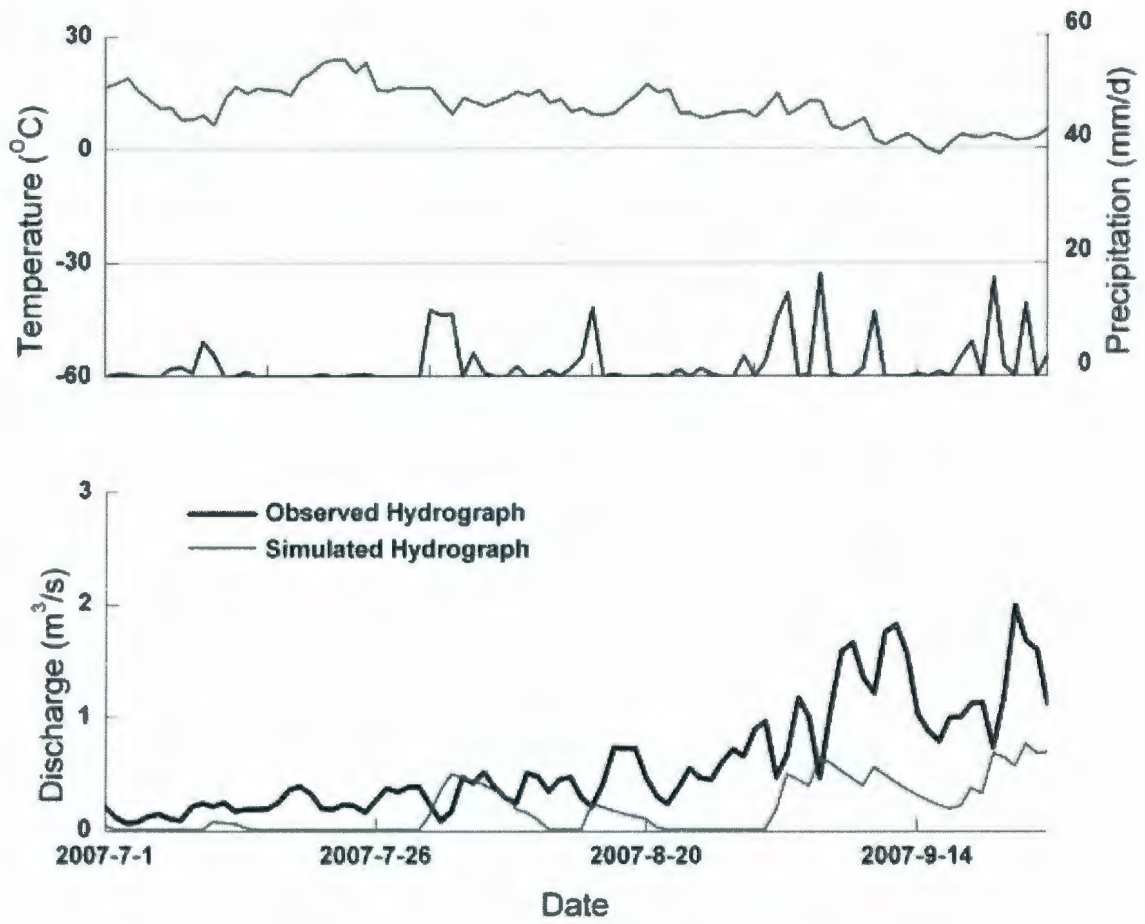


Figure 4.42 Simulated and observed daily hydrographs by SLURP for Station 5 in 2007

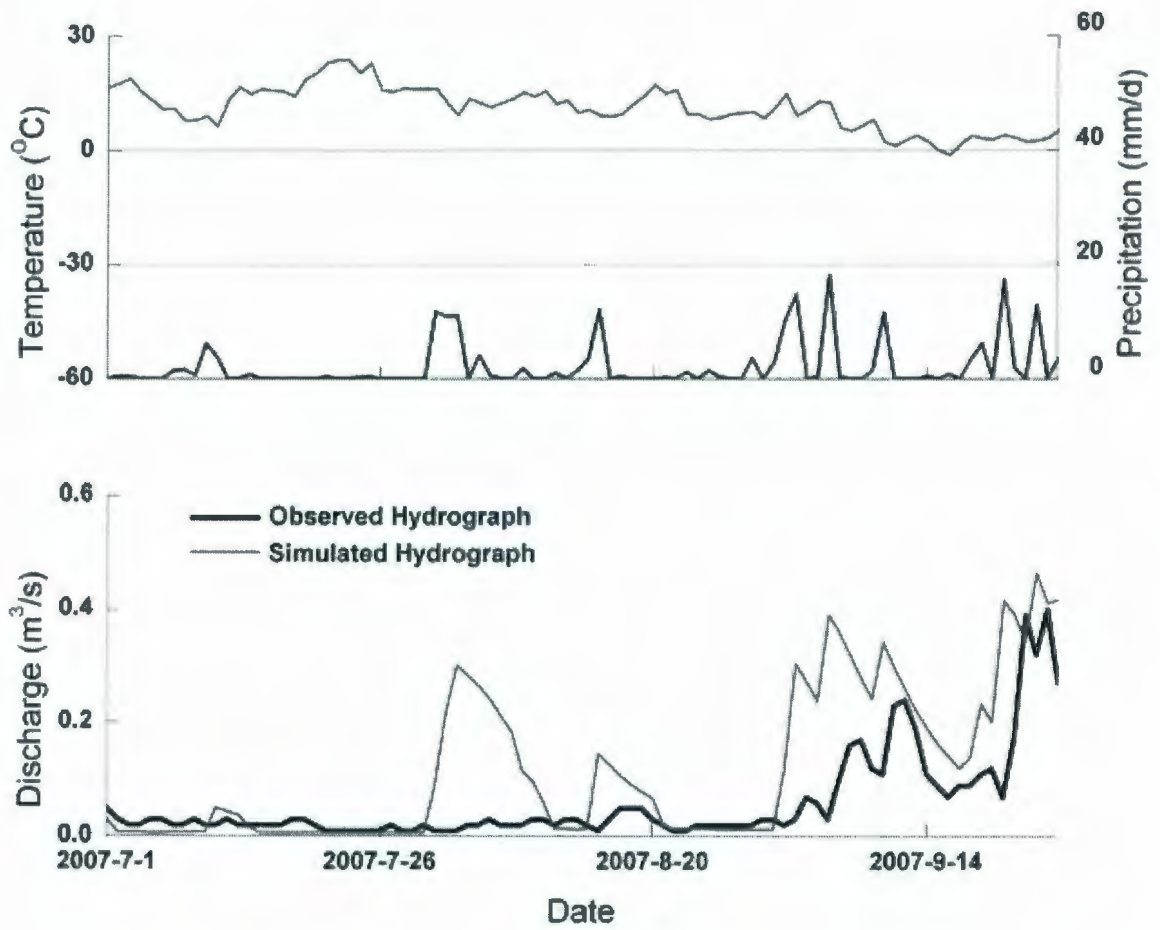


Figure 4.43 Simulated and observed daily hydrographs by SLURP for Station 6 in 2007

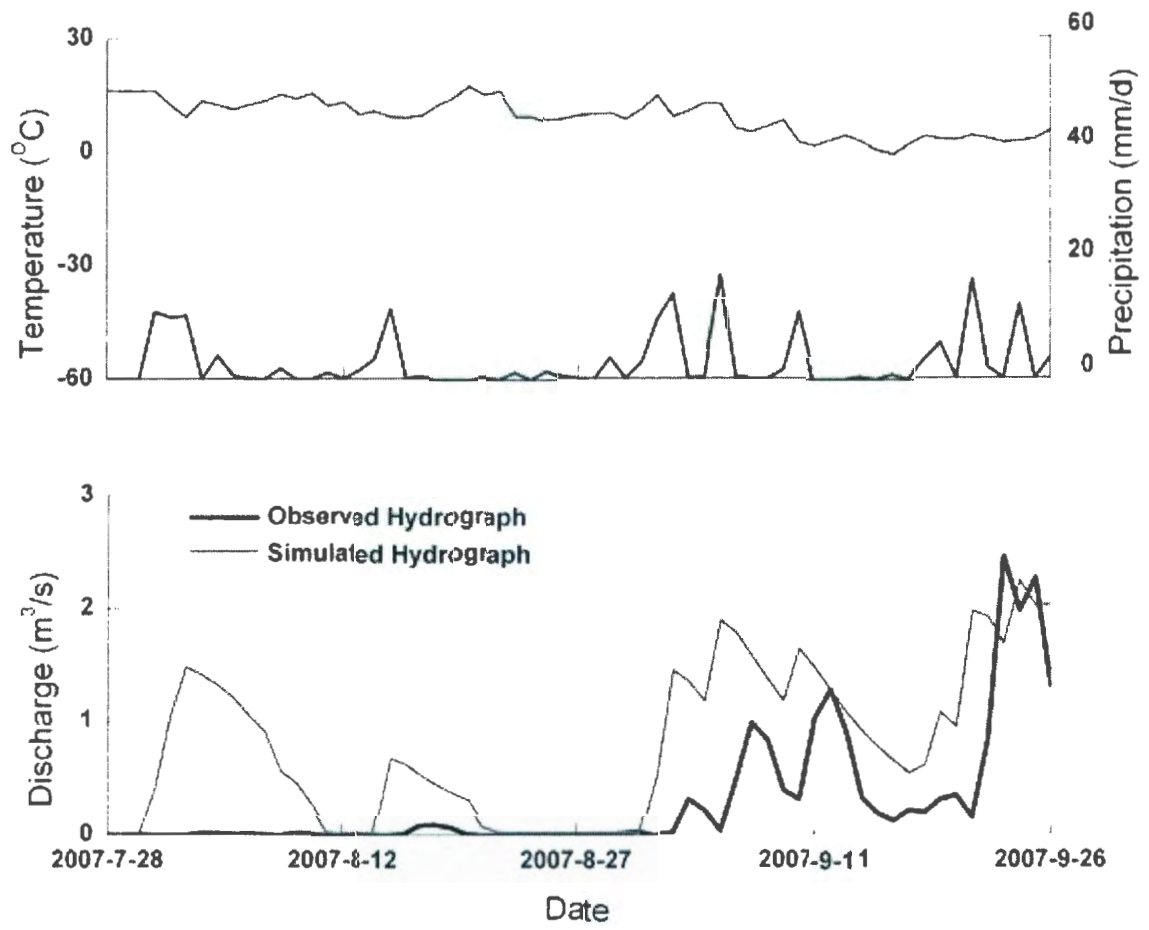


Figure 4.44 Simulated and observed daily hydrographs by SLURP for Station 7 in 2007

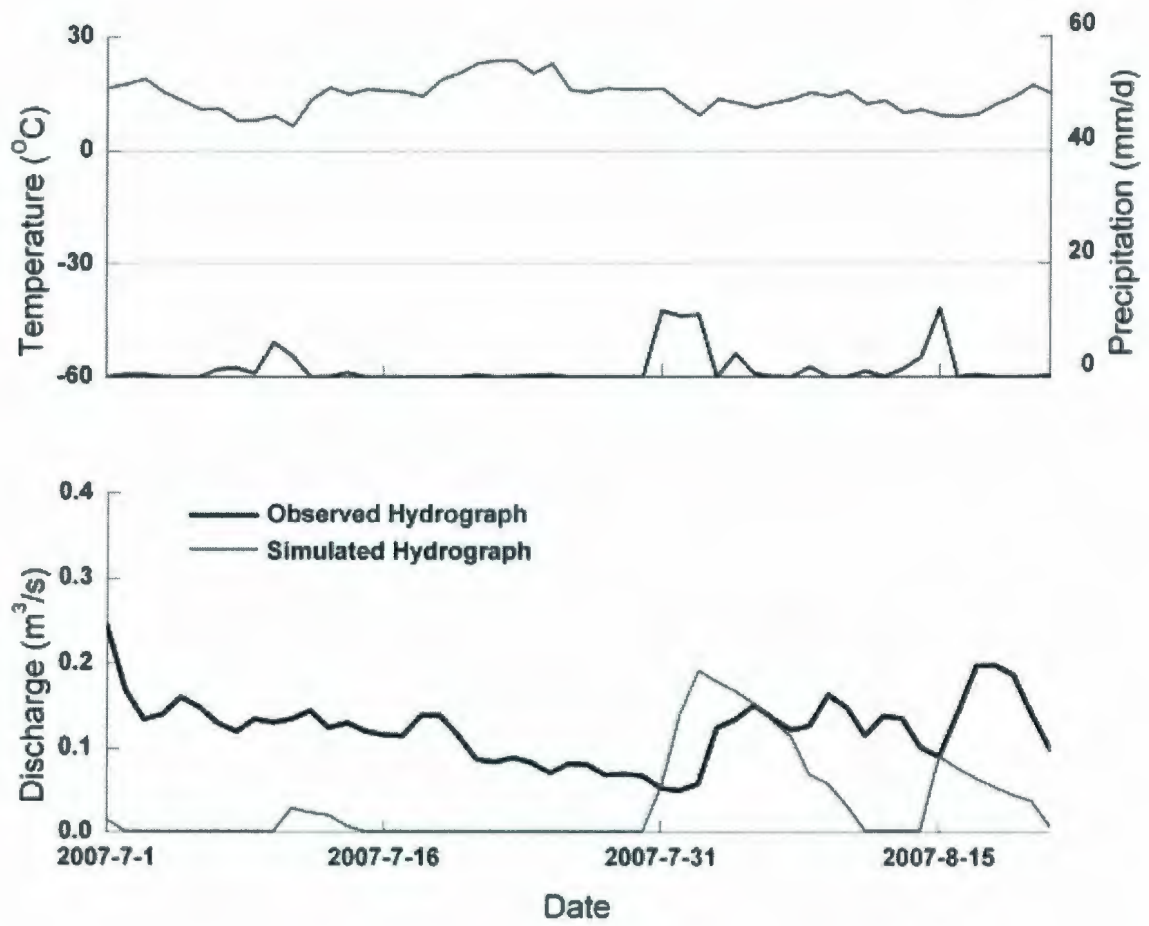


Figure 4.45 Simulated and observed daily hydrographs by SLURP for Station 10 in 2007

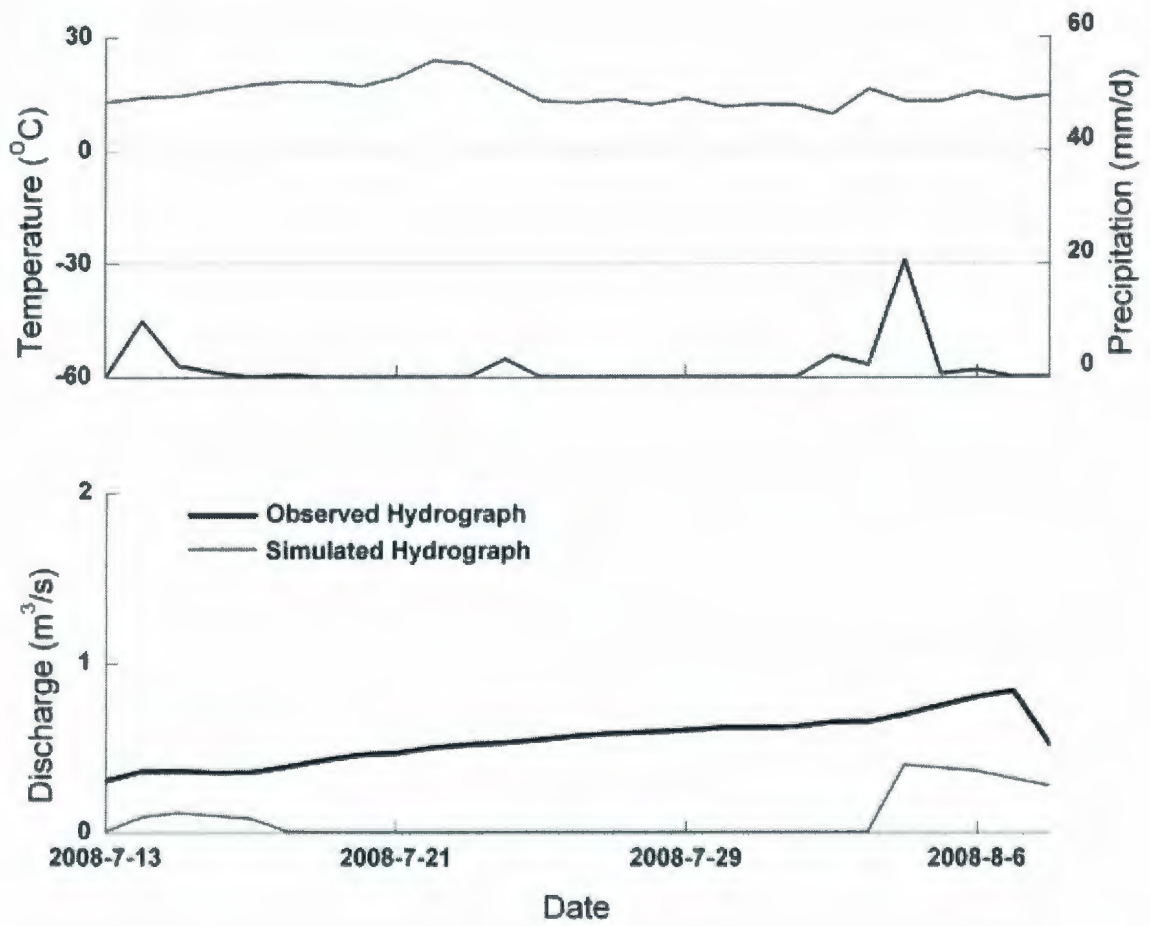


Figure 4.46 Simulated and observed daily hydrographs by SLURP for Station 5 in 2008

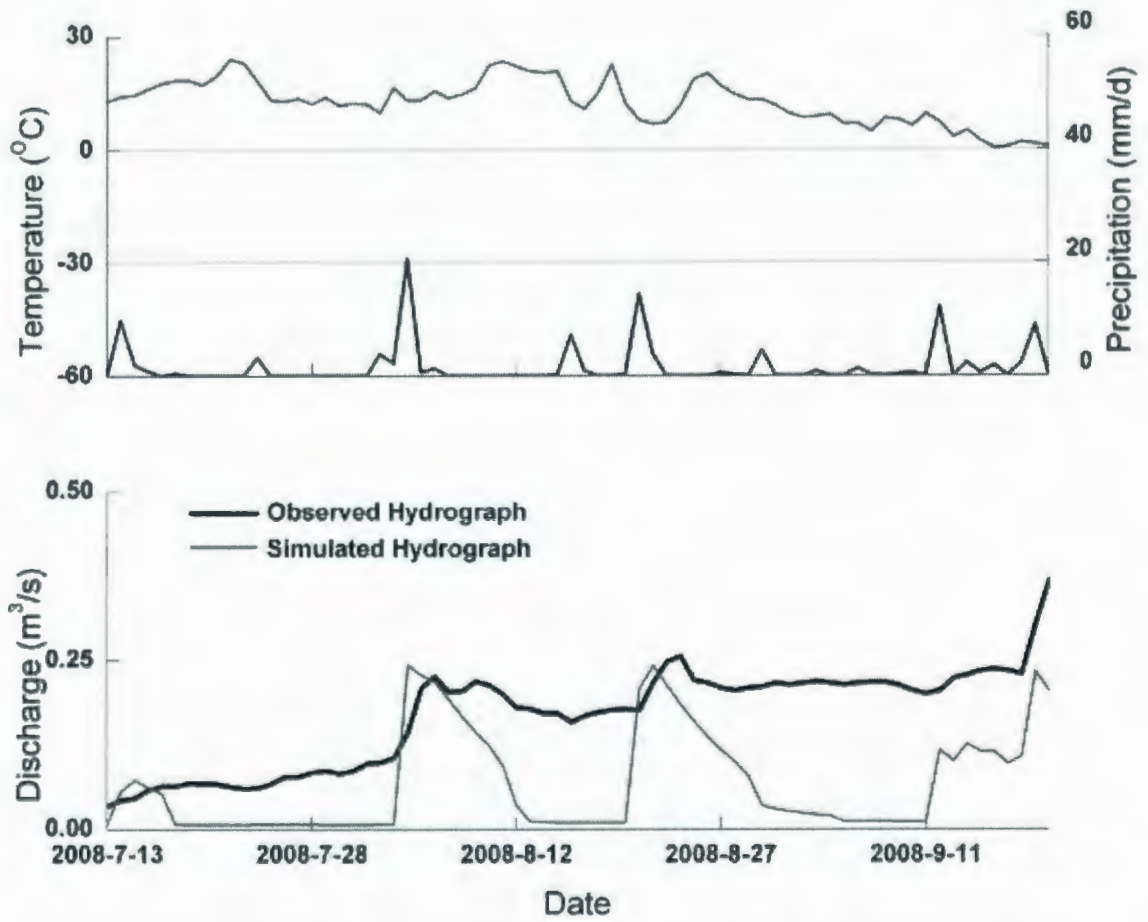


Figure 4.47 Simulated and observed daily hydrographs by SLURP for Station 6 in 2008

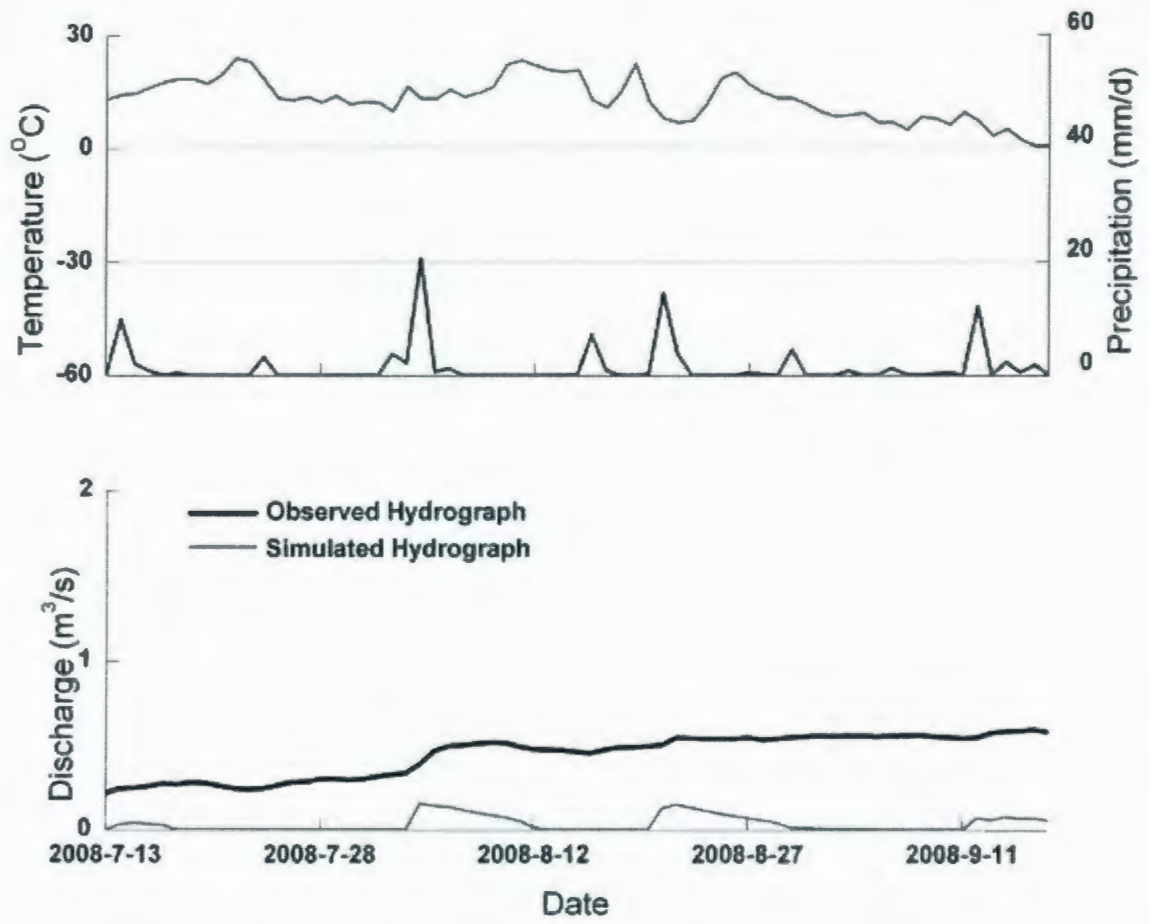


Figure 4.48 Simulated and observed daily hydrographs by SLURP for Station 10 in 2008

4.9 Summary

In this chapter, a semi-distributed, conceptual continuous hydrological model – SLURP was applied to model the Deer River Watershed and the Chesnaye Sub-basin. Results from the modelling of the Deer River Watershed show some weaknesses of SLURP of not considering the influences from the frost table and ponds, underestimating the water storage capacity of the organic soil layers and the errors of the built-in snowmelt routine. The DV values of the calibration and verification periods also indicate that the fluctuation of the simulated flow is not as intensive as that of the observed flow. This may be explained by the effect of permafrost layer which blocks the percolation of precipitation and snowmelt water and increases the runoff in the watershed during the snowmelt period. On the other hand, not removing enough volume of water from the system through the process of evapotranspiration can also overestimate the runoff during the summer period. Results from modelling the Chesnaye Sub-basin show that SLURP overestimates the summer runoff from rainfall events because of the underestimated evapotranspiration and not considering the effects from the frost table and local ponds. It is implied that modifications to the snowmelt algorithm and adding some routines regarding the frost table as well as the particular soil features may improve the model's performance. The next chapter presents the application of the WATFLOOD to the Deer River Watershed and the Chesnaye Sub-basin. The goal of this modelling study is to examine the robustness of WATFLOOD in the sub-arctic wetland system and compare it with SLURP. Detailed discussions and comparisons will be presented in Chapter 6.

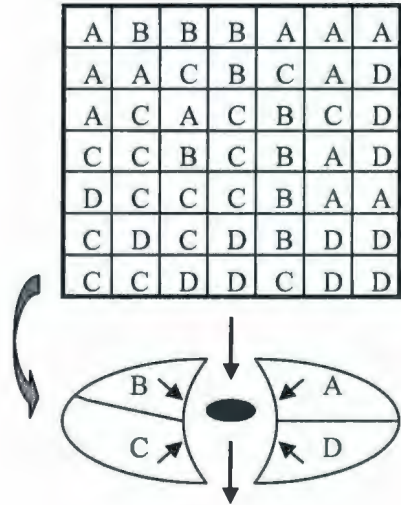
Chapter 5 Modelling of the Deer River Watershed by WATFLOOD

5.1 WATFLOOD

WATFLOOD is a widely used physically based hydrological model to forecast flood events or simulate watersheds without sacrificing the distributed features of hydrological and meteorological as well as the computational efficiency. As differentiated from SLURP, WATFLOOD is constructed based on the concept of Grouped Response Units (GRU) and the hourly time-step simulation. Each GRU is a fundamental computational element which contains various land covers and distributed hydrological parameters. Figure 5.1a illustrates the above concept that WATFLOOD combines all the 49 (7×7) grids into one GRU which has four land covers (A, B, C, and D). Then all the grids within the GRU are categorized into four sub-groups (A, B, C and D) with determined ratios based on the hydrological similarities defined by land cover types. The runoff response from each sub-group is subsequently calculated and routed downstream to the outlet of each GRU. All the runoff amounts from each land cover are accumulated and routed to the next GRU (Figure 5.1b). WATFLOOD assumes that similar land covers exist in regions of homogenous soil characteristics and topographic conditions.

As with most distributed hydrological models, WATFLOOD (Figure 5.2) only simulates part of the overall processes of the natural environment, including interception, infiltration, evapotranspiration, snow accumulation and ablation, interflow, recharge, baseflow, and overland and channel routing (Kouwen *et al.*, 1993; Kouwen, 2008).

(a) **Group Response Unit**
to deal with basin heterogeneity



(b) **Physically Based Streamflow Routing**

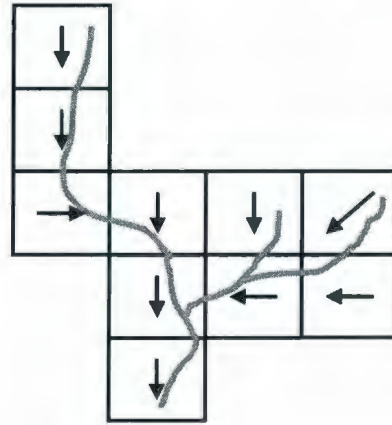


Figure 5.1 Group Response Unit and runoff routing concept (Donald, 1992)

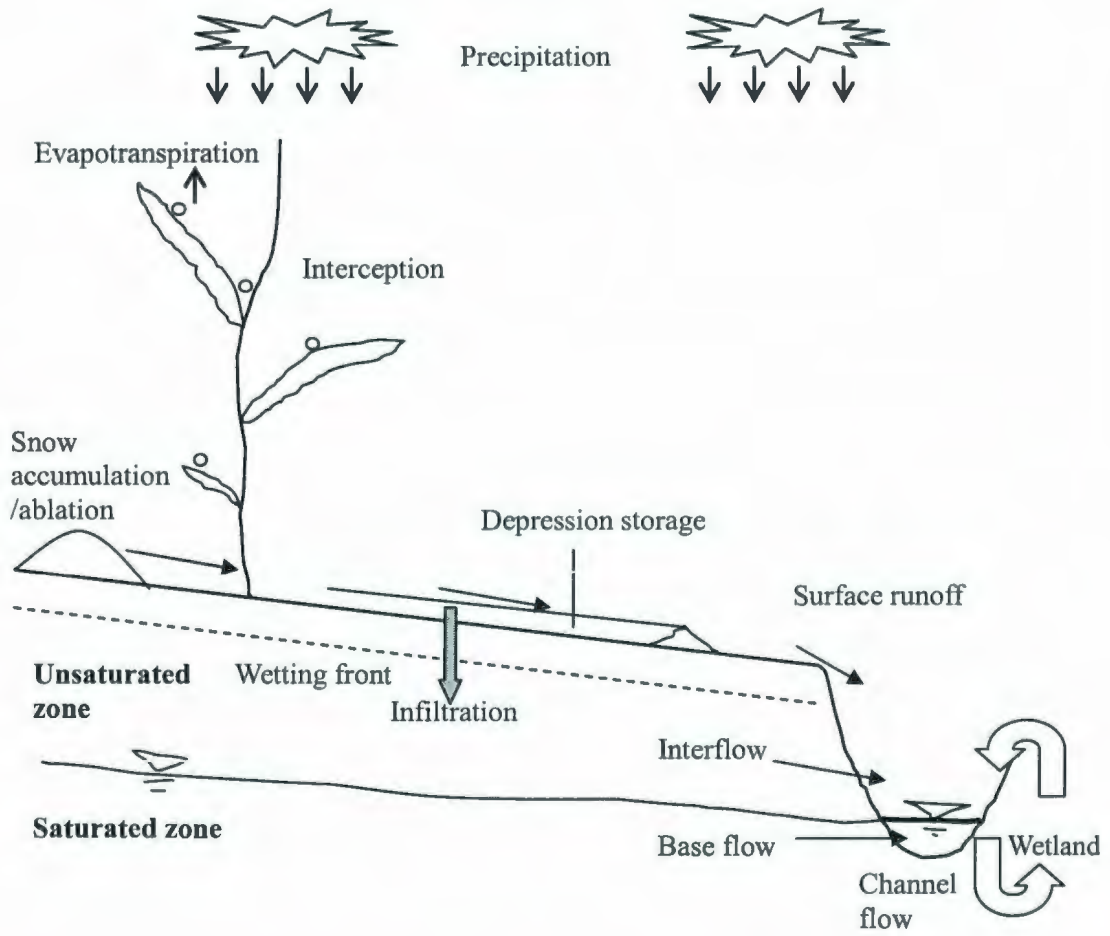


Figure 5.2 Schematic of the runoff generation algorithm in WATFLOOD (Kouwen, 2008)

5.1.1 Interception

Interception is calculated as the sum of two parts: interception evapotranspiration (IET) during the storm event (mm/h) and monthly maximum canopy storage (Rowe, 1983). IET is computed from (Linsley *et al.*, 1949):

$$IET = FPET \times PET \quad (5-1)$$

where $FPET$ is the factor which can be set to 1.0 during a precipitation event and 3.0 after the precipitation.

5.1.2 Surface Storage

Because of the interception, depression storage is assumed to be exponentially related with its maximum value (Linsley *et al.*, 1949):

$$D_s = S_d(1 - e^{-kP_e}) \quad (5-2)$$

where D_s is the depression storage (m^3); P_e is the accumulated rainfall excess (mm); S_d is the maximum value of depression storage (m^3); and k is the factor which decides how fast the depression storage can reach its top limit.

5.1.3 Infiltration

The following Philip Equation (Philip, 1954) is applied for representing the significant physical process of infiltration:

$$\frac{dF}{dt} = K \left[1 + \frac{(m - m_0)(Pot + D1)}{F} \right] \quad (5-3)$$

where F is the total depth of infiltrated water (mm); t is the total time (hour); K is the hydraulic conductivity (mm/h); m is the average moisture content of the soil to the depth

of the wetting front (percentage); m_0 is the initial soil moisture content (percentage); Pot is the capillary potential at the wetting front (mm); and DI is the depth of water on the soil surface (mm). Moreover, Pot could be calculated from:

$$Pot = 250 \log(K) + 100 \quad (5-4)$$

5.1.4 Initial Soil Moisture

WATFLOOD defines the ground into three layers: upper zone storage (UZS , unsaturated), intermediate zone storage (IZS , unsaturated), and lower zone storage (LZS , saturated). Initial soil moisture (m_0) represents the moisture content of the intermediate zone which affects the infiltration of precipitation and melting water:

$$m_0 = API / 100 \quad (5-5)$$

where API is the Antecedent Precipitation Index (Boken *et al.*, 2005) and explained by:

$$API_i = K_r (API_{i-1}) + P_i \quad (5-6)$$

where K_r is the recession constant in the model; and P_i is the amount of precipitation in hour i (mm).

5.1.5 Evapotranspiration

5.1.5.1 Potential Evapotranspiration

Depending on the availability of temperature and net radiation data, Priestley-Taylor equation, Hargreaves equation or estimating evapotranspiration from published values can be selected for the computation of potential evapotranspiration. The Priestley-Taylor equation is described below and used when both temperature and net radiation data is

available (Priestley and Taylor, 1972).

$$PET = \alpha \frac{s(T_a)}{s(T_a) + \gamma} (K_n + L_n) \times \frac{1}{\rho_w \lambda_v} \quad (5-7)$$

where PET is the potential evapotranspiration rate (mm/h); K_n is net short wave radiation ($\text{MJ}/\text{m}^2/\text{h}$); L_n is the net long-wave radiation ($\text{MJ}/\text{m}^2/\text{h}$); $s(T_a)$ is the slope of the saturation-vapour pressure temperature curve; γ is the psychrometric constant (0.066 $\text{kPa}/^\circ\text{C}$); ρ_w is the mass density of water (kg/m^3); λ_v is the latent heat of vaporization ($\text{MJ}/\text{m}^2/\text{h}$); and α is suggested to be 1.26 in the moist climates (De Bruin and Keijman, 1979; Stewart and Rouse, 1976). The result from this method has to be adjusted by:

$$PET = 0.05 \times PET + 0.95 \times PET \times \frac{1 - alb}{1 - albe} \quad (5-8)$$

where $albe$ is the all-wave albedo in which the radiation measurement is made; and alb is the all-wave albedo for each land class. It should be noted that Priestley-Taylor is advanced because it separates evaporation and transpiration without requiring dew point temperature and relative humidity. However, the coefficient α may bring in some uncertainties.

Hargreaves equation is applied where only temperature data is available (Hargreaves and Samani, 1982). It could be explained by:

$$PET = 0.0075 \times R_a \times C_t \times \delta_t^{1/2} \times T_{avg,d} \quad (5-9)$$

where R_a is the total incoming extraterrestrial solar radiation in the same units as evapotranspiration (mm); C_t is a temperature reduction coefficient which is determined by relative humidity; δ_t is the difference between the mean monthly maximum and mean

monthly minimum temperature ($^{\circ}\text{F}$); and $T_{avg,d}$ is the mean temperature ($^{\circ}\text{F}$). If either temperature or net radiation data is available, the original method is chosen to estimate the evapotranspiration from published values. These published values are considered to be potential evapotranspiration rates as results from Priestley-Taylor equation and Hargreaves equation.

5.1.5.2 Actual Evapotranspiration

The actual evapotranspiration is reduced from the potential evapotranspiration under different scenarios:

$$\begin{array}{ll}
 AET = PET & \text{if : } PET < IET \\
 AET = (PET - IET) \times UZSI \times FPET2 \times FTALL \times ETP & \text{if : } PET > IET \\
 AET = PET \times UZSI \times FPET2 \times FTALL \times ETP & \text{if : } IET = 0 \\
 AET = PET & \text{for : water - surface}
 \end{array} \quad (5-10)$$

where AET is the actual evapotranspiration rate (mm/h); IET is the interception evapotranspiration (mm/h); $FPET2$ is the second reduction coefficient (0.02-1.0); $FTALL$ is the forest vegetation coefficient (0.70 or 1.0); and $UZSI$ is the upper zone storage indicator which can be obtained by:

$$UZSI = \left[\frac{(UZS - PWP)}{(SAT - PWP)} \right]^{1/2} \quad (5-11)$$

where UZS is the water accumulation in the upper zone (mm); SAT is the soil saturation level (mm); and PWP is the permanent wilting point (mm). SAT and PWP can be calculated by the following equations:

$$PWP = FFCAP \times FULL \quad (5-12)$$

$$SAT = SPORE \times FULL \quad (5-13)$$

where *FFCAP* and *SPORE* are constants representing the field capacity and saturation point, respectively; and *FULL* is the theoretical depth at which all the soil pores are full of water (mm) and computed by:

$$FULL = \frac{RETN}{FCAP} \quad (5-14)$$

where *RETN* is the retention constant (mm); and *FCAP* is the field capacity constant.

5.1.6 Snowmelt

Snowmelt process is calculated by the widely used the degree-day method as (Anderson, 1973):

$$M = MF(T_a - T_{base}) \quad (5-15)$$

where *M* is the hourly snowmelt depth (mm/h); *MF* is the melting factor (mm/°C/h); *T_a* is the air temperature (°C); and *T_{base}* is the temperature at which snow starts to melt (°C).

5.1.7 Interflow

Infiltrated water, which is firstly stored in the upper zone storage (*UZS*), will penetrate downwards or horizontally. The horizontal flow is called interflow and can be estimated by:

$$DUZ = REC \times (UZS - RETN) \times S_i \quad (5-16)$$

where *DUZ* is the depth of upper zone storage that is released as interflow (mm); *REC* is the dimensionless coefficient; *UZS* is the water accumulation in the upper zone (mm); *RETN* is the retention constant (mm); and *S_i* is the internal slope (dimensionless).

5.1.8 Groundwater Recharge

Groundwater recharge is defined as water drainage from the upper zone to the lower zone and calculated in the model by:

$$DRNG = AK2 \times (UZS - RETN) \quad (5-17)$$

where $DRNG$ is the groundwater recharge (mm); and $AK2$ is an intermediate zone resistance parameter.

5.1.9 Overland Flow

Water is routed to the channel when the infiltration and depression capacity are both exceeded:

$$Q_r = (D1 - D_s)^{1.67} S_i^{0.5} A_b / R3 \quad (5-18)$$

where Q_r is channel inflow (m^3/s); $D1$ is surface storage (mm); D_s is the depression storage capacity (mm); A_b is the area of the basin element (m^2); and $R3$ is the combined channel roughness and length parameter.

5.1.10 Base Flow

Ground water depletion is related with base flow, which is described as:

$$QLZ = LZF \times LZS^{PWR} \quad (5-19)$$

where LZF is the lower zone function constant; LZS is the water accumulation in the lower zone (mm); and PWR is the coefficient in the lower zone function.

5.1.11 Channel Routing

The routing of water through the channel system is conducted by using a storage routing method (Kouwen, 2008) as shown in the following equation:

$$\frac{I_1 + I_2}{2} - \frac{O_1 + O_2}{2} = \frac{S_2 - S_1}{\Delta t} \quad (5-20)$$

where I is the inflow to the reach consisting of overland flow, interflow, base flow as well as channel flow from all upstream units (m^3/s); O is the outflow from the reach (m^3/s); S represents the storage (m^3/s); Δt is the time step (s); and subscripts 1 and 2 are the time steps. Inflow I can be calculated by:

$$I = Q + q_{in} \quad (5-21)$$

where Q is entering discharge from upstream boundary (m^3/s); and q_{in} is lateral flow (m^3/s) obtained from:

$$q_{in} = q_{int} + q_l + q_{lz} + q_{stream} - q_{loss} \quad (5-22)$$

where q_{int} is the interflow (m^3/s); q_l is the overland flow (m^3/s); q_{lz} is the base flow (m^3/s); q_{stream} is the precipitation falling on the stream (m^3/s); and q_{loss} is the less evaporation (m^3/s). The main channel flow can be computed by:

$$Q = \frac{1}{n} \frac{1}{w^{0.667}} A_{cs}^{1.667} S_s^{0.5} \quad (5-23)$$

where n is the Manning's roughness coefficient; w is the main channel width (m); A_{cs} is the main channel cross section area (m^2); and S_s is the internal slope.

5.1.12 Wetland Routing

Wetland routing is governed by the method proposed by McKillop *et al.*, (1999).

Interaction between the wetland and the channel is computed by Dupuit-Forchheimer discharge equation (Bear, 1979):

$$q_{o_{wet1,2}} = \frac{kcond}{2} (h_{wet1,2}^2 - h_{cha1,2}^2) \quad (5-24)$$

where $q_{o_{wet}}$ is the lateral wetland outflow (m^3/s); $kcond$ is the hydraulic conductivity (m/s); h_{wet} is the height of water in wetland (m); h_{cha} is the height of water in channel (m); and subscripts 1 and 2 are the time steps. During the wetland routing, the net income flows contributing to the channel and the wetland are calculated by:

$$\begin{aligned} q_{channel} &= q_{in} + q_{stream} - q_{loss} + q_{o_{wet}} \\ q_{wet} &= q_{int} + q_l + q_{lz} + q_{swrain} - q_{swevp} \end{aligned} \quad (5-25)$$

where $q_{channel}$ and q_{wet} are the net income flows of the channel and the wetland (m^3/s), respectively; q_{swrain} is the flow contribution from the precipitation (m^3/s); and q_{swevp} is the evaporation loss off the wetland surface (m^3/s).

5.1.13 Lake Routing

Water is routed through lakes using either a power function or a polynomial function as below:

$$\begin{aligned} Outflow &= b_1 \times Storage^{b_2} \\ Outflow &= b_1 \times Storage + b_2 \times Storage^2 + b_3 \times Storage^3 + b_4 \times Storage^4 + b_5 \times Storage^5 \end{aligned} \quad (5-26)$$

where $Outflow$ is the flow moving out of the lake (m^3/s); $Storage$ is the storage of the lake (m^3/s); and b_1 , b_2 , b_3 , b_4 , and b_5 are coefficients. If b_3 , b_4 , and b_5 are set to 0, the first power function will be assumed.

5.2 Watershed Delineation by TOPAZ and EnsimHydrologic

A 3 arc second (approximately 90 m) resolution DEM for the Deer River Watershed was obtained from the National Map Seamless Server of the USGS (USGS, 2007). The DEM was subsequently processed by TOPAZ which has strong capability of automated digital landscape analysis. Figure 4.3 displays the river network of the Deer River Watershed which was generated by TOPAZ. WATFLOOD is based on grid-cell calculation which differs from the sub-watershed concept in SLURP. Four output files from TOPAZ, which include a DEM file, a boundary file, a drainage direction file and an upstream drainage area file, were loaded into EnsimHydrologic[®] in order to generate the input files of the Deer River. Figures 5.3 to 5.5 show the boundary, elevation variation and channel network (flow directions) of the watershed in EnsimHydrologic[®].

The MAP file (.map file) which is required by WATFLOOD could be obtained by delineating the watershed file (.wsd file) into identical rows and columns. Here the entire DEM was evenly gridded into 48 rows and 54 columns because it requires each grid cell to be an exact square which means the unit distance on both longitude and latitude should be equal. Figure 5.6 displays the gridded cells and different colours stand for different elevations. Figure 5.7 shows the combination of gridded cells, boundary and channel network of the Deer River Watershed which are the basic components of a MAP file. Then dataset of land covers can be embedded into the MAP file by adding a GeoTIF format file. Flow direction of each grid cell can be displayed if necessary. Geological and land cover information can also be manually edited for each grid cell.

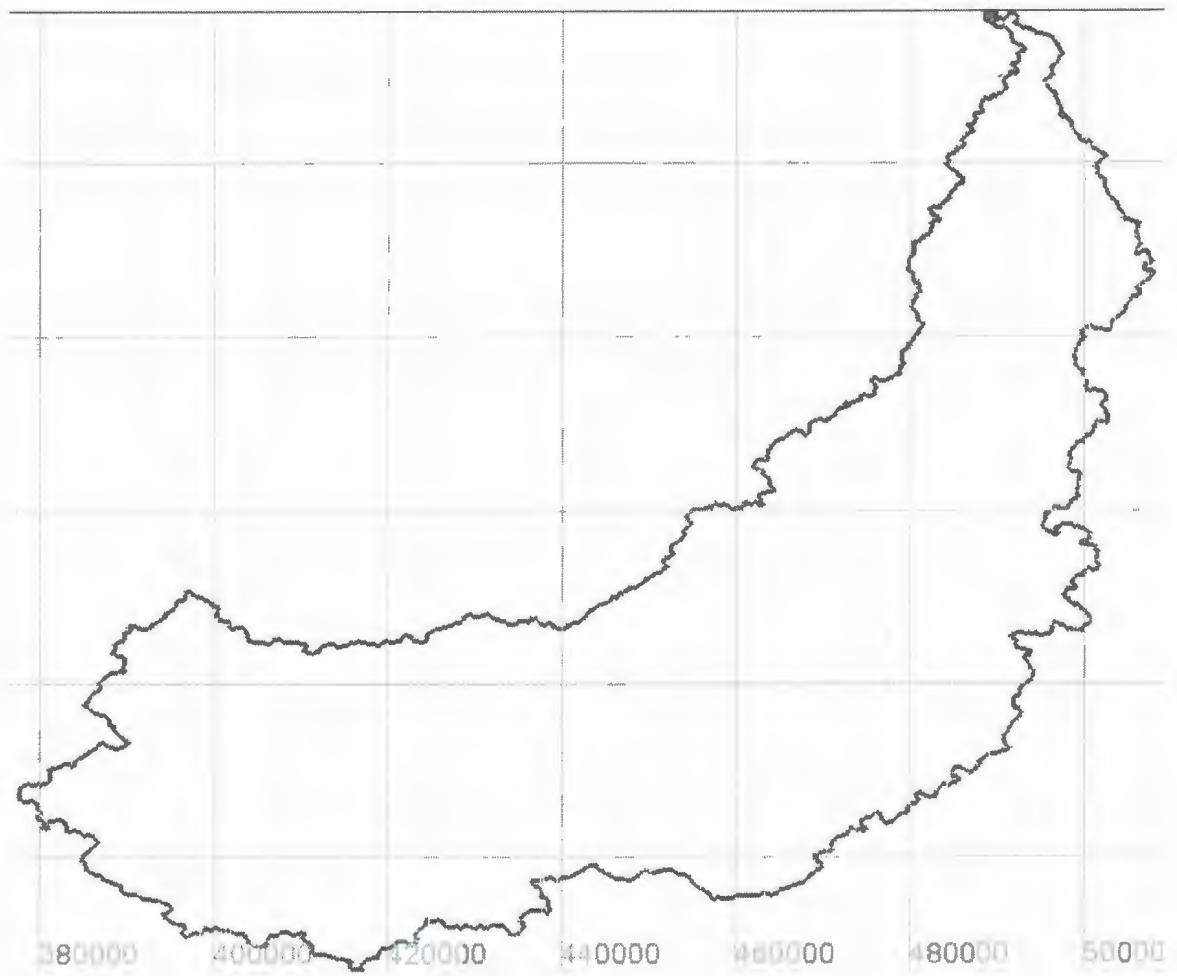


Figure 5.3 Boundary of the Deer River Watershed in EnsimHydrologic®

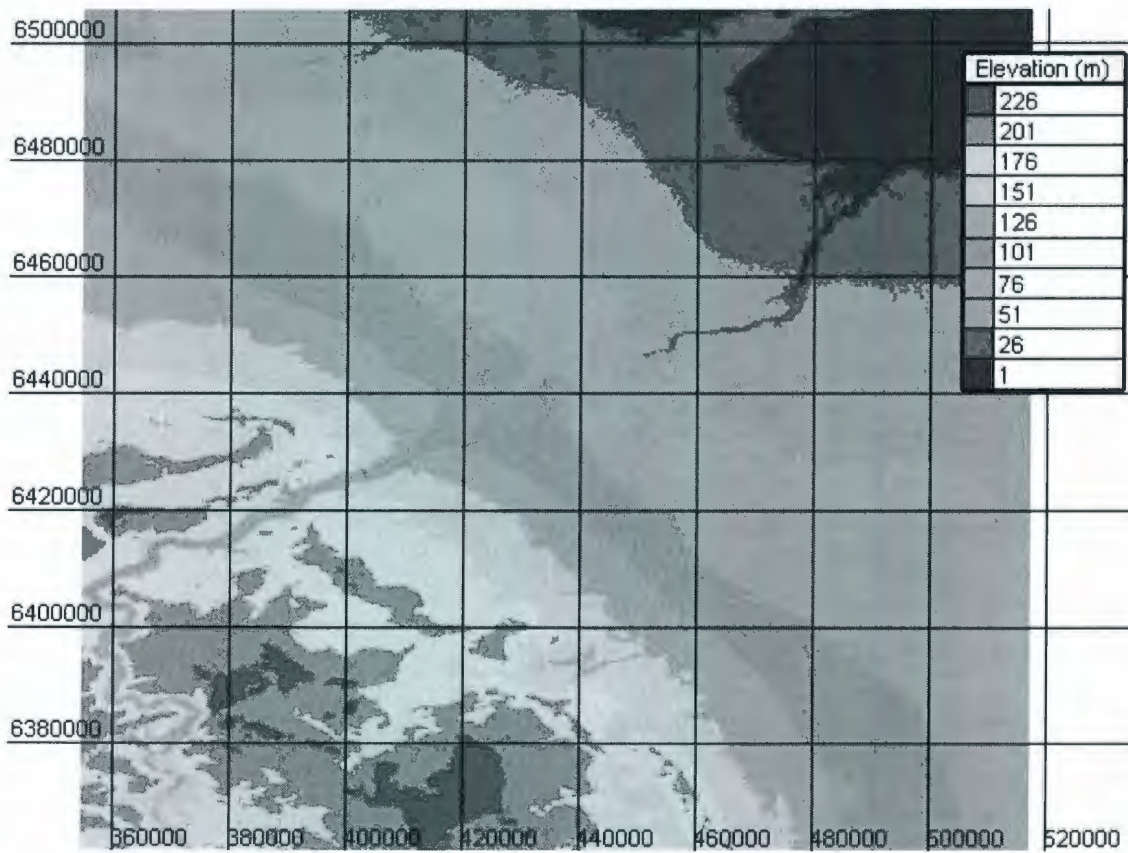


Figure 5.4 DEM of the Deer River Watershed in EnsimHydrologic®

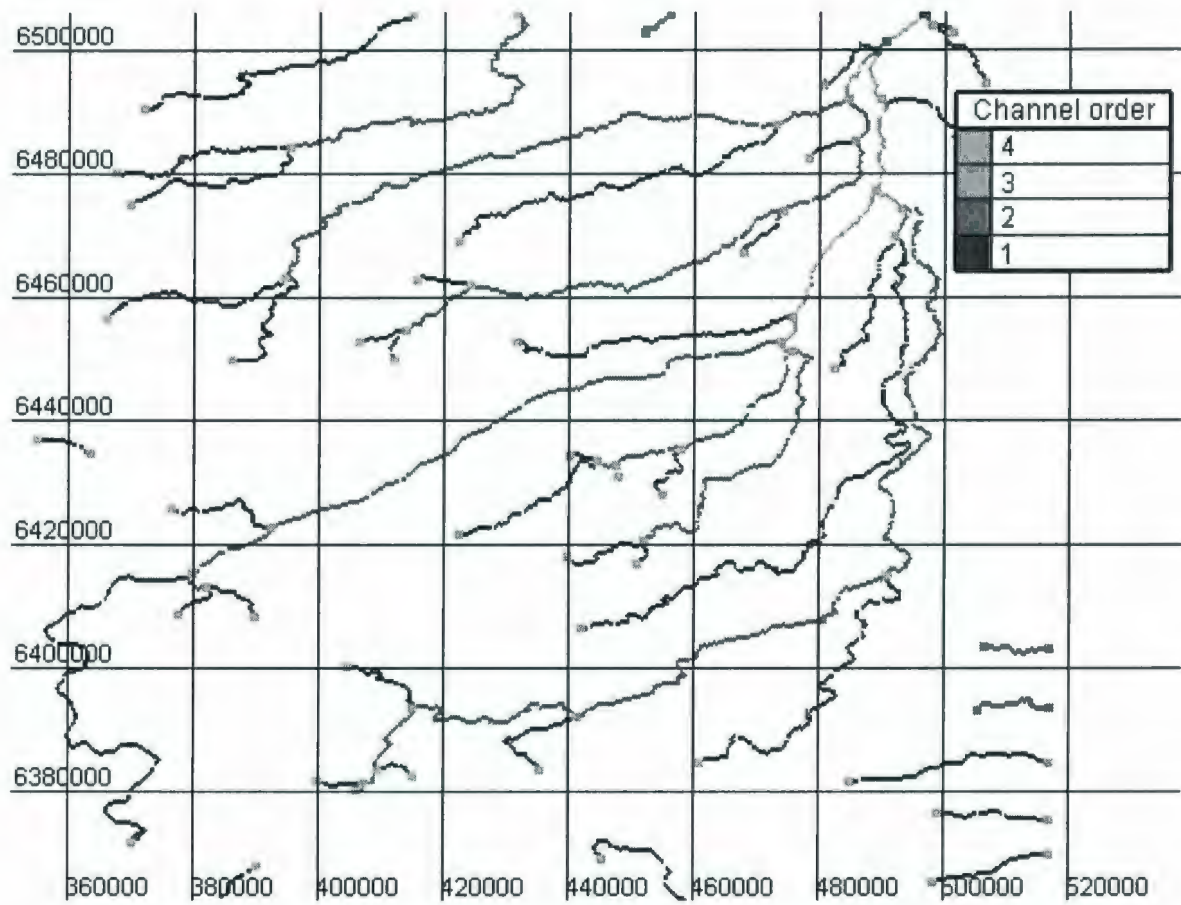


Figure 5.5 Channel network of the Deer River Watershed in EnsimHydrologic®

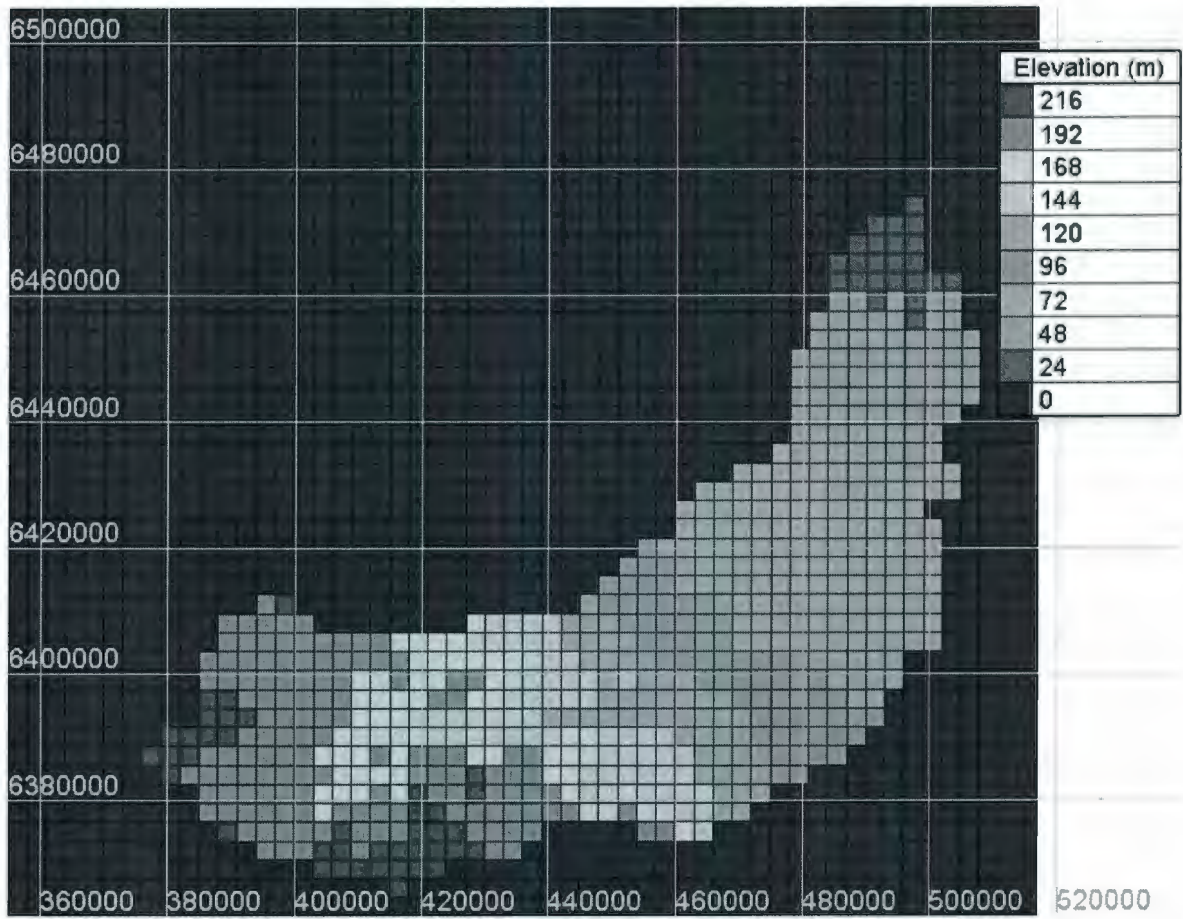


Figure 5.6 Gridded cells of the Deer River Watershed in EnsimHydrologic®

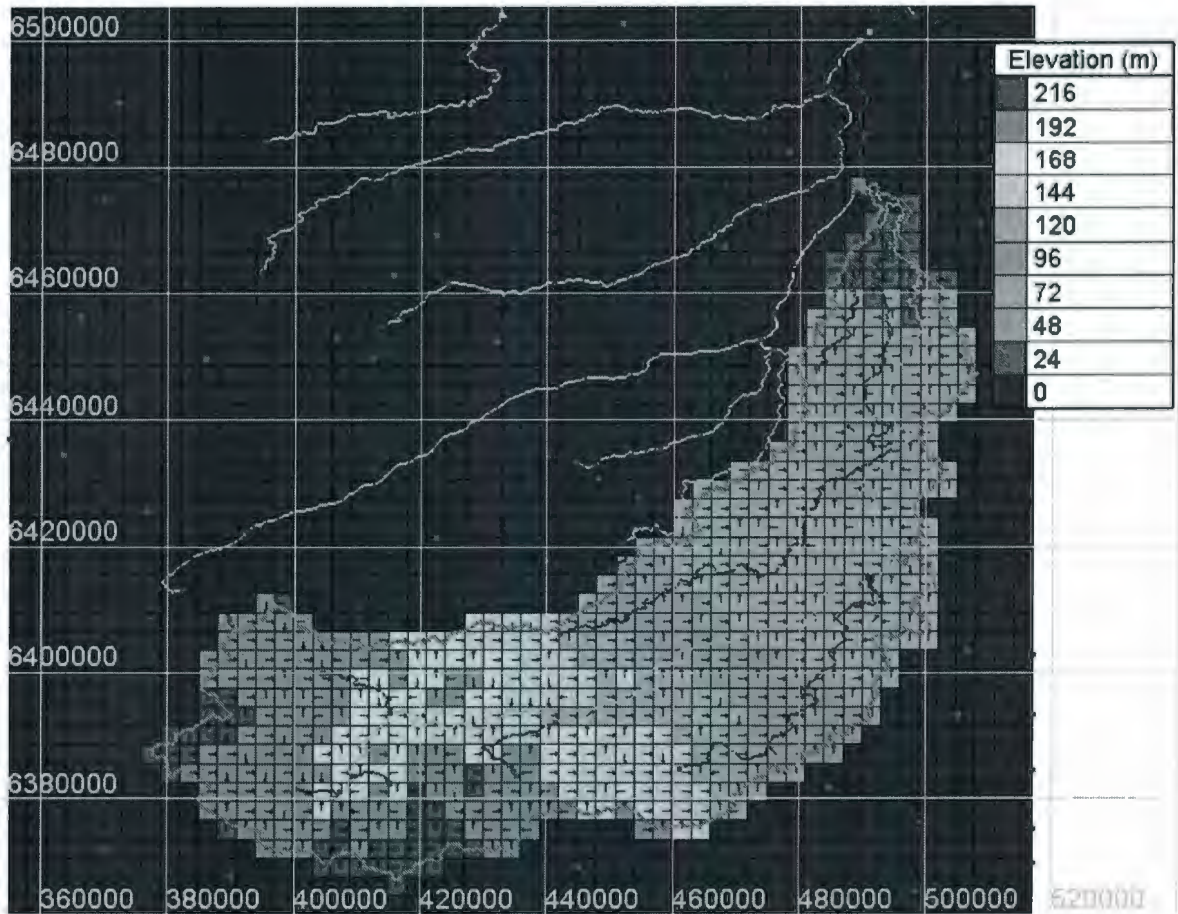


Figure 5.7 Gridded cells, boundary, elevation and channel network of the Deer River Watershed in EnsimHydrologic®

5.3 Land Cover Classification

Detailed land cover information of the Deer River Watershed is referred to Section 4.3.

5.4 Meteorological and Streamflow data

WATFLOOD requires all the input meteorological data, such as air temperature, precipitation, and net radiation as hourly. Hourly average temperature (1978 – 2004, Churchill-A Climate Station, ID: 5060600) was downloaded from the Environmental Canada. Hourly accumulated precipitation was obtained by evenly dividing daily accumulated precipitation into 24 hours. This method is recommended in the manual of WATFLOOD because it is applicable for most moderate rainfall events except some unusual high intensity ones. Hourly net radiation was estimated by WATFLOOD based on Hargreaves equation because the radiation data purchased from the Environmental Canada is not sufficient and complete.

WATFLOOD determines the values of meteorological parameters for each GRU using a modified version of the Reciprocal Distance Weighting Technique (Wei and McGuiness, 1973). The original RDWT method estimates the local values from observations at other stations as given by:

$$\theta_m = \frac{\sum_{j=1}^{n_s} \theta_j d_{mj}^{-k_s}}{\sum_{j=1}^{n_s} d_{mj}^{-k_s}} \quad (5-27)$$

where θ_m is the objective unknown value at location m ; n_s is the number of stations; θ_j is

the observation at station j ; d_{mj} is the distance from the location of station j to the point of m (km); and k_v is friction distance and usually set to 2.0. WATFLOOD divides each GRU into four quadrants and selects one nearest station for each quadrant. Those four stations are used in the above equation to derive the final values of the meteorological parameters for the GRU.

Daily stream flow data was obtained from the Water Survey Canada at the north of Belcher (D. River N. Belcher, 58°0'54" N 94°11'44" W, ID: 06FD002, 1978 - 2004). Hourly stream flow was prepared by setting each of hourly discharge as the daily discharge.

5.5 Sensitivity Analysis

WATFLOOD is a conceptual, mesoscale hydrological simulation model which focuses on flood forecasting and long-term hydrologic simulation using distributed precipitation data from radar or numerical weather models. Most of the parameters have been tested by sensitivity analysis to obtain the most significant ones. The parameters were individually adjusted by $\pm 5\%$, $\pm 15\%$ and $\pm 30\%$ and the results were represented by the fluctuation of model's efficiency. The Nash and Sutcliffe efficiency (NSE) was calculated as statistical measure of the goodness of fit of the WATFLOOD (Section 4.5).

Table 5.1 shows the sensitivity analysis results and indicates that base temperature for snowmelt ($^{\circ}\text{C}$), melt factor ($\text{mm}/^{\circ}\text{C}/\text{hr}$), lower zone drainage function parameter, lower

zone drainage function exponent, river channel Manning's roughness coefficient, reduction in soil evaporation due to tall vegetation, crude snow sublimation factor and porosity of the wetland or channel bank play significant roles in WATFLOOD. As shown in Figure 5.8, base temperature for snowmelt and crude snow sublimation factor are significant parameters because they control the rate and amount of the snowmelt in the spring. Lower zone drainage function exponent also has significance to the modelling because it dominates the volume of base flow that enters the channels. Moreover, snowmelt base temperatures of each land cover were set to be identical with the values used for SLURP. SLURP simulates the snowmelt processes using the air temperature as the critical temperature, whereas WATFLOOD uses snowpack temperature as the base temperature. Therefore, the parameters that should be calibrated in the automatic optimization runs of WATFLOOD include (from the most significant to the least significant):

- G. Lower zone drainage function exponent
- H. Base temperature for snowmelt
- I. Porosity of the wetland or channel bank
- J. Reduction in soil evaporation due to tall vegetation
- K. Crude snow sublimation factor
- L. Melt factor
- M. River channel Manning's roughness coefficient

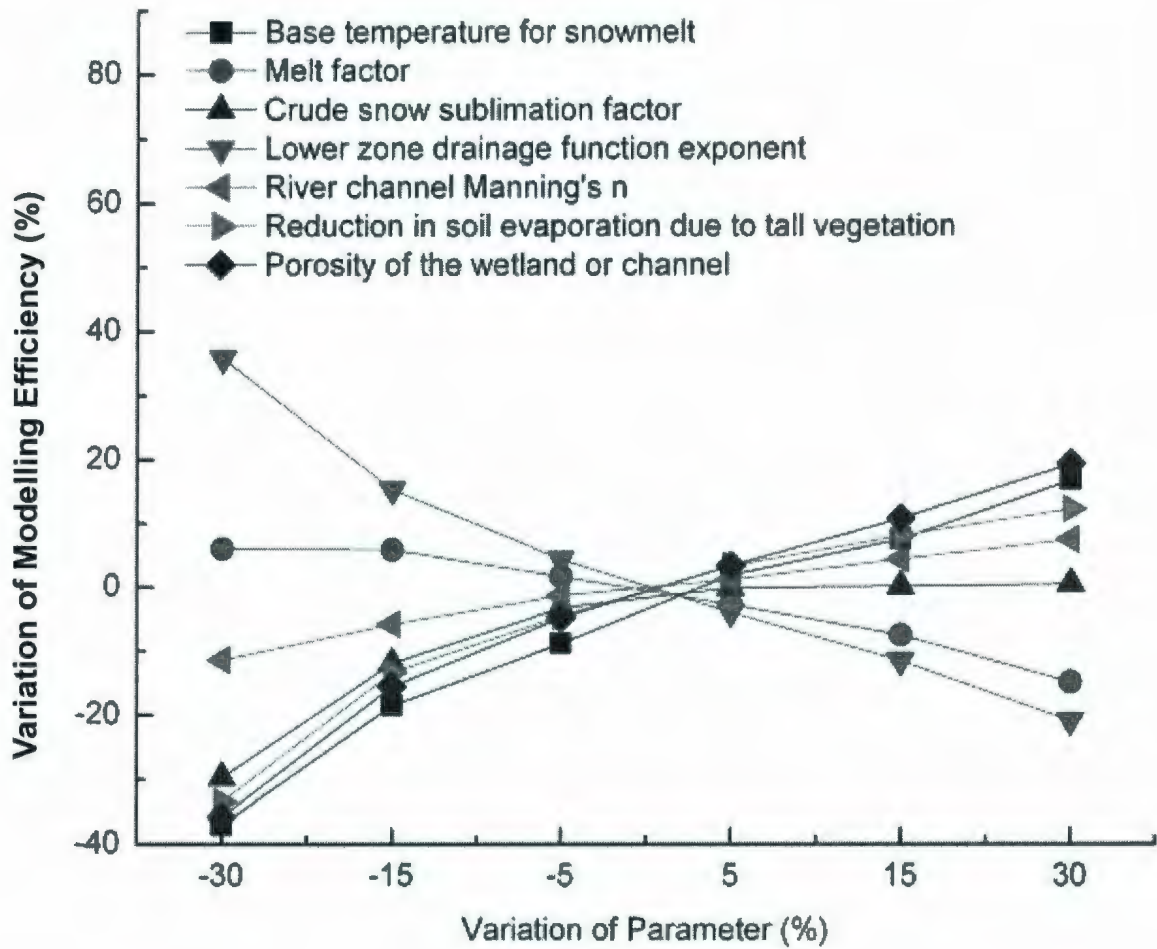


Figure 5.8 Sensitivity analysis of the key parameters of WATFLOOD

Table 5.1 Sensitivity analysis of WATFLOOD parameters
(The first 16 parameters in bold font can be automatically optimized in the model)

Variation of parameters		↓30%	↓15%	↓5%	↑5%	↑15%	↑30%
Explanation		Variation of Modelling Efficiencies (%)					
AK2	upper zone drainage resistance factor for bare ground	+1.4	+0.5	-0.1	-0.7	-1.2	-1.9
AK2FS	upper zone drainage resistance factor under snow	+0.2	-0.1	-0.3	-0.5	-0.7	-1.1
AK	soil permeability of bare ground (mm/h)	0	0	0	0	0	0
AKFS	soil permeability under snow (mm/h)	0	0	0	0	0	0
Albedo	the all-wave albedo	-0.4	-0.4	-0.4	-0.4	-0.4	-0.4
BASE	base temp for snowmelt (°C)	-37.1	-18.5	-8.8	+1.9	+7.5	+16.7
MF	melt factor (mm/°C/h)	+6.0	+5.9	+1.7	-2.7	-7.5	-14.9
NMF	negative melt factor (mm/°C/day)	-2.2	-1.0	-0.7	0	+0.5	+1.3
R3	overland flow roughness for bare pervious area	-0.4	-0.4	-0.4	-0.4	-0.4	-0.4
R3FS	overland flow roughness for snow covered pervious area	-0.4	-0.4	-0.4	-0.4	-0.4	-0.4
REC	interflow depletion coefficient	+0.1	0	0	0	-0.1	-0.3
RETN	upper zone specific retention (mm)	-0.4	-0.3	-0.3	-0.3	-0.3	-0.3
A5	API hourly reduction value	0	0	0	0	0	0
lzf	lower zone drainage function parameter	+3.1	+1.3	+0.4	-0.4	-1.2	-2.2
pwr	lower zone drainage function exponent	+35.8	+15.3	+4.4	-3.9	-11.5	-20.9
R2n	river channel Manning's roughness coefficient	-11.4	-5.8	-1.3	+1.2	+4.4	+7.4
ds	depression storage for bare ground (mm)	-0.4	-0.4	-0.4	-0.4	-0.4	-0.4
dsfs	depression storage for snow covered ground (mm)	-0.4	-0.4	-0.4	-0.4	-0.4	-0.4
flapse	lapse rate in °C per 100m (°C)	-0.4	-0.4	-0.4	-0.4	-0.4	-0.4
fpet	increase in interception evaporation for tall vegetation	-0.6	-0.5	-0.4	-0.3	-0.3	-0.2
ftal	reduction in soil evaporation due to tall vegetation	-33.5	-13.3	-4.5	+3.3	+8.1	+12.2
kcond	conductivity of the wetland (mm/h)	0	0	-0.1	-0.7	-1.6	-3.5
mndr	meandering factor	-	-	-	-0.4	-0.4	-0.4
R1n	flood plain Manning's roughness coefficient	-0.4	-0.4	-0.4	-0.4	-0.4	-0.4
sublim	crude snow sublimation factor (mm/h)	-29.7	-11.9	-3.2	-0.1	+0.1	+0.5
theta	porosity of the wetland or channel	-35.8	-15.5	-4.8	+3.4	+10.8	+19.3

5.6 Calibration

Calibration was conducted by using the 10-year data (1978 – 1987) and through both manual adjustment and built-in routine in the model. Initial soil moisture and initial snow cover which require initial estimates were manually adjusted to the values used SLURP. All the other parameters were calibrated or assigned values by taking reference from WATFLOOD manual's sample data at the Grand River (Kouwen, 2008) and Stadnyk (2008). After the optimization runs, the values of the parameters used in the watershed modelling are listed in Table 5.2.

Figures 5.9 to 5.18 show the daily modelling outputs during the calibration period (1978 – 1987). Table 5.3 reports the modelling NSE efficiencies and deviation of runoff volume (DV) of all the calibration years. The model's overall efficiency (-16%) is not as good as SLURP (52%); however, it performs well in some years. For instance, in 1979, its efficiency reaches 69% with accurate estimation of spring runoff. The efficiencies in some years are negative which may be explained by the lack of hourly precipitation, poor data resolution and simple snowmelt computation. The DVs indicate that the annual runoff volume of the majority of the calibration years are underestimated in the spring and overestimated during the summer and fall which can be explained by not considering the influences of frost table, existence of local ponds and highly porous soil.

Figures 5.19 and 5.20 show the monthly and annual modelling outputs during the calibration period (1978 – 1987). Table 5.4 reports the modelling efficiencies and DV of

monthly and annual results. It is clear that the monthly efficiency (-13%) is better than the daily efficiency (-16%) because the differences between simulated and observed flows are to some extent reduced. The annual modelling efficiency (NSE = -415%) and DV (293%) indicates that annual results are more inaccurate which can be explained the fact that WATFLOOD overestimates the fluctuation of the streamflow. Another possible reason is that WATFLOOD simulates the flows between wetlands and channels without sufficient data support from the field survey.

Table 5.2 Final Values of the parameters for each land cover used for modelling the Deer River Watershed

	Deciduous	Coniferous	Shrub	Marsh	Water	Impervious
AK2	0.55	0.55	0.55	0.55	0.051	5E-10
AK2FS	0.52	0.51	0.52	0.52	0.051	5E-10
AK	13.4	12	3	400	-0.1	0.1E-10
AKFS	1.2	1.2	3	400	-0.1	0.1E-10
Albedo	0.16	0.13	0.14	0.15	0	0.15
BASE	-0.32	-0.61	-0.93	-0.99	-0.03	-0.56
MF	0.13	0.13	0.17	0.17	0.13	0.15
NMF	0.10	0.10	0.10	0.10	0.10	0.10
R3	0.10	0.08	0.20	0.09	0.04	4
R3FS	0.1	0.05	0.20	0.10	0.04	4
REC	0.2	0.2	0.2	0.9	0.1	0.9
RETN	150	150	150	140	0.1	0.1
A5	0.985	0.985	0.985	0.985	0.985	0.985
lzf	0.1E-4	0.1E-4	0.1E-4	0.1E-4	0.1E-4	0.1E-4
pwr	2.05	2.05	2.05	2.05	2.05	2.05
R2n	0.018	0.018	0.018	0.018	0.018	0.018
ds	123	120	1.2E4	1.2E10	0	1
dsfs	223	220	220	2.2E10	0	1
flapse	0.75	0.75	0.75	0.75	0.75	0.75
fpet	3	4	4	4	1	0
ftal	0.85	0.85	1	1.3	1	1
kcond	0.75	0.75	0.75	0.75	0.75	0.75
mndr	1	1	1	1	1	1
R1n	0.05	0.05	0.05	0.05	0.05	0.05
sublim	0.10	0.10	0.22	0.22	0.30	0
theta	0.7	0.7	0.7	0.7	0.7	0.7

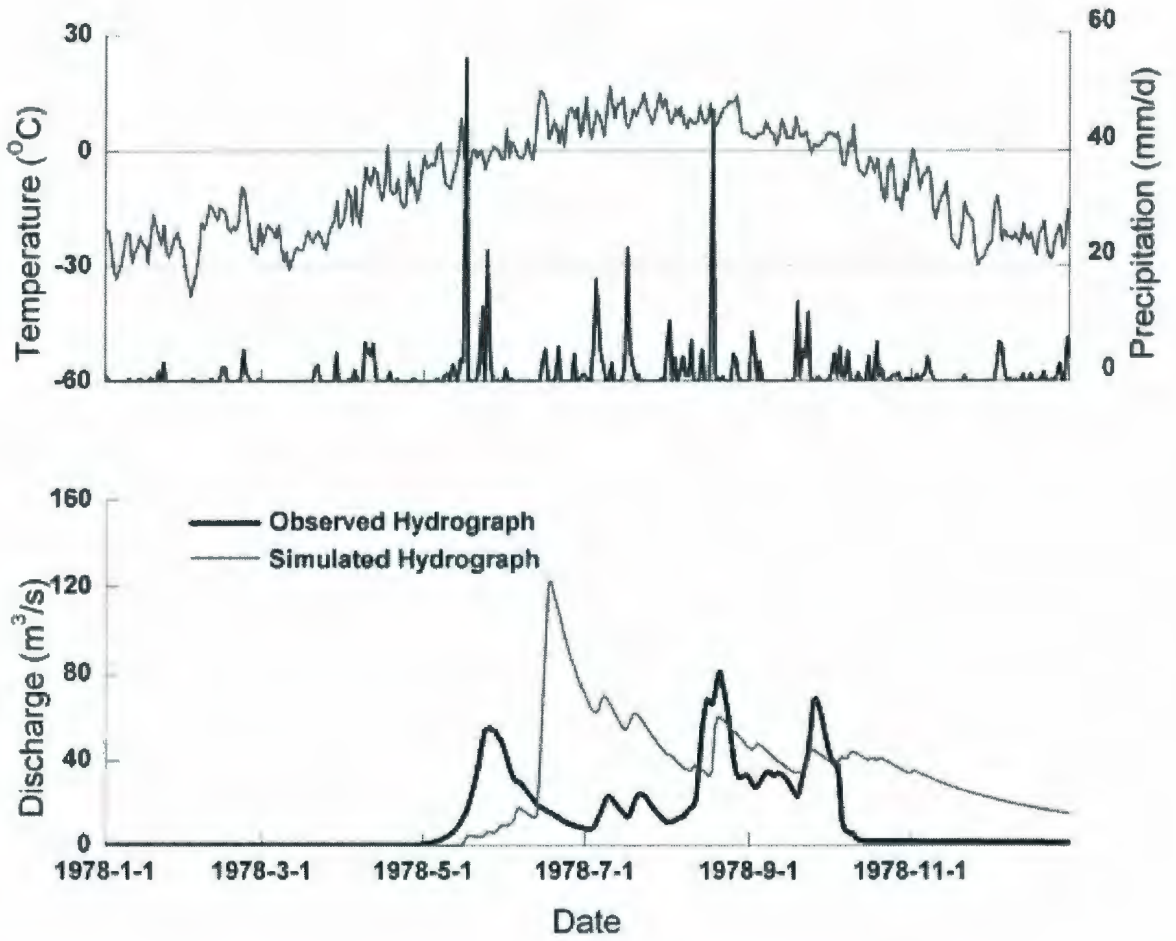


Figure 5.9 Simulated and observed daily hydrographs for the Deer River Watershed in 1978

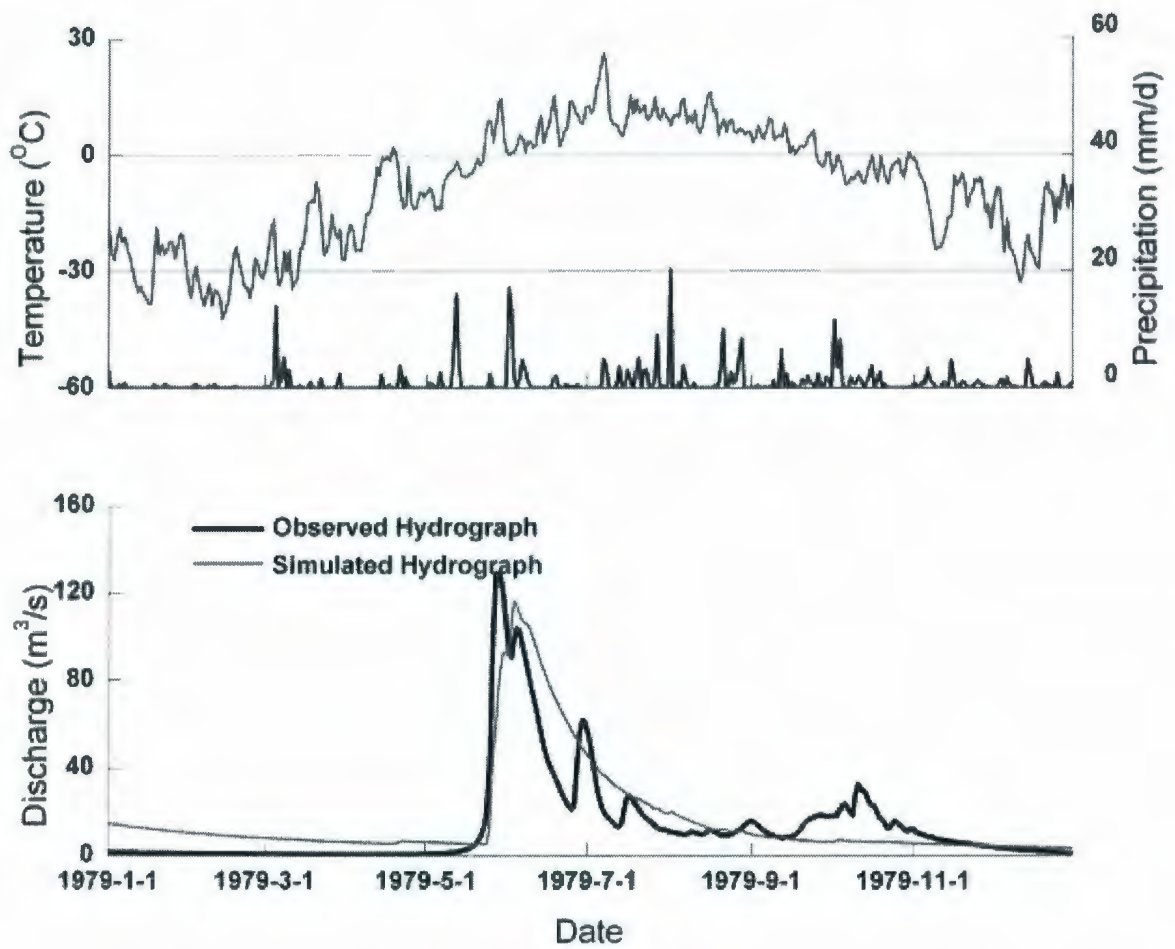


Figure 5.10 Simulated and observed daily hydrographs for the Deer River Watershed in 1979

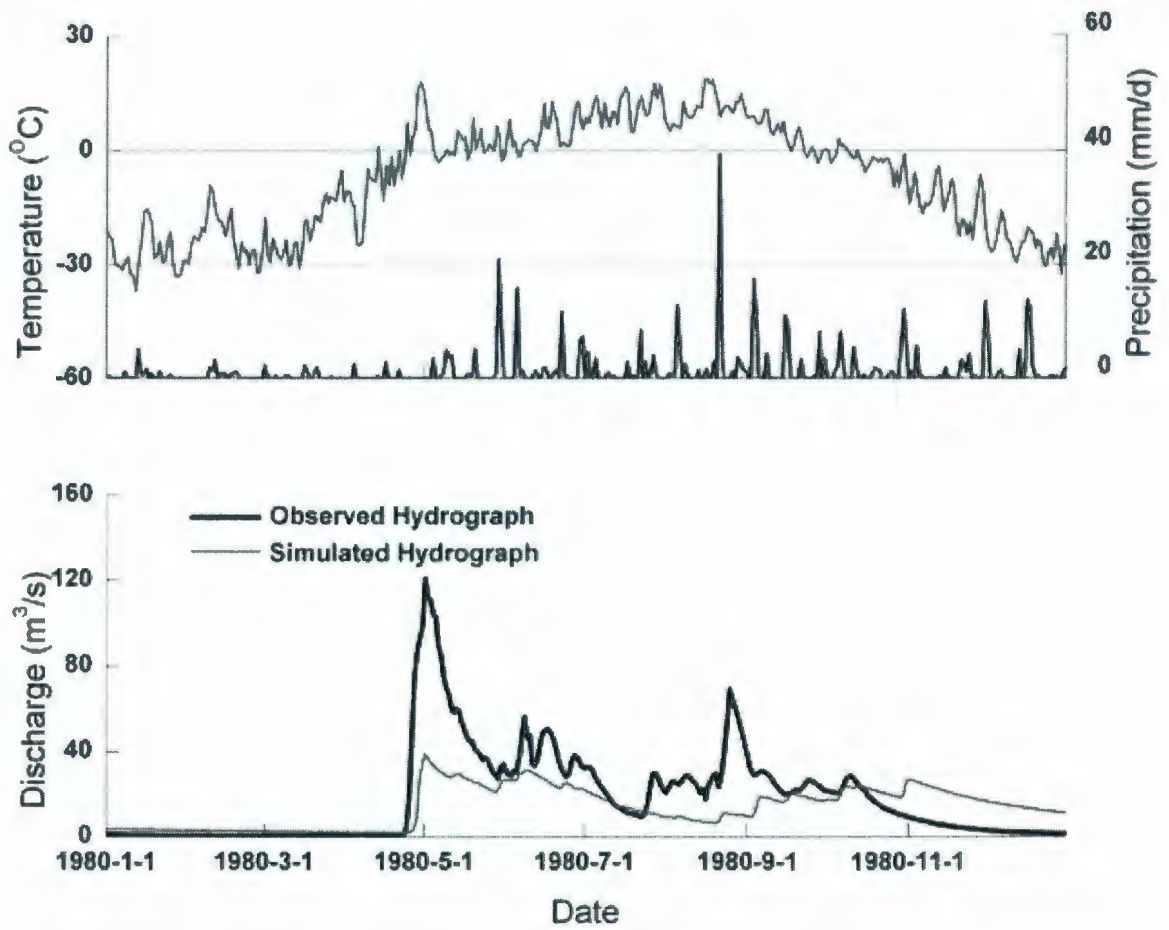


Figure 5.11 Simulated and observed daily hydrographs for the Deer River Watershed in 1980

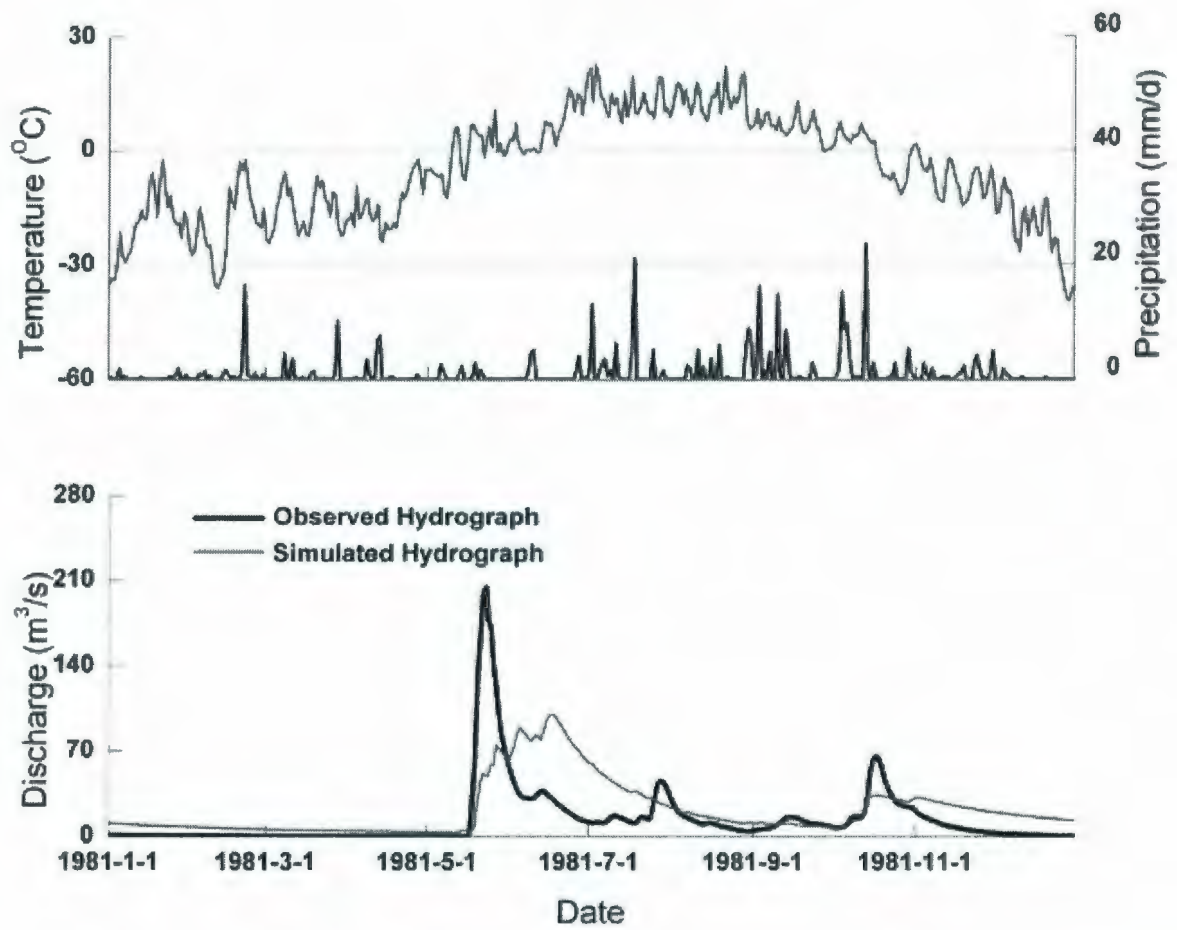


Figure 5.12 Simulated and observed daily hydrographs for the Deer River Watershed in 1981

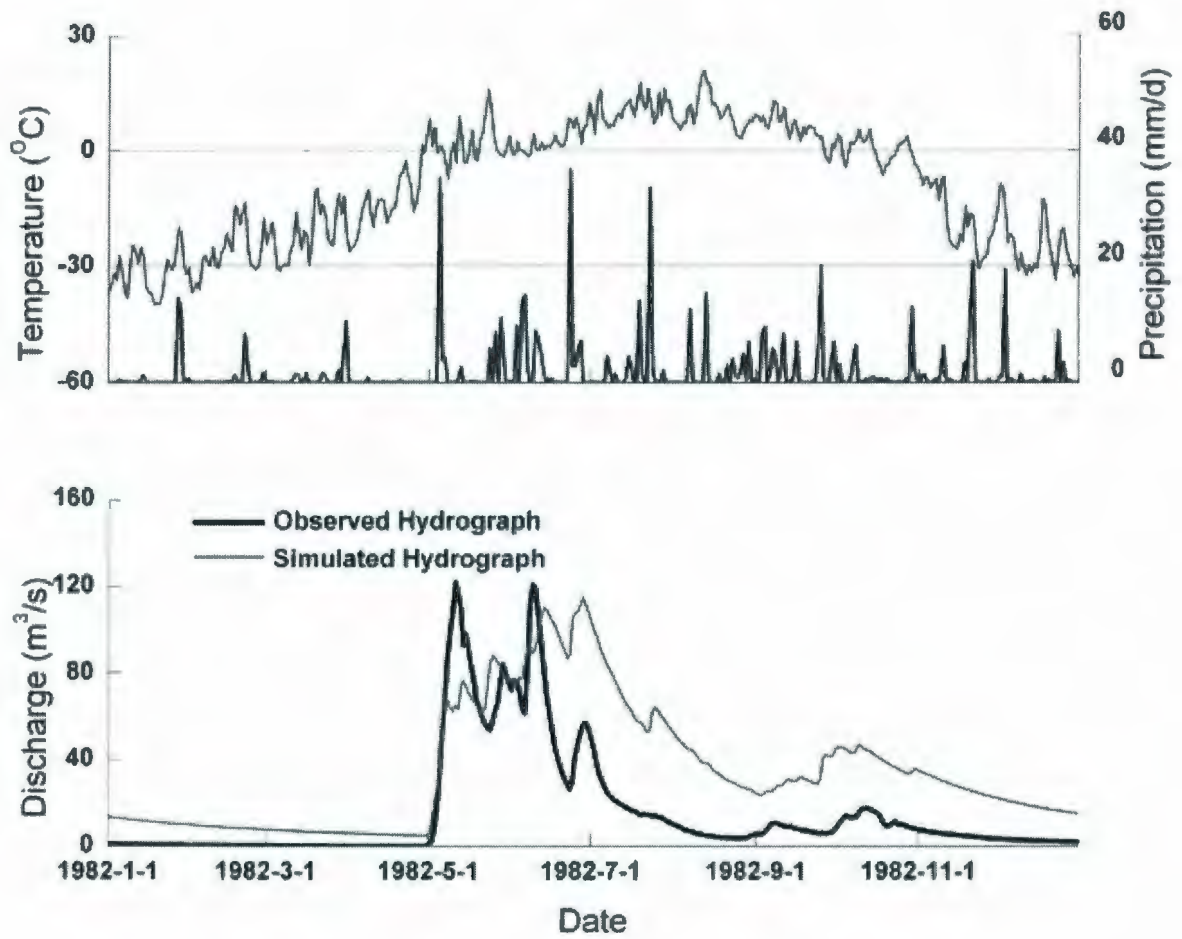


Figure 5.13 Simulated and observed daily hydrographs for the Deer River Watershed in 1982

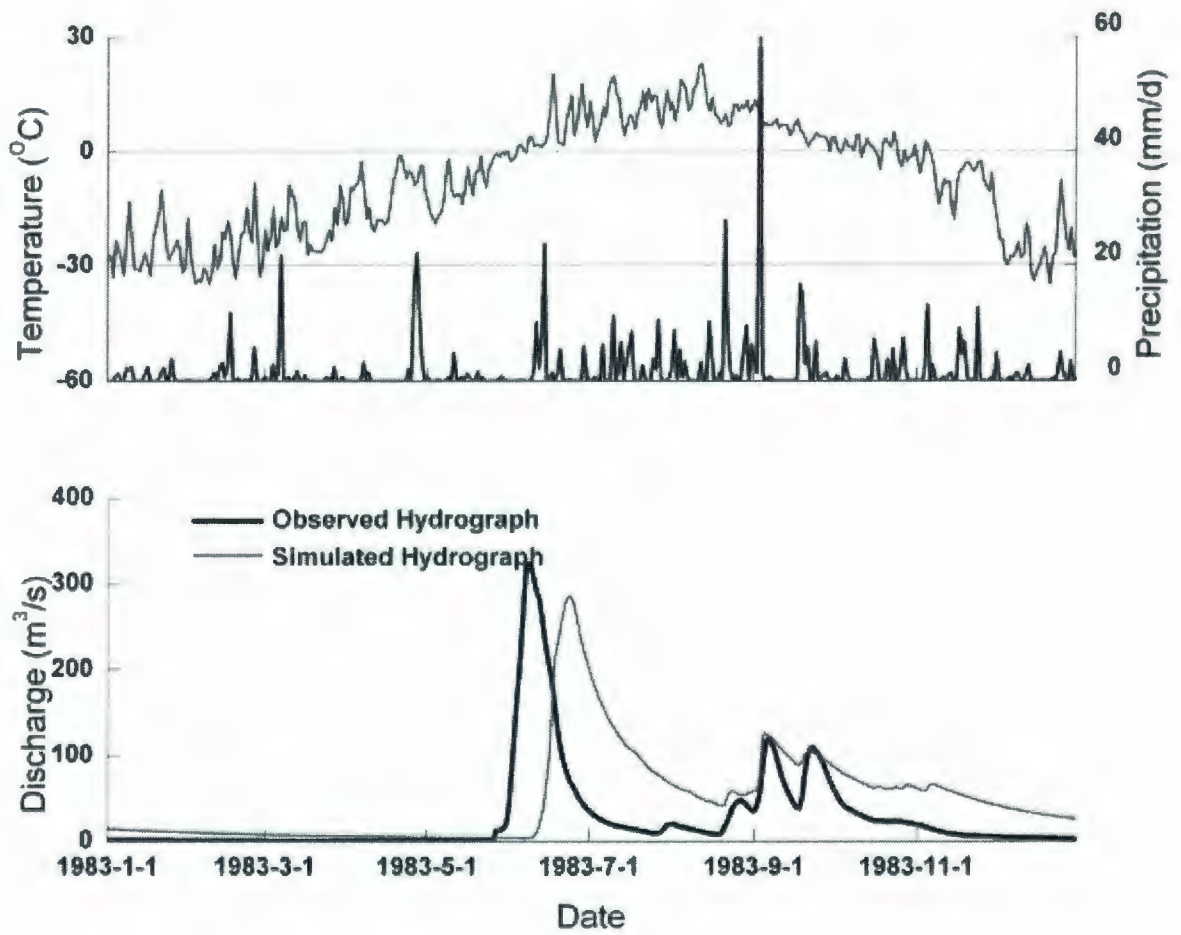


Figure 5.14 Simulated and observed daily hydrographs for the Deer River Watershed in 1983

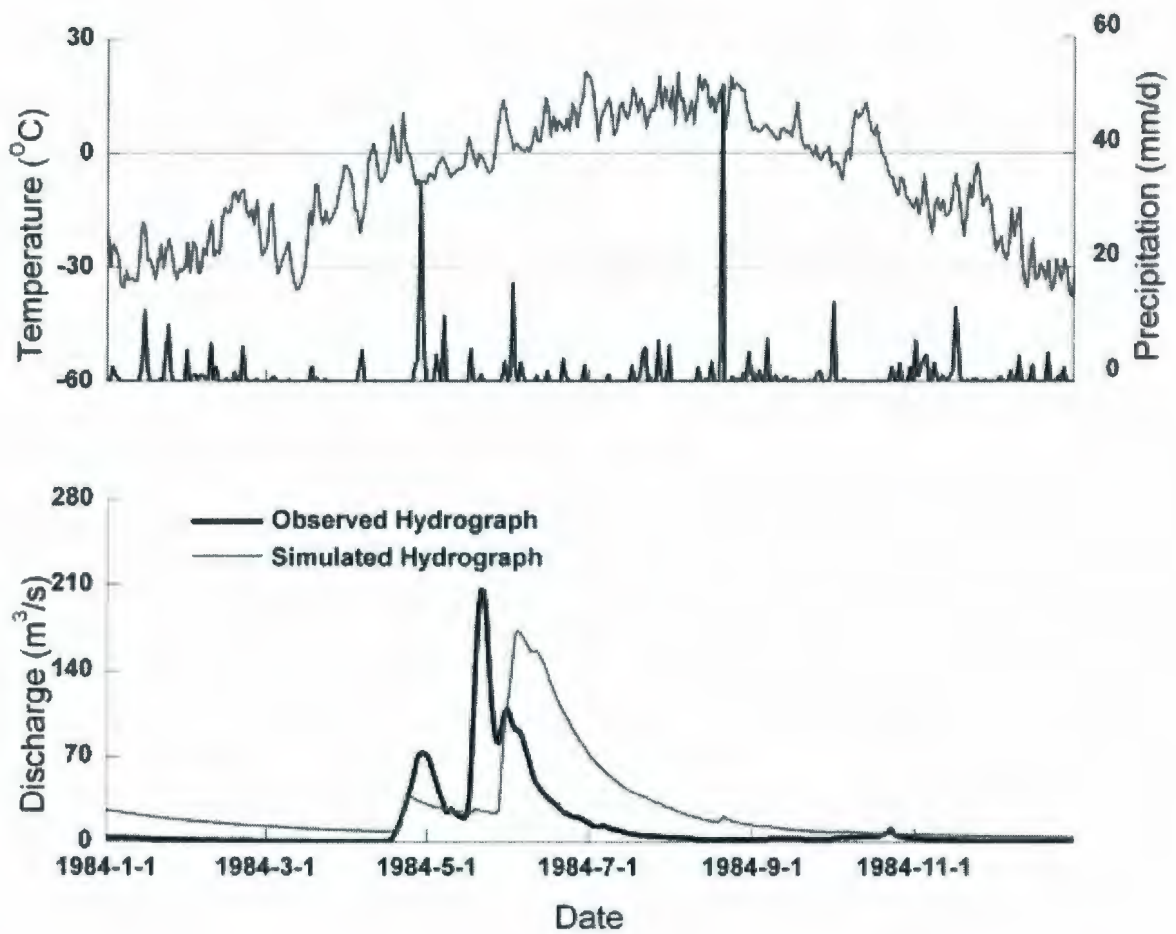


Figure 5.15 Simulated and observed daily hydrographs for the Deer River Watershed in 1984

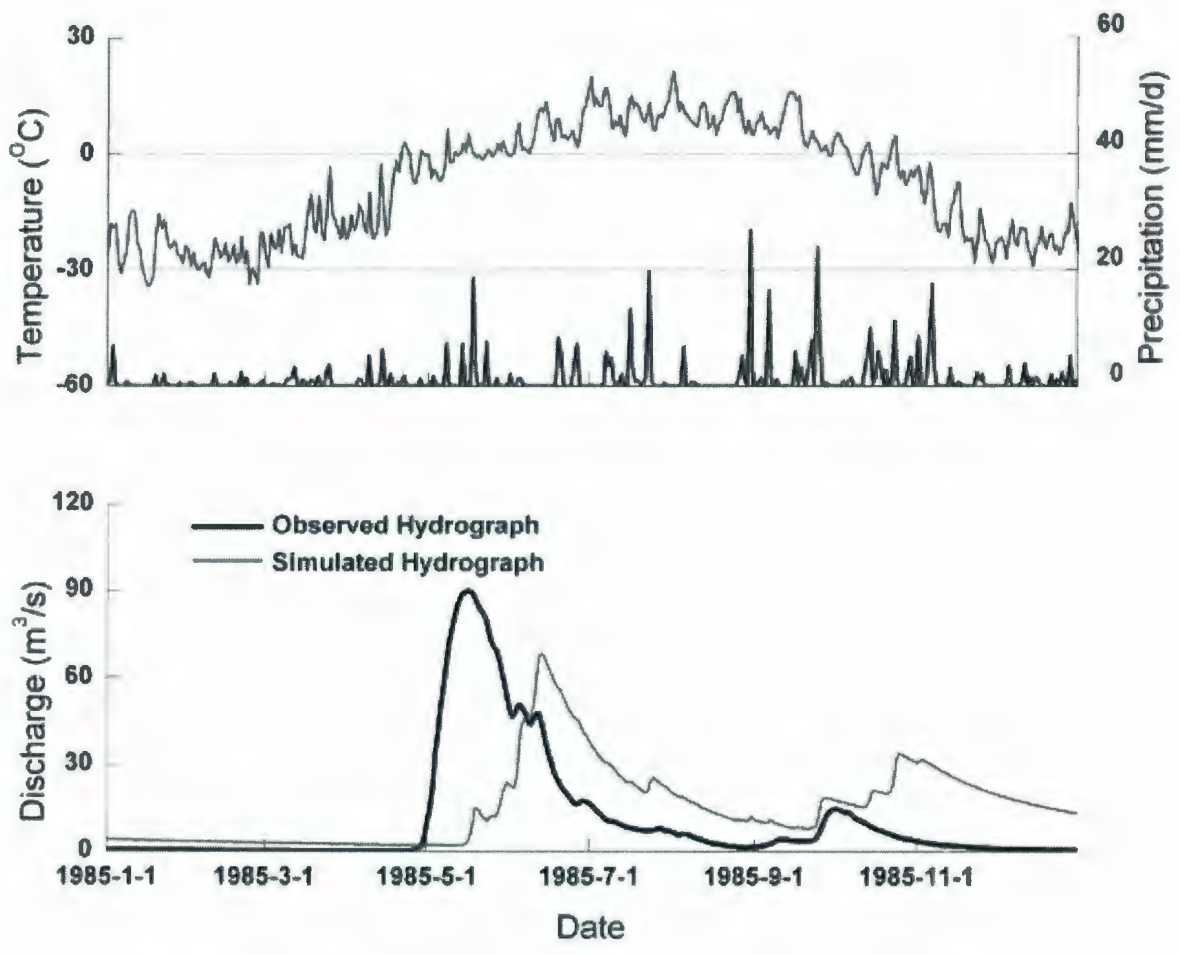


Figure 5.16 Simulated and observed daily hydrographs for the Deer River Watershed in 1985

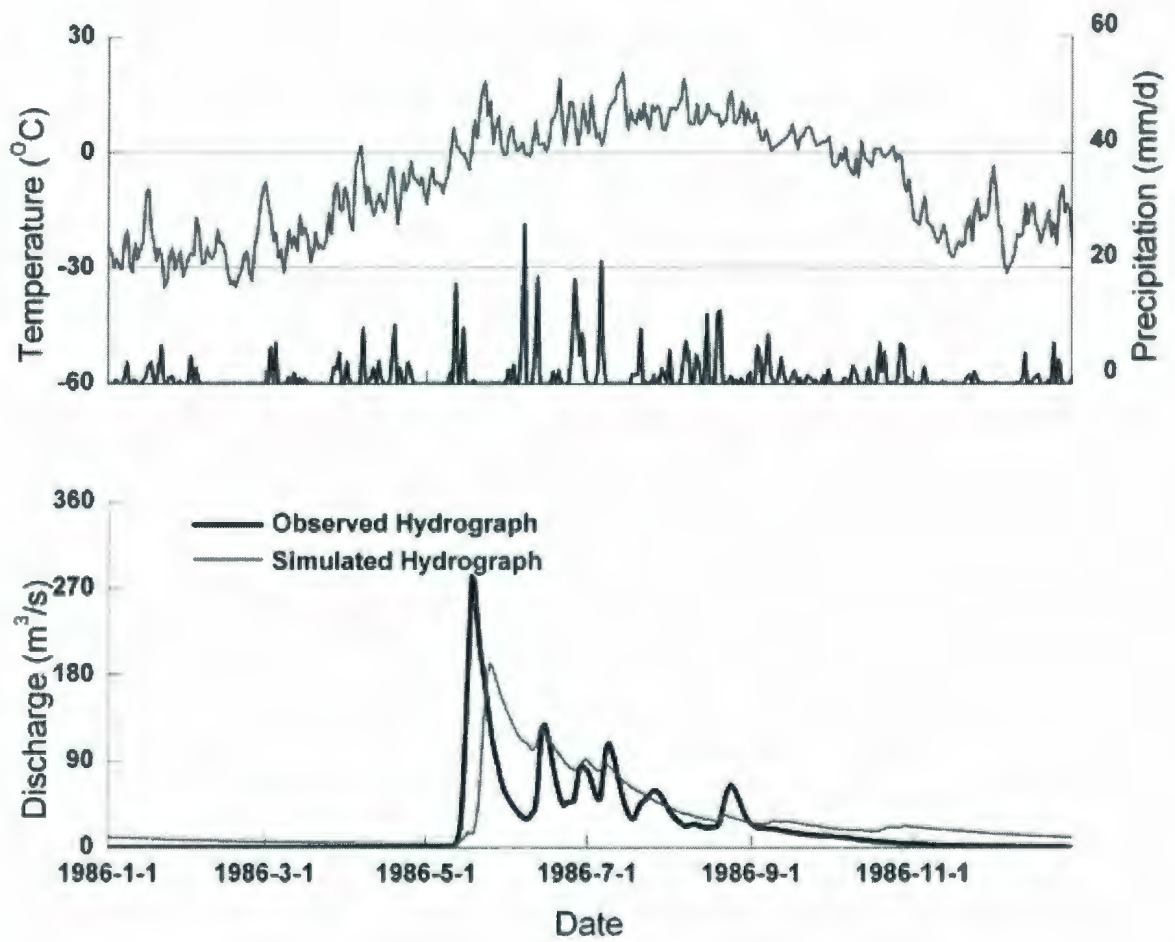


Figure 5.17 Simulated and observed daily hydrographs for the Deer River Watershed in 1986

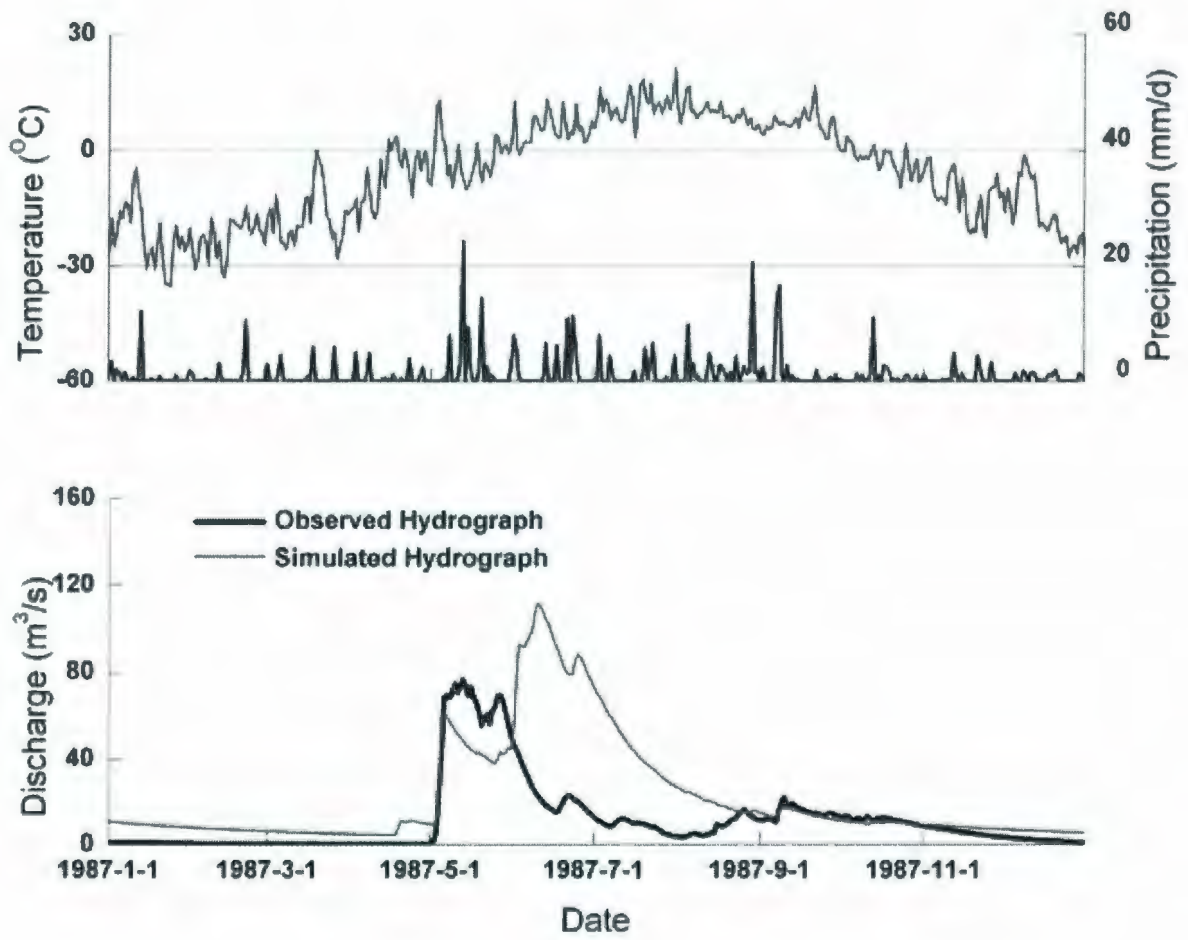


Figure 5.18 Simulated and observed daily hydrographs for the Deer River Watershed in 1987

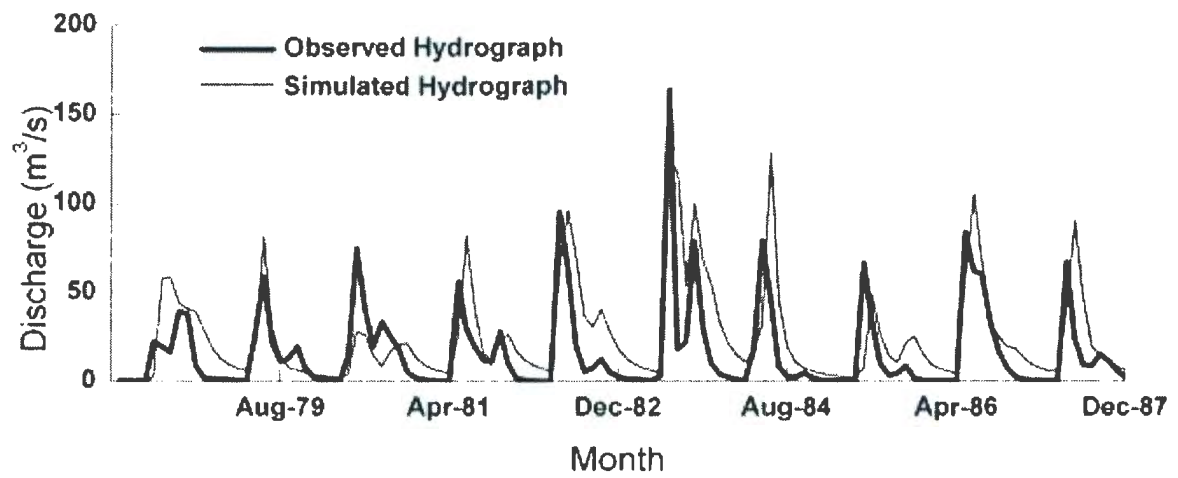


Figure 5.19 Simulated and observed monthly hydrographs for the Deer River Watershed from 1978 to 1987

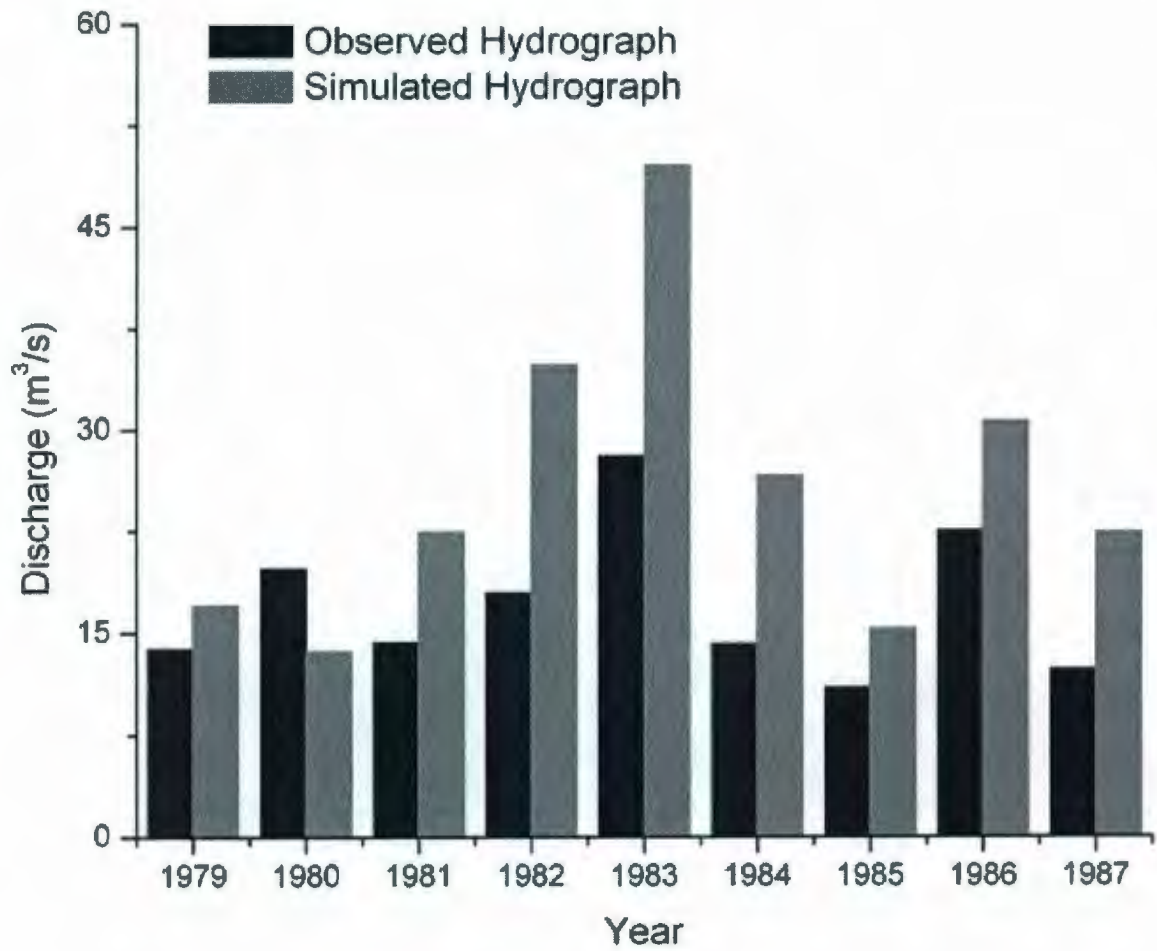


Figure 5.20 Simulated and observed annual hydrographs for the Deer River Watershed from 1978 to 1987

Table 5.3 Modelling efficiencies during WATFLOOD daily calibration in the Deer River Watershed

Year	NSE (%)	DV (%)
1978	142	110
1979	69	4
1980	30	-85
1981	7	-31
1982	22	-27
1983	-64	4
1984	-36	25
1985	-21	-55
1986	26	-18
1987	-48	41
Average.	-16	-3
Max.	69	110
Min.	-142	-85

Note: NSE is the Nash and Sutcliffe efficiency; and DV is the deviation of runoff volumes.

Table 5.4 Modelling efficiencies during WATFLOOD calibration in the Deer River Watershed

	NSE (%)	DV (%)
Monthly	-13	21
Annual	-415	293

Note: NSE is the Nash and Sutcliffe efficiency; and DV is the deviation of runoff volumes.

5.7 Verification

Modelling verification was performed the period between 1988 and 2004. Figures 5.21 to 5.37 show the modelled and observed hydrographs during the verification period. Table 5.5 reports the modelling efficiencies and DV. The overall efficiency for the verification years (-38%) is not as good as the calibration years (-16%). This might be attributed to the more intensive changes in climatic conditions, streamflow data measurement, a natural shifting of the channels or the change of meteorological data collection as discussed in Section 4.7. Nonetheless, the modelling results have good accuracy in some years. The year of 1990 is chosen as an example because it is a median year from a meteorological perspective (Figure 5.23). The modelling efficiency of this year is 58% with a DV of -35%. The negative DV implies that, as similar to the calibration years, the spring streamflow is underestimated during the snowmelt season due to the unconsidered influences from the frost table and ponds.

The results also indicate a delayed response of simulated spring peak runoff caused by snowmelt. For example, the simulated spring flow peak in 1989 is 40 days later than the observed one (Figure 5.22). This phenomenon may be due to the built-in snowmelt algorithm and the existence of the permafrost table. In WATFLOOD, the degree-day snowmelt algorithm starts snowmelt and transfers the water into the upper zone storage tank on any day if the snowpack temperature exceeds 0 °C. This can cause some uncertainties because the snow may not start melting due to the lack of radiation though the temperature is above the melt temperature. The snowmelt factor which determines the

snowmelt rate is a constant in WATFLOOD. This may cause that when the temperature is much higher than the melting base temperature, the simulated snowmelt is still not accelerated which disobeys the nature of the environment. Moreover, because the shallow permafrost table can prevent the water from infiltrating into the fast storage tank, the actual spring runoff occurs much quicker and the volume is greater than the simulated result. An interesting finding is that WATFLOOD has the sublimation factor of snow which enables the adjustment of melting process and following spring runoff. This sublimation process along with hourly basis calculation and wetland module could improve the simulation accuracy in the spring period. However, these modules have high requirement in sufficiency of hourly data which are usually difficult to meet. For example, in this study, hourly precipitation data was prepared by evenly distributing the daily data into 24 hours. However, this may lead to the fact that the intensities and durations of rainfall events are weakened and prolonged, respectively. Therefore, the instant runoff may be underestimated or delayed. The highly porous soil and numerous storage ponds are two significant reasons for the overestimation of the flow during summer and fall. High soil porosity and those seasonal ponds are capable of modelling great amount of precipitation and resulting in the fact that the simulated flows in summer and fall are higher than the observed ones. Figures 5.38 and 5.39 show the monthly and annual model outputs during the verification period (1988 – 2004). Table 5.6 reports the modelling efficiencies and DV of monthly and annual results. The monthly results are close to daily results whereas annual modelling efficiency (-312%) is much lower than the daily one (-38%) with a higher DV (148%).

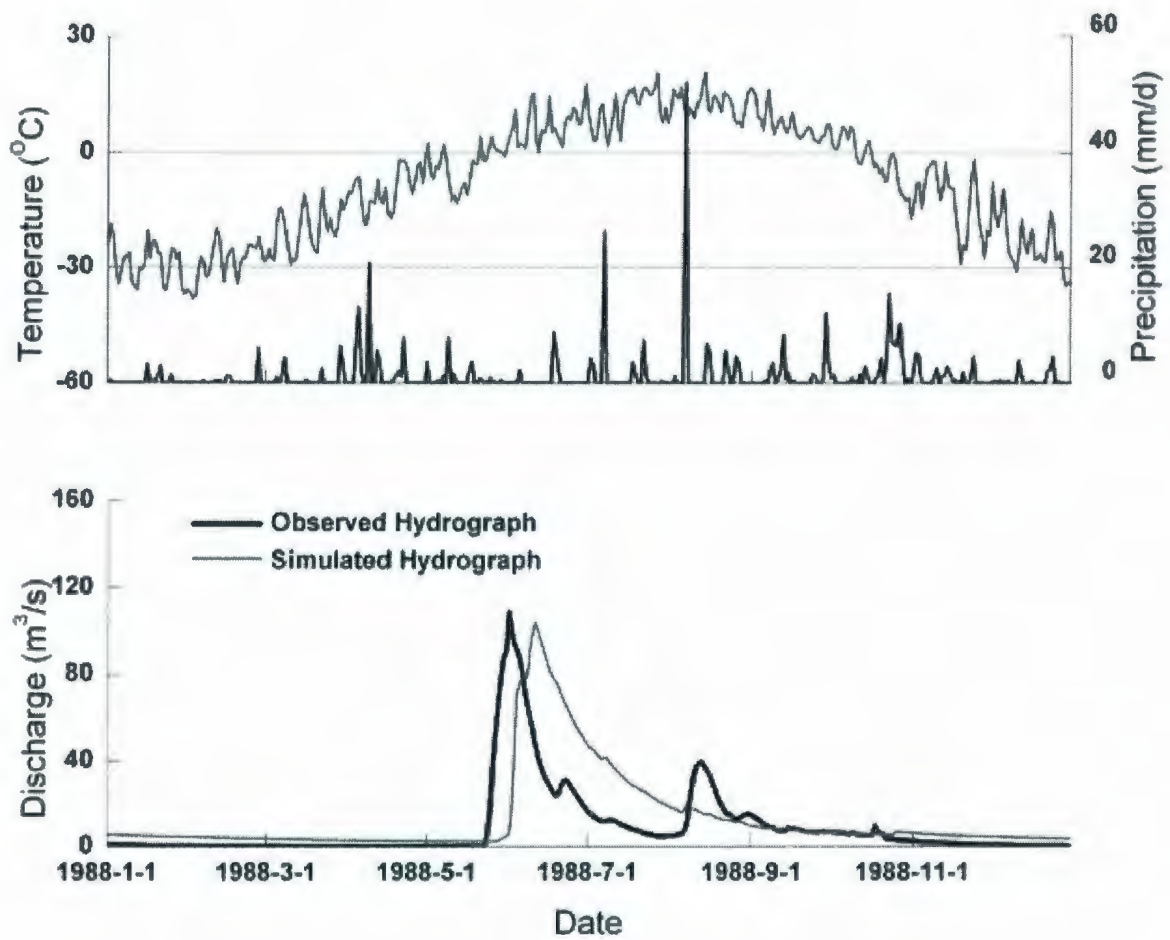


Figure 5.21 Simulated and observed daily hydrographs for the Deer River Watershed in 1988

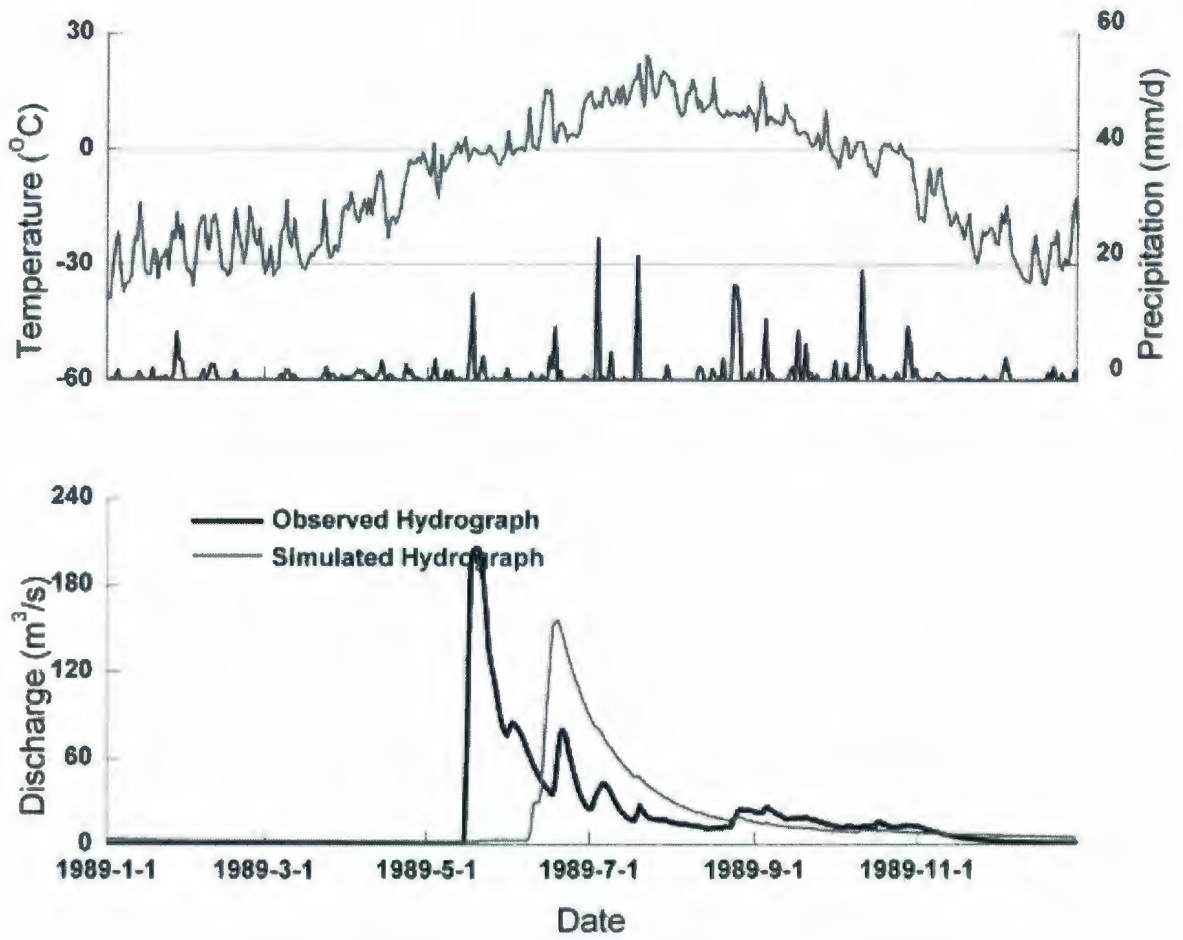


Figure 5.22 Simulated and observed daily hydrographs for the Deer River Watershed in 1989

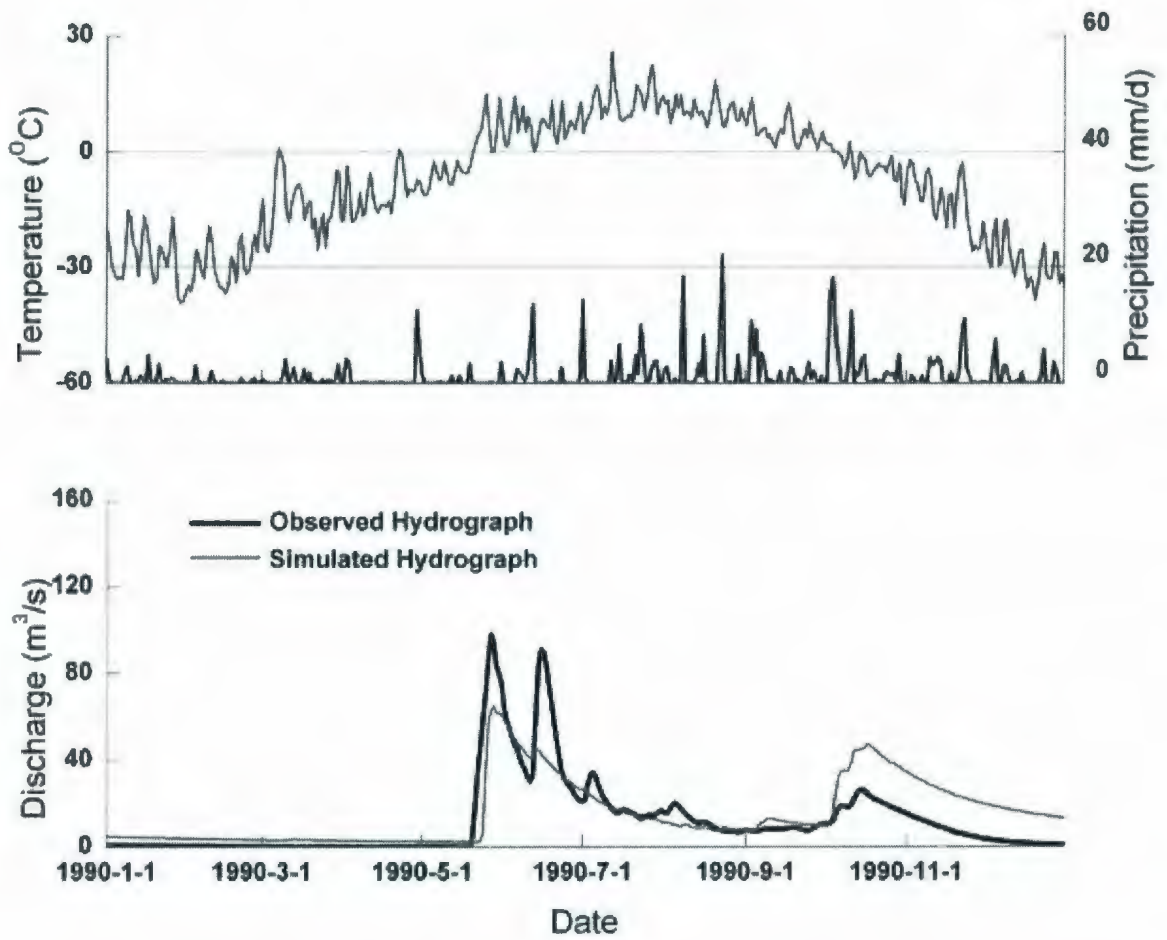


Figure 5.23 Simulated and observed daily hydrographs for the Deer River Watershed in 1990

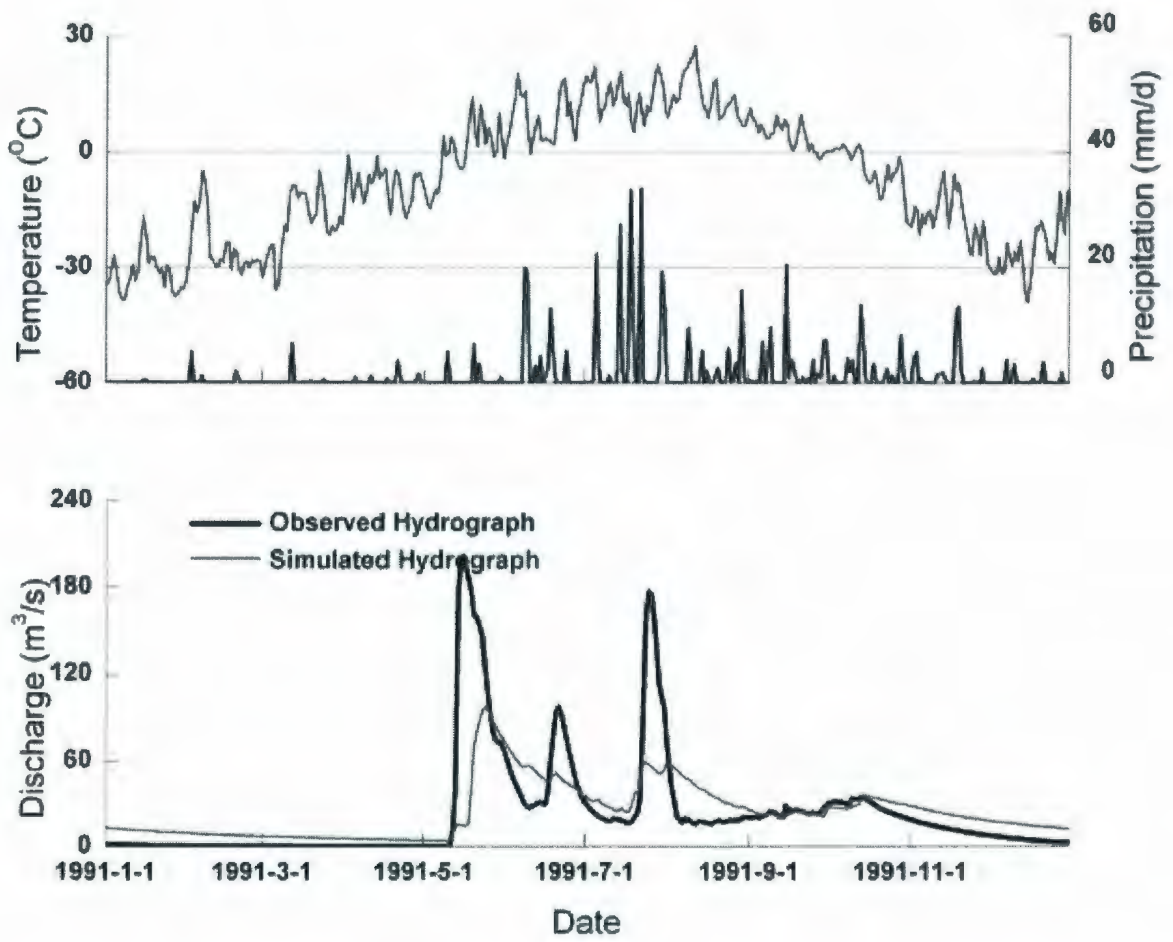


Figure 5.24 Simulated and observed daily hydrographs for the Deer River Watershed in 1991

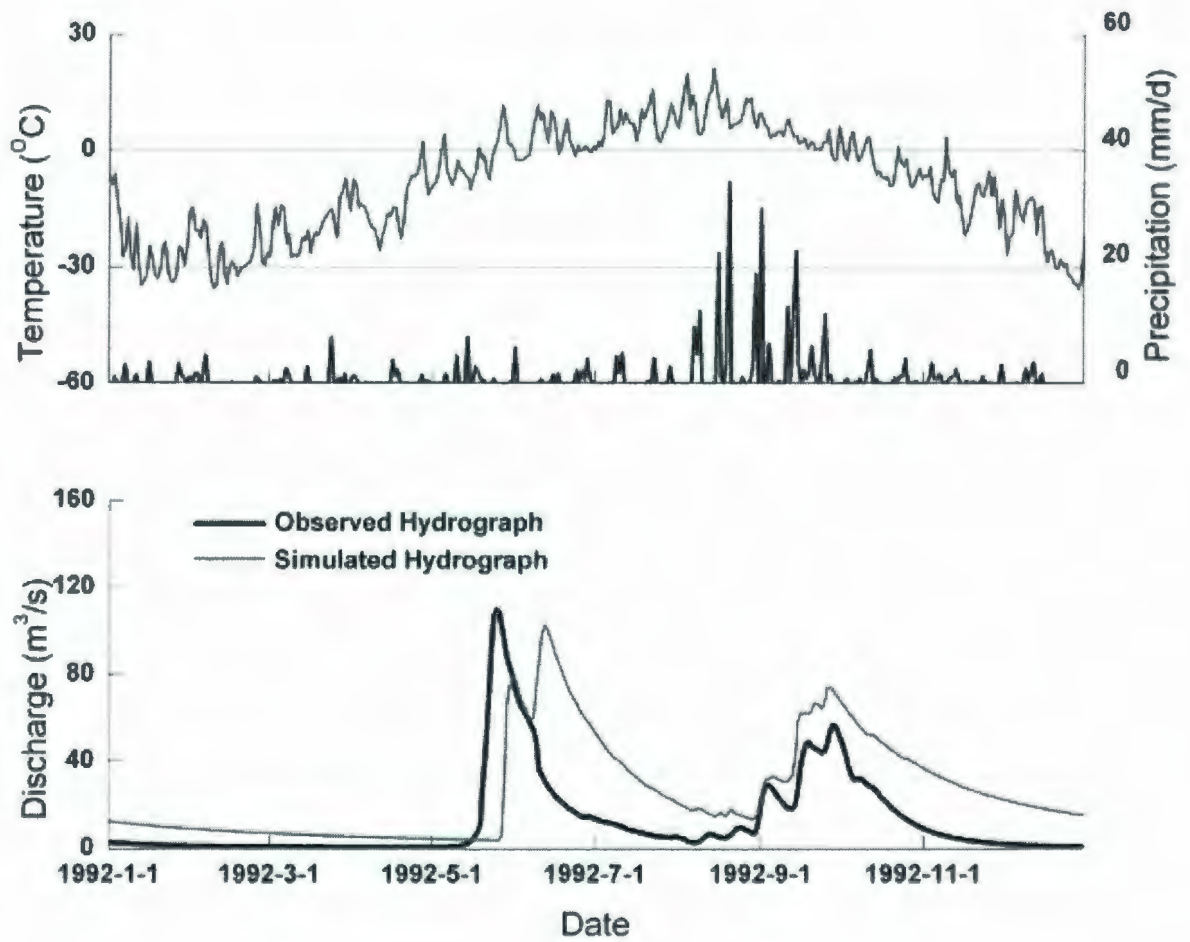


Figure 5.25 Simulated and observed daily hydrographs for the Deer River Watershed in 1992

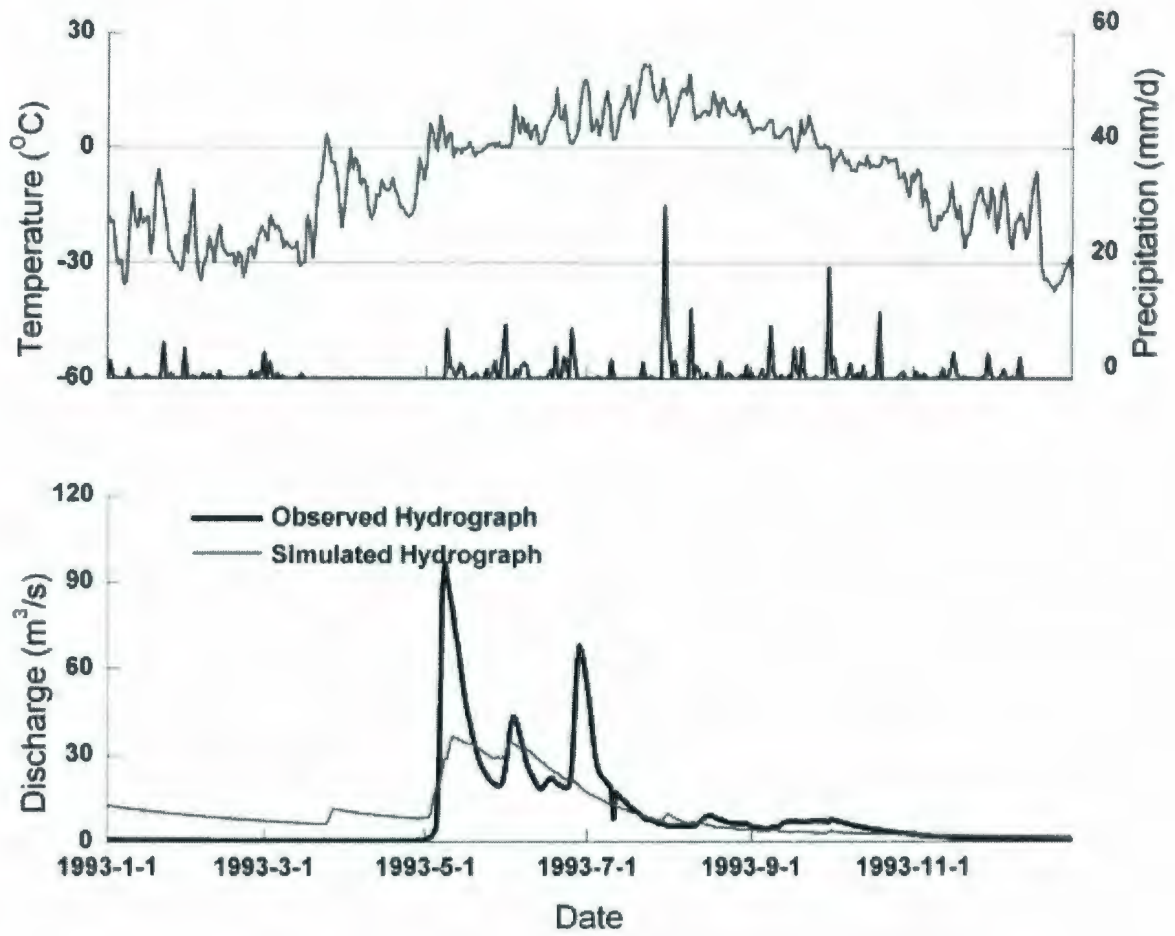


Figure 5.26 Simulated and observed daily hydrographs for the Deer River Watershed in 1993

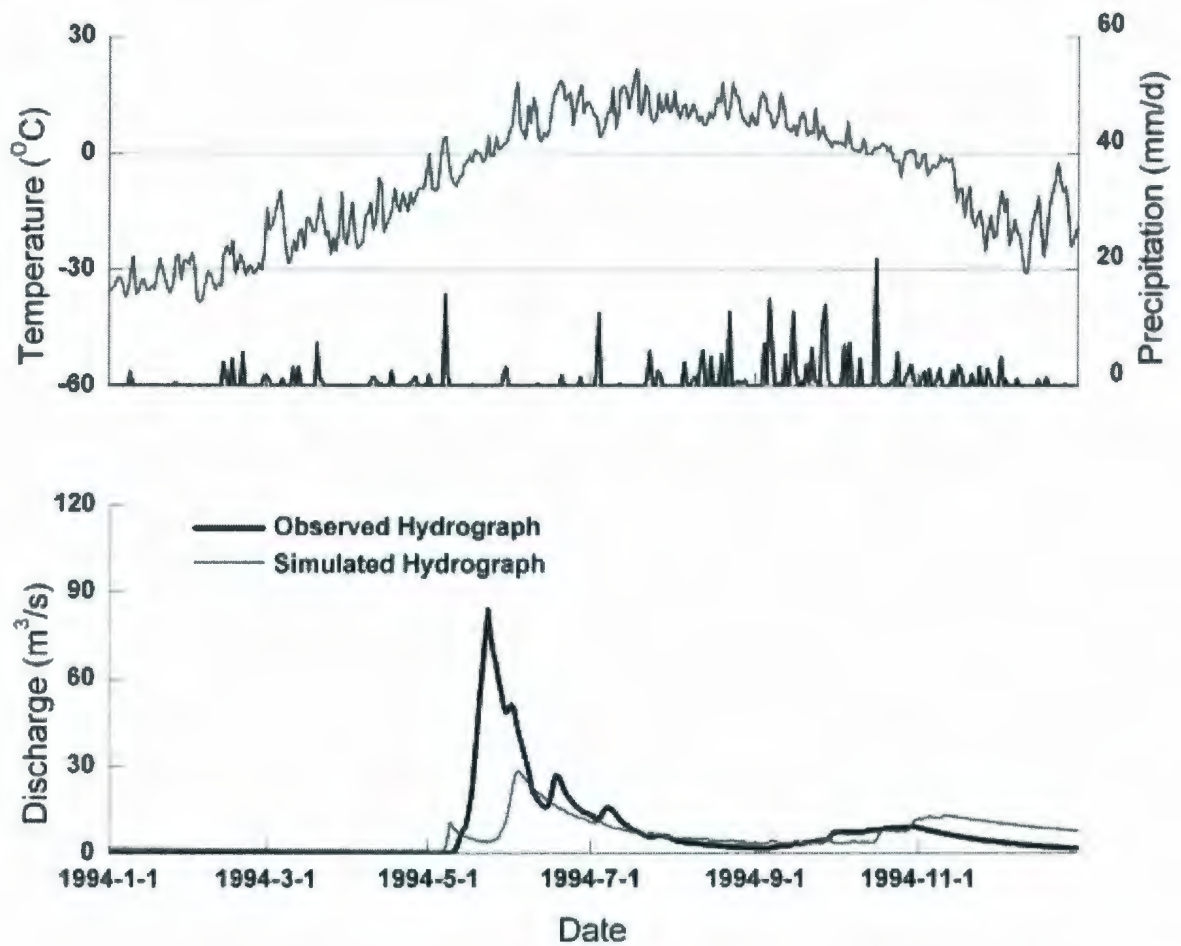


Figure 5.27 Simulated and observed daily hydrographs for the Deer River Watershed in 1994

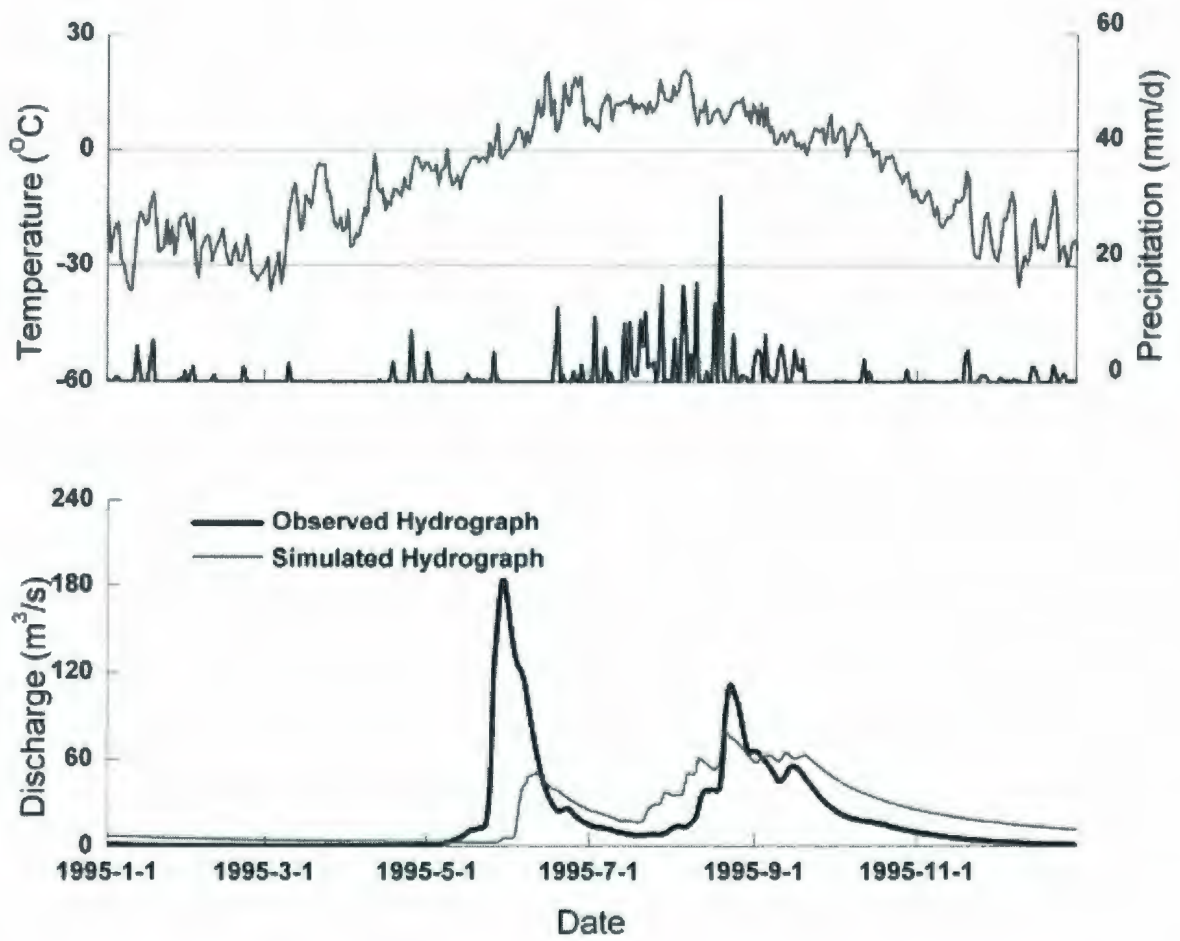


Figure 5.28 Simulated and observed daily hydrographs for the Deer River Watershed in 1995

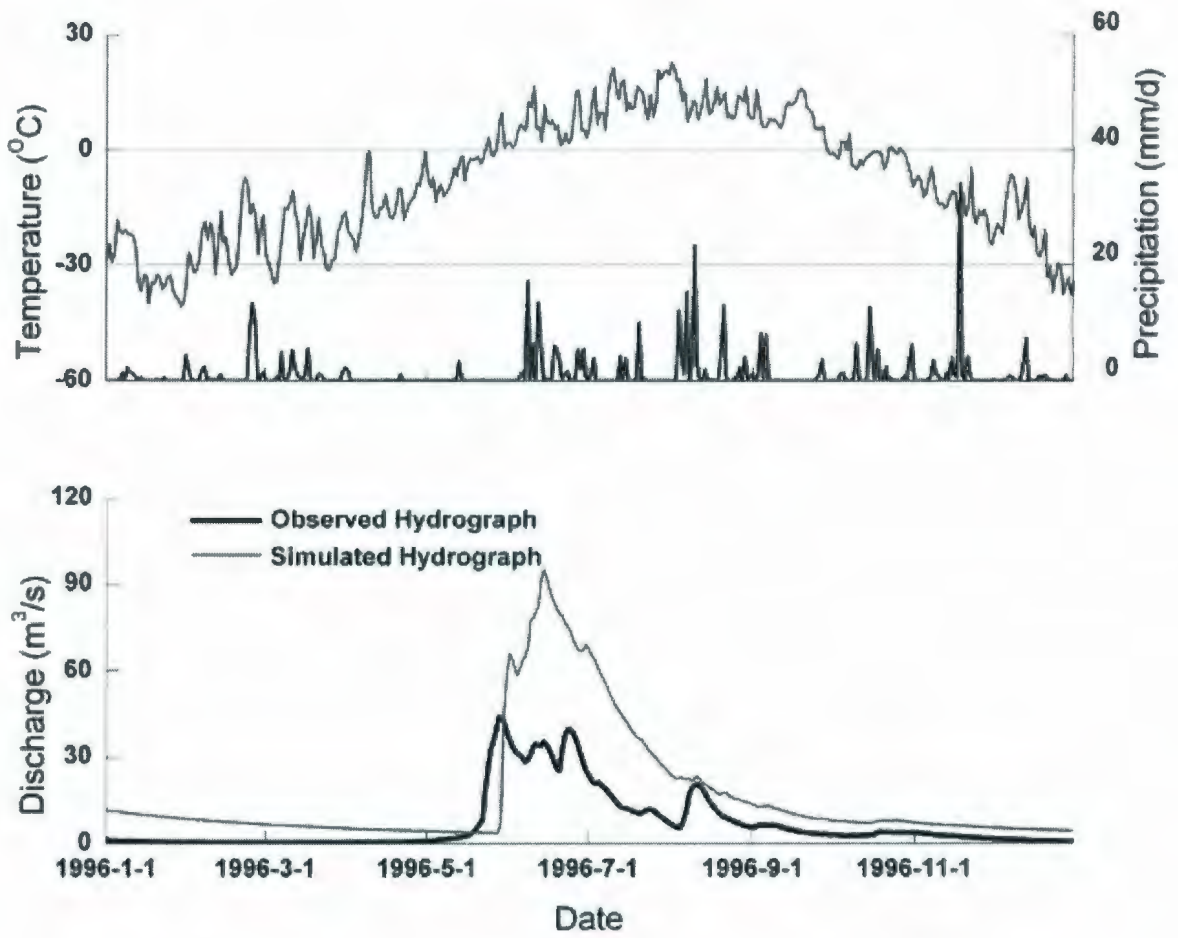


Figure 5.29 Simulated and observed daily hydrographs for the Deer River Watershed in 1996

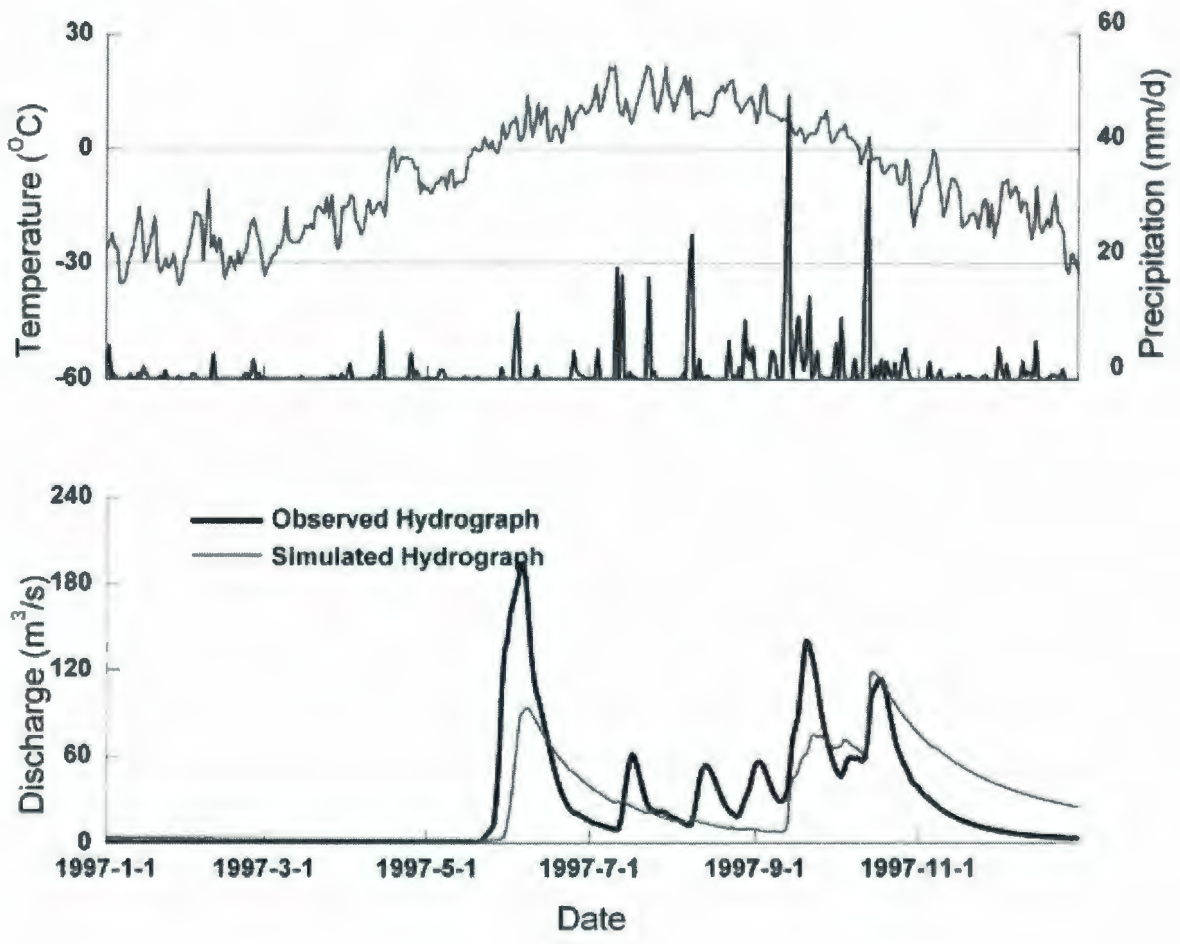


Figure 5.30 Simulated and observed daily hydrographs for the Deer River Watershed in 1997

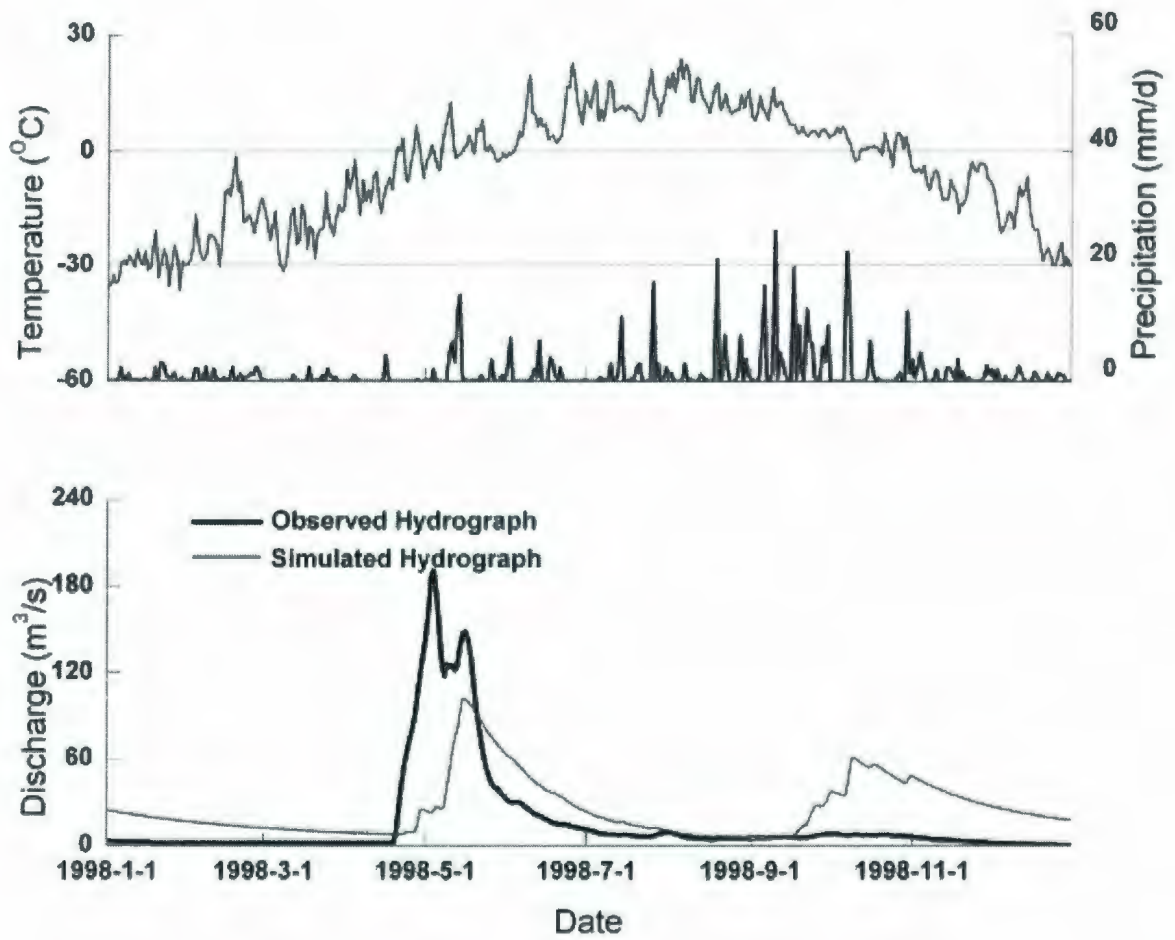


Figure 5.31 Simulated and observed daily hydrographs for the Deer River Watershed in 1998

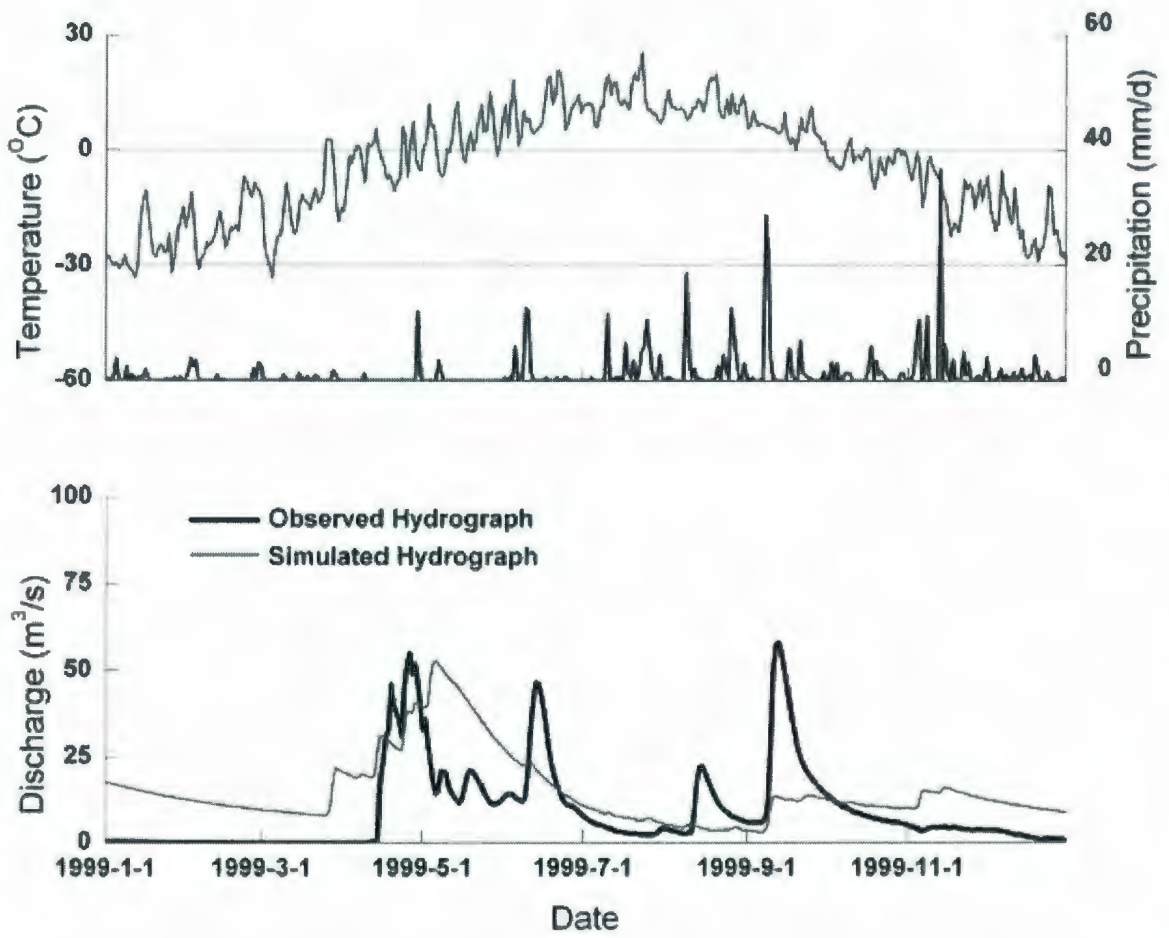


Figure 5.32 Simulated and observed daily hydrographs for the Deer River Watershed in 1999

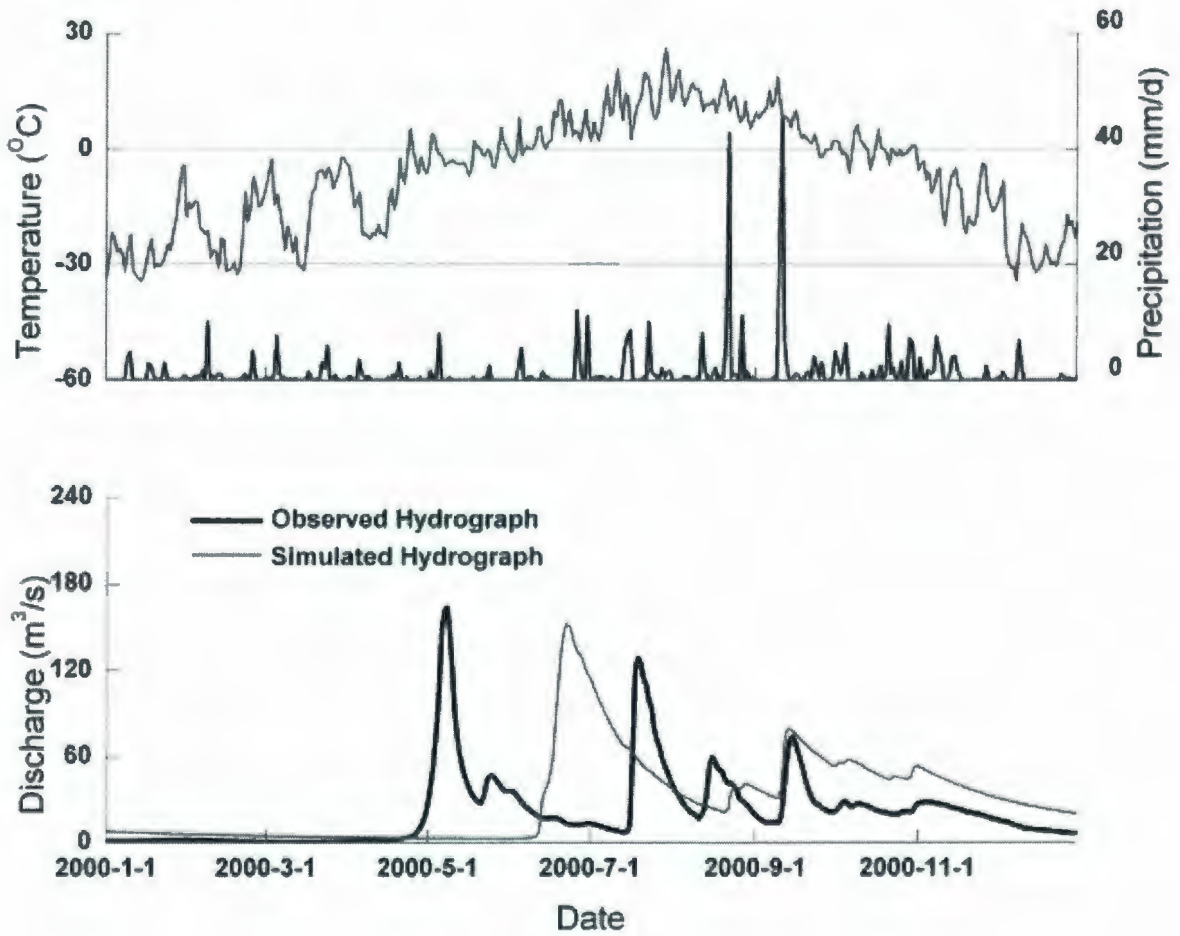


Figure 5.33 Simulated and observed daily hydrographs for the Deer River Watershed in 2000

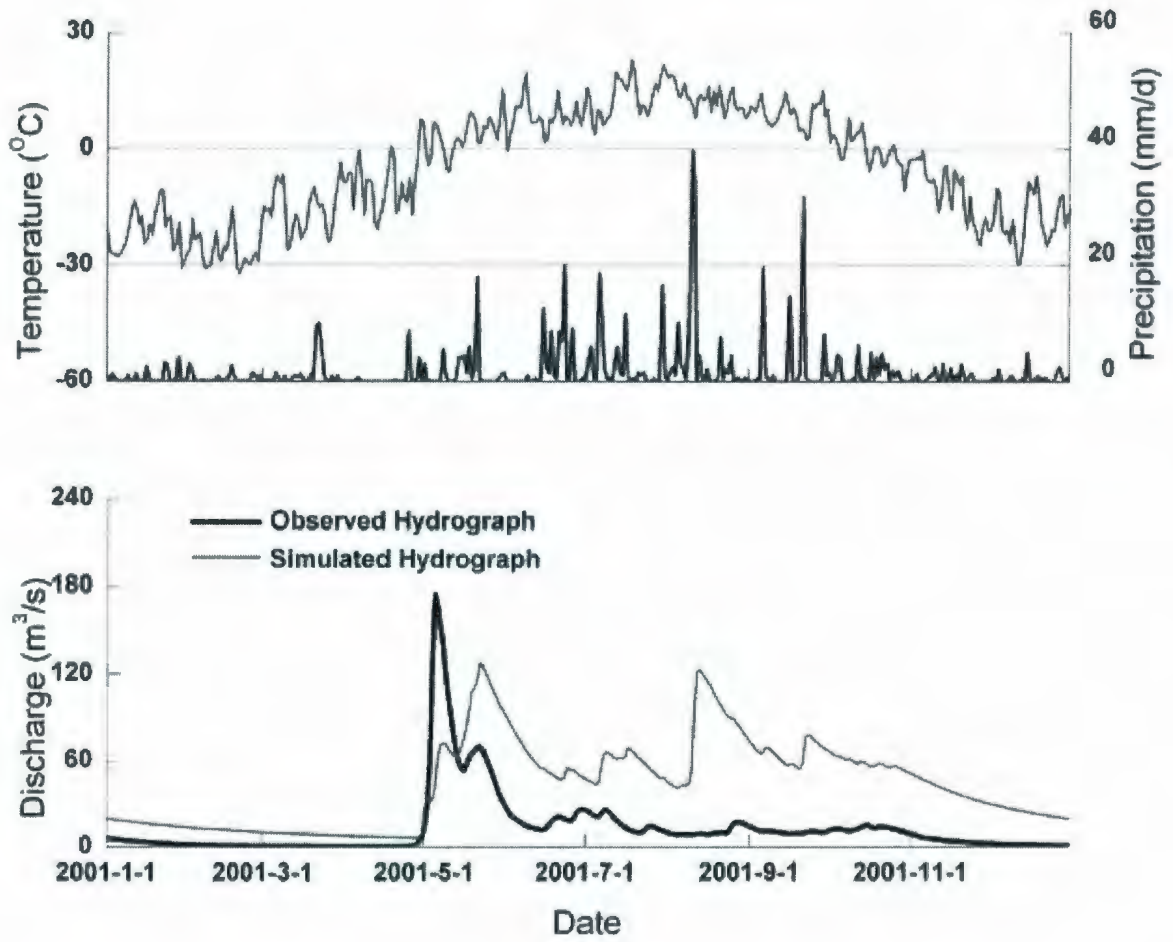


Figure 5.34 Simulated and observed daily hydrographs for the Deer River Watershed in 2001

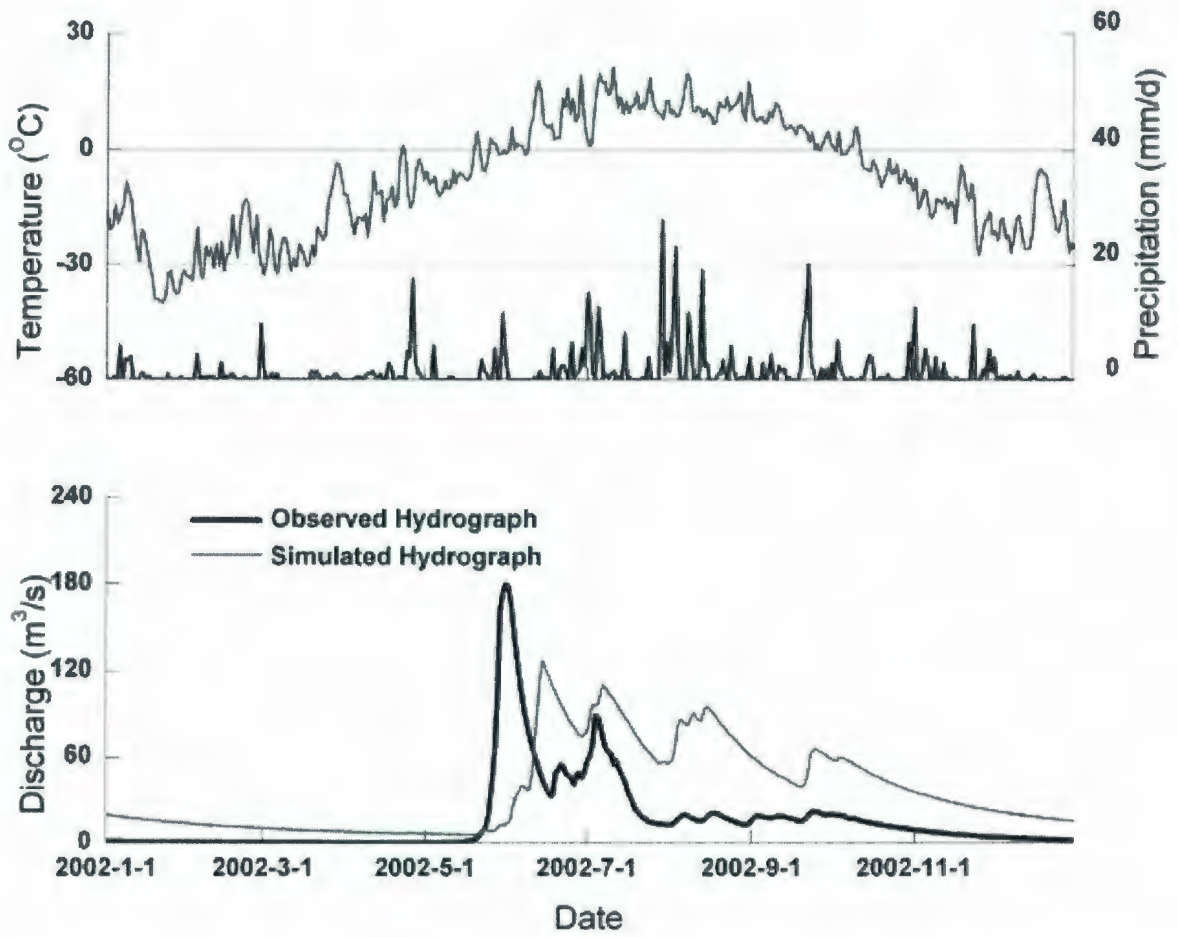


Figure 5.35 Simulated and observed daily hydrographs for the Deer River Watershed in 2002

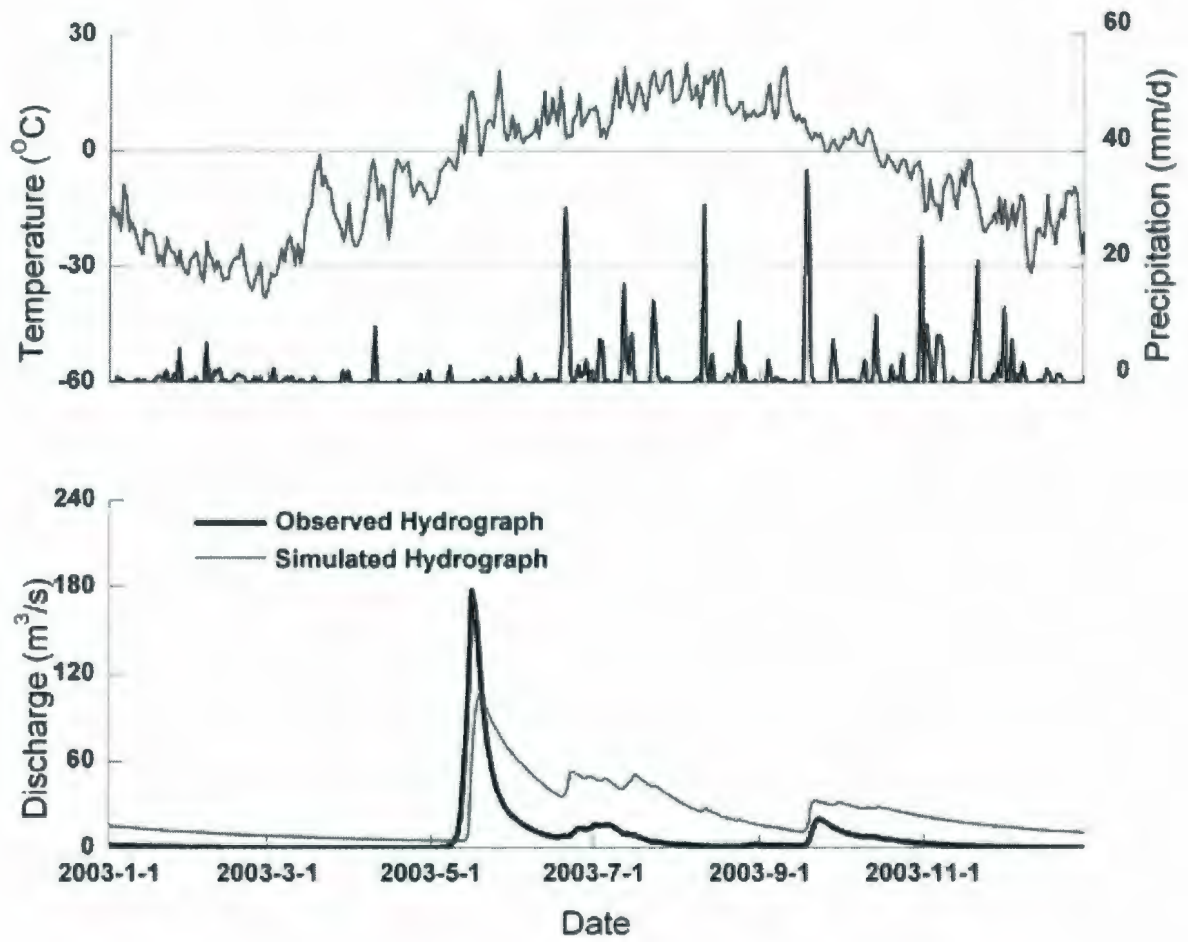


Figure 5.36 Simulated and observed daily hydrographs for the Deer River Watershed in 2003

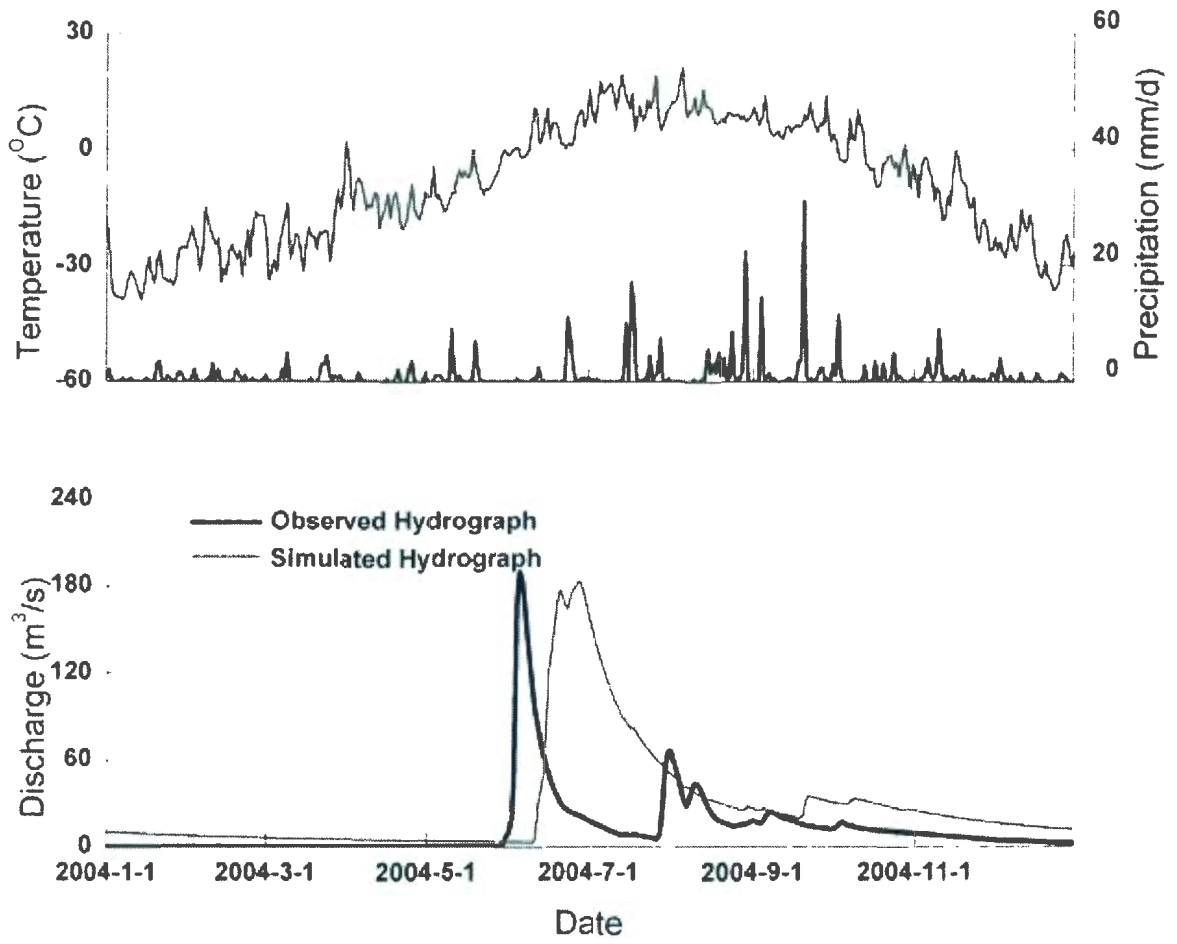


Figure 5.37 Simulated and observed daily hydrographs for the Deer River Watershed in 2004

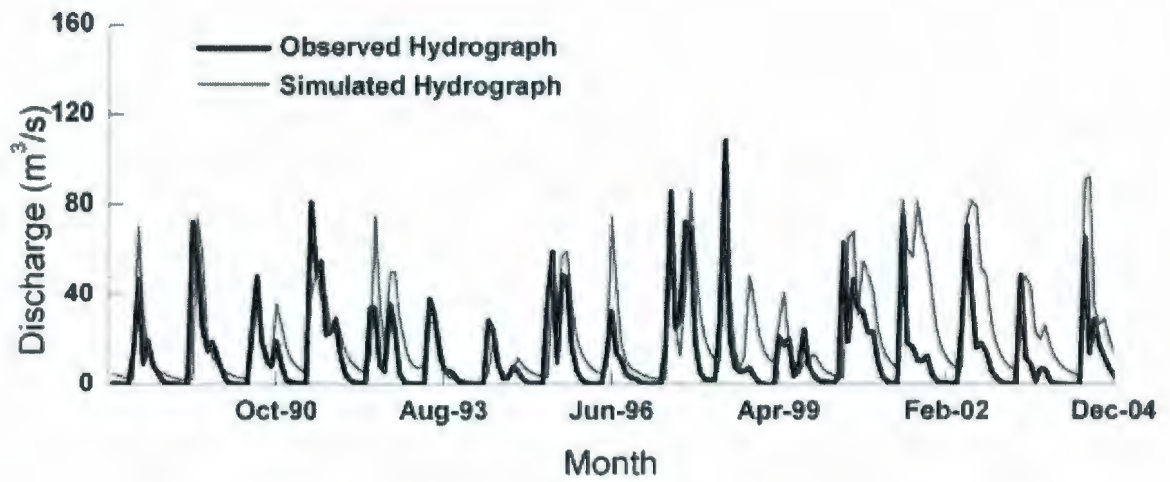


Figure 5.38 Simulated and observed monthly hydrographs for the Deer River Watershed from 1988 to 2004

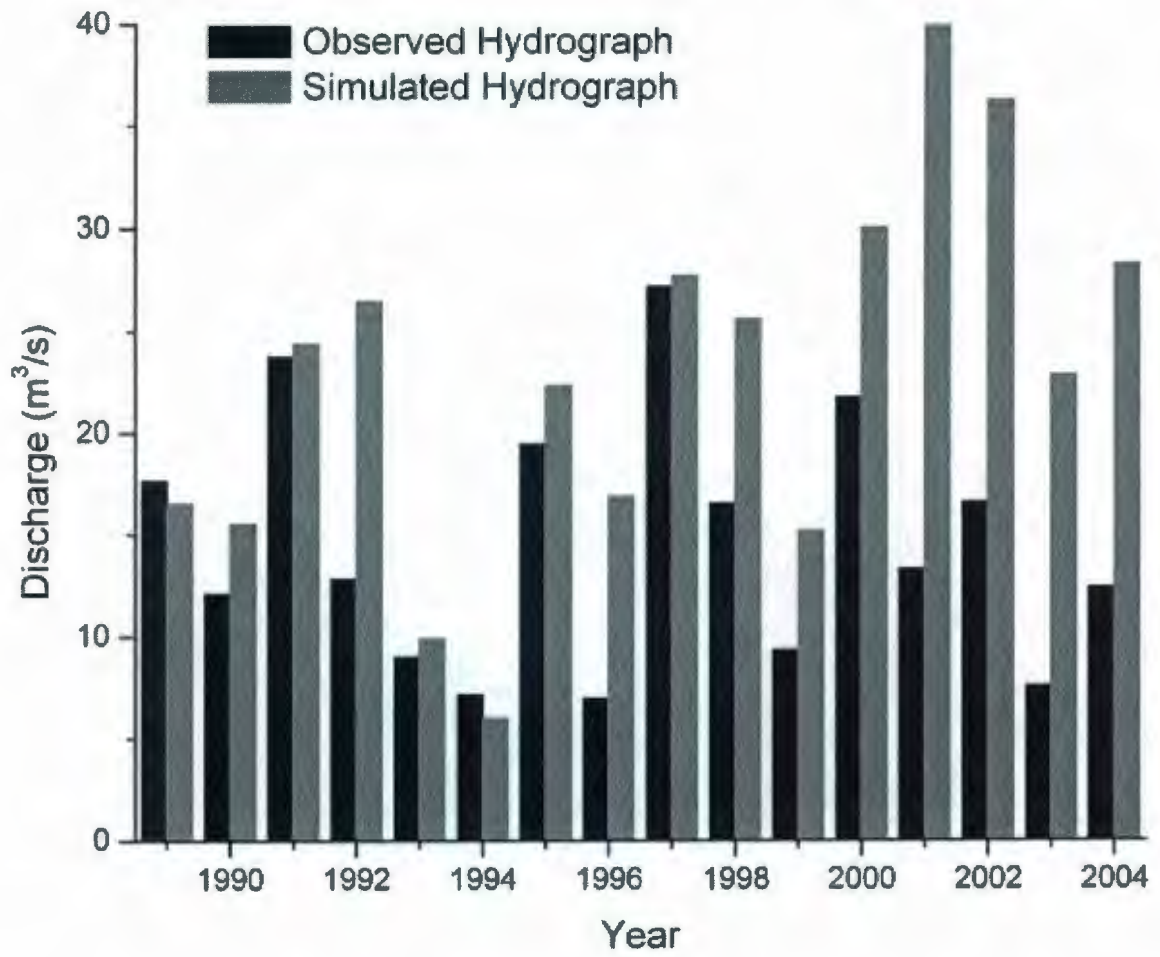


Figure 5.39 Simulated and observed annual hydrographs for the Deer River Watershed from 1988 to 2004

Table 5.5 Modelling efficiencies during WATFLOOD daily verification in the Deer River Watershed

Year	NSE (%)	DV (%)
1988	-6	32
1989	-34	-25
1990	58	-35
1991	40	-24
1992	-47	33
1993	52	-68
1994	22	-84
1995	21	-61
1996	-157	315
1997	46	-41
1998	13	-66
1999	-14	-31
2000	-109	34
2001	-208	68
2002	-75	13
2003	-24	-12
2004	-230	145
Average.	-38	11
Max.	58	315
Min.	-230	-84

Note: NSE is the Nash and Sutcliffe efficiency; and DV is the deviation of runoff volumes.

Table 5.6 Modelling efficiencies during WATFLOOD verification in the Deer River Watershed

	NSE (%)	DV (%)
Monthly	-3	28
Annual	-312	148

Note: NSE is the Nash and Sutcliffe efficiency; and DV is the deviation of runoff volumes.

5.8 Modelling of the Chesnaye Sub-basin

To further understand the hydrological features of the subarctic wetland in the summer time at a small scale basin and compare the results with those of SLURP, modelling work by WATFLOOD was also conducted for the Chesnaye Sub-basin.

5.8.1 Delineation of the Chesnaye Sub-basin

DEM file, boundary file, drainage direction file and upstream drainage area file generated from TOPAZ were loaded into EnsimHydrologic[®]. The entire DEM was divided into 50 rows and 50 columns as displayed in Figure 5.40. The basin is defined by its boundary and highlighted with different colours for elevation variation. Flow directions were also marked for each cell.

5.8.2 Land Cover

Detailed land cover data of the Chesnaye Sub-basin is referred to Section 4.8.2.

5.8.3 Meteorological and Streamflow data

Detailed meteorological and streamflow data is referred to Section 4.8.3.

5.8.4 Modelling Results

Modelling results from WATFLOOD (Figures 5.41 to 5.48) appear to be less accurate than those from SLURP. The estimated discharges of all the four stations are significantly lower than the observed ones; and even the responses to the rainfall events are not

obvious. This may be caused by using the same values of the modelling parameters as the ones used for modeling the entire Deer River Watershed. These parameters, such as upper zone storage and lower zone storage capacities are appropriate for the watershed but may need to be adjusted when modelling the Chesnaye Sub-basin. Besides the above uncertainty introduced by model parameters, resolution of the precipitation data which was converted from daily to hourly, could also affect the modelling accuracy and amplify the error. Moreover, the Hargreaves equation used in WATFLOOD is a rough estimation of the evapotranspiration and may also significantly reduce the runoff due to the overestimation. Simulated concentration times are days shorter than the observed ones due to the fact of descending permafrost table and enlarged soil water capacity. Buffering capability of local ponds should also be highlighted during the summer and fall months.

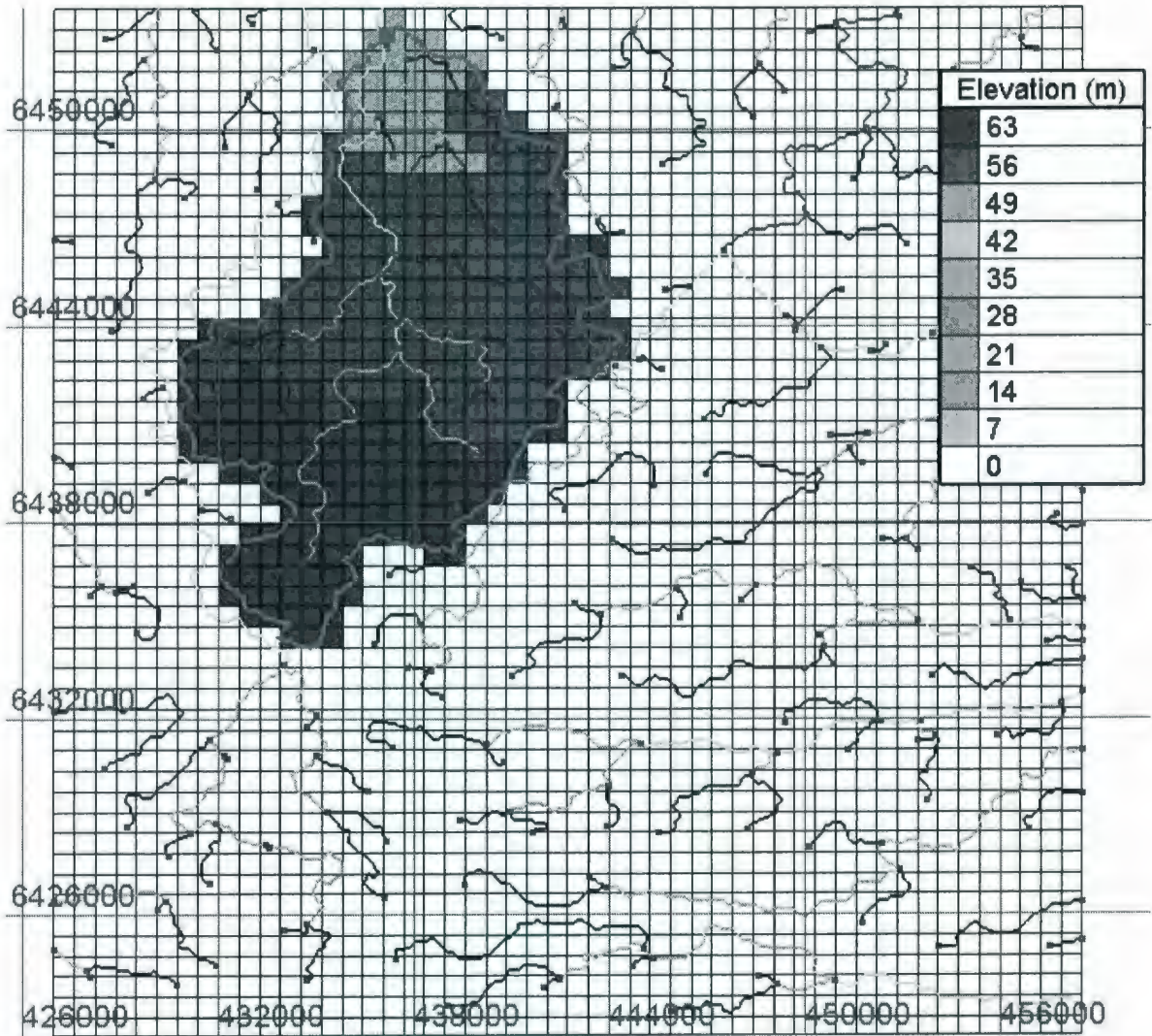


Figure 5.40 Gridded cells, boundary, elevation and channel network of the Chesnaye Sub-basin in EnsimHydrologic®

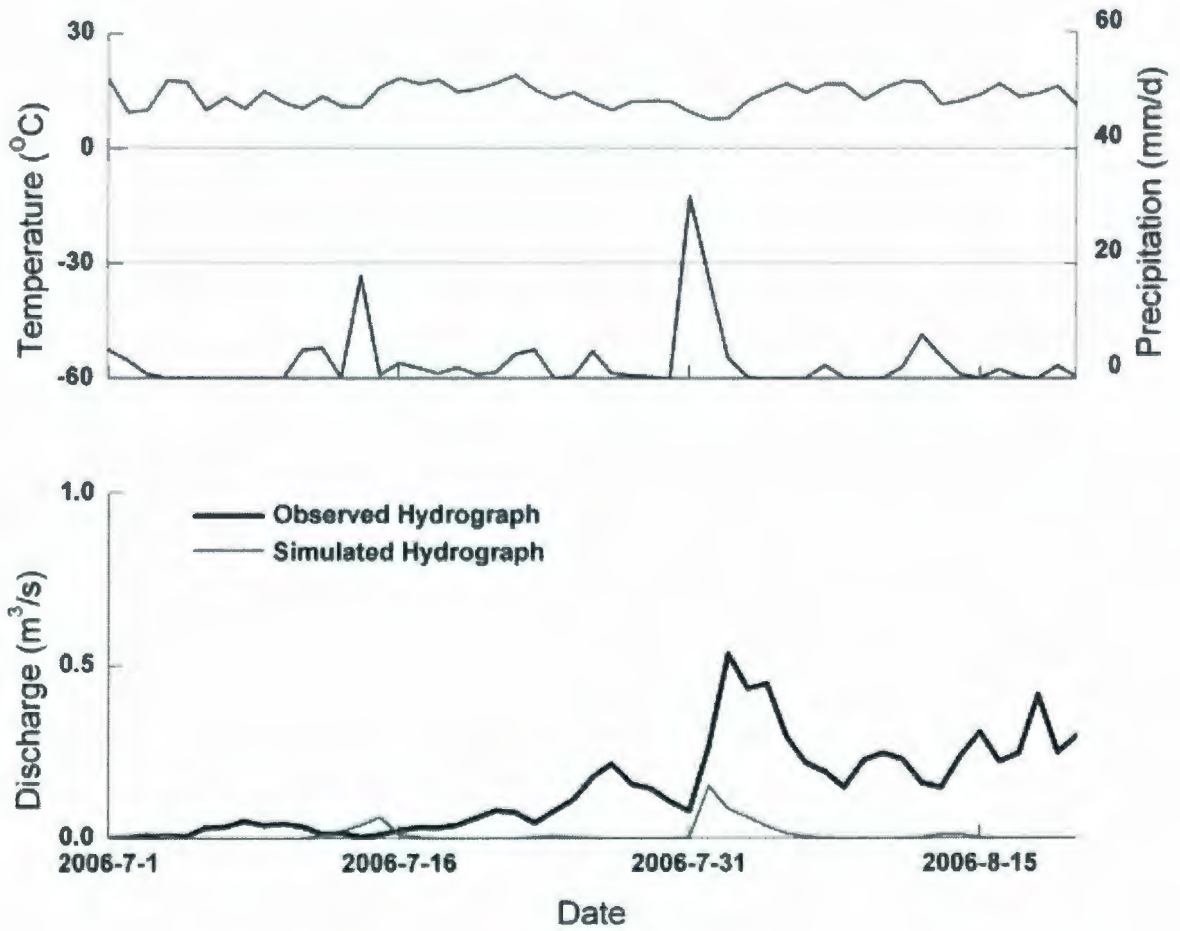


Figure 5.41 Simulated and observed daily hydrographs by WATFLOOD for Station 5 in 2006

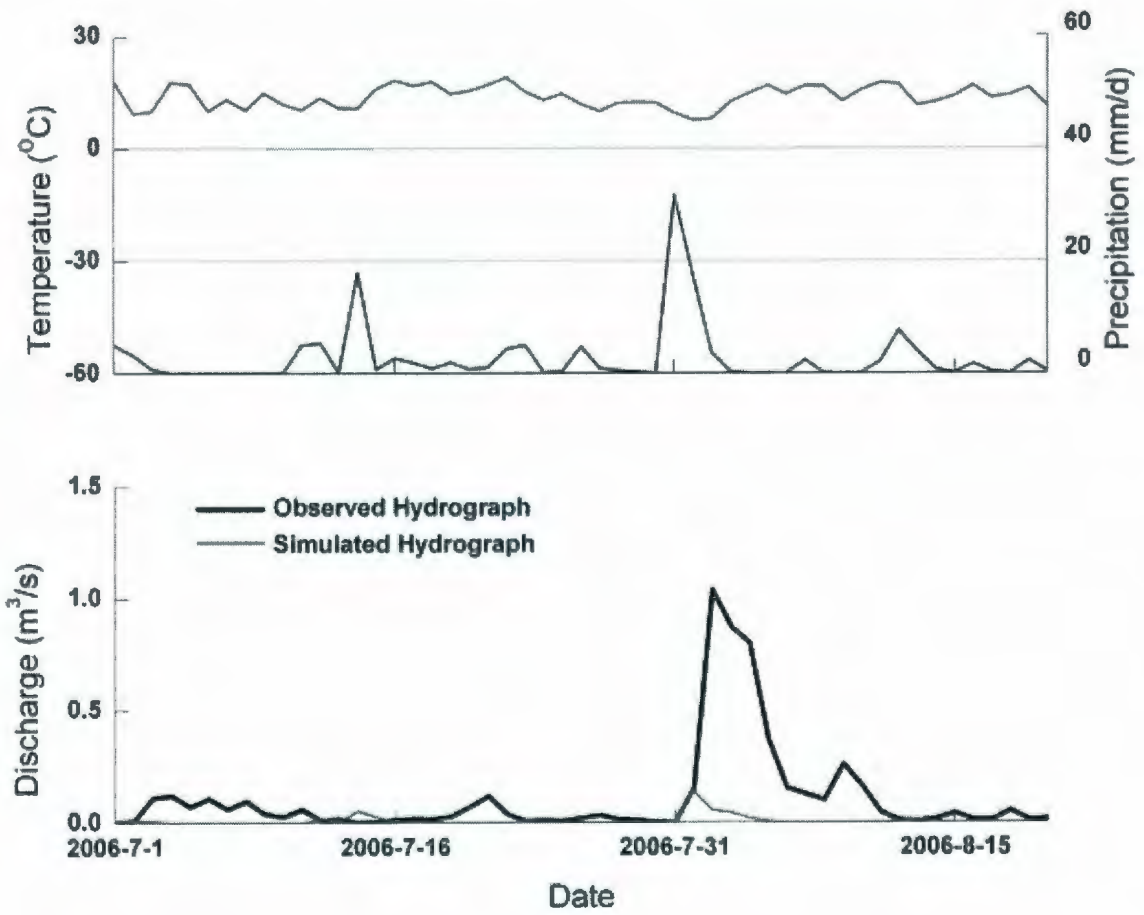


Figure 5.42 Simulated and observed daily hydrographs by WATFLOOD for Station 7 in 2006

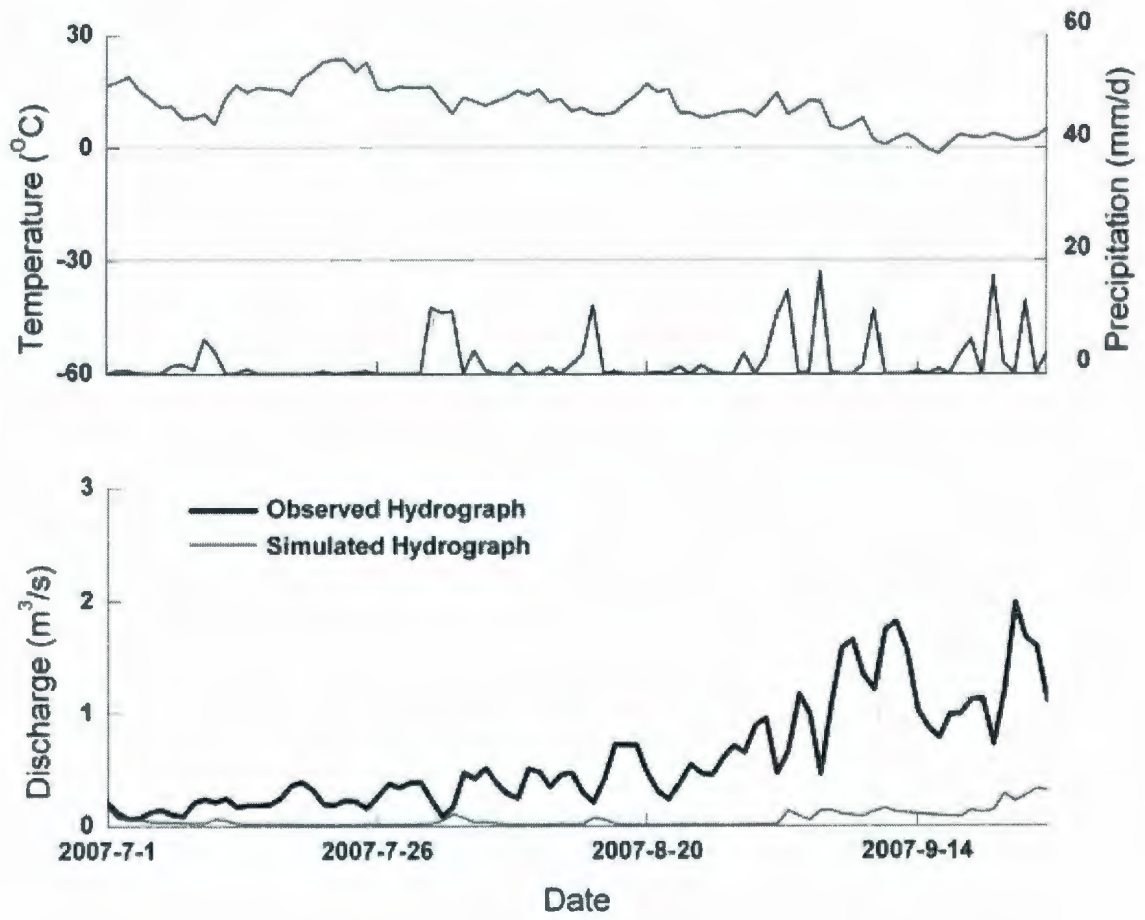


Figure 5.43 Simulated and observed daily hydrographs by WATFLOOD for Station 5 in 2007

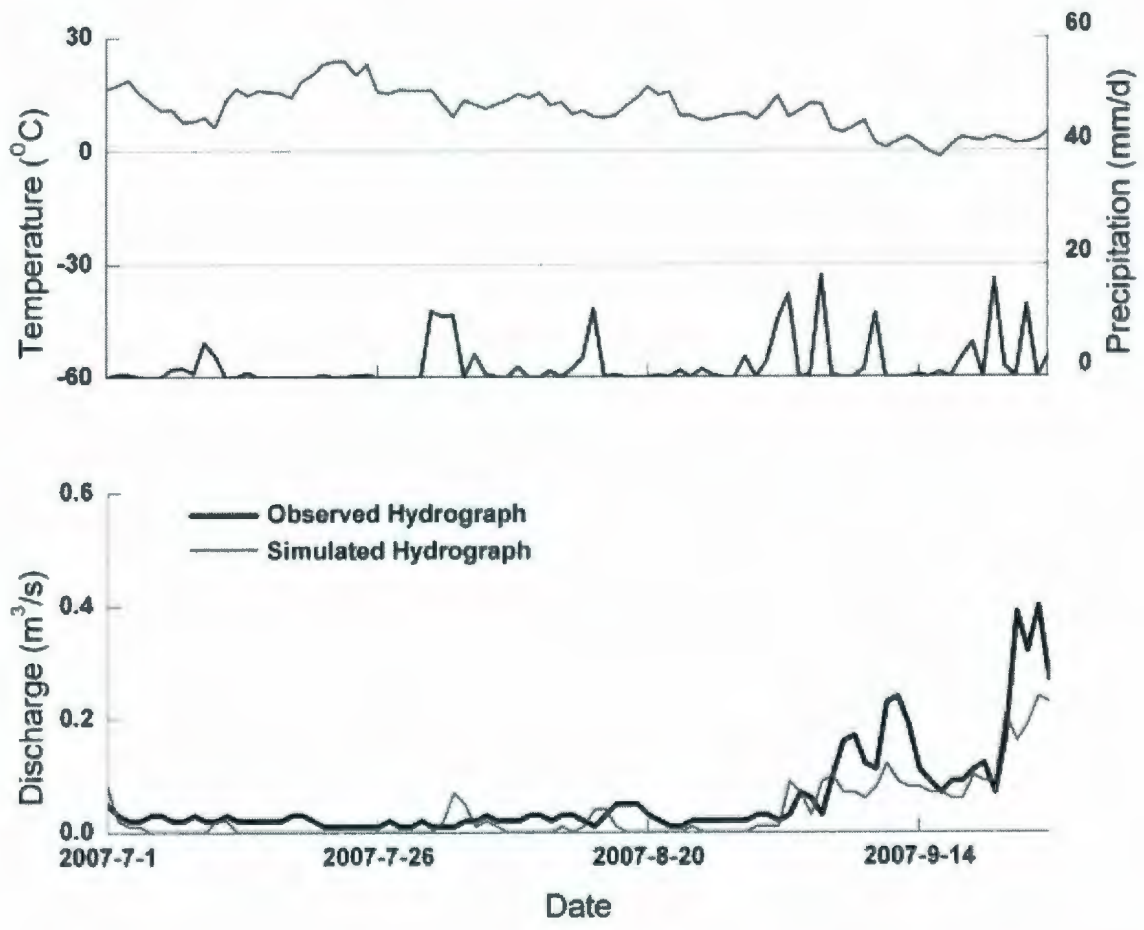


Figure 5.44 Simulated and observed daily hydrographs by WATFLOOD for Station 6 in 2007

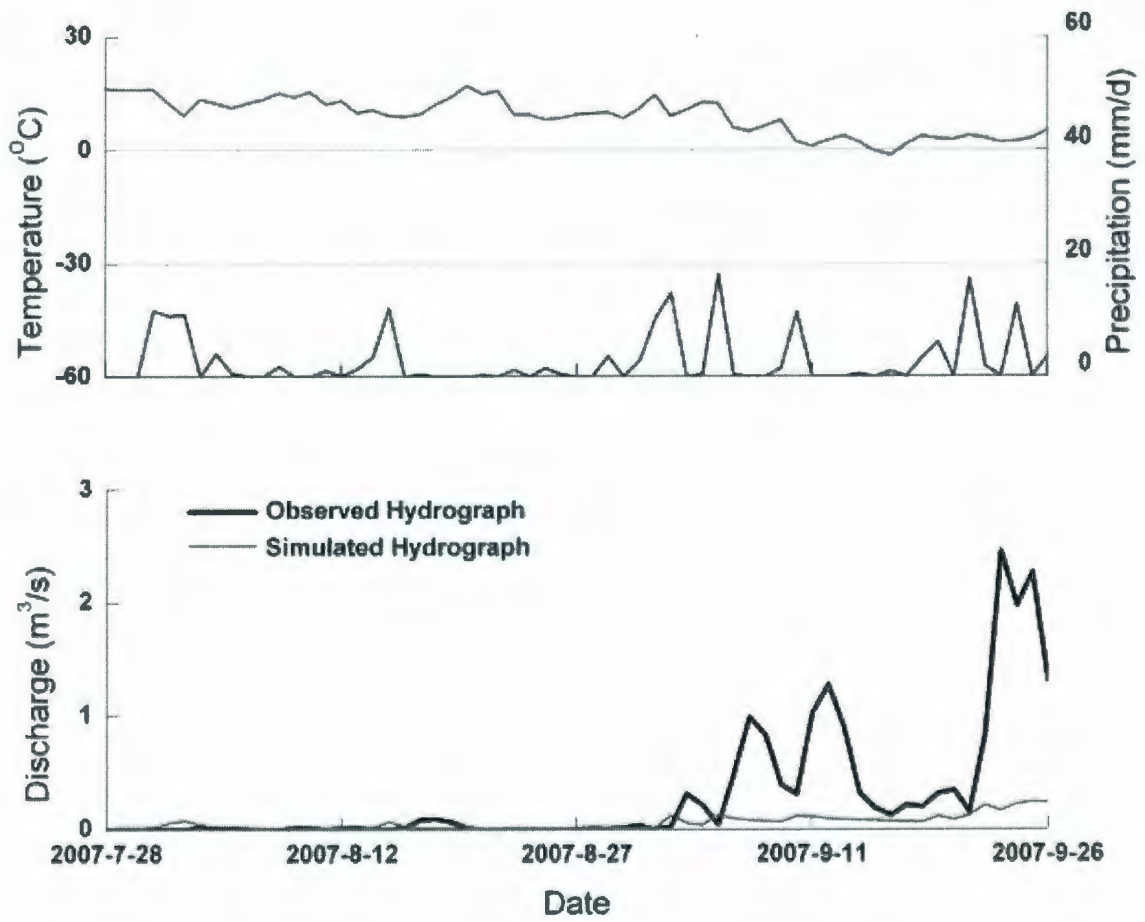


Figure 5.45 Simulated and observed daily hydrographs by WATFLOOD for Station 7 in 2007

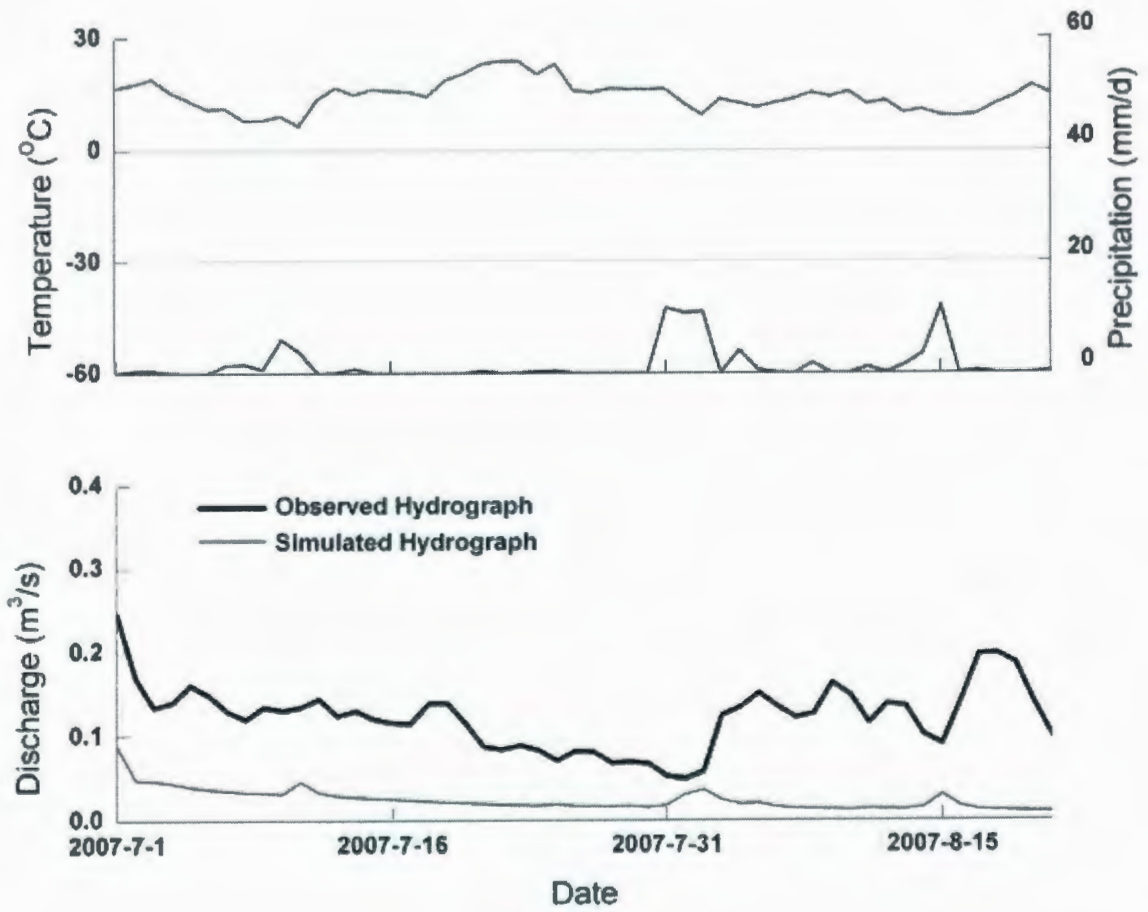


Figure 5.46 Simulated and observed daily hydrographs by WATFLOOD for Station 10 in 2007

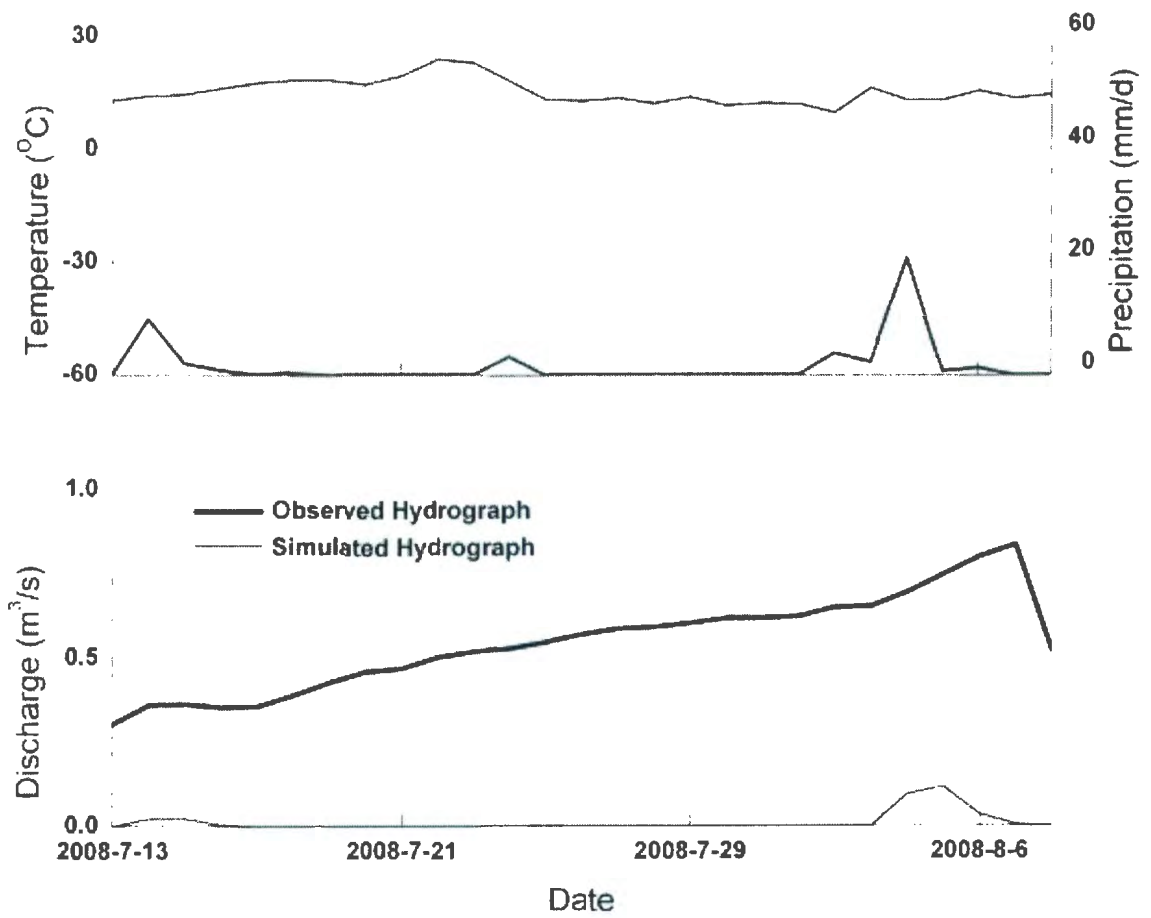


Figure 5.47 Simulated and observed daily hydrographs by WATFLOOD for Station 5 in 2008

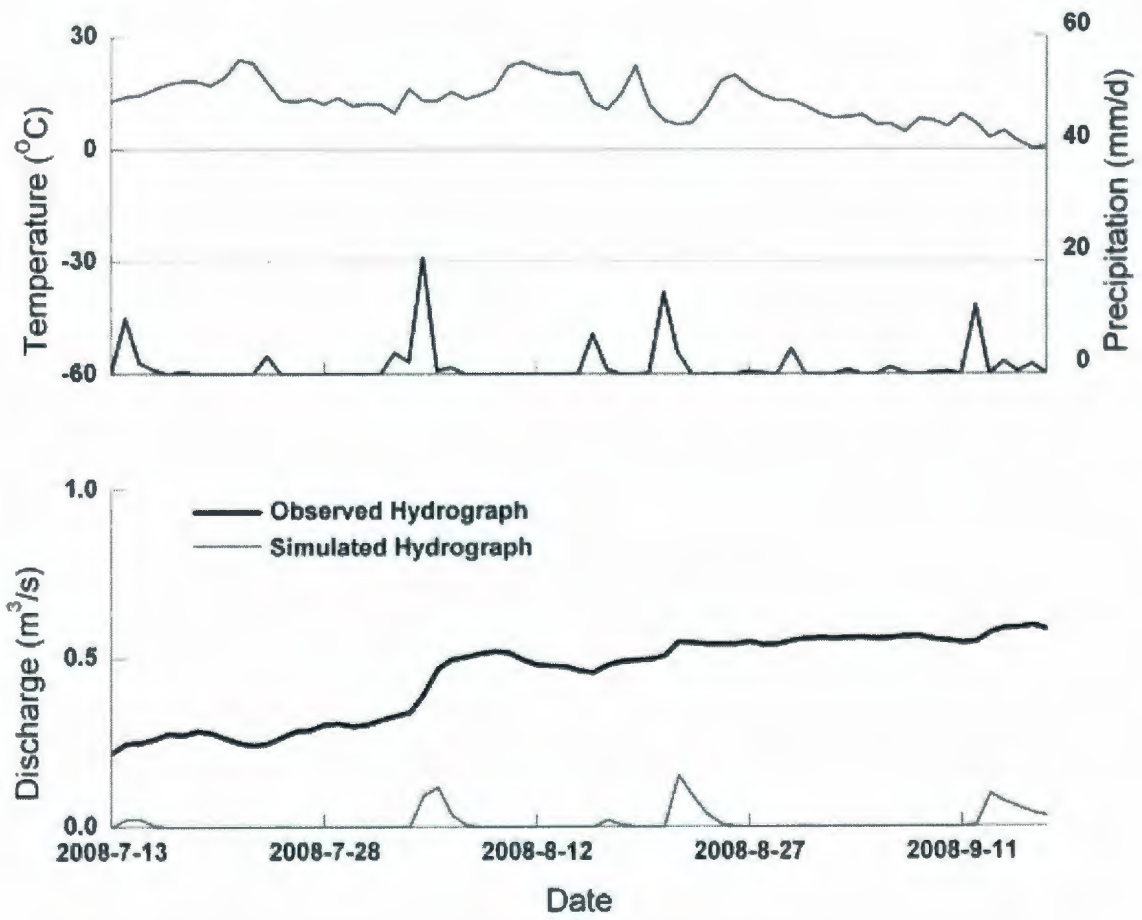


Figure 5.48 Simulated and observed daily hydrographs by WATFLOOD for Station 10 in 2008

5.9 Summary

In this chapter, WATFLOOD was used to simulate the hydrological processes of the Deer River Watershed and the Chesnaye Sub-basin. The modelling efficiencies of both calibration and verification periods are much lower than those of SLURP. This may be explained by the lack of hourly data, poor data resolution, extra complexities of the model, difficulties in optimization and time constraints to treat these two models evenly. For example, hourly precipitation data was prepared by evenly distributing the daily data into 24 hours which may weaken the intensities and prolong the durations of the rainfall events. The degree-day snowmelt algorithm and constant melt factor were discussed because it generates spring runoff wherever snowpack temperature exceeds 0 °C. Moreover, not considering the influences from the frost table, extremely high soil porosity and the ponds may also result in the inaccuracy of the modelling results. The DVs indicate that WATFLOOD underestimates the spring peak but overestimates the summer runoff. Simulation of the Chesnaye Sub-basin further shows that WATFLOOD is not as accurate as SLURP, indicating that the Hargreaves equation used in the modelling work overestimates the evapotranspiration.

The next chapter presents the discussion of the modelling results from both SLURP and WATFLOOD. Based on the results and the model structures, a comparison between these two models will also be presented.

Chapter 6 Comparison between SLURP and WATFLOOD

6.1 Introduction

SLURP and WATFLOOD are both conceptual, physically based, semi-distributed hydrological models which are used for simulating and predicting watershed features. Both of them have been developed in Canada and widely used since the 1970s. The basic computation concepts of the two models are different. SLURP divides a watershed into multiple ASAs, routes the runoff within each ASA and then among the ASAs to the basin outlet; On the other hand, WATFLOOD evenly divides a watershed into GRUs and routes the runoff within each GRU as well as along adjacent ones to the outlet. Of importance is that hydrological processes are also described differently by employing different equations in the two models. For example, SLURP divides the soil layers as fast storage and slow storage, whereas WATFLOOD separates the subsurface into upper zone storage, intermediate zone storage and lower zone storage. Though the two models have been individually applied to watersheds under different scenarios in the past decades, there is still lack of studies on comparing them and examining their efficiencies and capacities in modelling watersheds, especially the ones in the subarctic regions. This chapter is about to compare the two models through conceptual illustration as well as the real-world case study conducted in the Deer River Watershed.

6.2 Difference in Modelling Structure

One of the fundamental differences between SLURP and WATFLOOD is the modelling time step. SLURP is based on daily runoff calculation, whereas WATFLOOD computes the water discharge at hourly interval. In other words, WATFLOOD has a more advantageous and accurate calculation because it needs more detailed data input than SLURP does. However, it also implies that WATFLOOD may even compromise the modelling efficiency if the meteorological or streamflow data is not available in hourly.

Another major difference in modelling structure lies in the hydrological simulation unit. SLURP divides the whole watershed into multiple ASAs by TOPAZ. The D8 flow algorithm routes each DEM grid into the steepest of its eight neighbour grids and combines related grids to form an ASA. Each ASA is subdivided into areas of different land covers referred to satellite image. Surface runoff, interflow and groundwater flow are then accumulated from each land cover area within each ASA by using a time-contributing area relationship. Then the combined outflow is converted and accumulated to stream flow and eventually routed to the outlet of the watershed. A notable advantage of this ASA concept is that the outputs are available in raster format and able to be compared with satellite based models. Each ASA is not homogenous and contains multiple land covers with independent flow routing calculations based on the mean distances to the nearest streams. Moreover, SLURP is capable of recalculating downstream flow values based on transient internal system diversion. Additionally, the size of each ASA can be adjusted to vary over the entire range of possibilities. However,

there are some shortcomings of this ASA concept. For example, the watershed delineation may not be accurate for some topographical conditions, such as board plains where elevation hardly varies. Moreover, SLURP distributes point meteorological data to each ASA without any compensation or modification which simplifies the runoff computation but compromises the accuracies.

WATFLOOD evenly and symmetrically divides a basin into multiple functional units – GRU. Each GRU has identical DEM grids and various land covers with determined ratios. Surface runoff, intermediate flow and ground water flow are routed for each land cover type within each GRU and flow direction is determined by D8 algorithm to route the water flows to the next steepest neighbouring GRU. A prominent advantage of this GRU concept is that it is able to use radar meteorological data which is more accurate and reliable than distributed data from climate stations. Another major advantage is that it can incorporate necessary hydrological features without compromising the simplicity of computation and introducing any uncertainties caused by watershed delineation. Additionally, large size GRU (10 km × 10 km) is available in WATFLOOD which remarkably reduces the computation effort and input parameterization work. However, an inherent weakness of this concept is that the heterogeneity may be lost and only land covers differentiation within one grid could be derived. Moreover, flow direction determination of each GRU may also be inaccurate if its size is too large.

6.3 Difference in Simulation Methodologies

Basic model schemes of SLURP and WATFLOOD contain each necessary hydrological process as following description. The use of different equations for some processes could result in significant differences in modelling outputs.

6.3.1 Interception and Surface Storage

Interception is the first water re-distribution when precipitation occurs. SLURP treats the interception with leaf area index (*LAI*) as shown in Equation 4-10 (Spittlehouse, 1989). It computes the canopy interception from an empirical equation and only considers how flourish the vegetations are. On the other hand, WATFLOOD computes interception as the sum of two parts: interception evapotranspiration (*IET*) during a rainfall event (Equation 5-1) and maximum canopy storage (Linsley *et al.*, 1949). It combines the evapotranspiration during the rainfall with actual canopy storage to obtain the more accurate interception capacity. Surface storage could be understood as depression storage on the ground surface, such as ponds, lakes and reservoirs. It plays a significant role in affecting the water distribution because lakes or reservoirs could act as a buffer and prolong the concentration time. WATFLOOD calculates the surface storage as shown in Equation 5-2, whereas SLURP does not include surface storage and this amount of water could be distributed into canopy interception or fast storage.

Modelling results of WATFLOOD indicate that runoff from most of the rainfall events are underestimated than those of SLURP. For example, as shown in Figures 4.13 and 5.16,

simulated runoff from most of the rainfall events occur in September and October are underestimated by WATFLOOD compared with SLURP, implying that interception and surface storage may take much more water in WATFLOOD. The same conclusion can be observed in Figures 4.20 and 5.22.

6.3.2 Snowmelt Process

Snowmelt is one of the crucial natural processes because it determines the spring runoff, which is the majority water budget in subarctic wetland systems. Both SLURP and WATFLOOD utilize the degree-day method that relates the snowmelt rate with air temperature as shown in Equations 4-13 and 4-14, and Equation 5-15 (Anderson, 1973). It is indicated that SLURP employs an exponentially increasing snowmelt rate with date and WATFLOOD only concerns temperature difference. This difference, if under the same circumstances given time and temperature, may lead to the consequences that snowmelt is accelerated in SLURP but delayed in WATFLOOD.

Figures 6.1 and 6.2 emphasize the modelling difference by taking examples from 1979 and 1992. Results from WATFLOOD shows that spring peak later than the actual situation or the one from SLURP. Constantly melting assumption is able to delay the runoff because it does not consider the accelerating effect from raising temperature. Another feature that could be observed is that spring runoff estimated by WATFLOOD is much greater than the historical records or that of SLURP. Maximum fast storage and slow storage can be set and calibrated in SLURP which enables the soil layers to store as much water as required and adjust the channel runoff. On the other hand, WATFLOOD

does not have these parameters to control the water storage which means excessive water can be released as surface runoff. Moreover, WATFLOOD has a particular sub-model that deals with the water distribution within the wetland. It requires some properties of the wetland, such as wetland width, wetland porosity, the hydraulic resistance coefficient, channel width to depth ratio, and height of water in wetland and channels. However, these wetland properties are not available from the field investigation, which means they have to be estimated and calibrated during the calibration and generate some uncertainties.

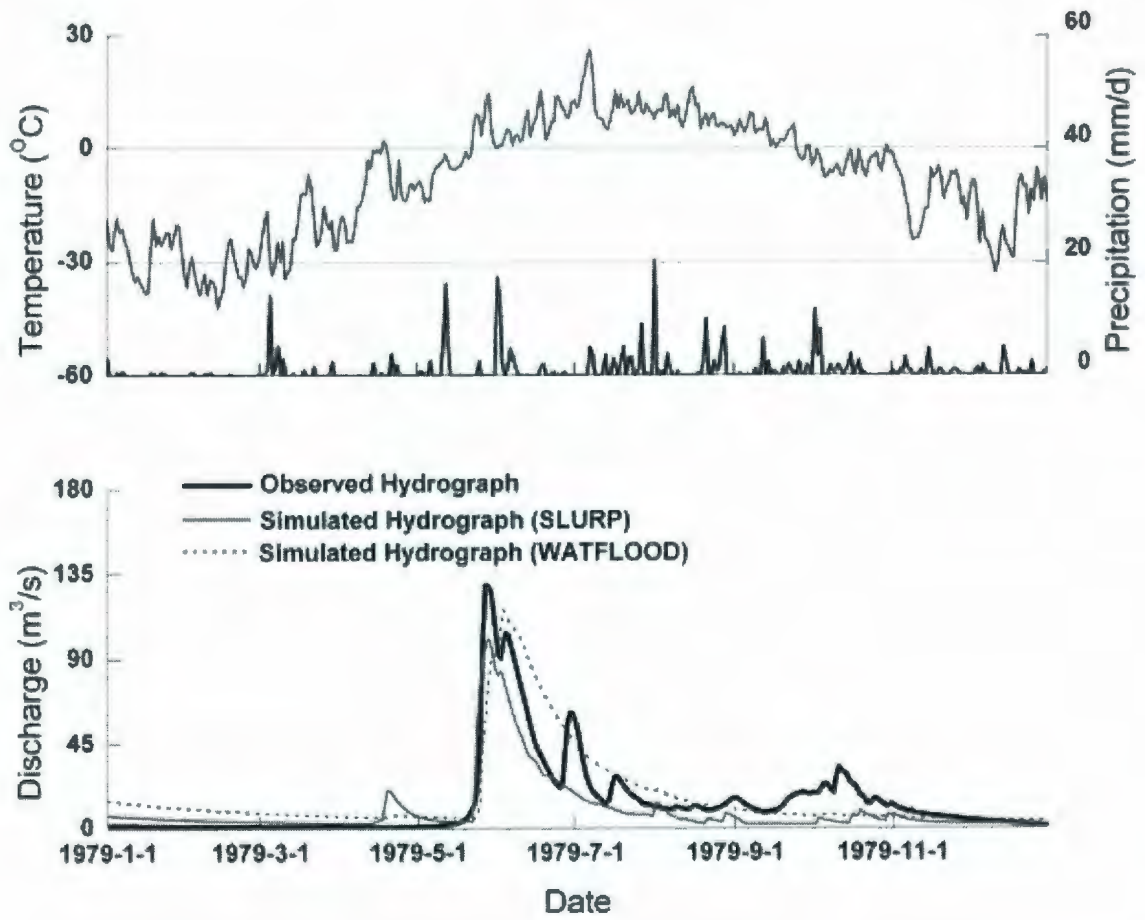


Figure 6.1 Simulated and observed daily hydrographs for the Deer River Watershed in 1979

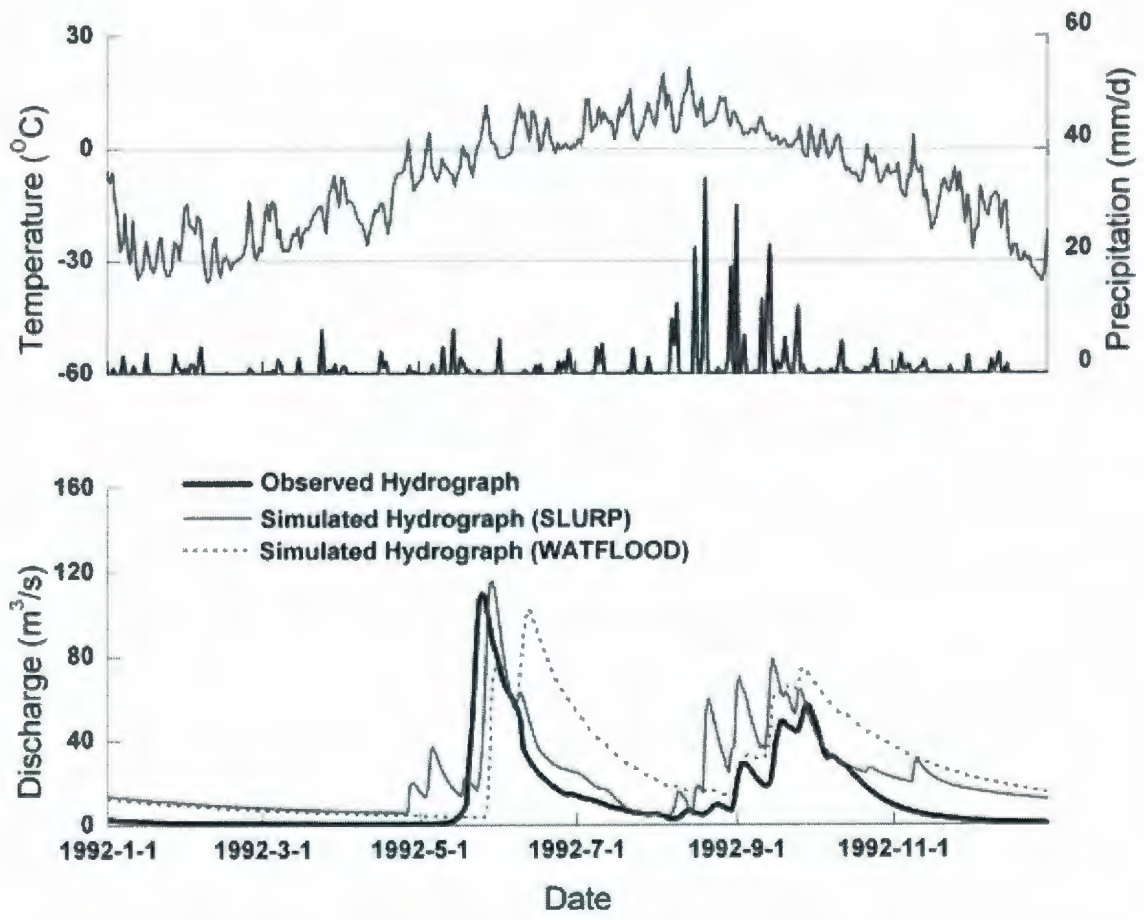


Figure 6.2 Simulated and observed daily hydrographs for the Deer River Watershed in 1992

6.3.3 Evapotranspiration

Evapotranspiration behaves as one of the dominant factors in hydrological modelling. Accurately evapotranspiration computing ensures the efficiency of modelling the water budget and stream discharge.

6.3.3.1 SLURP

In the modelling work of SLURP, Morton CRAE method (Morton, 1983) was chosen to estimate the actual evapotranspiration as shown in Equation 4-1. E_w and E_p could be expressed by:

$$E_p = R_T - \lambda f_T (T_p - T) \quad (6-1)$$

$$R_p = E_p + \gamma p f_T (T_p - T) \quad (6-2)$$

$$E_w = d_1 + d_2 (1 + \gamma p / \Delta_p)^{-1} R_p \quad (6-3)$$

where R_T is the net radiation for soil-plant surface at air temperature (mm eq./d); λ and f_T are the heat transfer coefficient and vapour transfer coefficient, respectively; T_p is the potential evapotranspiration equilibrium temperature ($^{\circ}\text{C}$); T is the air temperature ($^{\circ}\text{C}$); γ is the psychrometric constant (0.066 kPa/ $^{\circ}\text{C}$); p is the atmospheric temperature ($^{\circ}\text{C}$); d_1 and d_2 are set to 14 W/m² and 1.20, respectively; and Δ_p is the slope of saturation vapour pressure curve at T_p . R_T can be calculated by:

$$R_T = (1 - a)G - B \quad (6-4)$$

where a is the average albedo; G is incident global radiation (mm eq./d); and B is net long-wave radiation loss for soil-plant surfaces at air temperature (mm eq./d). a can be obtained by the following equations:

$$a = a_o[S + (1-S)(1-Z/330)] \quad (6-5)$$

$$a_o = \frac{a_z[\exp(1.08) - (2.16 \cos Z/\pi + \sin Z) \exp(0.012Z)]}{1.473(1 - \sin Z)} \quad (6-6)$$

$$a_z = a_{zz} + (1 - c_0^2)(0.34 - a_{zz}) \quad (6-7)$$

$$\begin{aligned} a_{zz} = a_{zd} &= 0.26 - 0.00012P_A(p/p_s)^{0.5}[1 + |\phi/42| + (\phi/42)^2] \\ 0.11 \leq a_{zz} &\leq 0.5(0.91 - \nu_D/\nu) \\ 0.11 \leq a_{zd} &\leq 0.17 \end{aligned} \quad (6-8)$$

$$p/p_s = [(288 - 0.0065H)/288]^{5.256} \quad (6-9)$$

$$\begin{aligned} c_0 &= \nu - \nu_D \\ 0 \leq c_0 &\leq 1 \end{aligned} \quad (6-10)$$

$$\begin{aligned} \nu_D &= 6.11 \exp[17.27T_D/(T_D + 237.3)] \\ \nu &= 6.11 \exp[\alpha'T/(T + \beta')] \end{aligned} \quad (6-11)$$

$$\begin{aligned} \cos Z &= \cos(\phi - \theta) \\ \theta &= 23.2 \sin(29.5i - 94) \end{aligned} \quad (6-12)$$

$$\begin{aligned} \cos Z &\geq 0.001 \\ S &= 0.53G/(G_o - 0.47G) \\ 0 \leq S &\leq 1 \end{aligned} \quad (6-13)$$

where a_o is the clear-sky albedo (Arnfeld, 1975); S is the ratio of observed to maximum possible sunshine duration; Z is the noon regular zenith distance of sun (dimensionless); a_z and a_{zz} are the regular and snow-free zenith values of clear-sky albedo, respectively; a_{zd} is the zenith value of dry-season snow-free clear-sky albedo; P_A is the long-term average precipitation (mm); p and p_s are atmospheric pressure and atmospheric pressure at sea level (kPa), respectively; ϕ and θ are the latitude and declination of sun (degree), respectively; H is the altitude (m); ν_D and ν are the saturation vapour pressures at T and T_D (kPa), respectively; T_D is the dew-point temperature ($^{\circ}\text{C}$); i is the month number; G_o is the clear-sky global radiation (mm eq./d) (Brooks, 1960); α' and β' are set to 17.27°C

and 237.3 °C when T is equal or greater than 0 °C or 21.88 °C and 265.5 °C when T is less than 0 °C, respectively; and c_0 is a constrained variable. G_o and G could be calculated by:

$$G_o = G_E \tau [1 + (1 - \tau / \tau_a)(1 + a_o \tau)] \quad (6-14)$$

$$G = S G_o + (0.08 + 0.30 S)(1 - S) G_E$$

$$G_E = (1354 / \eta^2)(\omega / 180) \cos z \quad (6-15)$$

$$\eta = 1 + (1/60) \sin(29.5i - 106) \quad (6-16)$$

$$\cos \omega = 1 - \cos Z / (\cos \phi \times \cos \theta) \quad (6-17)$$

$$\cos \omega \geq -1$$

$$\cos z = \cos Z + [(180/\pi)(\sin \omega) / \omega - 1] \cos \phi \times \cos \theta \quad (6-18)$$

$$\tau = \exp[-0.089(p/p_s / \cos z)^{0.75} - 0.083(j / \cos z)^{0.90} - 0.029(W / \cos z)^{0.60}] \quad (6-19)$$

$$\tau_a = \exp[-0.0415(j / \cos z)^{0.90} - (0.0029)^{0.5} (W / \cos z)^{0.30}] \quad (6-20)$$

$$\tau_a \geq \exp[-0.0415(j / \cos z)^{0.90} - 0.029(W / \cos z)^{0.60}]$$

$$W = v_D / (0.49 + T/129)$$

$$j = (0.5 + 2.5 \cos^2 z) \exp[c_1(p/p_s - 1)] \quad (6-21)$$

$$c_1 = 21 - T$$

$$0 \leq c_1 \leq 5$$

where G_E is the extra-atmospheric global radiation (mm eq./d); τ is the transmittance of clear skies to direct beam solar radiation (dimensionless); τ_a is the part of τ that is the result of absorption (Brooks, 1960); η is the radius vector of sun (dimensionless); ω is the angle the earth rotates between sunrise and noon (degree); z is the average angular zenith distance of sun (dimensionless); j and W are turbidity coefficient and precipitable water vapour (kPa), respectively (Robinson, 1966; Morton, 1978).

B is the net long-wave radiation loss with the surface at air temperature and could be calculated by the following equations:

$$B = \varepsilon \sigma (T + 273)^4 [1 - (0.71 + 0.007 v_D p/p_s)(1 + \rho)] \quad (6-22)$$

$$B \geq 0.05 \varepsilon \sigma (T + 273)^4$$

$$\begin{aligned}\rho &= 0.18[(1-c_2)(1-S)^2 + c_2(1-S)^{0.5}] p_s/p \\ c_2 &= 10(v_D/v - S - 0.42) \\ 0 &\leq c_2 \leq 1\end{aligned}\quad (6-23)$$

where ε , σ , and ρ are surface emissivity, Stefan-Boltzmann constant ($5.67 \times 10^{-8} \text{ W/m}^2/\text{K}^4$), and proportional increase in atmospheric radiation (W/m^2) due to clouds, respectively; and f_T and λ are the vapour and heat transfer coefficients, respectively. Following equations could be applied for calculation:

$$f_T = (p_s/p)^{0.5} f_z/\zeta \quad (6-24)$$

$$\begin{aligned}\lambda &= \gamma p + 4\varepsilon\sigma(T + 273)^3/f_T \\ 1/\zeta &= 0.28(1 + v_D/v) + \Delta R_T/[\gamma p(p_s/p)^{0.5} b_0 f_z(v - v_D)] \leq 1\end{aligned}\quad (6-25)$$

$$\begin{aligned}\gamma p &= (\gamma p_s)(p/p_s) \\ \Delta &= dv/dT = \alpha\beta v/(T + \beta)^2\end{aligned}\quad (6-26)$$

where f_z and γp_s are 28 W/mbar/m^2 and $0.66 \text{ mbar/}^\circ\text{C}$ when T is equal or greater than 0°C or 32.2 W/mbar/m^2 and $0.57 \text{ mbar/}^\circ\text{C}$ when T is less than 0°C , respectively; ζ is the stability factor; Δ is the slope of the saturation vapour pressure ($\text{kPa/}^\circ\text{C}$); and b_0 is a constant which is equal to 1.00.

The other variable parameters in Equations 6-1, 6-2 and 6-3 are T_p and Δ_p which are able to be estimated from:

$$T_p = T_p' + [\delta T_p] \quad (6-27)$$

$$[\delta T_p] = [R_T/f_T + v_D - v_p' + \lambda(T - T_p')]/(\Delta_p' + \lambda) \quad (6-28)$$

$$v_p = 6.11 \exp[\alpha T_p/(T_p + \beta)] \quad (6-29)$$

$$\Delta_p = \alpha\beta v_p/(T_p + \beta)^2$$

where $[\delta T_p]$ is the correction to T_p' in iteration process; v_p is the saturation vapour pressure at T_p (kPa); and T_p' , v_p' and Δ_p' are the initial values for T_p , v_p and Δ_p ,

respectively.

6.3.3.2 WATFLOOD

The method which has been used for WATFLOOD modelling is Hargreaves Equation (Hargreaves and Samani, 1982) because the hourly net radiation data is not available for the Priestley-Taylor Equation. The parameters in Equation 5-9 could be computed based on the following equations (Duffie and Beckman, 1980):

$$R_a = 15.392 \times d_r (w_s \times \sin \phi \times \sin \delta + \cos \phi \times \cos \delta \times \sin w_s) \quad (6-31)$$

$$d_r = 1 + 0.033 \times \cos \left(\frac{2\pi \times J}{365} \right) \quad (6-32)$$

$$\delta = 0.4093 \times \sin \left(\frac{2\pi \times J}{365} - 1.405 \right) \quad (6-33)$$

$$w_s = \arccos(-\tan \phi \times \tan \delta) \quad (6-34)$$

$$\begin{aligned} C_i &= 0.035(100 - w_a)^{1/3} & w_a &\geq 54\% \\ C_i &= 0.125 & w_a &< 54\% \end{aligned} \quad (6-35)$$

where d_r is the relative distance between the sun and the earth (dimensionless) and computed by Julian day (J); w_s is the sunset hour angle (radian); and ϕ and δ are latitude (degree) and solar declination (radian), respectively. The actual evapotranspiration then could be derived from Equation 5-10.

It is notable that Morton CRAE method computes the potential evapotranspiration by using modifications of the Penman Equation and replaces the wind function with a vapour transfer coefficient (f_T) in order to solve the energy balance and aerodynamic equations

for potential evapotranspiration. It is more logic but not widely accepted. The basic calculation requires mean daily temperature, dew-point temperature and net radiation. The advantage of this method is that it includes most of the important parameters which has been used in both Priestley-Taylor Equation and Penman Equation. However, the accuracy may not be good enough because most of the data are not fully distributed. Moreover, complicated calculations may result in more error. Contrastingly, Hargreaves Equation is chosen for modelling by WATFLOOD because hourly net radiation is not available for the whole simulation period and hence evapotranspiration has to be estimated by the relative location on the earth. The only required input is hourly air temperature. Wind speed, vapour pressure and other regular parameters in evapotranspiration computation are not necessary which defines this method as an empirically lumped estimation. Nonetheless, its accuracy might be acceptable because it simplifies some complicated climatic processes and avoids bringing in random errors.

Figures 6.3 and 6.4 show the cumulative monthly evapotranspiration calculated by SLURP and WATFLOOD at D. River N. Belcher from 1978 to 2004. It is obvious that summertime evapotranspiration estimated by the Hargreaves Equation is dramatically higher than the one computed by the Morton CRAE method. For example, the cumulative evapotranspiration of July in 1982 is computed as 105 and 48 mm by WATFLOOD and SLURP, respectively. Take August, 1995 as another example, the values of cumulative evapotranspiration are 128 and 51 mm for WATFLOOD and SLURP, respectively. This implies that the summertime discharge may be underestimated by WATFLOOD because it removes too much water from the system through the process of evapotranspiration (e.g.

Figures 5.11, 5.21, 5.24 and 5.30). On the other hand, it also implies that the summertime discharge may be overestimated by SLURP (e.g. Figures 4.22, 4.26, 4.28, 4.31 and 4.32). This conclusion can also be validated by the modelling results of the Chesnaye Sub-basin. Figure 6.5b displays the evapotranspiration estimated by WATFLOOD and SLURP at Station 5 in 2006. Compared with the simulated and observed hydrographs shown in Figure 6.5a, it indicates that the evapotranspiration is overestimated and underestimated by WATFLOOD and SLURP, respectively, resulting in underestimated and overestimated summertime discharge, respectively. Same evidences can also be viewed from Figure 6.6. More interestingly, Figures 6.5b and 6.6b show that evapotranspiration estimated by the FAO-56 Penman-Monteith Equation (Section 3.3.2) agrees with the results from SLURP because Morton CRAE model is also a modification from Penman Equation. These two methods seem to be more reliable than Hargreaves Equation where radiation is not considered.

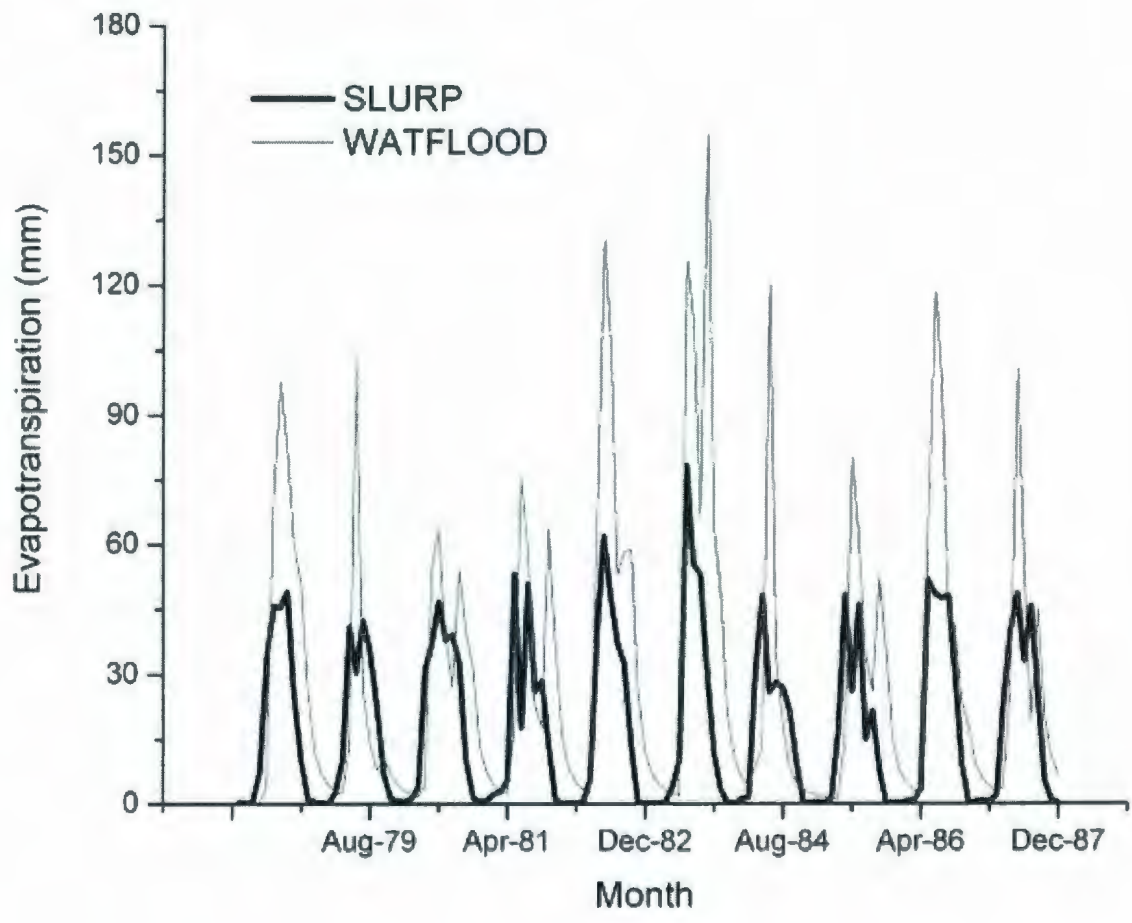


Figure 6.3 Monthly evapotranspiration at D. River N. Belcher from 1978 to 1987

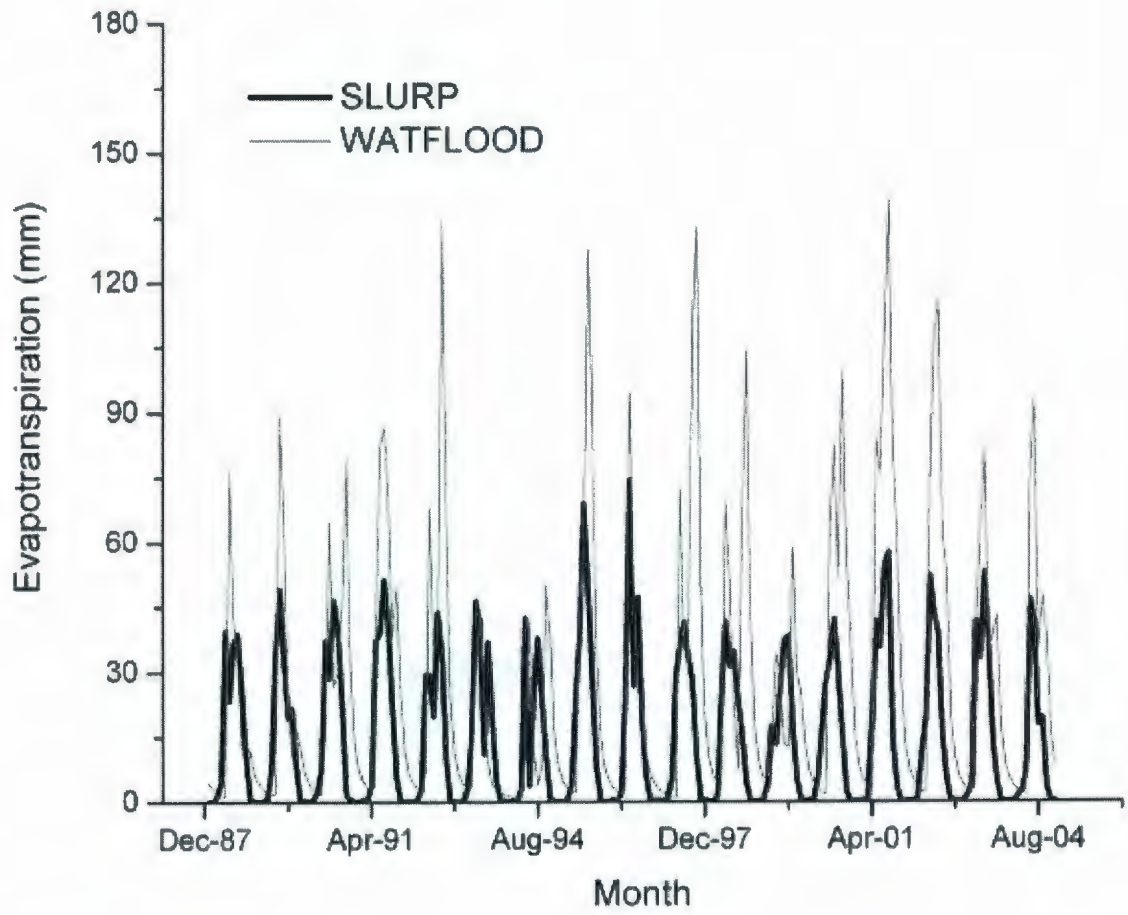


Figure 6.4 Monthly evapotranspiration at D. River N. Belcher from 1988 to 2004

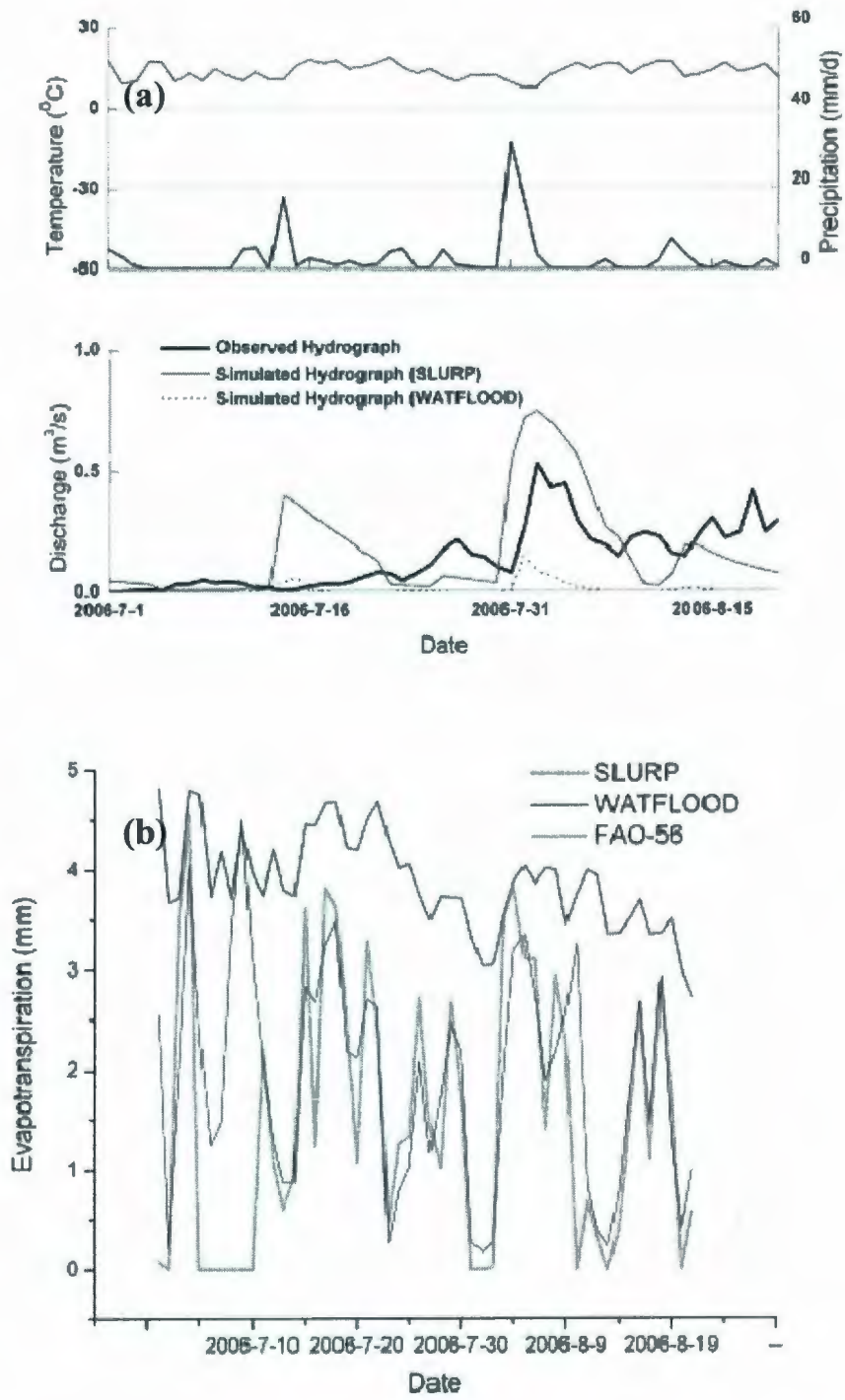


Figure 6.5 (a) Simulated and observed daily hydrographs (b) daily evapotranspiration for Station 5 in 2006

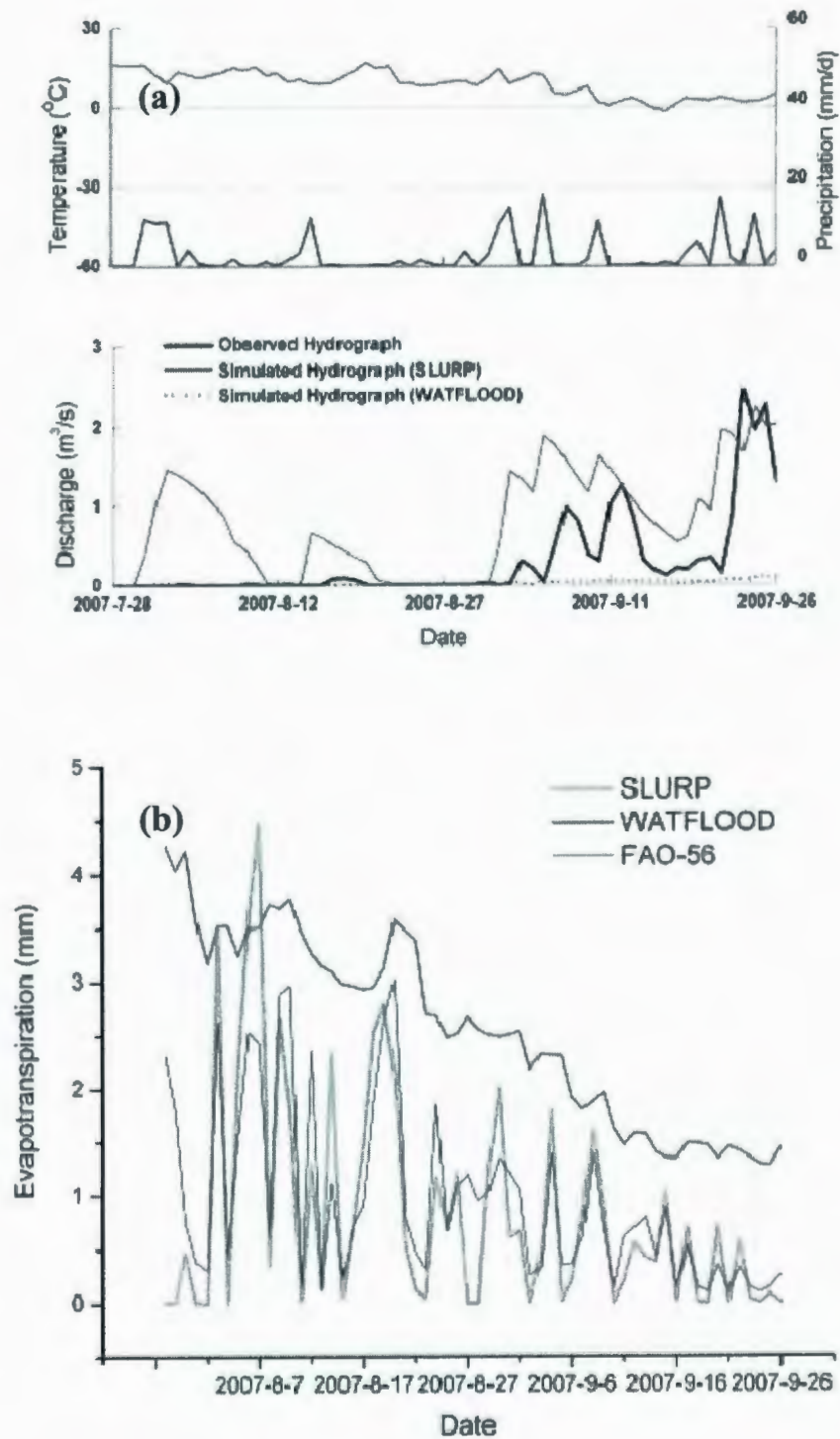


Figure 6.6 (a) Simulated and observed daily hydrographs (b) daily evapotranspiration for Station 7 in 2007

6.4 Difference in Modelling Results

SLURP and WATFLOOD have been calibrated and validated for the Deer River Watershed from 1978 to 2004. Moreover, both of them have been further applied on a small subcatchment - the Chesnaye Sub-basin in the summertime from 2006 to 2008 to testify their applicability at different scales. SLURP has better and more stable modelling performance than WATFLOOD in most of the modelling years (Figure 6.7 and Appendix B). The gap between the performances of these two models may be attributed to the following findings:

6.4.1 Spring Snowmelt and Runoff

Results from both the calibration and verification indicate that the snowmelt process in the spring (May - June) produces the highest peak discharge and the majority of the streamflow during the modelling period (1978 - 2004). Both of the simulated and observed spring flows in the years of 1979, 1980, 1982 and 1996 are good examples for this conclusion. This finding reveals that, in the subarctic wetland, snow accumulation is a major source of surface water; meanwhile the contribution from summer rainfall is relatively small. Moreover, the existence of the shallow permafrost table could restrict the infiltration of water which helps divert the snowmelt to form spring peak.

Peaks of the simulated spring flows, as shown in most hydrographs, are to some extent lower than the observed ones. This could be attributed to the combined effects of using meteorological data from the town of Churchill, snow sublimation, small ponds and

permafrost table. Meteorological data from the town of Churchill was used, which could influence the snowmelt processes and compromise the modelling accuracy. A large number of small ponds are stretching over the Deer River Watershed because of the sub-arctic wetland characteristics discussed in Chapter 2. These connected or disconnected ponds have a great potential of water storage which can form less streamflow during the snowmelt. On the other hand, the shallow permafrost table which delays the water penetrating to deep soil layers also plays significant role in amplifying the actual spring runoff. Therefore, the spring flows simulated by SLURP which does not consider these effects are lower than the observed ones. The simulation results also imply that there are some minor snowmelt events before the snow actually starts to melt. This can be explained by the built-in snowmelt algorithm and the optimized rain/snow division temperatures. The default degree-day snowmelt calculation in SLURP allows the snow to be depleted when the temperature exceeds the rain/snow division temperature. The division temperatures of all the six types of land cover were automatically optimized by SLURP to be lower than 0 °C, which means snowmelt is possible even the temperature is still not high enough for the actual melting. Some improvements such as modifications to the snowmelt algorithm or adding the consideration of the frost table are expected to promote the modelling efficiency of SLURP.

The simulated spring peak is always later than the actual peak for WATFLOOD. This delay is about 10 to 20 days in most of the years and it is inherently due to the ripening snowmelt algorithm that WATFLOOD uses. Base temperatures which control the melting process for each land cover were set to be identical with the values used in SLURP. These

values are appropriate for SLURP because it uses a parabolic interpolation to determine the melt rates which varies with time (Equation 4-5). However, these temperatures may cause impacts to the simulation of WATFLOOD because its snowmelt rate is a constant and not high enough to let the simulated peak match with the observed peak. In other words, the snowmelt process is somewhat slow, leading to the results that snow pack is depleted slowly and the peak flow is postponed.

6.4.2 Summer Rainfall Events

Both the modelling and observation results show that most of the small and moderate rainfall events during the summertime (July – August) do not generate significant runoff. This phenomenon is usually due to various reasons including canopy interception, depression storage, soil layer porosity, permafrost table descending and evapotranspiration. The dominant vegetation species in the Deer River Watershed are tundra, shrub and coniferous forest which have considerable interception capacity. Depression storage is referred to the numerous ponds in the wetland, which are able to receive and store a great amount of rainfall. The levels of these ponds fluctuate with the climatic conditions and behave to compensate the wetland water budget during dry season periods. The Deer River Watershed has a high soil porosity leading to a considerable water storage capacity. This attribute allows the water to infiltrate and stay in the deeper soil layer, and finally be released by the processes of evapotranspiration or drainage along the frost table. Descending frost table in the summertime releases more porous soil and intensifies the water storage capacity. Evapotranspiration is the most important natural process during the summer months because of the relatively high temperature and long

daylight period with high net radiation evaporates the water content from the wetland. This reduces antecedent moisture conditions so that runoff does not respond to regular rainfall. Only large rainfall events or continuous moderate rainfall events tend to generate runoff because the infiltration capability of the surface soil layer is saturated and excessive water could be routed into the channel system as streamflow.

6.4.3 Fall Rainfall Events

Rainfall events that occur in the fall months (September – October) generate much more runoff than during the summertime because the temperature is much lower and the net radiation is decreased which limits the evapotranspiration. However, this conclusion depends on whether rainfall happens frequently in the summer. A good example is the hydrograph of the year of 1984 (Figure 4.12). There is a large amount of precipitation (about 50 mm) in the late August. However, no obvious runoff is generated because rainfall rarely happens during that summer and the wetland storage is low. Another example can be found in the year of 1995 (Figure 5.28). A number of rainfall events occur during the summer and much of the runoff is consequently observed during August and September.

6.4.4 Rainfall-Runoff Relationship

The modelling results of SLURP indicate a time lag of 2 – 8 days between peaks of rainfall and runoff during the summer and fall months. As shown in Figure 6.8, a short-duration (30 hours) and high-intensity rainfall (59 mm in total) occurs during October 12th to 13th, 1997. Both the simulated and observed flow peaks show up on the

following day, indicating an approximately 2-day lag. Another series of high-intensity and moderate rainfalls (2 – 49 mm) occurs between September 12th and 20th, 1997. However, the peak flow is observed after a delay of 8 days. This delay may be due to the soil properties, land slope, infiltration process and the buffering capacity of wetland water storage. The same trend can also be found in the modelling results of WATFLOOD. As shown in Figure 6.9, a short-duration and high-intensity rainfall (60 mm) happens on September 3rd, 1983 and the flow peak appears on September 6th, 1983, with a delay of 3 days. Another series of moderate rainfalls (3 – 18 mm) can be observed between September 18th and 20th, 1983 with the peak flow showing up after 5 days interval.

A high-intensity rainfall event brings plenty water to the wetland surface which can easily exceed the infiltration capacity. After the fast storage tank is saturated, excessive water generates flashy runoff which contributes to the streamflow. Meanwhile, percolation allows water to occupy and fill the slow storage where the excessive water could gradually form the streamflow. This is the reason why a high-intensity rainfall has a steeper discharge response. If rainfall events are concentrated but more moderate, infiltration dominates re-distribution and gradually generates interflow and base flow. As a result, the discharge response is prolonged and gentler.

Moreover, ponds stretching over the watershed behave as buffers for precipitation and prolong the concentration time. This is one of the reasons why the simulated flow peaks are usually earlier than the observed ones. Neither SLURP nor WATFLOOD take such effect into consideration.

6.4.5 Uncertainty Analysis

Besides the reasons discussed above, there are reasons from other possible sources of uncertainty which could be summarized as follows.

6.4.5.1 Resolution of the modelling inputs

The horizontal resolution of the original DEM is $90\text{ m} \times 90\text{ m}$. Elevation of the whole watershed lies between 16 and 232 m. The majority of the watershed is plain wetlands which means the elevation vary slightly (Figures 3.1 and 3.6). Therefore, some depressions or convex surfaces could be ignored when applying TOPAZ, leading to errors determining flow directions and concentration areas. Resolution of the original NDVI data obtained from the SPOT vegetation program is $1\text{ km} \times 1\text{ km}$. To match the resolution of DEM, each NDVI value was uniformly distributed to 121 DEM grids ($90\text{ m} \times 90\text{ m}$). However, this conversion has 10 m error in the distribution and it sacrifices the accuracy of the land cover classification (Section 4.3). Moreover, there are a great number of small ponds which are not represented in the SPOT datasets because of the relatively low resolution. This could also contribute to some uncertainty to the modelling results.

6.4.5.2 Quality of the modelling inputs

Quality of the meteorological data and the streamflow data also influence the modelling accuracy. For example, the streamflow in some years (e.g. 2001, 2002, and 2003) are unreasonably low throughout the summer and fall months with plenty of precipitation. Some possible reasons can be summarized as streamflow data measurement, a natural

shifting of the channels or the change of meteorological data collection. This may help explain the significantly low modelling efficiencies (NSE) in these years. Another factor that could influence the modelling accuracy could be the source of meteorological data. All the meteorological data used in modelling the Deer River Watershed (1978-2004) was obtained from the weather station at the town of Churchill, which is about 80 km north to the Deer River Watershed. There should be more or less difference between the actual climatic conditions and the ones in Churchill, which could result in non-negligible inaccuracy of the modelling results.

6.4.5.3 Calibration of the modelling parameters

Calibration was implemented both manually and automatically through the optimization module of SLURP. However, some parameters may be assigned values varying from their actual ones. This problem could be mitigated if these parameters were obtained from the field measurement. For example, the snowmelt rates for different type of land cover were assigned fixed values from the reference of Metcalfe and Buttle (2001). However, these values may not be accurate for the Deer River Watershed and some differences between the simulated and observed spring peaks can be attributed to this.

On the other hand, Calibration was implemented both manually and automatically through the optimization runs of WATFLOOD. However, some parameters may be different from the actual values in the natural environment. Moreover, snowmelt base temperature, all-wave albedos of each land class as well as temperature lapse rate were set to be identical with values used in SLURP. This could also bring some errors to the

final modelling results.

6.4.5.4 Effects of permafrost table and ponds

The existence of permafrost table and ponds has considerable influence on water percolation and runoff generation. However, they are not considered in the computation of SLURP or WATFLOOD, which affects the modelling accuracy, such as the calculation of spring peaks and runoffs from rainfall events.

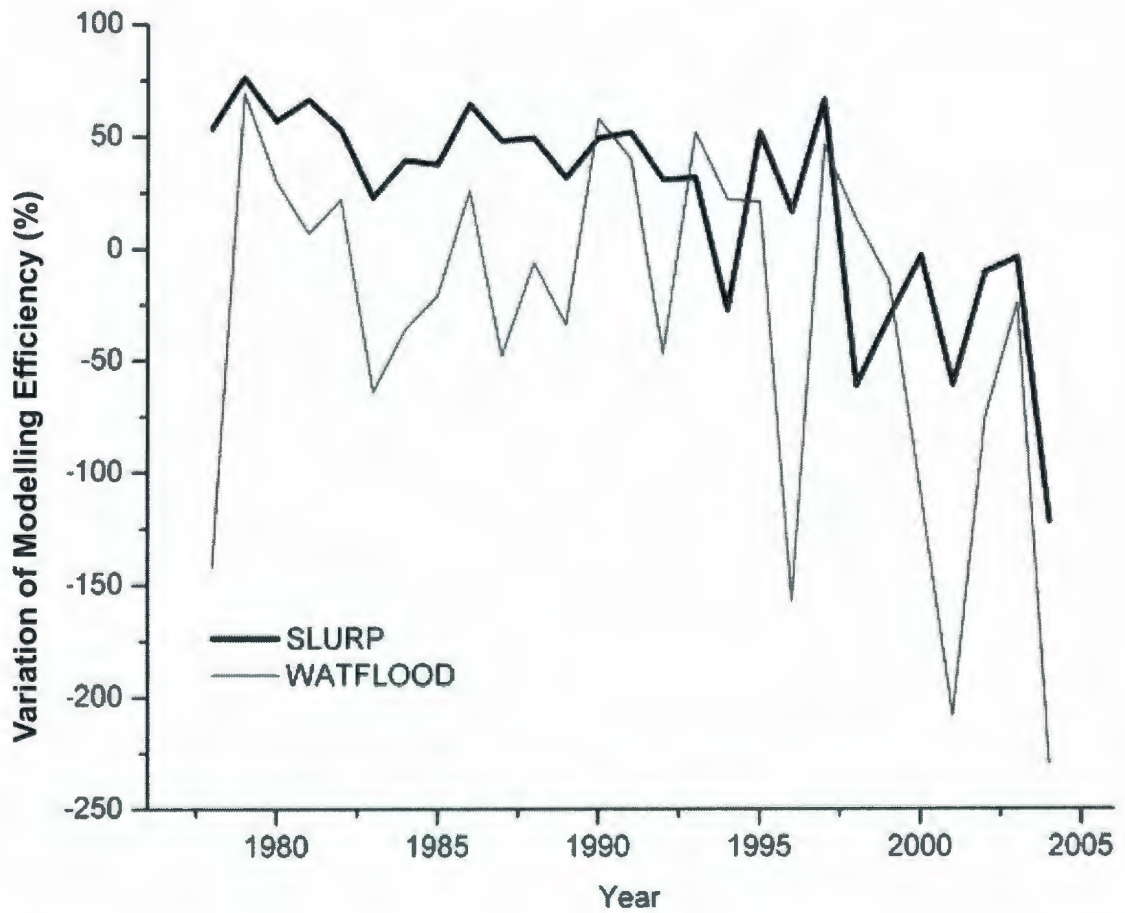


Figure 6.7 Variation of Modelling efficiencies for SLURP and WATFLOOD in the Deer River Watershed from 1978 to 2004

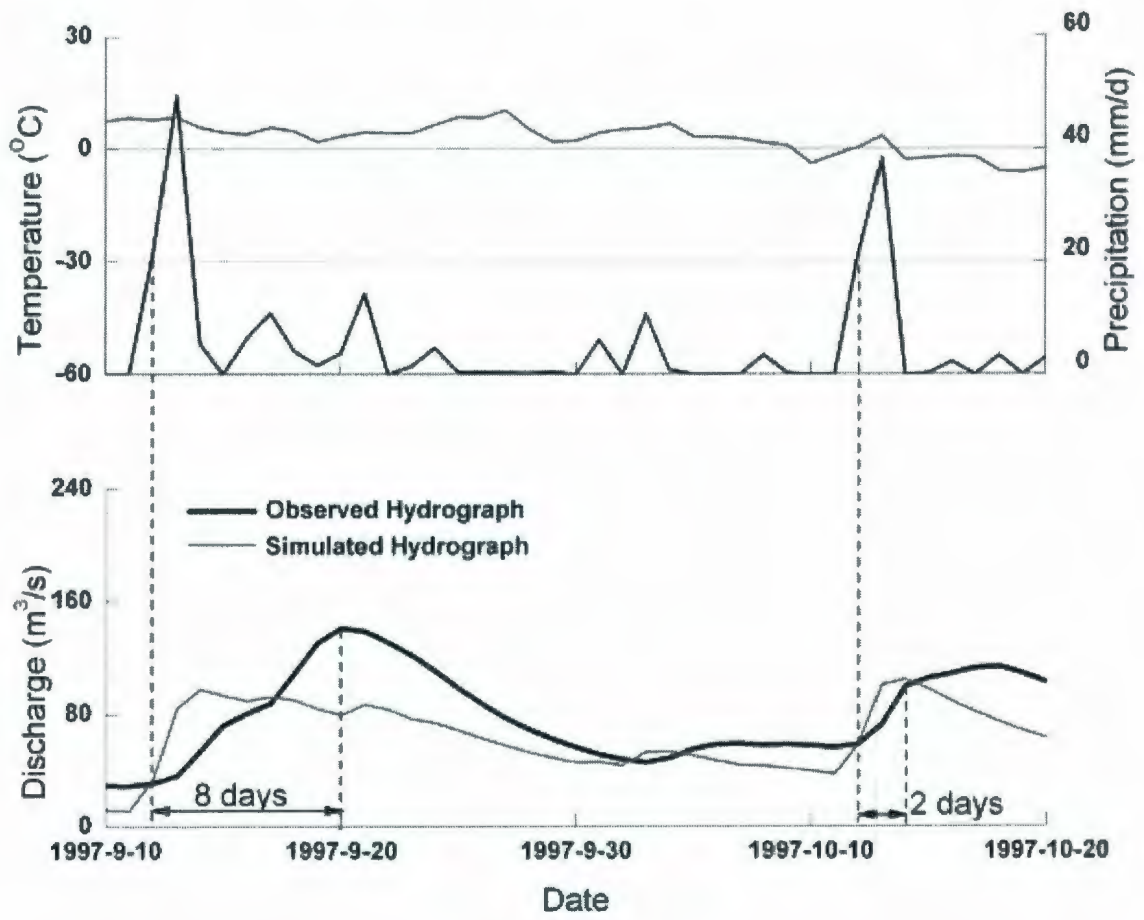


Figure 6.8 Response of daily discharge to the precipitation by SLURP in 1997

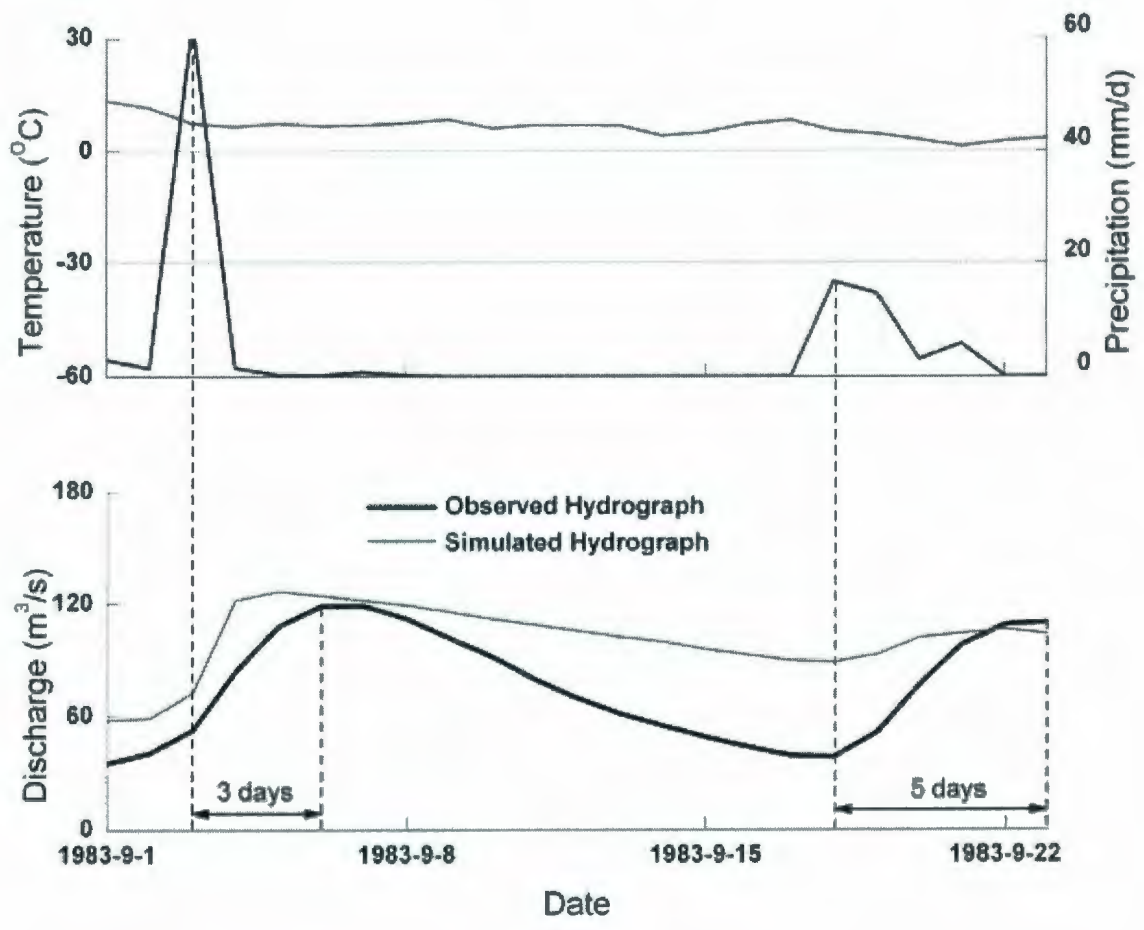


Figure 6.9 Response of daily discharge to the precipitation by WATFLOOD in 1983

6.5 Summary

SLURP and WATFLOOD was compared from the modelling structure, simulation methodologies, and modelling results in this chapter. SLURP employs an ASA concept with prominent advantages such as adjustable ASA size, heterogeneous land covers and efficient recalculations. Inaccuracies in watershed delineation and meteorological data distribution also reveal some of its shortcomings. The GRU concept embedded in WATFLOOD is capable of using fully distributed radar data and meteorological data from models. This reduces the effort of calculations without compromising any necessary process.

Modelling results indicate that interception and surface storage takes much more water in WATFLOOD because it considers the interception evapotranspiration. Snowmelt process and spring peak simulated by SLURP are earlier than that estimated by WATFLOOD in most of the calibration and verification years due to the fact that SLURP employs an exponentially increasing snowmelt rate with date. Not using meteorological data in the basin and not considering the existence of frost table and ponds in the Deer River Watershed appears to be the main reason for underestimating the spring peak in most years by both SLURP and WATFLOOD. Canopy interception, depression storage, soil layer porosity, descending permafrost table and evapotranspiration play key roles in determining the discharge responses to the rainfall events during the summertime and fall. Evapotranspiration estimated by the Morton CRAE method and the Hargreaves Equation implies that SLURP and WATFLOOD may underestimate and overestimate the

evapotranspiration, respectively, especially in the summertime. Other uncertainties, such as resolution and quality of the modelling inputs and calibration of the modelling parameters may also influence the modelling results.

Chapter 7 Conclusions and Recommendations

7.1 Summary

This research presents an integrated study of the hydrology of subarctic wetlands through field investigation and hydrological modelling. An extensive field investigation focusing on the hydrological features of the Deer River watershed near Churchill, Manitoba was conducted during May to September from 2006 to 2008. A monitoring network was established to collect hydrological and meteorological data for the in-depth understanding of the sub-arctic wetland attributes and modelling the hydrological processes in the watershed.

The 31-year data (1978 to 2008) presents steady elevations of both mean temperature and accumulative precipitation in the summertime (June 20th – October 3rd). Moreover, the 3-year observation at Rail Spur agrees with this increase of the summertime air temperature in both 2007 and 2008, which has higher maximum and lower minimum values as well as decrease in average as compared with those of 2006. Frost tables at stream banks show a reverse proportional relationship to their distances to the streams which reveals strong influence from the stream flow and subsurface flow. The subsurface flow which lies within organic layer moves ahead to the stream which could accelerate the thaw of frozen soil along its pathway. Lower albedo vegetations and greater insulation under deeper snow cover at near stream locations may also be considered as possible explanations. The frost table continuously descends through the summer time in the

monitoring years (2006-2008), indicating that air temperature is the primary factor. In addition, the frost table at the monitored transects are significantly shallower in 2007 than those in 2006 which may implicate the weather has become warmer. At these transects, the soil layers are more saturated as one gets closer to the stream channels. The data obtained from the automated weather station also indicates that, following the major recharge period of the snowmelt, soil moisture contents keep declining over time throughout the summer in the monitoring years. This is especially true for the shallow layers in the sub-arctic wetland. Throughout the monitoring season, the water discharge generally shows a descending trend before September due to insufficient precipitation and excessive evapotranspiration as well as expansion of the storage capacity of organic soil layers. A lag time of around 1-2 days between peaks of water discharge and rainfall events can be observed. Generally, the field investigation indicates that the monitored streams show a delayed response to precipitation due to the combined effects of shallow impermeable frost table, porous soil, and varied storage capacity of organic layer.

SLURP and WATFLOOD, two semi-distributed and physically based hydrological models were applied to simulate the hydrological processes of the Deer River Watershed during the period from 1978 to 2004. The results of the simulations done in this study indicate that the snowmelt process in the spring season usually produces the highest peak flow and the majority of the streamflow within a year. The finding reveals that the existence of the shallow permafrost table could alleviate the infiltration of water which enables the snowmelt to form spring peak flow. It is also shown that most of the small or moderate rainfall events during the summertime do not generate obvious runoff due to

canopy interception, depression storage, soil layer porosity, permafrost table descending, and evapotranspiration. Contrastingly, rainfall events that occur in the fall months result in much more runoff than that in the summertime because the evapotranspiration is hindered by the decreasing temperature and net radiation. Overall, the modelling results of SLURP indicate a time lag of 2 – 8 days between peaks of rainfall and runoff during the summer and fall months, indicating a considerable water storage capacity of the organic soil layer. To further test the applicability of these two models in a small scale subarctic wetland, simulation was conducted for a sub-watershed in the downstream of the Deer River in the summertime from 2006 to 2008. Results show that SLURP and WATFLOOD overestimates and underestimates the summertime runoff, respectively, which can be attributed to the difference in evapotranspiration computations.

SLURP and WATFLOOD has been compared from the perspectives of modelling structure, simulation methodologies, and modelling results. The concepts of ASA and GRU both have advantages and shortcomings. Snowmelt process and spring peak simulated by SLURP are earlier than that estimated by WATFLOOD in most of the simulation years due to the fact that SLURP employs an exponentially increasing snowmelt rate with date. Not considering the existence of frost table and ponds in the Deer River Watershed appears to be the main reason for underestimating the spring peak in most years by both SLURP and WATFLOOD. Moreover, in this study, WATFLOOD calculates the evapotranspiration using a rough estimation due to the lack of hourly radiation data. The results indicate Morton CRAE method and the Hargreaves Equation, which are employed by SLURP and WATFLOOD underestimates and overestimates the

evapotranspiration, respectively, especially in the summertime. Overall SLURP has better and more stable modelling efficiency than WATFLOOD in most of the simulation years in both the Deer River Watershed and the Chesnaye Sub-basin. Reasons could be summarized as the differences in snowmelt and evapotranspiration computation, uncertainties caused by arbitrarily converting daily data to hourly ones, model complexities and time constraints to treat WATFLOOD as even as SLURP.

7.2 Significance of Research

The contributions of this research can be summarized into two aspects: the field investigation of a typical subarctic wetland in the Hudson Bay Lowlands and the application of two semi-distributed models, SLURP and WATFLOOD, to the Deer River Watershed to gain the in-depth understanding of the hydrological features of the subarctic wetland system. The detailed contributions include:

- 1) Advancement of the knowledge about the climatic, geographical and hydrological characteristics of the subarctic wetlands through 3-year field monitoring and survey;
- 2) Delineation of the target watershed using River Tools[®] and TOPAZ and preparation of the inputs and datasets for running the two models;
- 3) Validation and application of SLURP and WATFLOOD in the Deer River Watershed to model the hydrological processes in the watershed;
- 4) Comparison of SLURP and WATFLOOD from modelling structures, simulation methodologies and modelling results. Assessment of the variation of modelling

parameters and justification of the applicability of the two models on subarctic wetlands; and

- 5) Decision support of wetland management and climate change impacts over the subarctic region.

7.3 Recommendations for Future Work

The culmination of this research has defined several initiatives that are central to the success of hydrological simulation in the subarctic wetlands. It was shown that despite the advancement of research of subarctic wetlands, there is still considerable work to be done to reveal in-depth understanding of the hydrological processes. There are some recommendations for future work.

The field work should be continuously conducted in the subarctic wetland to gain more information about the hydrological features. Frost table and water table should be more frequently monitored with longer probe at multiple transects. Soil moisture needs to be continuously monitored at multiple depths (e.g. 5cm, 25cm, and 50cm) along the stream banks. Hydraulic conductivity needs to be measured at each station once a month. More stations are recommended to be set up, especially in the midstream and upstream regions.

The snowmelt process of SLURP is based on a dynamic melting rate which mainly depends on the snowmelt rate in July and the Julian day's number. Further research is needed to modify the calculation by recalibrating the coefficients and variables.

WATFLOOD is also considered to be further justified about its snowmelt rate. Hourly net radiation data and detailed wetland parameters should be obtained for the future modelling work. Most of the parameters applied in SLURP and WATFLOOD are estimated and optimized through modelling calibration based on 10-year historical data. There could be some uncertainties because of the deviation from the actual conditions. Further uncertainties of the modelling work could be summarized as resolution and quality of the original data, conversion process of the original data, calibration of the parameters and the existence of permafrost and ponds.

The subarctic wetlands in the Hudson Bay Lowlands are threatened by pollutants carried by rivers or channels originated from Saskatoon or Alberta and flowing through agricultural lands. There is a need to embed a pollutant transport module into SLURP and WATFLOOD which can benefit the investigation of non-point source pollution and its impact on the vulnerable wetland system. Moreover, field survey focusing on the water quality needs to be done to support the modelling work.

References

- Abbott, M.B., Bathurst, J.C., Cunge, J.A., O'Connell, P.E., and Rasmussen, J. 1986. An Introduction to the European System: Systeme Hydrologique Europeen (SHE). *Journal of Hydrology*, 87: 61-77.
- Anderson, E.A. 1973. National Weather Service River Forecast System-Snow Accumulation and Ablation Model. National Oceanographic and Atmospheric Administration, Silver Springs, Md., Tech. Memo NWS_HYDRO-17.
- Allen, R.G., Pereira, L.S., D. Raes, D., and Smith, M. 1998. Crop evapotranspiration, guidelines for computing crop water requirements. FAO Irrig. and Drain. Paper 56, Food and Agric. Orgn. of the United Nations, Rome, Italy. 300 pp.
- Anderson, E.A. 1973. National Weather Service River Forecast System-Snow Accumulation and Ablation Model. National Oceanographic and Atmospheric Administration, Silver Springs, Md., Tech. Memo NWS_HYDRO-17.
- Arctic Council and the International Arctic Science Committee. 2004. Impacts of a Warming Arctic: Arctic Climate Impact Assessment. Cambridge University Press, Cambridge, UK.
- Armstrong, R.N., and Martz, L.W. 2008. Effects of reduced land cover detail on hydrological model response. *Hydrological Processes*, 22: 2395-2409.
- Arnfeld, A.J. 1975. A note on the diurnal, latitudinal and seasonal variation of the surface reflection coefficient. *Journal of Applied Meteorology*, 14: 1603-1608.
- Bastiaanssen, W.G.M. 1995. Regionalization of surface flux densities and moisture indicators in composite terrain: A remote sensing approach under clear skies in

- Mediterranean climates. Ph.D. dissertation, Landbouwwuniversiteit te Wageningen, Wageningen, The Netherlands.
- Bear, J. 1979. *Hydraulics of Groundwater*. McGraw-Hill, New York, N.Y.
- Bello, R., and Smith, J.D. 1990. The Effect of Weather Variability on the Energy Balance of a Lake in the Hudson Bay Lowlands, Canada. *Arctic and Alpine Research*, 22(1): 98-107.
- Bergström, S. 1992. The HBV model - its structure and applications. SMHI Reports RH, No. 4, Norrköping.
- Beven, K.J., Kirkby, M.J., Schofield, N., and Tagg, A.F. 1984. Testing a physically-based flood forecasting model (TOPMODEL) for three U.K. Catchments. *Journal of Hydrology*, 69: 119-143.
- Bicknell, B.R., Imhoff, J.C., Kittle, J.L., Donigian, A.S., and Johanson, R.C. 1997. *Hydrological Simulation Program--Fortran, User's manual for version 11*: U.S. Environmental Protection Agency, National Exposure Research Laboratory, Athens, Ga., EPA/600/R-97/080, 755 p.
- Bidlake, W.R. 2000. Evapotranspiration from a bulrush-dominated wetland in the Klamath Basin, Oregon. *Journal of the American Water Research Association*, 36: 1309-1320.
- Boken, V.K., Cracknell, A.P., and Heathcote, R.L. 2005. *Monitoring and predicting agricultural drought: a global study*. Oxford University Press, U.S.
- Boswell, J.S., and Olyphant, G.A. 2007. Modeling the hydrologic response of groundwater dominated wetlands to transient boundary conditions: Implications for wetland restoration. *Journal of Hydrology*, 332: 467-476.

- Brooks, F.A. 1960. *An Introduction to Physical Microclimatology*. University of California Press, Davis, Calif.
- Brown, L., Thorne, R., and Woo, M.K. 2008. Using satellite imagery to validate snow distribution simulated by a hydrological model in large northern basins. *Hydrological Processes*, 22: 2777-2787.
- Brubaker, K., Rango, A., and Kustas, W. 1996. Incorporating radiation inputs into the Snowmelt Runoff Model. *Hydrol. Proc.*, 464.
- Canadian Hydraulics Centre and Water Survey Canada. 2007. *Ensim Hydrologic Reference Manual*. Ottawa, Ontario, Canada.
- Carey, S.K., and Woo, M.K. 1998. Snowmelt hydrology of two subarctic slopes, southern Yukon, Canada. *Nordic Hydrol*, 29: 331-346.
- Carey, S.K., and Woo, M.K. 1999. Hydrology of two slopes in subarctic Yukon, Canada. *Hydrological Processes*, 13: 2549-2562.
- Carey, S.K., and Woo, M.K. 2000. The role of soil pipes as a slope runoff mechanism, Subarctic Yukon, Canada. *Journal of Hydrology*, 233: 206-222.
- Carey, S.K., and Woo, M.K. 2001. Spatial variability of hillslope water balance, wolf creek basin, subarctic Yukon. *Hydrological Processes*, 15: 3113-3132.
- Carey, S.K., Quinton, W.L., and Goeller, N.T. 2007. Field and laboratory estimates of pore size properties and hydraulic characteristics for subarctic organic soils. *Hydrological Processes*, 21: 2560-2571.
- Cary, L.E. 1984. Application of the U.S. Geological Survey's Precipitation-Runoff Modeling System to the Prairie Dog Creek basin, Southeastern Montana: U.S. Geological Survey Water-Resources Investigations Report 84-4178, 98 p.

- Cheng, C.T., Ou, C.P., and Chau, K.W. 2002. Combining a fuzzy optimal model with a genetic algorithm to solve multi-objective rainfall-runoff model calibration. *Journal of Hydrology*, 268: 72-86.
- Chiew, F., and McMahon, T. 1994. Application of the daily rainfall-runoff model MODHYDROLOG to 28 Australian catchments. *Journal of Hydrology*, 153: 383-416.
- Cho, J., Park, S., and Im, S. 2008. Evaluation of Agricultural Nonpoint Source (AGNPS) model for small watersheds in Korea applying irregular cell delineation. *Agricultural Water Management*, 95: 400-408.
- Corell, R.W. 2006. Challenges of Climate Change: An Arctic Perspective. *A Journal of the Human Environment*, 35(4): 148-152.
- Crawford, N.H., and Linsley, R.K. 1966. Digital Simulation in Hydrology: Stanford Watershed Model IV. Technical Report No. 39, Department of Civil Engineering, Stanford University, p. 210.
- Cunge, J.A. 1967. On the subject of a flood propagation method. *Journal of Hydraulic Research IAHR*, 7(2): 205-230.
- De Bruin, H.A.R., and Keijman, J.Q. 1979. The Priestley-Taylor evaporation model applied to a large, shallow lake in the Netherlands. *Journal of Applied Meteorology*, 18: 898-903.
- Dibike, Y.B., and Coulibaly, P. 2007. Validation of hydrological models for climate scenario simulation: the case of Saguenay watershed in Quebec. *Hydrological Processes*, 21: 3123-3135.
- Donald, J.R. 1992. Snowcover depletion curves and satellite snowcover estimates for snowmelt runoff modelling. Ph.D. Thesis, University of Waterloo, ON, Canada, 232.

- Dredge, L.A., and Nixon, M. 1979. Thermal sensitivity and development of tundra ponds and thermokarst lakes in the Manitoba portion of the Hudson Bay Lowlands. Geological Survey of Canada, Paper, 79-1C: 23-26.
- Drexler, J.Z., Snyder, R.L., Spano, D., and Paw U, K.T. 2004. A review of models and micrometeorological methods used to estimate wetland evapotranspiration. *Hydrological Processes*, 18: 2071-2101.
- Duffie, J.A., and Beckman, W.A. 1980. *Solar Engineering of Thermal Processes*. Wiley, N.Y., pp. 1-109.
- Duru, J.O., and Hjelmfelt, A.T. 1994. Investigating prediction capability of HEC-1 and KINEROS kinematic wave runoff models. *Journal of Hydrology*, 157: 87-103.
- Eaton, A.K., and Rouse, W.R. 2001. Controls on evapotranspiration at a subarctic sedge fen. *Hydrological Processes*, 15: 3423-3431.
- Fassnacht, S.R., Soulis, E.D., and Kouwen, N. 1999. Algorithm application to improve weather radar snowfall estimates for winter hydrologic modelling. *Hydrological Processes*, 13: 3017-3039.
- Galvão, P., Braunschweig, F., Trancoso, R., Neves, R., and Cooper, D. 2005. Modularity in integrated catchment modeling covering different time-scales. *Geophysical Research Abstracts*, 7, 08325.
- Granger, R.J. 1995. A feedback approach for the estimation of evapotranspiration using remotely sensed data. In: *Applications of Remote Sensing in Hydrology, Proceedings of the Second International Workshop, 18-20 October, 1994*, by G.W. Kite, A. Pietroniro and T. Pultz (eds.), Symposium No. 14, NHRI, Saskatoon, Saskatchewan, 211-222.

- Guerschman, J.P., Paruelo, J.M., Di Bella, C., Giallorenzi, M.C., and Pacin, F. 2003. Land cover classification in the Argentine Pampas using multi-temporal Landsat TM data. *International Journal of Remote Sensing*, 24(17): 3381-3402.
- Haberlandt, U., and Kite, G.W. 1998. Estimation of daily space-time precipitation series for macroscale hydrological modelling. *Hydrological Processes*, 12: 1419-1432.
- Hargraeves, G.H., and Samani, Z.A. 1982. Estimating potential evapotranspiration. ASCE, *J. Irrigation and Drainage Division*, 108(3): 225-230.
- Hayashi, M., Goeller, N., Quinton, W.L., and Wright, N. 2007. A simple heat-conduction method for simulating the frost-table depth in hydrological models. *Hydrological Processes*, 21: 2610-2622.
- Jing, L., and Chen, B. 2007. Fieldwork Manual for the Hydrological Investigation in the Deer River Watershed. Memorial University of Newfoundland, St.John's, NL, Canada.
- Kite, G.W. 1975. Performance of two deterministic models. In: *Application of Mathematical Models in Hydrology and Water Resources Systems*. Proceedings of the Bratislava Symposium, September, IASH Publication, 115: 136-142.
- Kite, G.W. 1997. Manual for the SLURP Hydrological Model V.11. National Hydrology Research Institute, Saskatoon.
- Kite, G.W. 2002. Manual for the SLURP hydrological model, v12.2. International water management institute, Colombo, Sri Lanka.
- Kouwen, N., Soulis, E.D., Pietroniro, A., Donald, J., and Harrington, R.A. 1993. Grouped response units for distributed hydrologic modeling. *Journal of Water Resources Planning and Management*, 119: 289-305.

- Kouwen, N. 2008. Manual for WATFLOOD/ WATROUTE - Hydrological Model Routing & Flow Forecasting System. University of Waterloo, Waterloo.
- Kustas, W.P., Rango, A., and Uijlenhoet, R. 1994. A simple energy budget algorithm for the snowmelt runoff model. *Water Resources Research*, 30(5): 1515-1527.
- Leavesley, G. 1983. Precipitation runoff modelling system. Denver, Colorado, USA' USGS Publ User manual.
- Leenders, E.E., and Woo, M.K. 2002. Modelling a two-layer flow system at the subarctic, subalpine treeline during snowmelt. *Water Resources Research*, 38(10), 1202. DOI: 10.1029/2001WR000375.
- Linsley, R.K., Kohler, M.A., and Paulhus, J.L.H. 1949. *Applied Hydrology*. McGraw-Hill, New York, N.Y.
- Mansell, R.S., Bloom, S.A., and Sun, G. 2000. A Model for Wetland Hydrology: Description and Validation. *Soil Science*, 165(5): 384-397.
- Martinec, J. 1975. Snowmelt runoff model for streamflow forecasts. *Nordic Hydrology*, 6: 145-154.
- McKillop, R., Kouwen, N., and Soulis, E.D. 1999. Modeling the Rainfall-Runoff Response of a Headwater Wetland. *Water Resources Research*, Am. Geophysical Union, 35(4), 1165-1177.
- Metcalf, R.A., and Buttle, J.M. 2001. Soil partitioning and surface store controls on spring runoff from a boreal forest peatland basin in north-central Manitoba, Canada. *Hydrological Processes*, 15: 2305-2324.
- Michaud, J., and Sorooshian, S. 1994. Comparison of simple versus complex distributed runoff models on a midsized semiarid watershed. *Water Resources Research*, 30:

593-605.

- Miller, N.L., and Kim, J. 2001. Coupled precipitation-streamflow simulations at the GAME/HUBEX Site: Xixian Basin. *Journal of Meteorological Society*, 79: 985-998.
- Moreda, F., Koren, V., Zhang, Z., Reed, S., and Smith, M. 2006. Parameterization of distributed hydrological models: learning from the experiences of lumped modeling. *Journal of Hydrology*, 320: 218-237.
- Morton, F.I. 1978. Estimating evapotranspiration from potential evaporation: practicability of an iconoclastic approach. *Journal of Hydrology*, 38: 1-32.
- Morton, F.I. 1983. Operational estimates of areal evapotranspiration and their significance to the science and practice of hydrology. *Journal of Hydrology*, 66: 77-100.
- O'Callaghan, J.F., and Mark, D.M. 1984. The extraction of drainage networks from digital elevation data. *Computer vision, graphics and image processing*, 28: 323-344.
- Park, S.Y., Lee, K.W., Park, I.H., and Ha, S.R. 2008. Effect of the aggregation level of surface runoff fields and sewer network for a SWMM simulation. *Desalination*, 226: 328-337.
- Parmley, R.O. 2000. *Hydraulic field manual*, 2nd Edition. McGraw-Hill Professional, New York, N.Y.
- Paw U, K.T., and Gao, W. 1988. Applications of solutions to non-linear energy budget equations. *Agricultural and Forest Meteorology*, 43: 121-145.
- Payette, S., Fortin, M.J., and Gamache, I. 2001. The Subarctic Forest-Tundra: The Structure of a Biome in a Changing Climate. *Bioscience*, 51(9): 709-718.
- Petrone, R.M., Price, J.S., Waddington, J.M., and Waldow, H. 2004. Surface moisture and energy exchange from a restored peatland, Québec, Canada. *Journal of Hydrology*,

- 295: 198-210.
- Philip, J.R. 1954. An infiltration equation with physical significance. *Soil Science*, 77(1): 153-157.
- Pietroniro, A., Leconte, R., Toth, B., Peters, D.L., Kouwen, N., Conly, F.M., and Prowse, T. 2006. Modelling climate change impacts in the Peace and Athabasca catchment and delta: III-integrated model assessment. *Hydrological Processes*, 20: 4231-4245.
- Priestley, C.H.B., and Taylor, R.J. 1972. On the assessment of surface heat flux and evaporation using large scale parameters. *Monthly Weather Review*, 100(2): 81-92.
- Price, J.S., and Waddington, J.M. 2000. Advance in Canadian wetland hydrology and biochemistry. *Hydrological Processes*, 14: 1579-1589.
- Price, J.S., Branfireun, B.A., Waddington, J.M., and Devito, K.J. 2005. Advances in Canadian wetland hydrology, 1999-2003. *Hydrological Processes*, 19: 201-214.
- Quick, M.C., and Pipes, A. 1977. U.B.C. Watershed Model. *Hydrological Sciences - Bulletin*, XXII(1): 153-161.
- Quinton, W.L., and Marsh, P. 1998. The Influence of Mineral Earth Hummocks on Subsurface Drainage in the Continuous Permafrost Zone. *Permafrost and Periglacial Process*, 9: 213-228.
- Quinton, W.L., and Roulet, N.T. 1998. Spring and Summer Runoff Hydrology of a Subarctic Patterned Wetland. *Arctic and Alpine Research*, 30(3): 285-294.
- Reeve, A.S., Siegel, D.I., and Glaser, P.H. 2000. Simulating vertical flow in large peatlands. *Journal of Hydrology*, 227: 207-217.
- Refsgaard, J.C., and Knudsen, J. 1996. Operational validation and intercomparison of different types of hydrological models. *Water Resources Research*, 32: 2189-2202.

- Richard, C., and Gratton, D.J. 2001. The importance of the air temperature variable for the snowmelt runoff modelling using the SRM. *Hydrological Processes*, 15: 3357-3370.
- Robinson, N. 1966. *Solar Radiation*. Elsevier, Amsterdam.
- Rouse, W.R., Douglas, M.S.V., Hecky, R., Hershey, A.E., Kling, G.W., Lesack, L., Marsh, P., McDonald, M., Nicholson, B.J., Roulet, N.T., and Smol, J.P. 1997. Effects of climate change on the fresh waters of arctic and subarctic northern America. *Hydrological Processes*, 11: 873-902.
- Rouse, W.R. 1998. A water balance model for a subarctic sedge fen and its application to climatic change. *Climatic Change*, 38: 207-234.
- Rouse, W.R. 2000. Progress in hydrological research in the Mackenzie GEWEX study. *Hydrological Processes*, 14: 1667-1685.
- Rowe, L.K. 1983. Rainfall interception by an evergreen beech forest, Nelson, New Zealand. *Journal of Hydrology*, 66: 143-158.
- Samani, Z., Bawazir, A.S., Bleiweiss, M., Skaggs, R., and Tran, V.D. 2007. Estimating Daily Net Radiation over Vegetation Canopy through Remote Sensing and Climatic Data. *Journal of Irrigation and Drainage Engineering*, 133(4): 291-297.
- Shah, S.M.S., O'Connell, P.E., and Hosking, J.R.M. 1996a. Modelling the Effects of Spatial Variability in Rainfall on Catchment Response. 1. Formulation and Calibration of a Stochastic Rainfall Field Model. *Journal of Hydrology*, 175: 67-88.
- Shah, S.M.S., O'Connell, P.E., and Hosking, J.R.M. 1996b. Modelling the Effects of Spatial Variability in Rainfall on Catchment Response. 2. Experiments with Distributed and Lumped Models. *Journal of Hydrology*, 175: 89-111.

- Shaw, D.A., Martz, L.W., and Pietroniro, A. 2005. A methodology for preserving channel flow networks and connectivity patterns in large-scale distributed hydrological models. *Hydrological Processes*, 19: 149-168.
- Shin, H.J., and Kim, S.J. Assessment of climate change impact on snowmelt in the two mountainous watersheds using CCCma CGCM2. *KSCE Journal of Civil Engineering*, 11(6): 311-319.
- Souch, C., Wolfe, C.P., and Grimmond, C.S.B. 1996. Wetland evaporation and energy partitioning: Indiana Dunes National Lakeshore. *Journal of Hydrology*, 184: 189-208.
- Spittlehouse, D.L. 1989. Estimating evapotranspiration from land surfaces in British Columbia. In: *Estimation of Areal Evapotranspiration*, IAHS Publication No. 177, 245-253.
- SPOT IMAGE and VITO. 2008. NDVI image of the Deer River Watershed in July, 2007. Retrieved 06/23, 2008, from <http://www.vgt.vito.be>
- St Laurent, M.E., and Valeo, C. 2007. Large-scale distributed watershed modelling for reservoir operations in cold boreal regions. *Canadian Journal of Civil Engineering*, 34: 525-538.
- Stadnyk, T. 2008. Mesoscale Hydrological Model Validation and Verification using Stable Water Isotopes: The isoWATFLOOD. Ph.D. Thesis, Department of Civil Engineering, University of Waterloo: Waterloo, ON.
- Stewart, R.B., and Rouse, W.R. 1976. A simple method for determining the evaporation from shallow lakes and ponds. *Water Resources Research*, 12(4): 623-628.
- Ström, L., and Christensen, T.R. 2007. Below ground carbon turnover and greenhouse gas exchanges in a sub-arctic wetland. *Soil biology and biochemistry*, 39: 1689-1698.

- Su, M., Stolte, W.J., and Van der Kamp, G. 2000. Modelling Canadian prairie wetland hydrology using a semi-distributed streamflow model. *Hydrological Processes*, 14: 2405-2422.
- Tao, T., and Kouwen, N. 1989. Remote sensing and fully distributed modelling for flood forecasting. *ASCE Journal of Water Resources Planning and Management*, 115: 809-823.
- Thorne, R. 2004. Simulating streamflow of a large mountainous catchment using different sets of climatic data. M.Sc. thesis, McMaster University, Hamilton.
- Todini, E. 1996. The ARNO rainfall-runoff model. *Journal of Hydrology*, 175: 339-382.
- United States Army Corps of Engineers. 1987. Streamflow synthesis and reservoir regulation (SSARR) model user manual. North Pacific Division, Portland, OR, USA.
- USGS. 2007. USGS 3 arc second DEM of the Deer River Watershed. Retrieved 15/05, 2007, from <http://seamless.usgs.gov/index.php>
- Van der Linden, S., and Woo, M.K. 2003. Application of hydrological models with increasing complexity to subarctic catchments. *Journal of Hydrology*, 270: 145-157.
- Waddington, J.M., Griffis, T.J., and Rouse, W.R. 1998. Northern Canadian Wetlands: Net Ecosystem CO₂ Exchange and Climatic Change. *Climatic Change*, 40(2): 267-275.
- Wang, J., Rich, P.M., and Price, K.P. 2003. Temporal response of NDVI to precipitation and temperature in the central Great Plains, USA. *International Journal of Remote Sensing*, 24(11): 2345-2364.
- Wei, T.C., and McGuinness, J.L. 1973. Reciprocal distance squared method, a computer technique for estimating area precipitation. Technical Report ARS-Nc-8. US Agricultural Research Service, North Central Region, Ohio.

- Weick, E.J., and Rouse, W.R. 1991a. Advection in the costal Hudson Bay Lowlands, Canada. I. The Terrestrial Surface Energy Balance. *Arctic and Alpine Research*, 23(3): 328-337.
- Weick, E.J., and Rouse, W.R. 1991b. Advection in the costal Hudson Bay Lowlands, Canada. II. Impact of Atmospheric Divergence on the Surface Energy Balance. *Arctic and Alpine Research*, 23(3): 338-348.
- Wessel, D.A., and Rouse, W.R. 1994. Modelling Evaporation from Wetland Tundra. *Boundary Layer Meteorology*, 68: 109-130.
- Williams, J.R., Jones, C.A., Kiniry, J.R., and Spanel, D.A. 1989. The EPIC crop growth model. *Transactions of the ASAE*, 32: 497-511.
- Winter, T.C., and Woo, M.K. 1990. In: Wolman, M.G., Riggs, H.C. (Eds.), *Hydrology of lakes and wetlands Surface Water Hydrology*, vol. 0-1. Geological Society of America, 159-187.
- Winter, T.C. 1998. Relation of streams, lakes, and wetlands to groundwater flow systems. *Hydrogeology Journal*, 7: 28-45.
- Winter, T.C. 2000. The vulnerability of wetlands to climate change: a hydrological landscape perspective. *Journal of the American Water Resources Association*, 32(2): 305-311.
- Woo, M.K., and Young, K. 2003. Hydrogeomorphology of patchy wetlands in the high arctic, polar desert environment. *Wetlands*, 23(2): 291-309.
- Woo, M.K., and Marsh, P. 2005. Snow, frozen soils and permafrost hydrology in Canada, 1999-2002. *Hydrological Processes*, 19: 215-229.
- Woo, M.K., and Thorne, R. 2006. Snowmelt contribution to discharge from a large

- mountainous catchment in subarctic Canada. *Hydrologic Processes*, 20: 2129-2139.
- Woo, M.K., and Young, K. 2006. High Arctic wetlands: Their occurrence, hydrological characteristics and sustainability. *Journal of Hydrology*, 320: 432-450.
- Xu, C.-Y., Tunemar, L., Chen, Y, and Singh, V.P. 2006. Evaluation of seasonal and spatial variations of lumped water balance model sensitivity to precipitation data errors. *Journal of Hydrology*, 324: 80-93.
- Yin, Z., and Williams, T.H.L. 1997. Obtaining spatial and temporal vegetation data from Landsat MSS and AVHRR/NOAA satellite images for a hydrologic model. *Photogrammetric Engineering & Remote Sensing*, 63(1):69-77.
- Zhang, Z., Kane, D.L., and Hinzman, D. 2000. Development and application of a spatially-distributed Arctic hydrological and thermal process model (ARHYTHM). *Hydrological Processes*, 14: 1017-1044.

Appendix A

This Appendix presents the coordinate margins of each sub-basin of the Deer River Watershed. All the coordinates are from delineation using River Tools®.

Table A.1 Coordinate margins of each sub-basin of the Deer River Watershed

Sub-basin #	Xmin	Xmax	Ymin	Ymax
1	-94.39875	-94.227083	57.532917	57.674583
2	-94.209583	-94.137917	57.80375	57.85875
3	-94.270417	-94.149583	57.719583	57.792083
4	-94.207917	-94.084583	57.997083	58.17375
5	-94.172083	-94.052917	58.072083	58.24625
6	-94.192083	-94.12625	57.98625	58.027917
7	-94.20375	-94.127917	57.91875	58.009583
8	-94.232083	-94.17875	57.93625	57.994583
9	-94.227917	-94.160417	57.875417	57.932083
10	-94.23625	-94.189583	57.869583	57.912917
11	-94.305417	-94.23375	57.83875	57.872083
12	-94.28125	-94.244583	57.912083	57.960417
13	-94.230417	-94.167083	57.797917	57.820417
14	-94.32625	-94.244583	57.79125	57.82875
15	-94.244583	-94.172083	57.920417	57.974583
16	-94.272083	-94.244583	57.867083	57.900417
17	-94.315417	-94.227917	57.82125	57.854583
18	-94.21375	-94.172083	58.150417	58.202083
19	-94.32875	-94.194583	57.985417	58.10875
20	-94.312917	-94.242917	58.014583	58.10875
21	-94.277083	-94.22125	58.115417	58.222083
22	-94.21875	-94.174583	58.182917	58.272917
23	-94.41625	-94.237917	57.949583	58.315417
24	-94.355417	-94.279583	57.58875	57.644583
25	-94.362083	-94.25625	57.632083	57.677083
26	-94.28875	-94.250417	57.672917	57.720417
27	-94.455417	-94.394583	57.504583	57.559583
28	-94.435417	-94.394583	57.567083	57.584583
29	-94.447917	-94.404583	57.577083	57.592917
30	-94.535417	-94.48125	57.564583	57.579583

Sub-basin #	Xmin	Xmax	Ymin	Ymax
31	-94.582917	-94.472917	57.48375	57.515417
32	-94.57625	-94.43625	57.45875	57.51125
33	-94.530417	-94.477083	57.512083	57.53875
34	-94.56125	-94.514583	57.500417	57.537917
35	-94.59875	-94.545417	57.48625	57.54375
36	-94.71875	-94.585417	57.53875	57.574583
37	-94.719583	-94.62125	57.519583	57.55375
38	-94.700417	-94.617083	57.479583	57.53875
39	-94.62375	-94.594583	57.48625	57.530417
40	-94.607917	-94.58125	57.50625	57.542083
41	-94.630417	-94.34625	57.565417	57.657917
42	-94.747083	-94.359583	57.540417	57.662083
43	-94.469583	-94.29625	57.63125	57.749583
44	-94.48125	-94.294583	57.649583	57.762083
45	-94.360417	-94.30625	57.667083	57.71125
46	-94.50625	-94.339583	57.88375	57.96625
47	-94.450417	-94.327917	57.870417	57.952083
48	-94.322083	-94.247917	57.845417	57.96125
49	-94.212917	-94.142917	57.764583	57.80625
50	-94.36375	-94.299583	57.822917	57.904583
51	-94.342917	-94.31125	57.874583	57.929583
52	-94.425417	-94.349583	57.84875	57.912083
53	-94.655417	-94.397917	57.78625	57.89375
54	-94.495417	-94.41125	57.744583	57.822917
55	-94.61875	-94.43125	57.707917	57.824583
56	-94.60625	-94.44875	57.744583	57.830417
57	-94.549583	-94.46125	57.789583	57.837083
58	-94.555417	-94.492083	57.834583	57.85875
59	-94.64625	-94.550417	57.78125	57.81625
60	-94.75625	-94.58375	57.747917	57.79375
61	-94.700417	-94.59875	57.712083	57.762917
62	-94.822917	-94.69125	57.692083	57.739583
63	-95.002917	-94.69625	57.667917	57.76375
64	-94.369583	-94.332917	57.797083	57.827917
65	-94.397917	-94.347083	57.75625	57.779583
66	-94.51625	-94.334583	57.727917	57.81625
67	-94.517917	-94.409583	57.657083	57.742917
68	-94.49375	-94.37625	57.654583	57.745417
69	-94.55375	-94.507917	57.642917	57.702083
70	-94.720417	-94.525417	57.64375	57.730417
71	-94.727083	-94.58625	57.570417	57.645417
72	-94.86625	-94.72625	57.420417	57.509583
73	-94.824583	-94.767083	57.50375	57.529583

Sub-basin #	Xmin	Xmax	Ymin	Ymax
74	-94.749583	-94.68125	57.47875	57.517083
75	-94.85375	-94.794583	57.50875	57.562917
76	-94.80375	-94.649583	57.625417	57.70875
77	-94.850417	-94.749583	57.637083	57.689583
78	-94.929583	-94.829583	57.437083	57.607083
79	-94.89875	-94.83125	57.61875	57.652083
80	-94.947917	-94.844583	57.642917	57.687083
81	-95.19125	-94.984583	57.71125	57.779583
82	-95.219583	-95.047083	57.622083	57.722917
83	-95.160417	-95.01125	57.59625	57.69875
84	-95.045417	-94.995417	57.615417	57.67625
85	-94.970417	-94.887917	57.557083	57.602083
86	-95.017083	-94.957083	57.609583	57.637083
87	-95.169583	-94.97375	57.544583	57.614583
88	-95.07375	-94.987917	57.54875	57.579583
89	-95.025417	-94.857083	57.390417	57.560417
90	-95.290417	-95.019583	57.490417	57.627917
91	-95.222917	-95.014583	57.409583	57.51875
92	-95.022083	-94.972083	57.457083	57.49875

NOTE: X and Y stands for longitude and latitude, respectively. Each sub-basin has maximum and minimum longitude and latitude. Sub-basin 4 is the study area, Chesnaye Sub-basin of our research.

Appendix B

Table B.1 Modelling outputs from SLURP and WATFLOOD from 1978 to 2004

Year	Cumulative Precipitation (mm)	Cumulative Evapotranspiration (mm)		Average Daily Runoff (m ³ /s)		
		SLURP	WATFLOOD	SLURP	WATFLOOD	Measured
1978	255.1	218.7	403.9	14.6	24.4	12.7
1979	142.5	194.6	204.4	9.9	17.0	13.9
1980	212.7	242.3	332.2	12.4	13.7	18.4
1981	172.1	203.1	325.2	17.9	22.5	14.4
1982	268.8	239.6	527.3	24.6	34.8	15.8
1983	297.0	248.6	610.2	35.7	49.6	27.9
1984	141.0	195.0	235.7	17.8	26.6	14.3
1985	197.6	184.4	325.4	17.0	15.3	11.1
1986	219.7	241.0	431.4	25.7	30.7	22.9
1987	176.4	227.1	299.6	17.0	22.5	11.6
1988	175.5	180.2	207.9	6.7	13.3	9.1
1989	155.2	172.6	232.9	15.8	16.5	17.6
1990	204.5	187.4	320.4	16.4	15.5	12.1
1991	296.0	202.0	419.9	28.6	24.4	23.8
1992	263.6	169.3	401.8	23.1	26.5	12.8
1993	151.3	177.6	135.1	10.4	9.9	9.0
1994	168.6	147.4	186.3	14.1	6.0	7.2
1995	285.0	224.1	397.3	17.2	22.3	19.4
1996	157.4	200.7	233.1	12.7	16.9	7.0
1997	306.4	185.4	462.5	22.1	27.8	27.2
1998	238.9	177.0	400.0	36.4	25.6	16.5
1999	204.7	159.1	253.6	18.4	15.2	9.3
2000	253.5	174.9	428.5	27.5	30.1	21.8
2001	349.9	225.0	615.3	33.9	43.1	13.3
2002	303.5	186.7	470.1	31.8	36.3	16.6
2003	283.5	188.2	344.4	23.3	22.9	7.6
2004	216.5	139.9	333.3	29.1	28.3	12.4



